RAPID-PROTOTYPING OF PDMS-BASED MICROFLUIDIC DEVICES

A Dissertation
Presented to
The Academic Faculty

by

Giorgio Gianini Morbioli

In Partial Fulfillment
of the Requirements for the Degree
Doctor of Philosophy in the
School of Chemistry and Biochemistry

Georgia Institute of Technology
AUGUST 2020

RAPID-PROTOTYPING OF PDMS-BASED MICROFLUIDIC DEVICES

Approved by:

Dr. Amanda M. Stockton, Advisor
School of Chemistry and Biochemistry
Georgia Institute of Technology

Dr. Christy C. O'Mahony
School of Chemistry and Biochemistry
Georgia Institute of Technology

Dr. Facundo M. Fernández
School of Chemistry and Biochemistry
Georgia Institute of Technology

Dr. Peter J. Hesketh
College of Engineering
Georgia Institute of Technology

Dr. Neha Garg
School of Chemistry and Biochemistry
Georgia Institute of Technology

Date Approved: June 19, 2020

ACKNOWLEDGEMENTS

I would like to thank my advisor, Dr. Amanda Stockton, for her support and guidance, and for giving me the opportunity to work in her group. During my time at Georgia Tech, she gave me the freedom to explore my creativity as a scientist and innovator, and she identified which mentoring approach was the best for me. She always celebrated our achievements, and motivated us to keep up with the good work. Thank you so much!

I would like to thank the other members of my committee: Dr. Facundo Fernández, Dr. Christy O'Mahony, Dr. Neha Garg and Dr. Peter Hersketh, for the suggestions to improve my thesis, my presentation skills, and for all the valuable professional advice I got throughout the years. I really appreciate all of it.

I would like to thank the members of the Stockton group for all these years together, in special: Nick Speller, Mike Cato, Zach Duca, Scot Sutton, Dedra Eichstedt, George Tan, Aaron Pital, Anna Simpson and Marshall Seaton. Thank you for making the lab more enjoyable.

I would like to thank the students and everyone who was involved in CHEM 2211 and CHEM 3211. In special Dr. O'Mahony, for always having the back of the TAs, and Dr. Johana Smeekens, for teaching me the tricks of the trade in the instrumental lab.

I also would like to thank Dr. Jiri Janata and Dr. Larry Bottomley for the teaching, mentoring and off-classroom conversations. They meant a lot for me.

I am grateful for all the friends I made during the years at Georgia Tech, which made graduate school a little easier: Dominic Sirianni (Dom), Stephen Zambrzycki, Nick Schulze, Alyssa Blake, Osiris Martinez-Guzman, Eric Drew, Krista Bullard, Andrés Caballero, Huijuan Xu, Yaro Vasyliv and Asta Quattrocchi. But most of all, I am grateful for the friendship of Larissa Simões Novelino (Time). You helped me through the most difficult phase of grad school – the beginning. And the middle. And the end.

I am thankful for the members of home away from home: Derek Saez (I am the captain now), Brian Malaga, Fernando Senhora (menino Fernando), Thomas Cantrell, Vin Pham, Megan MacQueen, Mirelis Rivas Soto, Yulliza Henao-Barragan and Jayaram Natajaram. Thank you for the laughs, parties and conversations. In special, I want to thank Timur Tankayev, for all his assistance with math and coding, always fueled by coffee; Mina Georgieva, for her assistance in statistical analysis for several papers; and David Fialho, for all the chemistry discussions.

I would like to thank my friends from always: Anderson (Dodói), Marcus Vinicius, Maurício Daniel (Yena), Guilherme (Vegetal), Pedro Ivo (Dorado), Lucas Quintal (Psycho), Lucas Sponton (Urso), Isaías (Minas), Luis Felipe (Pininho), Diego Golinelli (Deabo), Ricardo Kita (Yoshi), Glauco (Pombo), Natan, Walter (Glô), Adriano Aquino (Mestre Draculino), Márcio Bocelli, Juliana Tamara (Amiguinha) and Giulianna Denari (Giu). In special, Mateus (Arroz), Elias (Abu), Thiago Mazzu (Monstrão) and Pedro Dias (Taxinha), for always being there for me.

I would like to thank all the support and infrastructure of the Georgia Institute of Technology, in form of its human resources, in special Mr. Scott Elliot, for his support and

training in the machine shop at the George W. Woodruff School of Mechanical Engineering at Georgia Tech. I am indebted to Mr. David Bostwick in the Bioanalytical Mass Spectrometry core at the Petit Biotechnology Institute at Georgia Tech, for all the training, teaching and patience.

I would to acknowledge the funding agency CNPq (Science without borders, Grant No. 205453/2014-7) for the scholarship support, and the State of Georgia, USA, for the financial support, without which this work would not be possible.

I would like to thank my parents, William and Helena, for understanding the missed birthdays, holidays and celebrations, and for supporting me from the distance. I would also like to thank my siblings, Guilherme and Giovanna, for the encouragement and for the late-night calls.

Finally, I thank Renata. Through thick and thin, close together or far away, you were there for me. You always understood me. You helped me to become a better person. I am thankful for having you in my life, which is a happier place now. I love you.

TABLE OF CONTENTS

LIST OF TABLES

LIST OF FIGURES

LIST OF SYMBOLS AND ABBREVIATIONS

%	Percentage
µm	Micrometer
µTAS	Micro Total Analytical Systems
2D	Two-Dimensional
3D	Three-Dimensional
A	Pre-Exponential Factor
A.U.	Arbitrary Units
ABTS	2,2'-Azino-Bis (3-Ethylbenzothiazoline-6-Sulphonic Acid
ANOVA	Analysis of Variance
Ar	Cross-sectional area
ASSURED	Affordable, Sensitive, Specific, User-Friendly, Rapid and Robust, Equipment-Free and Deliverable
ATR	Attenuated Total Reflectance
C.I.	Confidence Interval
ca.	Circa
CAD	Computer Aided Design
CATF	Cellulose Acetate Transparency Film
C_{geo}	Geometric constant of the channel
cm	Centimeter
CMYK	Cyan, Magenta, Yellow, Black
COM	Common (pin)
cP	Centipoise
D	Debye

Da	Daltons
DAQ	Data Acquisition System
DC	Direct Current
df	Degrees of Freedom
DI	De-Ionized Water
DPI	Dots Per Inch
E.C.	Enzyme Commission Number
EOF	Electroosmotic Flow
ESI	Electrospray Ionization
F	F-value
FTIR	Fourier Transform Infrared Spectroscopy
GLUE	Green, Low-Cost, User-Friendly, Elastomeric
h	Hours
H	Channel height
i.d.	Internal Diameter
I/O	Inlet / Outlet
k	is the rate constant
kg	Kilograms
kPa	Kilopascal
Le	Length of the channel
LOC	Lab-On-a-Chip
M	Molar
m	Meter
max	Maximum
MEMS	Microelectromechanical Systems

min	Minutes
mL	Milliliter
mm	Millimeter
mmol	Millimolar
MS	Mass Spectrometry
MoS	Mean of Squares
NC	Normally Closed
nm	Nanometer
NO	Normally Open
^{o}C	Degrees Celsius
Pa	Pascal
PAP	Print-And-Peel
PDMS	Polydimethylsiloxane
PEEK	Polyetheretherketone
PPI	Pixel per Inch
PMA	Programmable Microfluidic Arrays
PSA	Pressure Sensitive Adhesive
PTF	Polyester Transparency Film
PVA	Poly(vinyl) alcohol
PVAc	Poly(vinyl) acetate
PVC	Poly(vinyl) Chloride
PWR	Power
Q	Fluid flow
R	Universal gas constant
RGB	Red, Green, Blue

R_H	Fluidic resistance of the channel
RMS	Root-mean-square
rpm	Revolutions per Minute
s	Seconds
SPD	Speed
SS	Sum of Squares
T	Temperature
Th	Thomson
U	Units
UV	Ultraviolet
UVO	Ultraviolet Ozone
V	Volts
W	Watts
w	Channel width
δ	Film thickness
$\Delta G^{\ddagger}$	Activation Energy
ΔP	Backpressure
η	Dynamic viscosity of the fluid
$\theta_{water\text{-}glass}$	Water-Glass Contact Angle
$\theta_{water\text{-}PDMS}$	Water-PDMS Contact Angle
μL	Microliter
μPADs	Microfluidic Paper-Based Analytical Devices
ω	Rotational speed

SUMMARY

Microfluidics uses the manipulation of fluids in microchannels to accomplish innumerous goals, and is attractive to analytical chemistry because it can reduce the scale of larger analytical processes. The benefits of the use of microfluidic systems, in comparison with conventional processes, include efficient sample and reagent consumption, low power usage and portability. Most microfluidic applications require a development process based on iterative design and testing of multiple prototype microdevices. Typical microfabrication protocols, however, can require over a week of specialist time in high-maintenance cleanroom facilities, making the iterative process resource-intensive and prohibitive in many locations. Rapid prototyping techniques can alleviate these issues, enabling faster development of microfluidic structures at lower costs. Print-and-peel techniques (PAP), including wax printing and xurography, are low-cost fast-prototyping tools used to create master molds for polydimethylsiloxane (PDMS) miniaturized systems.

In this work, three different methods were created to improve the rapid-prototyping of PDMS-based microfluidic devices. Using the wax printing method, PDMS microdevices can now be fabricated from design to testing in less than 1 hour, at the cost of $0.01 per mold, being one of the fastest and cheapest methods to date. If extensive fluidic manipulation is required, xurography becomes the method of choice. The xurography technique presented here is the most rapid tool to fabricate PDMS-based microdevices to date, presenting turnaround times as fast as 5 minutes. The first hybrid technique that can be used either as a PAP or a scaffolding method is also presented here, using the same

materials and fabrication process. The green, low-cost, user-friendly elastomeric (GLUE) rapid prototyping method to fabricate PDMS-based devices uses white glue as the patterning material, and is capable of fabricating multi-height molds in a single step, improving even further the development of PDMS microfluidic devices.

Device fabrication is only one of the steps in the iterative process of designing a fully-functional microfluidic tool. The design of the microdevice itself plays a crucial role in its performance, which directly impacts processes conducted in miniaturized devices. In this work, the influence of hydrodynamic resistance in sample dispersion on a microfluidic multiplexer was studied using paper-based analytical microfluidic devices (μPADs) as the testbed. When microfluidic devices are not rationally designed, and when the influence of fluidic resistance is not taken into account, sample dispersion can be biased. A bias can influence the output of colorimetric enzymatic assays supported on these microstructures, which are the most common applications of μPADs, demonstrating the need for rational design of microdevices.

The third essential component of developing microfluidic devices is their effective testing, especially when incorporating active pumping elements on-chip. To overcome issues in the manual operation or coding for operation of microvalves, a program that can automatically generate sequences for fluidic manipulation in microfluidic processors was written in Python, with the only inputs required from the user being reservoir positions, mixing ratio and the desired input and output reservoirs. To further improve testing and avoid the use of fixed mounts, a modular system was created to aid the testing of devices with different designs, another advance in the area. This research enables better design and testing of microfluidic devices in shorter times and at lower costs, enabling improvements

in the interfacing between different unit operations on-chip, a challenge in the microfluidics area. More than that, it also makes this area, traditionally confined into expensive cleanroom facilities, available to more research groups worldwide.

CHAPTER 1. INTRODUCTION

1.1 Background

In 1990, Manz *et al.* [1] first proposed the concept of micro total analytical systems (μTAS). These systems would be capable of performing all steps of an analytical process in an integrated miniaturized platform [1] with comparable or better performance than their macroscale analogs. Now, 30 years after the first proposition of such systems, we are able to miniaturize and automate multiple laboratory analytical processes [2], including clinical [3] and drug discovery research [4], and a diverse array of *in situ* analysis. These analyses can range from field-deployable autonomous analysis in challenging locations [5] to environmental monitoring [6], as envisioned by researchers in the early 1990's [1]. These advancements were only made possible by the development of the microfluidics field [7] and improvement of microfabrication techniques.

Microfluidics is the study and manipulation of fluids in channels of reduced dimensions (*i.e.* in the order of μm) [7], with flow rates in the order of mL min^{-1} to nL min^{-1}. Microfluidics presents intrinsic characteristics such as low sample and reagent consumption, low power usage, and portability [7–9], in comparison with conventional macroscale processes, which is attractive to both analytical chemistry and μTAS fields (Figure 1-1).

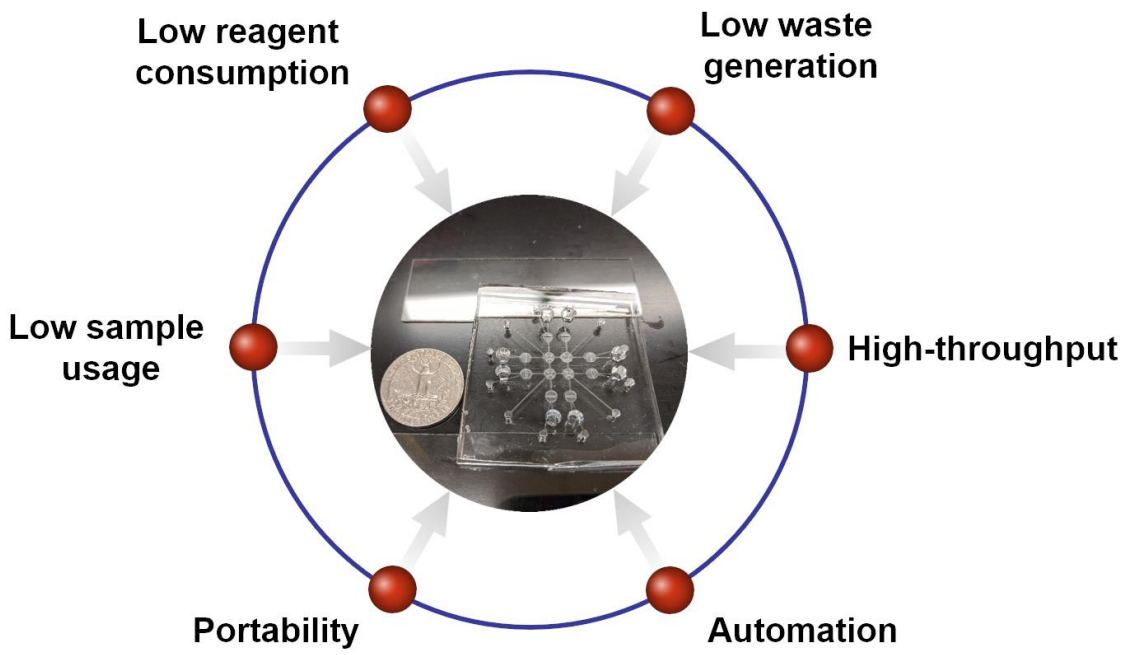

Figure 1-1 – Intrinsic characteristics of microfluidics that are attractive to analytical chemistry.

When fluids are confined into microchannels, they behave differently than at the macroscale, giving microfluidics unique physical and chemical characteristics. This is due to the different contributions of the dominant physical properties at the microscale, including viscosity, fluidic resistance and density [10].

The most well-known parameter used to characterize microfluidic systems is the Reynolds number, a dimensionless number defined by Equation 1:

$$Re = \frac{\rho u L e}{\eta} \tag{1}$$

Re is the Reynolds number;

ρ is the specific mass of the fluid (kg m^{-3});

u is the average velocity of the fluid (m s^{-1});

Le is the hydraulic diameter (m);

η is the dynamic viscosity of the fluid (Pa s).

The Reynolds number is an estimate of the ratio of convective forces over diffusional forces, used to characterize a flow as laminar (*Re* < 2100) or turbulent (*Re* > 4000), exemplified in Figure 1-2 [10].

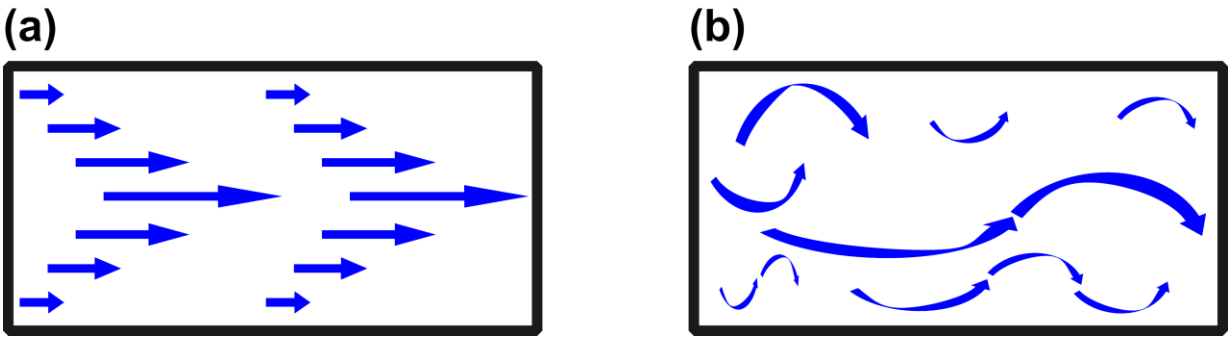

Figure 1-2 – (a) Laminar and (b) turbulent flow depiction.

The flow can be described by the incompressible Navier-Stokes Equations (Equation 2), which are a set of equations derived from the balance of forces (gravity, pressure, and viscosity) and conservation of momentum considering an infinitesimal volume of fluid [10],

$$\rho g - \frac{\partial p}{\partial x} + \eta\left(\frac{\partial^2}{\partial x^2} + \frac{\partial^2}{\partial y^2} + \frac{\partial^2}{\partial z^2}\right) u(x,y,z) = \rho \frac{\partial u(x,y,z)}{\partial t}$$

$$\rho g - \frac{\partial p}{\partial y} + \eta\left(\frac{\partial^2}{\partial x^2} + \frac{\partial^2}{\partial y^2} + \frac{\partial^2}{\partial z^2}\right) v(x,y,z) = \rho \frac{\partial v(x,y,z)}{\partial t} \quad (2)$$

$$\rho g - \frac{\partial p}{\partial z} + \eta\left(\frac{\partial^2}{\partial x^2} + \frac{\partial^2}{\partial y^2} + \frac{\partial^2}{\partial z^2}\right) w(x,y,z) = \rho \frac{\partial w(x,y,z)}{\partial t}$$

p is the driving pressure (Pa);

ρ is the specific mass of the fluid (kg m^{-3});

u,v,w are the velocity vectors (m s^{-1});

t is the time (s);

η is the dynamic viscosity of the fluid (Pa s);

g is the gravitational acceleration (m s^{-2}).

For low Reynolds number (*i.e.* Re << 1), the inertial forces are negligible when compared to the viscous forces, and the Navier-Stokes Equation (Equation 2) can be simplified to the Stokes Equation (Equation 3), which does not contain the non-linear inertial terms, and, therefore, is much simpler to solve. For its simplicity, the Stokes equation is useful to describe fluids behavior in microfluidic systems that satisfy the Re << 1 condition.

$$\rho g - \frac{\partial p}{\partial x} + \eta \left(\frac{\partial^2}{\partial x^2} + \frac{\partial^2}{\partial y^2} + \frac{\partial^2}{\partial z^2} \right) u(x,y,z) = 0$$

$$\rho g - \frac{\partial p}{\partial y} + \eta \left(\frac{\partial^2}{\partial x^2} + \frac{\partial^2}{\partial y^2} + \frac{\partial^2}{\partial z^2} \right) v(x,y,z) = 0 \quad (3)$$

$$\rho g - \frac{\partial p}{\partial z} + \eta \left(\frac{\partial^2}{\partial x^2} + \frac{\partial^2}{\partial y^2} + \frac{\partial^2}{\partial z^2} \right) w(x,y,z) = 0$$

For the low Reynolds number condition, laminar flow profiles are observed, meaning that for two (or more) separate streams of fluids meeting and co-flowing in a microchannel, mixing will happen due to diffusion at the interface of the streams, rather than inertial shear stress due to turbulence [10]. This characteristic is a blessing or a curse, depending on the intended application. For example, the creation of a Ag electrode inside of a 200 μm microchannel [11] is made possible by the laminar nature of the flow of the reagents, but the combination of sample and reagents to perform an assay in a microfluidic device is difficult due to the lack of turbulent mixing. In order to promote better mixing in microdevices, several design strategies have been developed over the years [12].

Fluidic resistance is another important parameter to be considered during microfluidic system development, which can be estimated by the Hagen-Poiseuille law (Equation 4).

$$R_H = C_{geo} \frac{\eta \, Le}{Ar^2} \quad (4)$$

R_H is the fluidic resistance of the channel (Pa m^{-3} s);

η is the dynamic viscosity of the fluid (Pa s);

Le is the length of the channel (m);

Ar is the cross-sectional area (m^2);

C_{geo} is the geometric constant of the channel.

Fluidic resistance is important when designing pressure-driven microfluidic devices, such as sample multiplexers, in which an undesired unbalance of hydrodynamic resistance can impact the output of an assay conducted on such device [13]. The fluidic resistance is also important because it is directly proportional to the pressure drop within a microchannel, which means that for a 10-fold decrease in the radius of a microfluidic channel there is a 100-fold increase in the pressure within the device for the same flow rate [10], which can limit device's application [8]. It is relevant to stress that this parameter only provides an approximation of the real increase in pressure experienced by the device, because it does not account for other relevant physical properties like fluid interactions with the channel (surface tension, for example). This makes material choice and surface chemistry also relevant, and these factors must be accounted for when envisioning the end application of the devices. The need to control fluidic resistance by controlling channel geometry and surface chemistry, therefore, also dictates the choice of fabrication technique.

The first microfluidic devices were fabricated in hard substrates such as glass and oxidized silicon (Si/SiO_2), using methods borrowed from the microelectronics industry, such as micromachining and photolithography [10]. Using these techniques, the iterative

process of microfluidic device development (design, fabrication and testing) becomes expensive and time consuming, requiring specialists operating expensive equipment inside a high-maintenance cleanroom environment. These requirements make the development of microfluidic devices cost-prohibitive to researchers worldwide [8].

To reduce time and cost associated with the development of microfluidic structures, rapid-prototyping tools were created [8,9,14–18], with different levels of investment, complexity and feature resolution. The use of the ubiquitous PDMS [2], in conjunction with these fast-prototyping techniques have boosted research in microfluidics: there is a (conservative) estimate that approximately 10% of all research in microfluidics has been conducted in PDMS-based devices [9]. This estimate demonstrates that the creation of new rapid-prototyping tools for PDMS-based microfluidic devices can reach many research groups, improving even further the development of μTAS.

The creation of rapid-prototyping microfabrication tools, besides the critical evaluation of these techniques, become necessary to broaden the microfluidics userbase, by eliminating the need for expensive cleanroom environments and highly trained personnel [9,19]. Low-cost, user-friendly, greener methods put this technology at the hands of researchers in in-development countries, students and hobbyists everywhere [9,19], making microfluidics an inclusive research area.

1.2 Thesis Organization

This thesis is organized as it follows: Chapter 2 presents the importance of the rational design of microfluidic devices, and how sample dispersion based on fluidic resistance impacts the colorimetric output of enzymatic assays conducted in microfluidic platforms. This study was conducted on microfluidic devices fabricated in a paper matrix with wax printing technology, owing to the simplicity of fabrication of these devices and short turnaround times. Despite fundamental differences in fluid transportation in a porous matrix versus open channels, these findings are relevant to the rational design of other devices created using other fabrication methods, such as the ubiquitous PDMS. PDMS devices account for ~10% of all studies, so a more widely applicable approach to study the influence of the design of microfluidic devices requires fabrication of microstructures with this elastomer. However, historically, device fabrication with PDMS has had long turnaround times using conventional microfabrication processes. To alleviate this issue, rapid-prototyping techniques can be used to fabricate molds for PDMS microfluidic devices.

In Chapter 3, I critically review the current literature associated with prototyping tools available to fabricate PDMS-based microdevices, comparing advantages, disadvantages and feature resolution of each method. In this chapter, I also present insights towards each one of the steps of the iterative microfabrication process (Design, Fabrication and Testing).

In Chapter 4, I demonstrate how wax printing can be used not only to fabricate microfluidic paper-based analytical devices, but also to fabricate master molds for

miniaturized PDMS systems. The biggest advantage of this method is the short time for prototyping relief molds (< 1 min); however, most of the device fabrication using this method is dedicated to curing the elastomer (3 h at 60 ^{o}C) on the mold. This relatively low curing temperature of PDMS is required to avoid deformations of the wax molds, at the cost of increased fabrication times. To alleviate this issue, I coupled wax printing mold fabrication with microwave thermal treatment of PDMS, reducing curing times from 3 h to 25 min; an ~86% improvement in processing time was achieved, while preserving wax mold features. This method significantly decreases the time associated with prototyping microdevices, from design to testing in one hour, while reducing the costs associated with the development of microfluidic tools. In addition to these improvements, another innovation brought by this method is the microwave annealing processing of PDMS-glass bonding to irreversibly seal hybrid devices after UVO exposure, posing as an alternative to conventional thermal annealing processes (2 h in a conventional oven x 30 min microwave treatment).

The full potential of microwave treatment of PDMS could not be reached using wax printing as the patterning method, due to thermal restrictions imposed by the mold. Moreover, channels fabricated by wax printing are low aspect ratio (height / width), which is useful for applications such as capillary electrophoresis, but increase the fluidic resistance of the microdevice in larger device footprints. If extensive fluidic manipulation is required in a microdevice, a method that can generate taller molds is preferred. In Chapter 5, I discuss how xurography, coupled with the microwave processing of PDMS gives rise to one of the fastest prototyping methods in literature for PDMS-based microdevices to date. This print-and-peel patterning method enables the fabrication of

molds with different heights, depending on the tape substrate used, or even the fabrication of multi-height molds, by the stacking of layers of tape. The greatest advantage of this method, however, is the circumvention of temperature limits imposed by wax molds. Depending on the tape substrate used to fabricate the molds, microfluidic devices can be fabricated in as fast as 5 min, from design to testing.

Chapter 6 presents an innovative PDMS microdevice fabrication method, which uses water-soluble white glue as the patterning material to fabricate relief molds for elastomer-based microfluidics: the Green, Low-cost, User-friendly, Elastomeric (GLUE) method. This method is the first of its kind, because it is the first method that can be used either as a print-and-peel technique or as a scaffolding-removal tool, using the same process and patterning material. Another advantage of this innovative tool is the ability to create multi-height master molds in a single step, avoiding the multiple mask alignment steps required in conventional photolithography.

Device fabrication is only one of the steps in the iterative process of designing a fully-functional microfluidic tool. After fabrication, it is necessary to test microdevice capabilities, but often the testing system does not match modified versions of devices nor allow for rapid modifications of the testbed apparatus. This, in turn, limits alterations in the design of the microfluidic device. Modifications in the design of microdevices should not have to be constrained to the testing system. In Chapter 7, I explore the improvement of the testing of the iterative design process of microfluidic devices. An automated low-cost modular system was developed to operate pneumatic-actuated microfluidic chips, compatible with PDMS-based microdevices fabricated using the methods presented in Chapters 4, 5 and 6.

Chapter 8 presents a summary of conclusions of this body of work, and suggestions for prospective studies that can be derived from the findings described above. I also present future directions and perspectives that I envision for the microfluidics field.

1.3 Contributions to the Field

The research projects described in this thesis represent a significant contribution to the microfluidics field. More than that, this work gives researchers, hobbyists and students worldwide the opportunity to study and use this technology, which has been traditionally developed by resource-rich research groups with access to cleanroom environments.

I first proved how the design of devices impacts the readout of colorimetric assays performed in three-dimensional microfluidic paper-based analytical devices. This study demonstrated the need for a rational design of microfluidic structures, and it is a step towards the adoption of these devices as point-of-care diagnostic tools, by reducing the bias generated by undesired uneven fluidic dispersion. This work on device design (Chapter 2) was published in Analytical Chemistry [13].

Second, I present a critical evaluation of the rapid-prototyping tools available in literature to fabricate PDMS-based microfluidic devices. I present insights about each step of the development process of microfluidic devices (Design, Fabrication, Testing); the costs associated with each fabrication technique; the resolution of features that can be achieved by each tool; and low-cost options to each one of the techniques, to facilitate the access to this technology by researchers in resource-limited sites. A manuscript was

prepared (Chapter 3), and it was submitted for publication to Analytica Chimica Acta (05/16/2020).

Third, I improved wax printing technology to fabricate PDMS-based microfluidic devices [17] by coupling it with microwave treatment to cure PDMS [20]. The combination of these technologies created one of the fastest prototyping methods in the PDMS-based microfluidics field, reducing the processing time to 1 h design-to-device [17]. The work on wax printing and microwave treatment (Chapter 4) was published in Sensors & Actuators B [8], and a provisional patent application was filed.

Fourth, the full potential of microwave curing of PDMS was explored by changing the patterning method from wax printing [8,17] to xurography [18]. Without the thermal limitations imposed by wax molds, PDMS curing times were reduced from 25 min to 5 min, a remarkable 80% improvement in processing time. When compared with conventional soft-lithography, the improvement in processing time is even more astonishing: from 24 h to 5 min, a 99.7% improvement. Also, the low startup costs (~$300.00) associated with the acquisition of a cutter plotter, a conventional microwave oven and tape as consumable material puts this technology in the hands of anyone interested in microfluidics, from hobbyists to pre-college labs. The work on xurography and microwave treatment (Chapter 5) was published in Sensors & Actuators B [9], and a provisional patent application was filed.

Fifth, to the best of our knowledge, we created a unique microfabrication method that can be used either in a Print-and-Peel approach or as a scaffolding tool (Chapter 6). Using non-toxic white school glue as the patterning agent, we created a green fabrication

tool that does not require organic solvents and does not generate toxic waste. This innovative method can create multi-height relief molds for PDMS-based microfluidics in a single step, without requiring any mask alignment steps. This work was published in ACS Applied Polymer Materials [19], and a provisional patent application was filed.

In Chapter 7 I discuss the testing of microfluidic devices, and how this important step of microfluidic device development has been neglected. A modular approach has been proposed to alleviate the issues with fixed testbeds, and a Python code has been written to automate fluidic manipulations in fluidic processors. To lower the costs associated with research on complex fluidic processing, an Arduino-based system was built, in contrast to the standard use of conventional commercial Data Acquisition systems (DAQs). The use of an automated low-cost modular system improved the testing of microfluidic devices, which will both speed up research in the area, while also giving the opportunity to researchers and microfluidics enthusiasts around the world to explore this field. A manuscript is in preparation for submission to Lab-on-a-Chip by July 2020.

CHAPTER 2. RATIONAL DESIGN OF MICROFLUIDIC DEVICES

2.1 Abstract

Paper-based devices are a portable, user-friendly and affordable technology that is one of the best analytical tools for inexpensive diagnostic devices. Three-dimensional microfluidic paper-based analytical devices (3D-μPADs) are an evolution of single layer devices and they permit effective sample dispersion, individual layer treatment, and multiplex analytical assays. Here, we present the rational design of a wax-printed 3D-μPAD that enables more homogeneous permeation of fluids along the cellulose matrix than other existing designs in the literature. Moreover, we show the importance of the rational design of channels on these devices using glucose oxidase, peroxidase, and 2,2'-azino-bis (3-ethylbenzothiazoline-6-sulphonic acid) (ABTS) reactions. We present an alternative method for layer stacking using a magnetic apparatus, which facilitates fluidic dispersion and improves the reproducibility of tests performed on 3D-μPADs. We also provide the optimized designs for printing, facilitating further studies using 3D-μPADs.

2.2 Introduction

Microfluidic paper-based analytical devices (μPADs) are low-cost analytical tools that are easily manufactured, manipulated, transported and stored [21], which makes μPADs attractive for diagnostic applications and meets the requirements of the World Health Organization in the ASSURED Challenge (Affordable, Sensitive, Specific, User-friendly, Rapid and robust, Equipment-free and Deliverable) [22]. Three-dimensional microfluidic paper-based analytical devices (3D-μPADs) consist of a stack of single layer μPADs [23–29], and are a natural evolution of single layer systems [30–41] due to: *i*) individual treatment of layers or the use of different materials in different layers [42], which can demand independent and sometimes incompatible treatments; *ii*) sample dispersion from ten to thousand-fold, which favors multiplexed assays [26]; *iii*) enclosing of intermediate layers, which protects the reagents stored on the device without the need for an additional toner layer [43] and *iv*) integration of sample preparation steps into the device, which includes separation and washing [23,44].

In order to allow fluid permeation through the device it is necessary to maintain intimate contact between adjacent hydrophilic zones, which can be done either irreversibly (Figure A-1, Appendix A), in which the layers cannot be separated after assembly without damaging the device [25,26,45,46]; or reversibly (Figure A-2, Appendix A), where it is possible to separate layers after assembly [23,28,29,44]. Among these methods of layer assembly, the use of tape and cellulose powder is the most laborious one, requiring precise alignment and addition of cellulose powder in each spot, which hinders mass production [26]. The use of adhesive spray, on the other hand, may be the most appropriate method for mass production of irreversibly-bound paper-based devices [25]. Reversibly-bound

origami μPADs are advantageous in comparison with irreversibly bound microchips, as they eliminate the need for extra layers of tape [26] or coating steps [25], and they are more useful for step-by-step studies [23] or in fluidic dispersion studies due to the ease of post-testing analysis [44]. The designs arrived at via reversible origami μPADs can be made into irreversible μPADs via multiple methods including hybrid origami / double-sided tape glued systems [47].

Patterns of fluidic distribution on the device depend on the design of the paper-based microchip (Figure A-3, Appendix A) [25]. However, it is relevant to note how the design of the 3D-μPAD could affect fluidic dispersion on the cellulosic matrix and, therefore, the use of the device itself [44]. Fluidic dispersion on paper-based devices is especially relevant in enzymatic assays supported on the cellulosic matrix, because these reactions are time-sensitive: the longer the enzymatic reaction proceeds, the higher amount of product is generated, enhancing the detected signal in those areas, whether colorimetric [21], electrochemical [27] or fluorescent [29]. If there is a preferential path of fluidic dispersion favoring some reaction zones, then a positive bias will be observed in those zones, impacting the figures of merit of the analytical method. Therefore, the design of paper-based microfluidic devices is critical for their successful application [44].

In this paper we present a new paper-based microchannel design and demonstrate how channel design influences fluidic permeation of the cellulosic matrix and the read-out measurements of the assay. We use colorimetric glucose determination by the glucose oxidase enzymatic assay as a model, as this system has been consistently used in conjunction with μPADs since the first report of this technology [48], and permits a rapid comparison between systems [37]. Moreover, we also present a new method of layer

assembly using an external magnetic apparatus, facilitating fluidic dispersion studies and improving the reproducibility of tests performed on 3D-μPADs. We also demonstrate how an excess of sample and an increase in reaction time improve the colorimetric response using our model enzymatic assay.

2.3 Materials & Methods

2.3.1 Reagents

Glucose oxidase from *Aspergillus niger* (Enzyme Commission Number (E.C.) 232-601-0), peroxidase from horseradish (E.C. 232-668-6), 2,2-azino-bis(3-ethylbenzothiazoline-6-sulfonic acid) diammonium salt (ABTS) and D-(+)-trehalose dehydrate from *Saccharomyces cerevisiae* were purchased from Sigma-Aldrich (St. Louis, MO). D-(+)-glucose was purchased from VWR (Solon, OH), red fountain pen ink was purchased from Waterman (Paris, France) and sodium hydrogen phosphate anhydrous (ACS, 99.0% min.) was purchased from Alfa Aesar (Ward Hill, MA). All reagents were used as received.

2.3.2 Paper-Based Devices Fabrication

Origami paper-based microchip devices were designed using CorelDraw® X7 software (Figure 2-1a), and printed on Whatman No. 1 chromatography paper (letter size) using a Xerox Phaser® 8580 wax printer (Figure 2-1b). The patterned sheets were

submitted to thermal treatment in an oven (150 ºC for 2 min, Figure 2-1c) to melt the wax through the entire thickness of the paper in order to create hydrophobic barriers [35]. The design files (Figure 2-1d) and specifications are available in the Electronic Supporting Information (Figure A-4, Appendix A). The origami paper-based microchip devices were folded along the white lines, aligning the edges of adjacent layers and superimposing one layer onto another (Figure 2-1e), obtaining a final device with 25 x 25 mm dimensions. Folding instructions are presented in the Appendix A (Figure A-5).

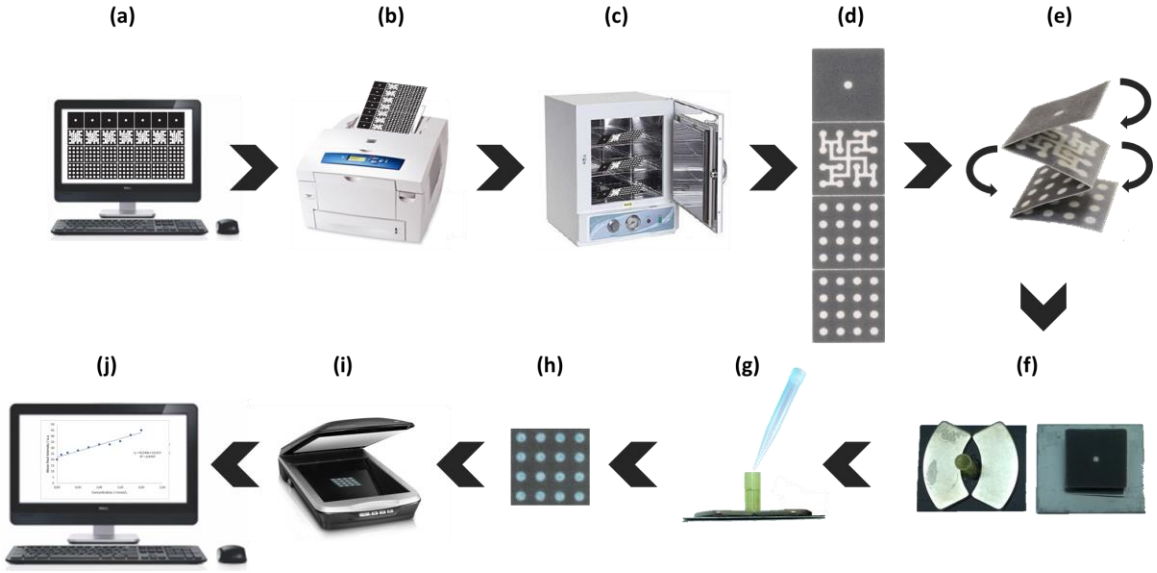

Figure 2-1 – Step-by-step fabrication and use of a µPAD with optimized flow path. (a) Microdevice design. (b) Wax printing. (c) Melting and permeation of wax on paper. (d) Cut microchip. (e) Folding of the device. (f) Insertion into the magnetic apparatus. (g) Sample introduction. (h) Bottom of the device after the assay. (i) Device digitalization. (j) Image analysis.

2.3.3 Magnetic External Apparatus

Two flat magnetic stainless steel sheets were recovered from machine shop scrap and were cut in the following dimensions: 39 × 48 mm, as presented in Figure 2-1f. Flatness

was assessed by visual inspection. The top sheet was perforated in the center, and a cut pipette tip was glued onto it (Figure 2-1f). The bottom part was perforated 16 times, in a 4 × 4 configuration, according to the bottom layer of the paper-based microdevices. The paper-based devices were introduced between the top and bottom metal sheets, aligning the holes of the apparatus with the pattern of the paper-based device (Figure 2-1g). To keep the whole apparatus together a pair of neodymium magnets were used (curved pieces in Figure 2-1f) [49].

2.3.4 Incremental Permeation Study

A red ink solution (0.5 mL ink: 10 mL deionized (DI) water) was applied at the top of the magnetic apparatus containing one paper-based device, in 5 μL increments (0 to 70 μL). This experiment was performed at least in triplicate for each of the volumes and for each of the 5 studied designs.

2.3.5 Permeation Study Recording

A Logitech® HD Pro Webcam C920 was fixed in the base of a universal support to record the bottom of the device during fluid permeation. The magnetic apparatus containing the paper-based device was positioned above the camera, and 70 μL of the red ink solution was applied at the top of the magnetic apparatus, recording each device for 15 min. At least 15 devices for each of the 5 studied designs were recorded. Video recordings of the fluid permeation on each studied design are available in the publisher's website.

2.3.6 Enzymatic Assay

A volume of 1 µL of a 25 mmol L^{-1} ABTS redox indicator in water was pipetted onto each one of the 16 spots in the bottom layer of the 3D-µPAD. After complete dryness of the spots (~30 min), 1 µL of a solution containing glucose oxidase (120 U mL^{-1}), horseradish peroxidase (300 U mL^{-1}) and trehalose (0.6 mol L^{-1}) in phosphate buffer (0.1 mol L^{-1}; pH 6.0) was added to each spot in the bottom layer of the 3D-µPAD, and allowed to dry ~30 min for complete dryness of the spots [37]. The standard of complete dryness minimized differences in color due to variation in reaction time and facilitates the analysis by yielding a more robust quantitative readout. The 3D-µPAD containing reagents was folded and placed in the external magnetic apparatus, and 65 µL of a 2 mmol L^{-1} glucose standard solution diluted in water was applied at the top of the magnetic apparatus. After 10 min the paper-based device was removed from the magnetic apparatus and after complete dryness (~30 min) the device read-off was digitalized in a flatbed scanner. This experiment was performed at least in triplicate for the original and optimized designs. This experiment was repeated with a longer reaction time (20 min), and with an increased sample volume (80 µL of a 2 mmol L^{-1} glucose standard solution and 20 min of reaction time). The average color intensity in the RGB channel was obtained using Adobe Photoshop® CC 2015 software (but another open source software could be also used, such as ImageJ (http://imagej.nih.gov/ij).

2.4 Results & Discussion

2.4.1 Layer Assembling Method

The reversible method for layer assembly using an aluminum housing with screws [29] can be problematic, as the torque applied to each one of the 4 screws can introduce a force imbalance into the system that can heterogeneously compress the device and induce a bias in fluidic dispersion in the 3D-μPAD. Using 2 flat stainless-steel plates united by strong Nd magnets alleviates this issue, as the force applied to keep the layers of the paper-based device together is more uniform. As this method minimizes variation in fluidic permeation, improvement in the figures of merit for the analytical method should also be expected [44].

2.4.2 Permeation Study

As seen in Figure 2-2 and in the video recordings of ink permeation on the devices with different designs (available in the publisher's website), the use of the original design presented in literature [25] creates a preferential path for fluidic permeation to the central spots in the bottom layers of the device. This bias can influence the results of enzymatic assays, which are time dependent. This behavior is due to the smaller hydrodynamic resistance of the path traveled by the fluid (Figure A-6, Appendix A) [50].

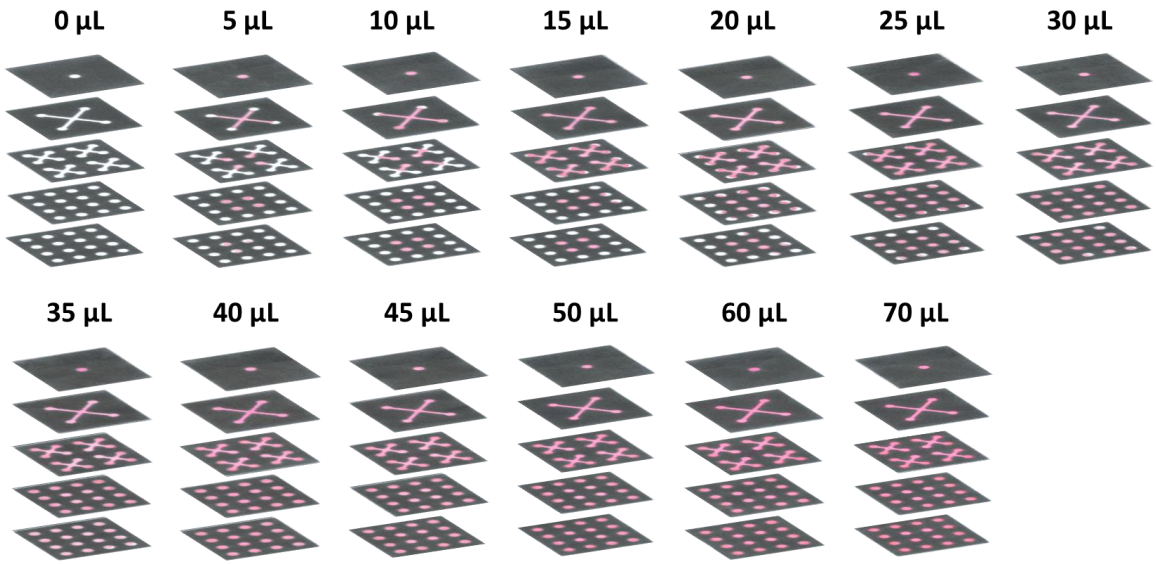

Figure 2-2 – Incremental fluid dispersion study using a design provided in literature [25]. Volumes of test dye solution were applied at the top of the device (in 5 µL increments) and permeated from top to bottom. Each device was unfolded and the image digitalized after 30 min. There is a preferential dispersion through the central spots, as observed in devices housing 5 to 20 µL. These images are presented in an exploded view to ease visualization, and represent experimental data. Original digitalization of the experimental results is available in the Appendix A (Figure A-7).

In the first iteration of device optimization, an additional layer was added to the original design [25] to ameliorate preferential fluidic dispersion (Figure A-8 and Figure A-9). The dispersion of fluid was more homogeneous in this design, with no apparent preferential paths. However, an extra layer was introduced in the device, which adds a minor additional degree of fabrication complexity [25].

Two other optimization designs were tested (Figure A-10 to Figure A-13) that have the same number of layers as the original design. The combination of these designs led to the fully optimized design (Figure 2-3), which incorporates just 4 layers and displays homogeneous fluidic dispersion [44]. This design presents a longer hydrophilic path for

each channel in the second layer, which in turn led to the same hydrodynamic resistance for all fluidic connections and homogeneous fluidic dispersion in this device. These longer hydrophilic paths increase the overall hydrodynamic resistance of the device (83.6 mm of total length, 1.9 mm of width) as compared to the original design (63.3 mm of total length, 1.9 mm of width) (Figure 2-2), but have been rationally designed such that the hydrodynamic resistances of all pathways are equivalent.

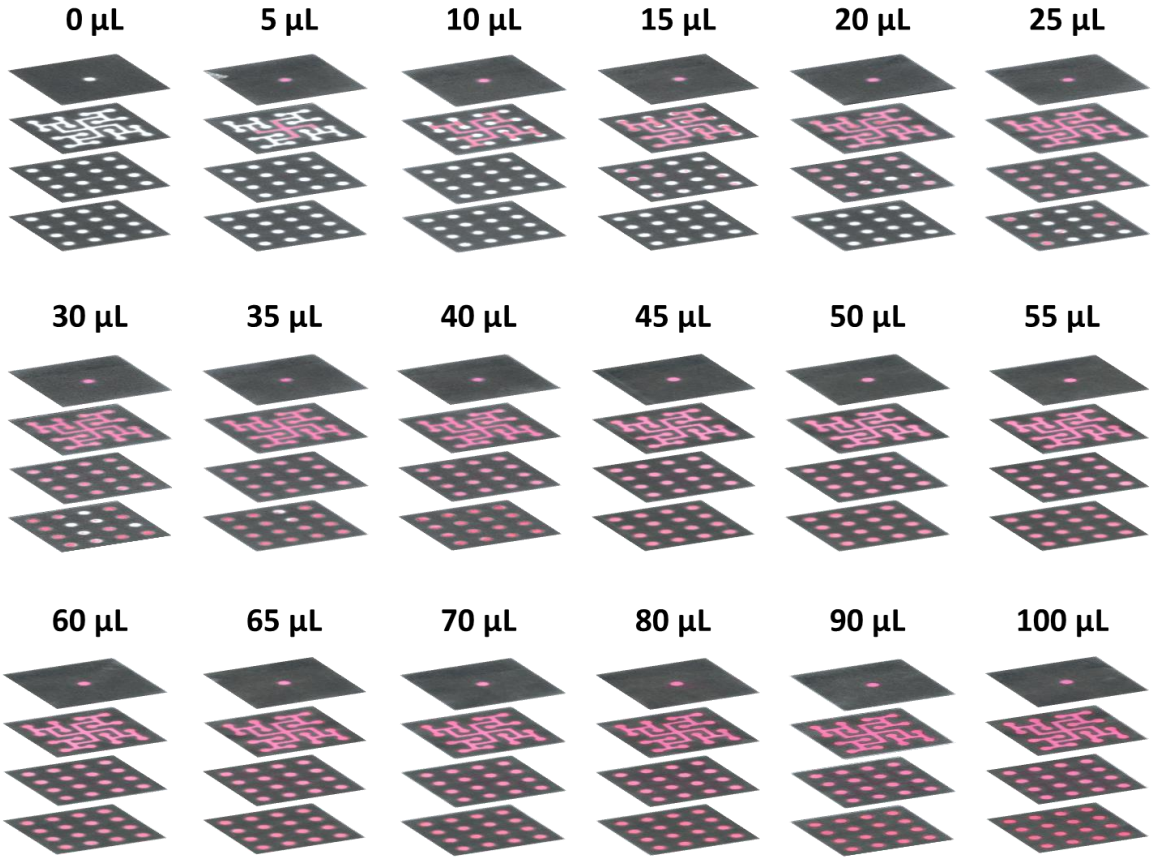

Figure 2-3 – Optimized paper-based microchip design. This design contains only 4 layers, and permits a more homogeneous dispersion of fluid in the device. It can comport 100 µL of sample without leaking. These images are presented in an exploded view to ease visualization, and represent experimental data. Original digitalization of the experimental results is available in the Appendix A (Figure A-14).

As can be seen in Figure 2-3, volumes as small as 40 μL can reach all the spots in the bottom layer of the optimized device. However, a small excess of liquid (65 μL) provides better results with the enzymatic assay. The improved performance is due to the prolonged hydration of the bottom spots, where the sample can interact with enzymes and redox indicator, which enables the enzymatic reactions to proceed further to completion. In order to evaluate the volumetric liquid capacity of the devices we have added an excess of fluid (up to 100 μL) at the top of the magnetic apparatus. We did not observe any leaking when excess fluid was applied to the devices, indicating that the system can hold larger volumes of fluid. This characteristic can be exploited further to improve the limit of detection and limit of quantification of enzymatic assays supported on these devices.

2.4.3 Enzymatic Assay

When the original design is used in conjunction with the enzymatic assay there is a difference in the mean pixel intensity of the 4 central spots and the 12 peripheral ones (Figure 2-4a, original data in Table A-1, Appendix A). This difference is statistically significant (*t*-test, C.I. 95%, Table A-2 and Figure A-17, Appendix A), supporting our initial hypothesis that different hydrodynamic resistances introduce a bias in the colorimetric output. The optimized design with equal hydrodynamic resistances (Figure 2-4b), however, shows no statistical difference between the spots (*t*-test, C.I. 95%, Table A-2 and Figure A-17, Appendix A). There is a slight color intensity decrease observed in the optimized design in comparison with the original design (Figure A-15), because the increased hydrodynamic resistance in the optimized design has reduced rate of fluid flow

resulting in a reduced reaction time in comparison with the original design (available in the publisher's website). If higher coloration intensity is desired, more sample can be added to the device. An increase in sample volume and in reaction time result in a statistically significant increase in the colorimetric signal, with a decrease in the variance of data (Figure A-18, Table A-3and Table A-4, Appendix A). These results prove that assays can be unbiased or biased based on the μPAD design, and that the rational μPAD design presented here enables unbiased μPAD assays.

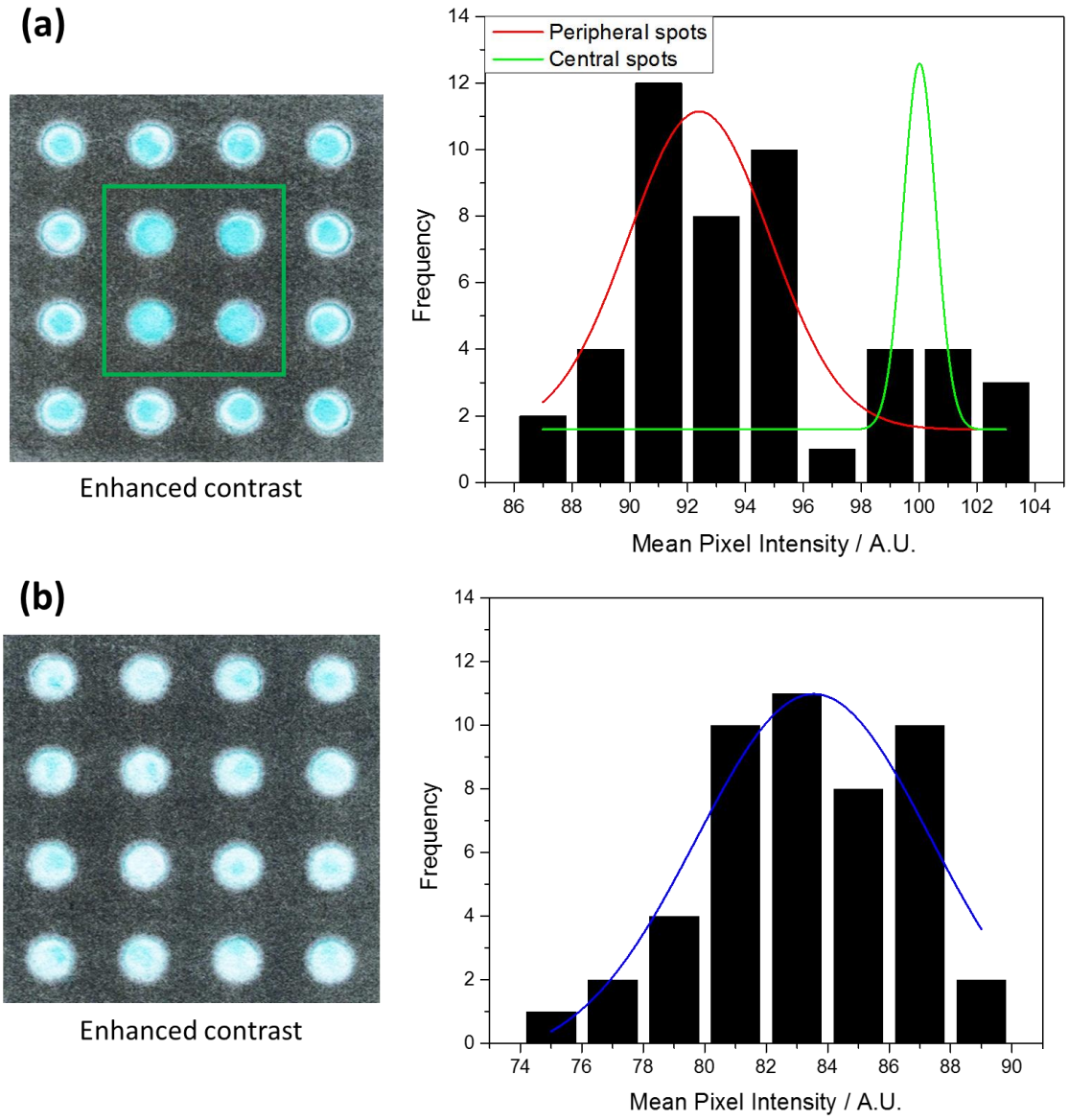

Figure 2-4 – Statistical comparison between colorimetric enzymatic assay for glucose determination. (a) Original design [25]. There is a higher signal developed in the 4 central spots (inside the green square) than in the peripheral spots. (b) Optimized design. There is no significant statistical difference between the central and peripheral spots coloration. Original digitalized images are provided in the Supporting Information (Figure A-15, Appendix A).

Limits of detection and quantification of enzymatic assays can be improved with an excess of sample volume. This increase is because an increase in sample volume results in a statistically significant increase in the colorimetric signal for solutions with the same concentration (Figure A-18, Table A-3and Table A-4, Appendix A). There is a more intense color in the detection zone because *i)* the enzymatic reaction can proceed longer and *ii)* because of the concentration power of the paper that allows for rapid evaporation of solvent (Figure A-19, Appendix A). More analyte reaches the bottom layer, which contains the enzymatic assay reagents, so more colored product is formed (Figure A-19, Appendix A). The colored products formed in the detection zones are stable, and the device digitalization can be performed even 72 h after the assay has been performed, without signal losses (Figure A-20, Appendix A).

2.4.4 Practical Guidelines to Design Unbiased Devices

When designing microfluidic devices, it is important to follow some ground rules to avoid biasing the outputs. The first insight is that the rational design of each layer is critical. The design rule is to ensure that channels have the same hydrodynamic resistance for every branch in a single layer (for example, the second layer in Figure 2-3) [51]. While this design rule is inherently for a 2D system, a 3D device is made of 2D structures layered together: an uneven fluidic hydrodynamic resistance in one 2D layer will affect the final output of the entire 3D structure.

The second insight is specific to 3D-μPADs. If two hydrophilic channels are brought into contact in adjacent layers, this will create a path of smaller hydrodynamic

resistance, as observed in Figure 2-2, analogous to a short-circuit in an electrical circuit [50]. Hydrophilic channels of adjacent layers should be connected just when the fluid has fully-completed the first layer, as shown in Figure 2-3 (with obvious exclusions for cases in which this is desirable, such as in a flow divider) [52].

The third insight is also specific to 3D-μPADs. Each layer of the device should maximize usage of the material, such as the second layer of the device depicted in Figure 2-3. This is due to the fact that the effectiveness of layer assembling is layer-dependent: A higher number of layers diminishes the efficacy of the layer assembling method, resulting in a fewer number of functional devices [25], or requires more steps in assembly of irreversibly-bound 3D-μPADs (Figure A-22, Appendix A) [26]. The layer assembly method itself also can influence the output, as discussed in the Layer Assembling Method Section, so we suggest magnetic apparatus to avoid biasing in 3D-μPADs.

2.5 Conclusion

The 3D-μPAD systems provide multiple advantages including sample distribution, multiplexed assays, and individualized treatment of layers. Here, we have shown that the method of assembling layers and the 3-dimensional design of paper-based devices play a critical role in assay performance. It is critical that all fluidic paths in the sample distribution layer present the same hydrodynamic resistance to avoid the creation of preferential fluidic paths, which are responsible for output differences. Moreover, the layer assembly method should ensure evenly distributed force across the entire 3D-μPAD system to avoid preferential fluidic paths, which is more facile when the microfluidic device

contains fewer layers. We have introduced a device that optimizes the production of 3D-μPADs and assay performance. Further work utilizing this device and these design principles with other assays and on relevant samples is warranted and encouraged. This work furthers the development of low-cost diagnostic tools, improving reproducibility and other figures of merit using a 3D paper-based platform.

2.6 Acknowledgements

The authors would like to thank the funding agencies FAPESP (Grant No. 2011/13997-8), CNPq (Grant No. 131306/2013-8 and 205453/2014-7) by the scholarships and financial support to the Instituto Nacional de Ciência e Tecnologia de Bioanalítica – INCTBio (FAPESP Grant Nr. 2008/57805-2 / CNPq Grant Nr. 573672/2008-3), the Georgia Institute of Technology (Georgia Tech) and the State of Georgia, USA. We gratefully acknowledge M.Sc. Larissa Simões Novelino (Georgia Institute of Technology, USA) for the AutoCAD drawings.

CHAPTER 3. RAPID-PROTOTYPING OF PDMS-BASED MICROFLUIDIC DEVICES

3.1 Abstract

Micro total analytical systems (μTAS) are attractive to multiple fields that include chemistry, medicine and engineering due to their portability, low power usage, potential for automation, and low sample and reagent consumption, which in turn results in low waste generation. The development of fully-functional μTAS is an iterative process, based on the design, fabrication and testing of multiple prototype microdevices. Typically, microfabrication protocols require a week or more of highly-skilled personnel time in high-maintenance cleanroom facilities, which makes this iterative process cost-prohibitive in many locations worldwide. Rapid prototyping tools, in conjunction with the use of polydimethylsiloxane (PDMS), enable rapid development of microfluidic structures at lower costs, circumventing these issues in conventional microfabrication techniques. Multiple rapid-prototyping methods to fabricate PDMS-based microfluidic devices have been demonstrated in literature since the advent of soft-lithography in 1998; each method has its unique advantages and drawbacks. Here, we present a tutorial discussing current

rapid prototyping techniques to fabricate PDMS-based microdevices, including soft-lithography, print-and-peel and scaffolding techniques, among other methods specifically comparing resolution of the features, fabrication processes and associated costs for each technique. We also present thoughts and insights towards each step of the iterative microfabrication process, from design to testing, to improve the development of fully-functional PDMS-based microfluidic devices at faster rates and lower costs.

3.2 Introduction

Micro total analytical systems (μTAS) are structures that can perform tasks of large macroscale analytical tools in an integrated small footprint device [14]. These chemical sensing systems, envisaged by Manz *et al.* in 1990 [1], became attainable with the development of the microfluidics field [7], and are attractive to diverse areas, including *in situ* environmental monitoring [6], off-site autonomous analysis in challenging locations [5], bioanalytical chemistry [53], separations science [54,55], epigenomic studies [56,57], drug discovery [4] and clinical chemistry research [3].

Microfluidic tools are appealing for use in multiple arenas owing to their intrinsic characteristics, namely: *i)* lightweight and small volume [54], which enables portability; *ii)* low consumption of power, reagent and sample, which results in *iii)* low waste generation [54]; *iv)* capability of integrating sample pretreatment steps on a small unit, reducing sample handling and minimizing sources of contamination [1,54]; and *v)* enhanced analytical performance, in terms of separation performance and multi-component analysis [1].

The development process of microfluidic devices, like all analytical tools, is based on iterative design, fabrication and testing of multiple prototypes (Figure 3-1). Typical microfabrication protocols, such as photolithography and micromachining of glass or oxidized silicon (Si/SiO_2) substrates, can require a week or longer of a specialist's time in a high-maintenance cleanroom facility. These requirements make the iterative process resource-intensive and cost-prohibitive in many locations [8]. Rapid prototyping techniques can alleviate such issues, enabling more efficient development of microdevices.

Rapid-prototyping methods are essential components of iterative design processes [58], because these methods reduce the time required to fabricate testable devices and streamline production chains [8,59]. Soft-lithography, developed in the late 1990s by the Whitesides group at Harvard University, was the first method to rapid-prototype microfluidic devices using polydimethylsiloxane (PDMS) soft-elastomers [14]. This pioneering work boosted research in microfluidics because it enabled start-to-finish manufacture of microdevices within 24 h. However, the primary limitation of this method is use of SU-8 mold fabrication, which uses conventional photolithography and wet-etching processes [14] that continue to require cleanroom facilities and skilled personnel. Since this first rapid-prototyping method to achieve microfluidic devices, alternative processes were created to fabricate relief molds for soft-elastomer-based microfluidic devices.

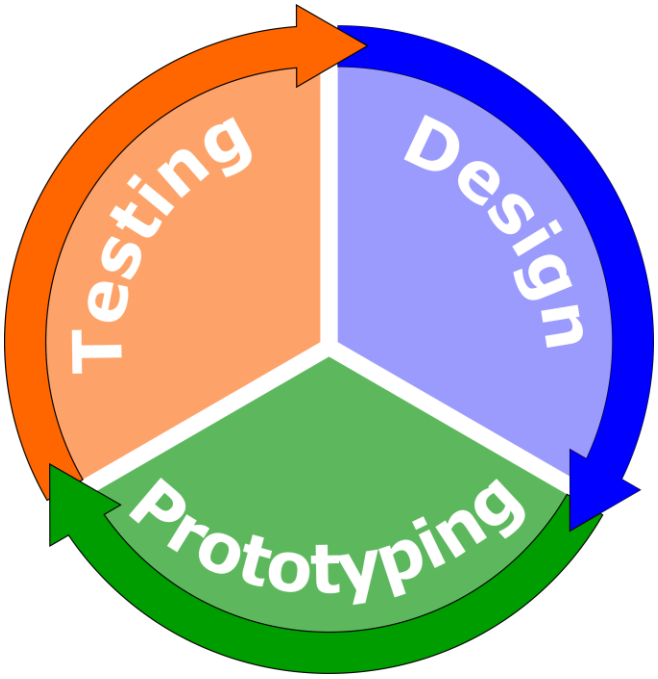

Figure 3-1 – Iterative design process diagram.

In this step-by-step tutorial review we discuss different rapid-prototyping approaches to fabricate PDMS-based microfluidic devices. Although there are alternatives to this material, such as poly (methyl methacrylate) (PMMA) [60], cyclicolefin copolymer (COC) [61], thermoset polyester (TPE) [62] and polyurethane (PU) [63], to cite a few, we focus this tutorial on techniques that use PDMS as the fabrication material of choice, due to its readily available nature, ease of use and application, non-toxicity, and abundance of information in literature [64]. We initially discuss general techniques that can be used to decrease time and complexity of each step of the iterative microfabrication process. A discussion on the current rapid prototyping methods available in literature is provided, and we critically evaluate each method in terms of cost, ease of fabrication and feature resolution. We also include a perspective on the combination of techniques and methods

that can meet the needs of the user in terms of cost, resolution and fabrication time. Finally, we include thoughts and insights for future research on microfabrication, which will enable the use of this technology by researchers, hobbyists, and schools worldwide at reduced costs and faster rates.

3.3 Elastomeric microfluidics - PDMS

Conventional materials used in microfabrication such as silicon and glass [65] do not allow for the fast turnaround times required to develop new microfluidic tools, are cost-prohibitive and require high startup costs [9]. Elastomeric materials have surpassed the limitations imposed by conventional microfabrication processes [2] due to their ease in processing. Styrenic thermoplastic elastomers (TPE) [66], polyurethane rubbers (PU) [63,67], and silicones [14,68] are a few examples of elastomeric materials available for fabrication of microfluidic devices. From these elastomers, it is undeniable that PDMS is the most popular [69]. It is estimated that more than 10% of studies on microfluidics employ PDMS as the substrate of choice [9].

PDMS is a very versatile material, but it has some well-known limitations, including swelling in the presence of organic solvents [70], the absorption of molecules into the polymer matrix [71], and its intrinsic hydrophobicity [72]. It is therefore necessary to consider PDMS properties when designing a microfluidic device for an intended final application [69].

3.3.1 PDMS Properties

Polydimethylsiloxane (Figure 3-2) has been the workhorse of exploratory research in the microfluidics field [7], owing to its intrinsic properties such as: optical transparency [73], flexibility [5], biocompatibility [74], thermal stability [75], surface modification potential [76–78], and commercial availability.

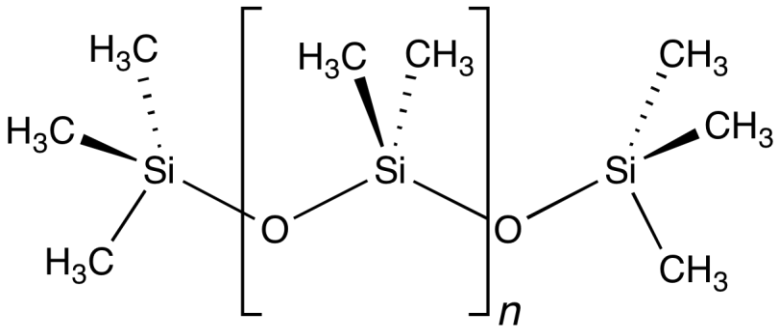

Figure 3-2 – Polydimethylsiloxane (PDMS) structure.

Sylgard 184® is a two-part silicone commercial elastomer from Dow Corning that has been extensively used in soft-lithography [14–16,75,79], with the closest competitor being RTV-615® from Momentive [80]. The curing agent is mostly composed of vinyl terminated poly(dimethylsiloxane) and surface-modified silica fillers [75] that act as elastic reinforcers [81]. The elastomer base is mostly composed of poly(dimethyl, methylhydrogen siloxane) and a platinum-based catalyst [75]. When mixed, a platinum-catalyzed olefin hydrosilylation reaction takes place through a Chalk-Harrod mechanism (Figure 3-3): *i)* oxidative addition of the hydrosilane into the platinum catalyst; *ii)* coordination of the olefin to the metallic center; *iii)* migratory insertion of the olefin into

the platinum-hydrogen bond (rate-limiting step) and *iv)* reductive elimination of the alkylated silane, restoring then the platinum catalyst [82].

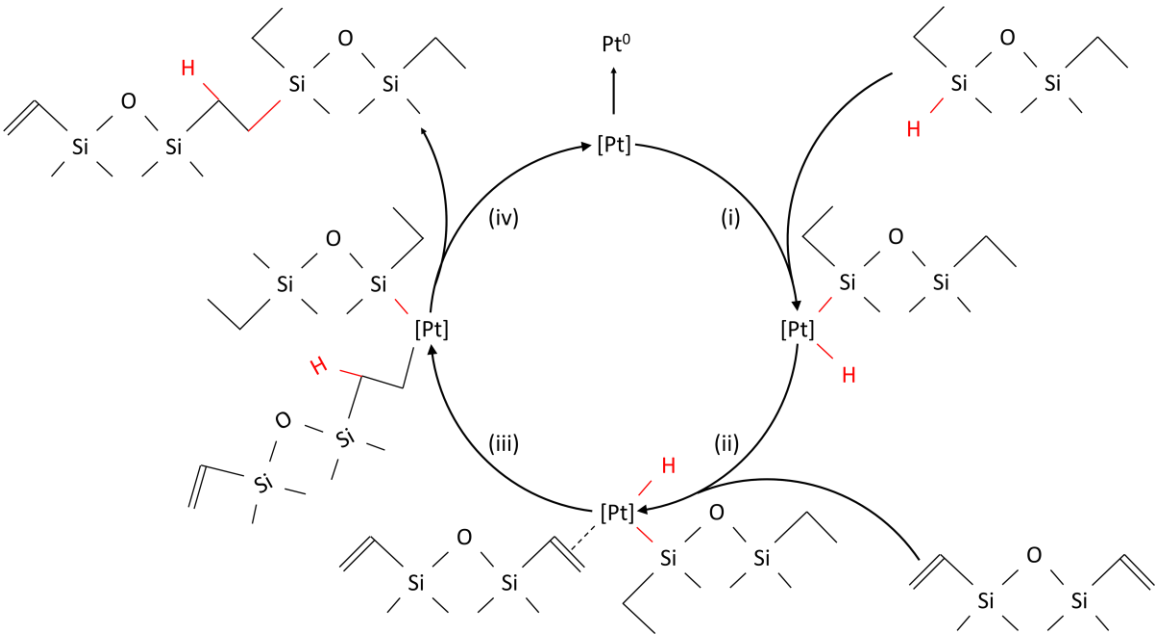

Figure 3-3 – Proposed Chalk-Harrod mechanism for platinum-catalyzed hydrosilylation of PDMS. (i) Oxidative addition of the hydrosilane into the Pt catalyst. (ii) Coordination of the olefin to the Pt catalyst. (iii) Migratory insertion of the olefin into the platinum-hydrogen bond (rate-limiting step). (iv) Reductive elimination of the alkylated silane. Eventually the Pt catalyst is reduced towards Pt^0 nanoparticles. Reprinted (adapted) with permission from ref. [82]. Copyright 2016, American Chemical Society.

The Dow Corning recommended ratio of PDMS elastomer base prepolymer to curing agent is 10:1 [83], which is the most utilized and characterized ratio in the field [5,8,14,17,54,56]. The concentration of curing agent changes the crosslinking density of the final material, and can be used to tune PDMS mechanical properties [84]. Compression testing performed by Wang *et al.* [84] showed that the elastic modulus of PDMS polymeric

networks increases linearly with the amount of curing agent, for the range from 2.9%$_{(w/w)}$ to 16.7%$_{(w/w)}$. However, higher concentrations of curing agent cause a decrease in the elastic modulus of the final material [85], due to the disruption of the polymeric network [84] and the formation of voids introduced by the unbalanced stoichiometry between the cross-linker and base polymer [84,85]. The use of PDMS materials fabricated with different curing agent ratios can be advantageous during some fabrication steps of microfluidic devices, namely the bonding step (Section 3.5.1 Layer bonding).

The curing of PDMS might be inhibited by the presence of some organometallic compounds, organotin catalysts, polysulfides, polysulfones, amines, urethanes, sulfur and amine-containing materials [83]. This becomes important during the selection of the fabrication method to rapid-prototype PDMS-based microfluidic devices (Section 3.6 Rapid-prototyping techniques), because these components might be present in the mold materials, such as 3D printer thermoplastic resins [86,87], inhibiting the cure of PDMS.

3.3.2 Degassing

Soft elastomers are molded against a master mold before curing and assume the shape of the master after curing which creates the channels necessary for fluidic transport [14]. To ensure reproducibility between devices fabricated with the same mold, it is essential that the mold design is transferred consistently to the elastomer. Inconsistent patterning can lead to increased surface roughness of the PDMS channels, which are detrimental for applications such as capillary electrophoresis [17]. The most common problem during patterning is trapping of air bubbles in the elastomeric matrix in proximity

to channels or other important features. These cavities can entrap sample, reagents and solvents, and can interfere with fluid transport, separations [17] and detection.

When PDMS is poured over a mold and cured using a conventional convection oven, the bubbles within the PDMS layer will rise to the top of the elastomer and disappear if the thickness of the elastomer film is < 5 mm. This is due to an increase of pressure inside the bubble (consequently reducing the density of the bubble) and the difference in densities of the materials (air, mold, and elastomer). This "pour and leave" method requires the least effort, but drawbacks include: *i)* some bubbles can remain on the final cured polymer; *ii)* due to the high viscosity of PDMS, there is not enough time for the air bubbles to escape the polymer matrix of thicker PDMS layers, which leads to trapped bubbles; and *iii)* for higher temperatures, curing of PDMS can occur prior to the elimination of entrapped air bubbles.

The most common method for degassing PDMS involves the use of a vacuum chamber [8,14,17,18,86] where the prepolymer-curing agent mixture is placed into a vacuum chamber and the differential pressure between the internal pressure of an air bubble and the pressure of the vacuum chamber make the bubbles coalesce, rise to the surface and escape the mixture. This method requires a vacuum chamber and a container at least 3 times larger than the volume of material being degassed, and its major disadvantage is the time required to complete the process (~ 30 min, depending on the amount of PDMS being degassed and the vacuum pump used). Depending on the size of the mold, it is also possible to pour the elastomer mixture on the mold and then place the mold inside the vacuum chamber, which can speed up the degassing process due to the potentially smaller path travelled by bubbles.

The fastest method to degas PDMS requires a centrifuge spinning at 3200 rpm, and can be completed in 2 min [88]. To overcome the need for a centrifuge, a low-cost alternative was presented by Soe and Nahavandi [89], where tightly capped centrifuge tubes containing the mixture to be degassed were attached to the stirrer attachment of an electric hand mixer, degassing the elastomer in 5 min. It should be stressed that the centrifuge tubes were balanced in the attachment to avoid accidents [88].

Other common strategies are the extraction of bubbles entrapped in deep features of the mold with a plastic probe and the removal of superficial bubbles with compressed air, from a distance, to avoid PDMS spillage [90].

3.3.3 Curing

At room temperature, the curing reaction of PDMS (Figure 3-3) requires 48 h [83], and is the simplest and lowest cost approach to cure the elastomer, at the cost of increased fabrication time. A heat cure in a conventional oven can decrease curing time to within hours, and is the most common approach [14,17,91,92]. This method only requires a laboratory oven or a hot plate. Higher temperatures (above 100 ^{o}C) promote faster curing of PDMS and are often used in conjunction with conventional SU-8 molds, without having an adverse effect on the master mold or on the PDMS channels.

When alternative mold fabrication methods are used, thermal limitations of the mold can limit curing temperatures. For example, when wax printing is used as the patterning method for the mold, high temperatures negatively impact the integrity of

positive relief features of the mold. Therefore, mild temperatures are best suited for curing PDMS on wax molds in a conventional oven, which results in longer processing periods (3 h at 60 ^{o}C) [17].

The use of microwave radiation is an alternative to PDMS thermal curing [8,20]. Microwave processing can enhance the curing rates of thermosetting polymers [93], improving turn-around times for fabrication of PDMS-based microdevices [8]. This enhancement is due to the intrinsic properties of microwave processing, in which the energy of the microwave electromagnetic radiation is converted into heat throughout the volume of the material in microwave active materials [8,93]. This mode of heating is unlike transfer via thermal gradients utilized in purely convection-based thermal processes. For a complete discussion on the topic, we refer the reader to reference [8].

When there are no restrictions imposed by the patterning method, with regard to the temperature stability of the mold, microwave processing of PDMS gives rise to the fastest curing method, as demonstrated by Speller and coworkers [9]. Using xurography of Kapton tape (stable to 700°C) to create the molds, these authors cured PDMS in a microwave in as little as 90 s, depending on the microwave-active substrate the Kapton tape was adhered to [9]. Aside from the speed, the use of a commercial microwave oven makes this low-cost processing method attractive for coupling to other inexpensive patterning tools [8,9,20]. However, there are some drawbacks regarding the use of microwave curing of PDMS, namely: *i)* this method is incompatible with conventional SU-8 molds patterned on Si wafers, due to cracking of the SU-8, and causes the silanization agent to bond irreversibly with the PDMS, which leads to destruction of the mold; *ii)* commercial microwave ovens have hot spots and cold zones, which can generate partially-

cured structures, or create thermal stress at the interface of the zones with different temperatures on the surface of the devices, and *iii)* due to the fast curing rate, there is not enough time to release thermal stress from the surface of the device, which can cause deformation at the top of the elastomeric device.

3.3.4 Low molecular weight oligomer extraction

After curing, low molecular weight oligomers (LMWO) and unreacted base prepolymer remain trapped in the PDMS polymer network [94,95]. The presence of these species is related to the degree of cross-linking in the polymer [95], and ultimately, with the ratio of prepolymer to curing agent. When the conventional 10:1 ratio is used, approximately $3\%_{(w/w)}$ of PDMS remains in the material as low molecular species [95], which can "leach" from the bulk [94–96]. While for some applications this phenomenon is desirable, such as the fabrication of thin film transistors [95], in microfluidics this oligomer chemical leaching can potentially interfere with the final application of the device [94,96]. LMWO in the PDMS bulk matrix are responsible for hydrophobic recovery of PDMS surfaces after plasma surface treatment [72], which can impact the fluidic transport in microfluidic channels [97], leading to the creation of bubbles due to de-wetting of the channel surface and the change of electroosmotic flow with time [94].

To address this issue, a solvent extraction of the oligomers from the PDMS bulk is usually performed [94–96] using the appropriate solvent system [70]. The use of this approach, however, presents 3 main problems, namely: *i)* long extraction periods are not compatible with rapid-prototyping turnaround times; *ii)* the use of batches of organic

solvents increases the waste generated, and is not compatible with the principles of green chemistry [98]; and *iii)* PDMS swelling upon contact with organic solvents is a well-known effect [70]. Although it is expected that channels return to their original dimensions after drying, to the best of our knowledge there has been no systematic study on the impact of solvent extraction on the final dimensions and surface roughness of PDMS channels, and we encourage research in this field. Swelling of PDMS is problematic at the microscale because microfluidic channels present high surface to volume ratios [2], and dimensional changes can be detrimental to some microfluidic applications [8,17].

Another strategy to minimize the impact of LMWO on hydrophobic recovery of plasma treated PDMS is the use of thermal aging [99]. This method is based on the extended curing of PDMS, which diminishes the amount of low molecular weight species within the polymer. However, like solvent extraction, the extended thermal aging treatment (up to 14 days) is not compatible with rapid-prototyping tools, evidencing an opportunity in the field. The use of microwave treatment accelerates PDMS curing [8,9], and it might be used to improve thermal aging of the bulk material in shortened times.

3.3.5 PDMS surface modification

A more definitive approach to render hydrophilicity to PDMS, and hinder non-specific adsorption of hydrophobic analytes on the polymer, is the use chemical surface modification [97]. As Zhou *et al.* presented in their review on the topic [97], there are mainly three approaches in which this modification can be performed, namely: gas-phase modification, wet chemical processing and a combination of both.

3.3.5.1 Gas-phase modification

The most utilized gas-phase process for PDMS modification is oxidation of the polymer using an O_2 RF plasma [14] to generate silanol groups on the surface of the PDMS [100]. This material processing procedure usually has 2 purposes: it is mostly used to bond PDMS to PDMS or PDMS to glass [14], completely sealing the microfluidic channel (Section 3.5.1.4 Irreversible bonding), but it also lowers the water-PDMS contact angle, from $\theta_{water\text{-}PDMS} = 110^o$ to 58^o [94], allowing for fluidic manipulation on chip. Although the PDMS surface recovers its hydrophobicity over time, this method can be completed within minutes [14], which is ideal for coupling with rapid-prototyping tools for exploratory studies. When used in conjunction with the LMWO extraction protocol, plasma oxidation of PDMS lowers the water-PDMS contact angle, from $\theta_{water\text{-}PDMS} = 105^o$ to 30^o [94], for longer periods [97].

Another common gas-phase approach to modify PDMS is the use of ultraviolet ozone (UVO) treatment [81,100], which also creates polar moieties on the elastomer's surface and lowers the water-PDMS contact angle, from $\theta_{water\text{-}PDMS} = 110^o$ to 55^o, after 30 min of exposure [81]. This treatment requires a processing time longer than the plasma surface treatment (over an order of magnitude) [81], but it is still complete within 30 minutes, compatible with rapid-prototyping ideals. The UVO treatment is also used to bond PDMS to glass (Section 3.5.1.4 Irreversible bonding) in the fabrication of hybrid PDMS-glass devices [101].

Chemical vapor deposition is another gas-phase strategy to modify the PDMS surface [97,102], but the need for specialized tools and reagents not commercially available

[102] limits its use with rapid-prototyping tools, because it increases fabrication costs and turnaround times substantially. Also, some coatings with metal oxides, such as TiO_2 [103], damage the PDMS surface, hindering microfluidic applications [97].

3.3.5.2 Wet chemical processing

A wet chemical approach to increase PDMS hydrophilicity is to oxidize the surface to create hydroxyl groups using oxidizing reagents such as an acidic peroxide solution [104]. Zhou *et al.* [97] reported that Slentz *et al.* [76] oxidized the PDMS surface by immersion in a 1 M solution of NaOH for 24 h. However, the authors of the review [97] misunderstood the described protocol [76], in which an oxygen plasma cleaner was used to oxidize the PDMS surface prior to further modification, instead of a wet chemical treatment with a strong base. The immersion of cured PDMS in a room temperature NaOH solution does not create silanol groups, although some studies [105] suggest the formation of alcohol groups on the PDMS surface due to the oxidation of the methyl groups of PDMS upon base treatment.

After creating silanol reactive groups on the surface of the material, sol-gel reactions can be performed to modify the PDMS surface in a more definitive way [76,77,97,104,106]. Sol-gel is the most common wet chemical processing to modify the PDMS surface, which can be performed *in situ* either in channels or on open PDMS surfaces [77,104]. The use of silane-based precursors such as tetraethoxysilane (TEOS) and 3-aminopropyltriethoxysilane (APTES) increase the wettability and electroosmotic flow of PDMS channels, retaining the material hydrophilicity for up to 200 days, hindering

its hydrophobic recovery [77]. The advantages of these modifiers include the use of aqueous solutions rather than strong organic solvents to perform the modification, which does not promote excessive PDMS swelling upon reaction [70], and is compatible with plasma exposure after modification [77], which enables bonding of the modified PDMS to either PDMS or glass to create sealed channels [14].

The modification presented by Beal *et al.* [77] does not modify the PDMS matrix itself, due to the lack of hydroxyl groups at the surface of native PDMS. These authors did not perform an oxidation step prior to the use of silane reagents. The sol-gel process requires hydroxyl groups to proceed, which will undergo a condensation reaction with the silane precursors to form the Si–O–Si bonds [107]. The most probable mechanisms by which the modification reported in [77] occurs are: *i)* via the hydroxyl groups of the surface-modified silica fillers added to PDMS [75], which can continuously react with other silane precursors to form silica [108]; or *ii)* via the grafting of silane precursors on the PDMS surface [77] and the subsequent condensation reactions between silanes to form silica [108].

Another approach for *in situ* wet chemistry PDMS modification is the use of dynamic coatings [97], analogous to common procedures performed in capillary electrophoresis [54]. The addition of modifiers into the running buffer or carrier fluid improves the wettability of the channels [97], which also diminishes the formation of bubbles, one of the most common issues in microfluidics [109]. The use of ionic surfactants [110] or ionic liquids [111] in the buffer also diminishes the unspecific adsorption of analytes on PDMS [97], another common issue when using this material to fabricate microchips. The hydrophobic moiety of amphiphilic molecules adsorbs onto PDMS

hydrophobic surface, while the hydrophilic moiety is exposed to the solvent [97,110,111], changing the surface properties of PDMS. When using this strategy, important considerations include *i)* the ionic strength of the medium; *ii)* how the modifiers affect the sample, the reagents and the other constituents of the buffer; *iii)* how the modifiers impact the detection method of choice, and *iv)* the critical micellar concentration (CMC) of the modifier, because concentration higher than the CMC can cause partitioning of the sample between the micelles and the buffer (which is desired in some applications, such as Micellar Electrokinetic Chromatography (MEKC) [111]).

The use of dynamic coating is the most compatible method with rapid-prototyping fabrication techniques, because it is performed during the testing phase, and it does not increase the fabrication time substantially.

3.3.5.3 Hybrid methods

Hybrid methods use a combination of gas-phase processes and wet chemistry to modify the surface of PDMS permanently [97]. First, the gas-phase modification is performed on native PDMS to oxidize its surface and generate silanol groups on it [100], either via an O_2 RF plasma [14] or a UVO exposure treatment [81,100]. After that, the oxidized PDMS surface can be treated with the appropriate silane [77,97,104], or it can be bonded to create sealed channels and then treated [77,104]. The use of hybrid methods is also compatible with rapid-prototyping microfabrication tools, because of the short times required to oxidize the PDMS surface using the gas-phase processes [14,81,100], in comparison with the wet chemistry oxidation method [104].

3.4 Practicalities in the design of microfluidic devices

For an in-depth discussion on the design of microfluidic devices, we refer the reader to excellent papers in the area [13,50,90,112,113]. In this tutorial review, we present some general practical aspects that should be considered during the design stage, which can impact the fabrication of devices using rapid-prototyping tools.

3.4.1 General considerations

While there are no universal formulas that yield perfectly functional microfluidic devices on the first try, there are strategies that can be employed to design microstructures more efficiently, minimizing the number of iterations required to attain a working microdevice. The first step involves the measurement of all equipment, tools and substrates available in the makerspace. These dimensions define the limits of the devices that can be fabricated within those facilities.

It is also necessary to consider the resolution and the minimum achievable features of the chosen fabrication method before designing the microfluidic device. Typically, fabricated features present an offset from the designed dimensions, and this difference depends on the fabrication method. Lithography methods achieve the highest resolution amongst rapid-prototyping tools, ranging from hundreds of nm to μm [75], and display smaller offsets, while other lower cost options, such as print-and-peel or scaffolding methods tend to achieve poorer resolutions, on the order of hundreds of μm [8,9,15,16,18,86], with offsets ~100 μm. These factors should be considered during the

design phase, especially if the fabrication tool presents a bias towards the patterning orientation (vertical vs. horizontal) [9]. Another geometric consideration when using PDMS to rapid-prototype microfluidic devices is that PDMS exhibits a shrinkage of ~1% after curing [2,75], and this difference should be accounted for during the design step. Some companies take this shrinkage into consideration when fabricating molds [114] and resize masks accordingly, so it is important to know if this is the case beforehand, or if the proper resizing should be performed by the researcher.

Multiple device positioning and orientation on a single substrate should also be considered for optimal usage of materials [90]. In a conventional soft-lithography mold, adding as many devices as possible on a single Si wafer is important due to the costs of materials, processing time and labor [14]. This requirement is not necessarily true for low-cost rapid prototyping tools when focusing on exploratory studies, but the incorporation of different modifications of the initial design on the same substrate can lead to better usage of resources and lower processing times between fabrication cycles (Figure 3-4).

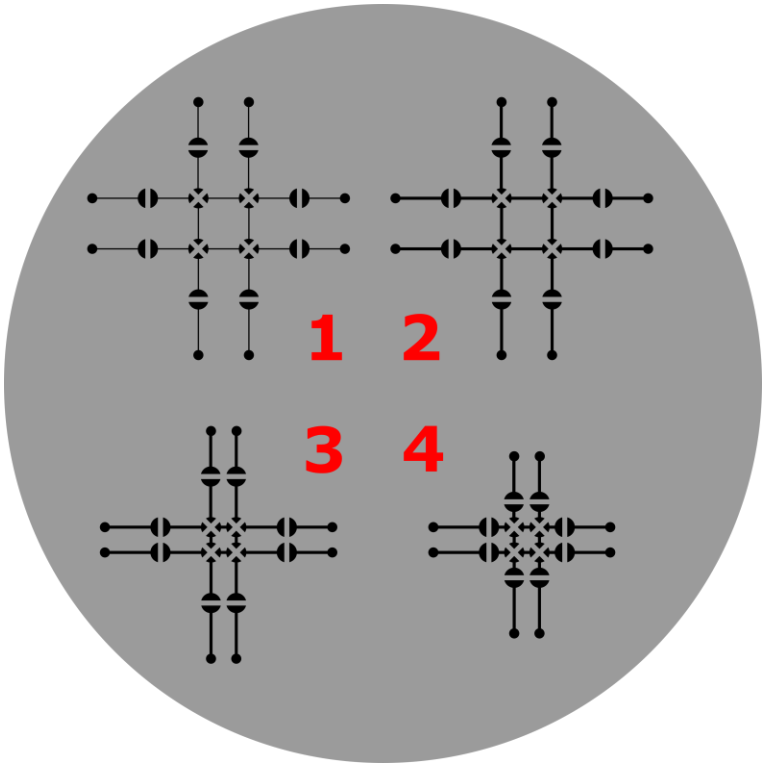

Figure 3-4 – Four iterations of an initial design for a 2x2 fluidic processor in the same fabrication cycle, improving material usage and decreasing fabrication costs.

3.4.2 Design software

The most used software to design microfluidic devices is Autodesk AutoCAD®, with the most support online [90]. Other alternative software that also can be used to design devices are CorelDraw®, or the freeware Inkscape [115]. However, it should be mentioned that some of these software present compatibility issues with some of the patterning tools (e.g. Inkscape incompatibility with vector data required by the ULS laser cutter interface). Therefore the ability to prototype devices should be tested before a major project takes place, using a simple testing model.

The power of design software relies on the fact that layers can (and should) be used when designing microfluidic devices. The first layer of the project is often a geometric shape with the dimensions of the substrate that will contain the device [90,114], providing the boundary to the design. A second layer of the project often contains major construction lines for the most critical features in the design, which will be hidden during the fabrication step. This is valuable for subsequent iterations of the design, saving time when making minor modifications (*i.e.* change in dimensions or positioning of few features), reducing duplication of effort. Another advantage of the use of layers within a project is particularly realized in the design of multilayer microdevices, in which alignment of features across layers plays a major role in device function. A practical tip when designing microfluidic devices is to check for repeated lines on the design [116], because they will result in multiple replications of the same feature, which may impact the final dimensions of the mold and subsequently device performance. Another practical tip, when designing multi-height masks, is to keep masks in different layers of the same project, using a different color scheme for each layer [90], which facilitates the design process by aligning critical features. For the fabrication of the masks, layers can be selected to include only desired features.

3.4.3 Device features

When designing microdevices to be fabricated by replica molding using PDMS, mechanical properties of the elastomer can place limitations on device feature sizes [75,90]. When the aspect ratio of features (height / width) becomes larger than 10:1, the

walls may adhere to each other across the narrow gap before or during bonding, deforming the structure (Figure 3-5a) [75,90]. This can be prevented by washing the features with an ionic surfactant (such as SDS), followed by a rinse with heptane [75]. For enclosed channels, the aspect ratio (defined as height of channel / distance between walls) cannot be smaller than 1:10, or the channel can collapse on itself due to the lack of structural support (Figure 3-5b) [75,90].

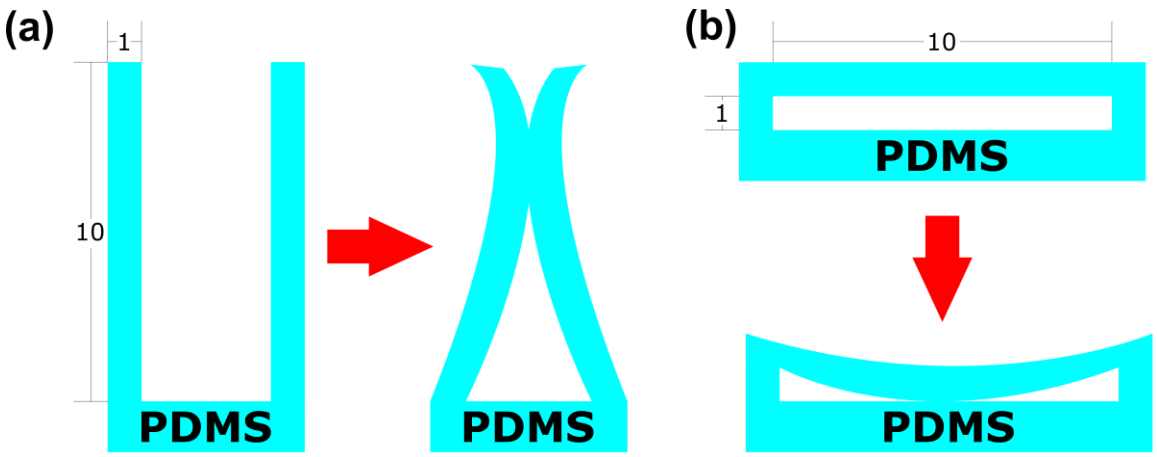

Figure 3-5 – Geometric considerations during the design phase of microfluidic devices fabrication. (a) Depiction of walls adhering to each other when features are fabricated with aspect ratio 10:1 or larger. (b) Depiction of channel collapse when features are fabricated with aspect ratio 1:10 or smaller.

3.4.4 Multi-height molds

Depending on the fabrication method of choice (Section 3.6 Rapid-prototyping techniques), multi-height molds might require the design of multiple masks [54] which result in features with different heights. The presence of alignment marks becomes imperative in such masks [90,114] to enable the correct positioning of features on the master mold. Stanford University's Shared Scientific [114] Facilities provides template

alignment marks, and AutoCAD® template files for chip design. It is important to stress that the aspect ratio limitations of the final PDMS fluidic channels [75,90] should be considered when designing multi-height molds, not only the height of individual layers.

3.4.5 Bonding and multi-layered devices

Passive PDMS microfluidic devices (herein defined as microfluidic devices comprised of only channels and reservoirs, operated using external equipment, such as syringe pumps) usually can be cured on a master mold, and then simply placed on another surface and are ready to use, depending on the application [17].

More complex devices with active components (*e.g.* active microfluidic valving [80]) require the combination of multiple layers of elastomer [117]. Integration between layers is critical for device function. For example, pneumatic [117] or hydraulic [118] actuation lines strategically placed over regions in the fluidic layer enables transfer of fluids when sequentially actuated [119]. However, the inadvertent crossing of actuation and fluidic lines can interfere with fluidic transfer in the device [114]. Modification of features of the actuation channel at the junction, particularly channel dimensions, can avoid the formation of improper valves [114] (Figure 3-6c).

Additionally important for device function is how the microchip connects to the external world. Depending on the external testing apparatus, access to the chip can be from both sides of the chip, or from a single side. When both sides of the chip can be accessed, there is more flexibility in the design of the microchip, because no via holes through layers

are required, simplifying connectivity (Figure 3-6a). When only one side can be accessed, the actuation channels (or the fluidic channels, depending on the testbed) must be reconfigured (*e.g.* from Figure 3-6a to Figure 3-6b), based on locations of inlets, outlets and channels of the subsequent layer.

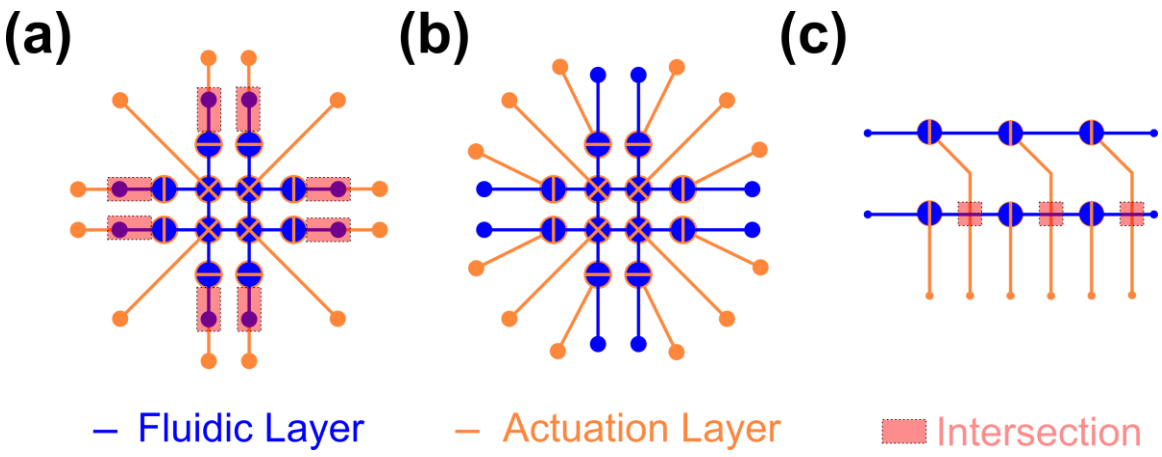

Figure 3-6 – Chip connectivity configurations. (a) In this design of a 2x2 microfluidic processor, there is some overlap between the fluidic and the actuation layer (marked by dotted pink boxes), but if access to the external world can be achieved from both sides of the microchip, there is no need to punch holes through layers. (b) A redesign of the microchip depicted in (a), removing overlap between layers by redesigning the actuation lines. (c) The inadvertent creation of valves (marked by dotted pink boxes) due to intersections of features on different layers.

It is also important to consider the fabrication method which will be employed during the design step of the development of a microfluidic device. Lithographic tools and print-and-peel methods generate microfluidic channels that are mirror images of the molds, while scaffolding tools generate channels with the same absolute configuration of the mold. Furthermore, more than one method can be used, and the assembling orientation of different layers should be also considered.

3.5 Device fabrication

After curing, the patterned PDMS is often assembled into a device prior to use. The patterned surface can be brought into contact with a flat surface, such as glass [17], to form a reversibly-sealed PDMS device [8], due to the van der Waals interactions between surfaces upon contact [54,120]. For applications that do not require high flow rates nor high internal pressures within channels (< 35 kPa [120]), this approach is adequate and requires the least number of steps [8]. The difference in pressure required to move fluids through the channels in these systems is usually generated by the application of a vacuum to the outlet [121], rather than pushing fluids through via the inlet (*e.g.* using a syringe pump). For a more detailed discussion on reversible sealing methods, we refer the readers to the reviews from Anwar *et al.* [121] and Temiz *et al.* [122].

3.5.1 Layer bonding

For applications that require higher pressures (> 200 kPa [120]), reversible bonding between PDMS and a rigid surface is not strong enough to sustain chip integrity, hence delamination of devices is common. In these cases, more robust bonding methods are recommended [8], such as adhesive bonding [123], sandwich bonding (SWB) [124], or the irreversible bonding of PDMS to the substrate via PDMS surface modification [14,81].

3.5.1.1 General considerations

A functional microfluidic device must store and transport fluid, typically through channels, without leaking. Both surfaces to be bonded must be flat and clean (both the

patterned PDMS surface and the backing substrate) to enable conformal contact of PDMS to the substrate surface. Regardless of the bonding method of choice, the substrates to be bonded must be clear of dust, glass particles, and organics [54], which can hinder contact between surfaces, resulting in trapped air at the interface and/or delamination under operation pressures or during manipulation.

To clean glass substrates to create hybrid PDMS-glass devices, a common strategy is to use a piranha solution (3:1 mixture of H_2SO_4 : H_2O_2 – caution, extremely oxidizing!) to remove all organic residues from the glass surface [54]. As recommended by Landers *et al.* [54], the use of ammonia-based window cleaner can accomplish this task more easily and more safely. We use window cleaner and lint-free wipes to clean our glass substrates, followed by a heating step in an oven to aid ammonia evaporation, increasing our chip bonding success rate.

To clean PDMS substrates, wiping the PDMS surface with lint-free wipes and water followed by either ethanol [54] or isopropanol rinses provide good results. If deeper cleaning is required, a sonication step may improve results, although care must be taken due to PDMS swelling in organic solvents [70]. Complete drying prior to bonding is imperative, as residual moisture may compromise this step. Additionally, holes, reservoirs and features in the device can trap liquid and thus require extra attention. After rinsing the surfaces, a blow dry with compressed nitrogen might be performed to remove any remaining solvent from the clean surface. Drying with a compressed air system is not usually recommended, as these systems often contain contaminants such as oil, which hinders PDMS bonding. Placing the devices into an oven or on a hot plate may additionally aid in solvent removal [90].

Another common tip in forums such as Research Gate [125] is to use Scotch® tape to remove large dust particles attached to the PDMS or glass surfaces. The quality of the tape used for this purpose is important: low-quality adhesive tapes tend to transfer adhesive to the PDMS surface, impacting final bonding. The tape can also be used to aid device storage for short periods of time, protecting clean surfaces from dust and other particulate deposition.

3.5.1.2 Adhesive bonding

For PDMS-based devices, the adhesive bonding technique can generate chips that can withstand pressures in the order of 200 kPa [123]. This technique uses partially-cured PDMS as the glue between the patterned fully-cured PDMS and the flat substrate [123,124]. A flat stamping substrate is prepared beforehand by spin coating freshly mixed PDMS onto it (Figure 3-7a). The fully-cured patterned PDMS is then placed on top of the spun PDMS (Figure 3-7b), and after uncured PDMS is transferred to its surface (Figure 3-7c), the patterned PDMS coated with uncured PDMS is placed on top of a clean flat substrate (Figure 3-7d). The uncured PDMS is cured to form the seal (Figure 3-7e) [123].

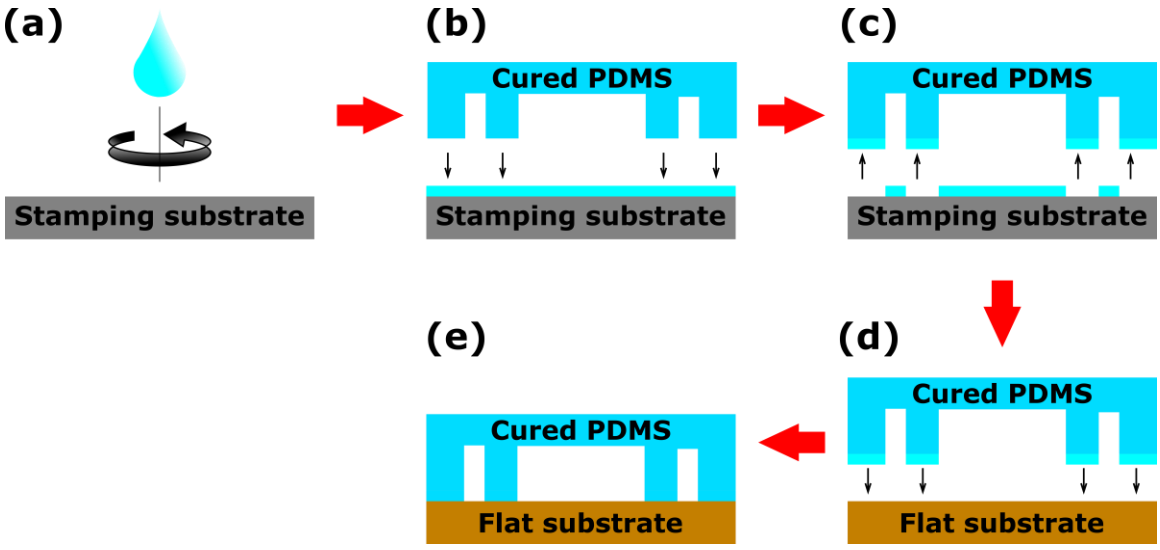

Figure 3-7 – Adhesive bonding method. (a) A clean flat substrate is spin-coated with fresh PDMS. (b) A fully-cured patterned PDMS piece is placed on top of the fresh PDMS. (c) Fresh PDMS is transferred from the flat surface to the patterns in the patterned PDMS that is in contact with the substrate. (d) The patterned PDMS containing the uncured PDMS is placed on top of a clean flat substrate, and (e) the uncured PDMS is cured, forming the adhesive bonding between the patterned PDMS and the flat substrate.

Deceptively simple at first glance, this method can trap uncured PDMS into channels, clogging them and rendering the device unusable [124]. This method requires a spin-coater to generate the PDMS thin film, which may not be readily available. The extra PDMS curing step must be performed at lower temperatures to avoid channel deformation [124] (20 min at 120 ^{o}C) [123], and this method does not permit realignment after initial contact due to PDMS transfer.

3.5.1.3 Sandwich bonding (SWB)

The Sandwich bonding (SWB) method relies on mechanically enclosing the patterned PDMS and the flat surface with a surrounding excess of PDMS [124]. This strategy allowed the researchers to obtain hybrid PDMS-glass microchips capable of withstanding burst pressures in the order of 1.0 ± 0.1 MPa [124]. Technically speaking, this method is not an irreversible bonding technique, because the glass-PDMS interface is composed of van der Waals interactions [54,120], instead of chemically bonded. The sandwich bonding process is depicted in Figure 3-8.

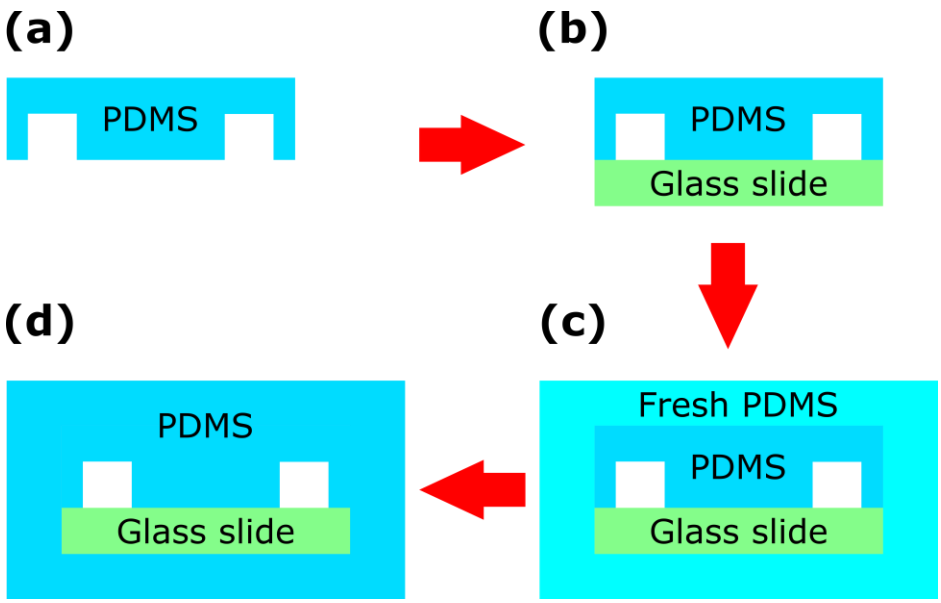

Figure 3-8 – Sandwich bonding method. (a) A patterned PDMS device is (b) reversibly bonded to a flat surface. (c) Fresh PDMS is cast around the whole structure, sandwiching the patterned PDMS and the flat surface. (d) After curing, the patterned PDMS and the flat surface are enclosed in PDMS.

This technique does not require additional instrumentation, which makes it a low-cost option to conventional irreversible bonding techniques [14,81], but does have the drawback of reduced burst pressures. The biggest advantage of the SWB method is the self-regeneration ability of microchips fabricated with this method: after a leakage is noticed, fluids are pumped out of the chips, and the device is baked again at 120 ^{o}C in an oven, allowing for *i)* the removal of the fluid from the PDMS-glass interface [124] and *ii)* a second thermal treatment that strengthens the bonding [123] and reseals the channel. Another advantage of this method is the "forgiveness" during chip alignment, *i.e.* it is amenable to repositioning of the features after unsuccessful alignment attempts. The extra PDMS curing step adds 40 min to fabrication, increasing fabrication time.

Although not tested, this method seems to be compatible with microwave curing [8,9], which might further reduce overall fabrication times. Another feature not tested, but with potential is the use of PDMS as the base substrate, creating a PDMS-only microfluidic device, in analogy to scaffolding techniques [19].

3.5.1.4 Irreversible bonding

The modification of a PDMS surface to bond it to another PDMS surface or to a glass slide was reported in the first publication regarding the rapid-prototyping of microfluidic devices using soft-lithography [14]. As a result, irreversible bonding is one of the most ubiquitous device fabrication methods [54]. The fundamentals of the surface modification of PDMS were described in detail in Section 3.3.5 PDMS surface modification.

The biggest advantage of these methods is the amount of information readily available in literature, both theoretical and technical [14,54,81,126]. Another advantage realized by these method is fast bonding times, when using gas phase methods to modify the PDMS surface, such as O_2 RF plasma [14] or ultraviolet ozone (UVO) treatment [81,100], although extra thermal annealing post-processing [120] might increase turn-around times for devices. The alternative to this extra thermal step is to use a microwave-assisted thermal treatment [8], instead of the conventional oven thermal treatment, which can be performed at a fraction of the time, or else using no thermal annealing method at all. The gas-phase processing of PDMS surface in conjunction with microwave-assisted thermal treatment to bond microfluidic devices is the most compatible method with rapid-prototyping ideals.

The disadvantages of this method include the need for a plasma cleaner [14] or UVO cleaner [81,100], and the size limitation of devices, dictated by the size of the equipment available [19]. Another disadvantage of this method is the short time available to perform the bonding step before the PDMS surface recovers its hydrophobicity [124], requiring some skill from the operator, and also little room for misalignment errors, due to irreversible bonding of layers upon contact [127]. Some authors recommend the use of a lubricant between layers, either DI water or methanol [128,129], to increase the working time and allow for realignment during bonding. However, our group experiences bonding issues when the relative humidity of the air is elevated, so we recommend the use of methanol, if needed.

Another irreversible bonding technique was developed by the Quake group in 2002 [130], called the off-ratio bonding method [54]. In this method, individual PDMS layers

are fabricated with different prepolymer to curing agent ratio (e.g. Layer A 5:1 ratio, Layer B 20:1 ratio) and are pre-baked. Then, these layers are put into contact and are submitted to a second thermal treatment to bond the layers together. The proposed mechanism behind this method is the diffusion of curing agent and prepolymer across the interface, leading to curing the polymer at the interface during the thermal processing, thus sealing the device [54].

A drawback to the off-ratio method is the different mechanical and optical properties of the individual layers [19,127], where an ideal method would use the same ratio for all individual layers. Lai *et al.* [127] demonstrated that partially cured elastomeric layers prepared using the 10:1 ratio of PDMS elastomer base prepolymer to curing agent can be bonded together and withstand standard microfluidic operation pressures (138 kPa to 310 kPa).

Although the off-ratio method to bond layers requires an extra thermal processing step, it is compatible with rapid-prototyping patterning techniques, especially scaffolding methods [19,131,132], discussed in details in Section 3.6.6 Scaffolding techniques. This happens because if PDMS is used as the backing substrate in the scaffolding method (*e.g.* in a 5:1 ratio), the PDMS being poured over the scaffold should be mixed with a different ratio (*e.g.* 20:1), enabling bonding between the different layers. This combination of patterning method (scaffolding) and bonding method (off-ratio method) exhibit the advantage of not limiting the blueprint of the chip by the size of equipment available in the laboratory, other than the oven.

3.5.2 Interfacing: how to plug-and-play a lab-on-a-chip

As presented by Temiz *et al.* [122] in their excellent review on the topic, one of the biggest challenges in the microfluidics field is still the interface between microdevices and the outer world. These challenges are often neglected during the first design iterations of devices, but become apparent during the testing phase. Therefore, there are significant benefits to considering the challenge of interfacing early in the design process.

3.5.2.1 Reservoir fabrication

For PDMS-based microfluidics, the first interfacing challenge arises from the creation of the fluidic reservoirs or fluidic connections. The most common approach is to punch holes of the desired size in the cured PDMS using a biopsy punch [8,90,110]. When punching the reservoirs, it is important to keep the cutter perpendicular to the surface of the PDMS [90], so fluidic connections can be made properly. The cut should be performed from the patterned side [90], which avoids problems with parallax misalignment. The punch goes through the PDMS in a continuous straight motion, and the punch should not be twisted in a corkscrew motion, to preserve the edges of the hole [133] (Figure 3-9a and b). The punch must be sharp, otherwise holes will not be cut, but ripped instead [133]. A practical tip to prolong the sharpness of the tool is to place a sacrificial piece of PDMS under the active piece during cutting. A practical tip to align holes is to use a needle to center the tool on the desired region.

When a clean cut is not obtained, small pieces of PDMS can be generated and fall into fluidic channels, clogging them and rendering the device inoperable. Another problem with ripped edges of reservoirs is that fluidic connections will be compromised due to imperfect sealing between the PDMS and the connector [122], resulting in leakage. For these reasons, it is preferable to punch reservoirs prior to bonding whenever possible.

Depending on the rapid-prototyping method of choice, sometimes it is not possible to punch the holes prior to bonding (e.g. Scaffolding techniques, Section 3.6.6), requiring additional care during this step. Also, the thickness of the membrane being punched should be measured prior to the cut, to avoid damaging the underlying layer.

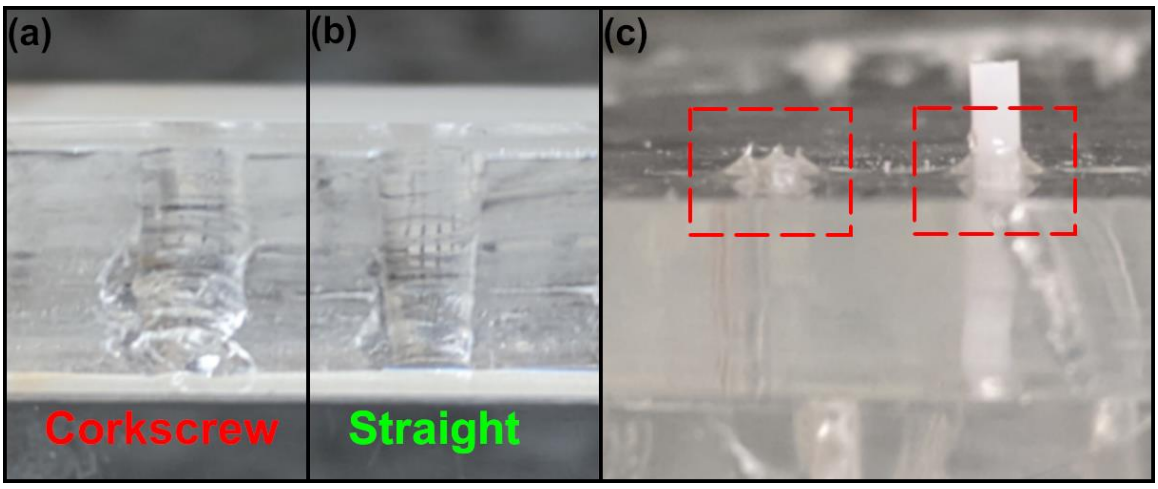

Figure 3-9 – Reservoir fabrication. Cross-section of reservoirs fabricated using a 3-mm biopsy punch, in a (a) corkscrew motion, and (b) in a straight motion. (c) Reservoirs fabricated by casting PDMS around a pole (white piece in the picture). Mounds generated by PDMS shrinkage around the poles are marked with red dotted boxes.

Another alternative to create reservoirs is to place posts on top of the features of the mold, and cure the PDMS around these posts [14]. A practical tip is to use a dab of white glue to place the posts on the mold [19], as this material is compatible with PDMS and is water soluble, with the caveat that excess glue will change the shape of the reservoir. Also, the glue must be fully-cured prior to PDMS thermal curing, otherwise water present in the glue will generate bubbles around the posts during the cure. The use of posts to create fluidic connections avoids the issues of punching holes in PDMS, but its characteristics might not be compatible with some testing systems. When PDMS is cured around a pole, the shrinkage of PDMS [75] leaves a meniscus around the pole (Figure 3-9c), instead of the flat surface obtained by punching the holes (Figure 3-9b), distorting surface flatness. The pole method is more compatible with scaffolding rapid-prototyping techniques [19,131], because it does not require a hole punching step.

3.5.2.2 Connections

With input / output reservoirs present in the device, the microfluidic chip can be connected with peripheral equipment, including pumps, tubing and detectors [122]. Often neglected, connections are most likely to cause leakage in an integrated microfluidic system [122].

The simplest connections are enabled by the insertion of tubing into the PDMS chip [122]. If the size of the reservoir is slightly smaller than the outer diameter of the tubing, the compression of the PDMS around the tubing is enough to seal the connection, and acts as a gasket [122] for pressures below 300 kPa [133], which is within the pressures required

for many microfluidic applications [120]. The biggest advantage of this method is that insertion connections do not require adhesives and are reversible [133], meaning that they are very compatible with rapid-prototyping tools and disposable devices [122], as long as the PDMS is not torn during the removal / insertion of the connection and that the integrity of the device bonding step was strong. Connectors can be made from stainless steel tubes [134] or glass capillary tubes [122], although connections made from trimmed pipet tips are not uncommon [8]. The latter approach is useful for rapid tests, because the pipet tip can be cut until a firm connection can be achieved between the PDMS and the pipette tip. The use of individual interconnectors is straightforward, but they suffer from drawbacks including: *i)* the mechanical stress applied to the flexed PDMS at the connection [133] can be enough to delaminate the device and / or crack the PDMS, causing leaks; *ii)* lack of control regarding the amount of tubing inserted in the chip, which may cause entrapment of bubbles and fluids at the connection, increasing dead volumes in the device and permitting cross-contamination [122], blocking the passage of fluids, or change the operating pressure of the device; *iii)* perforation of PDMS membranes, which may cause pieces of PDMS to fall into the channel or into the tubing, creating blockages, and *iv)* as the chip design increases in complexity, the connections become more densely populated [122,133], which may result in structural integrity problems in the device. Reversible connectors are preferred during the development phase of microfluidic devices, due to the need to test several iterations of a design [133], which is the most compatible approach for use in conjunction with rapid-prototyping tools.

An improvement in reversible connectors was achieved by Atencia *et al.* [135], using magnets around the tubing and gaskets, mounted on above and below the

microfluidic device. The advantage of this method is the repeatability provided by the magnets. With PDMS chips, however, special care must be taken, as the force applied by magnets is dependent on the distance between them [135], which may cause channel collapse, and rapid-prototyped structures may vary in size. Also, this method is not feasible for complex geometries [122], because of the bulky size of magnetic connectors.

For more permanent connections, adhesives can be used to improve connection, such as the use of epoxy adhesives around PDMS devices [136], although this encapsulation technique is more closely related to fixed mounts [122] than to adhesives sticking on PDMS. The drawback to fixed-mount connectors is that the design of the microfluidic device becomes limited by the testbed, while it is often desirable to make modifications to the design of a microfluidic device independent of the testing system. Improvements in versatility of fixed-mount connectors remains an unresolved challenge in rapid iterative microfluidic testing.

The lack of uniformity of connections for microfluidic devices is another shortage in the area [122]. The standard for microfluidics is the use of Luer Locks, which may not be compatible with fabrication methods available [122], given the number of new techniques developed every year. Some groups have attempted to standardize fluidic connectors [137], inspired by connectors from the microelectronic industry, such as USB ports [122], although this alternative may be more appropriate for either fixed testbeds or for final products.

3.5.2.3 Chip reusability

Rapid-prototyped PDMS-based microfluidic devices are intended to test device designs, fabricate proof-of-concept devices and, ultimately, to discard bad ideas faster. These rapid-prototyped devices are not intended to be used continuously nor stored for long periods, and likely should not be due to the inherent polymer characteristics of PDMS as it ages [99]. The adsorption of analytes on PDMS [97] and the hydrophobic recovery of the PDMS surface [94–96] are the most common issues regarding extended PDMS usage. One of the issues arising from hydrophobic recovery is the presence of bubbles in microfluidic channels, due to the solution de-wetting of the channel surface [94], and in some extreme cases, the impossibility of flowing solution through the hydrophobic channels, for channels with low aspect ratios and high fluidic resistance.

When a PDMS device must be reused after a long period of inactivity, and the polymer has neither been treated to extract low-molecular weight oligomers [94–96], nor has its surface been modified permanently [76], there is an alternative to render the channels surface hydrophilic again. Flushing channels with an oxidizing acidic peroxide solution [104] will create hydroxyl groups at the surface of the channel (Section 3.3.5.2 Wet chemical processing), which will render the device hydrophilic and it will allow for the passage of fluids. It is relevant to stress that this approach is only useful for structures without active valving components, as the creation of hydroxyl groups on two different surfaces in contact will inevitably result in bonding these surfaces by condensation reactions. This approach also might change the surface roughness of the channels, which might impact the performance of the device.

An easier approach to reuse a stored PDMS-based microfluidic device is the use of surfactants, described in Section 3.3.5.2 Wet chemical processing. However, this approach is only useful if the surfactant was used during the first use of the device, otherwise results will not be comparable.

3.6 Rapid-prototyping techniques

As van Dam stated in his excellent PhD thesis [2], one of the reasons PDMS achieved tremendous research interest is due to its ability to tinker with, once the mold is available, because no specialized facilities are required to work with this elastomer. But the fabrication of molds by conventional methods [14] requires resource-intensive cleanroom facilities [8], imposing a limitation for the development of microfluidic technology. Several alternative methods have been created over the years to rapid-prototype PDMS-based microfluidic devices without the need for cleanrooms or skilled personnel, which we discuss here. Table 3-1 presents a summary of rapid-prototyping techniques for PDMS-based microfluidics.

Table 3-1 – Rapid-prototyping techniques for the rapid fabrication of PDMS-based microfluidic devices

Class	Method	Description	Channel Specs.	Degree of Difficulty	Fabrication Time	Advantages	Disadvantages	Cost	Reusability	Ref
Lithography	Soft-Lithography (Gold standard)	Designs are printed on transparency films with high-resolution printers. Conventional photoresist (*e.g.* SU-8) is spun on Si wafer, soft-baked, exposed to high-energy radiation under the mask. Photoresist is revealed with solvent, hard-baked and the mold is silanized.	Minimal channel resolution: 20 µm; Channel height: 1 to 200 µm	High	24 h	High fidelity; High resolution; Multiple casts on the same mold.	Requires a cleanroom for high-resolution molds; Requires high-skilled personnel; Reduced turnaround times	High	Indefinitely	[14]
	PCB lithography	PCB master molds are fabricated by exposing a photomask on top of the board followed by chemical wet etching	Mold width: ~100 µm; Mold height: 16 µm	Medium	3 h	Does not require deposition of photoresist on PCB; Low-cost of molds. Low initial investment	Low quality of PDMS channels due to poor resolution of molds	Low	Indefinitely	[138]

Table 3-1 continued

	Low-cost contact PVAc lithography	PCB master molds are coated with PVAc emulsion, exposed to UV radiation and revealed with water, followed by a second radiation exposure	Minimum channel width: 30 µm; Height: 30 to 140 µm	Low	1.5 h	High resolution; Simplicity; Low-cost of molds. Low initial investment	Multiple exposure steps; Use of hazardous diazo photoinitiators	$0.05 per mold	Indefinitely	[139]
	Direct lithography	Direct UV irradiation of cured PDMS, followed by a wet etching	Minimum width: 2 to 5 µm; Heights: 3 to 10 µm	Low	13 h	Simplicity; Few processing steps	Long processing times; Caustic waste generation; Low aspect ratios	Low	No	[140]
Print-and-Peel	Laser printing	Deposition of toner particles on a flexible substrate to form the mold	Minimal line resolution: 70 µm; Minimal separation distance: 400 µm; Channel height: 10 µm.	Low	1.5 h	Simplicity. Low-cost of molds. Low initial investment	Relatively large separation between channels; High fluidic resistance.	$0.01 per mold (75 mm by 25 mm).	Up to 5 times	[15,16]
	Shrinky-Dinks	Molds are laser printed on a thermoplastic sheet, and shrunk using a thermal processing	Minimum width: 65 µm; Height: 50 µm	Low	22 min	Simplicity. Low-cost of molds. Low initial investment	2 thermal treatment steps	Low	Up to 5 times	[141]

Table 3-1 continued

	Wax printing	Deposition of wax on a flexible substrate to form the mold; Thermal reflow of the wax to smooth patterns. PDMS pouring and curing. Channels cleaning and bonding.	Minimal line resolution: 160 µm -before reflowing, 350 µm -after reflowing; Minimal separation distance: 300 µm; Channel height: 13 µm.	Low	1 hour (microwave processing); 3 hours (conventional curing).	Simplicity; Fast turnaround times when coupled with microwave processing; Low-cost of molds.	Multiple steps; Low channel resolution. High fluidic resistance.	$0.01 per mold (75 mm by 25 mm).	No	[8,17]
	Xurography	Tape is adhered to a backing substrate and cut using a cutter plotter. Tape excess is removed from the mold.	Minimum width: 32 µm; Heights: Variable (substrate-dependent)	Low	5 min	Simplicity; Low-cost of molds; Low initial investment	Difficulty in removing small cut features from the mold; Lack of scalability	Low	Indefinitely	[9,18]
	Razor writing	PDMS is spun on top of an adhesive layer and cured. PDMS thin film is cut using a cutter plotter, small features are removed from the substrate, and a flat PDMS slab is bonded to this structure	Minimum width: 100 µm; Height: N/A;	High	3 h	Minimal material usage (PDMS only)	Requires a spin coater; 3 thermal processing steps	Low	No	[142]

Table 3-1 continued

	3D printing	Mold is printed in a thermoplastic resin in 3 dimensions	Minimum width: 250 µm; Height: 500 µm	Medium	2 h	Simplicity	Requires a 3D printer (high initial investment); Different resolutions in each axis (x,y,z)	Medium	Indefinitely	[86]
Scaffolding	Template embedding	Nylon threads are embedded in PDMS. After curing, the Nylon threads are removed from the matrix by immersion in organic solvents and tension at the end of the thread	Width: 50 to 250 µm; Height: N/A;	Low	N/A	Simplicity; Low-cost of molds; Low initial investment	Organic solvent waste generation, limited designs	Low	No	[143]
	3D printing (ABS)	Scaffold is 3D-printed in ABS resin	Width: 90 to 500 µm; Height: N/A;	Medium	12 h	Incorporation of functionalities	Organic solvent waste generation, Increased surface roughness; Requires a 3D printer	Medium	No	[132]
	3D printing (Wax)	Scaffold is 3D-printed in wax	Width: 250 µm; Height: N/A;	Medium	48 h	Substrate availability	Requires a custom 3D printer, Organic solvent waste generation	Medium	No	[144]

Table 3-1 continued

	3D printing (PVA)	Scaffold is 3D-printed in PVA	Width: 59 µm; Height: 298 µm;	Medium	4 h	Water-solubility of molds;	Special handling of PVA filaments; Long times for channel cleaning	Medium	No	[131]
	Liquid molding	Selective hydrophilization of PDMS, followed by water application	Width: 100 to 1000 µm; Height: 40 µm;	Low	2 h	Simplicity; No waste generation	Cannot generate multi-height molds; Long thermal processing	Low	No	[145]
Hybrid	GLUE	Molds are fabricated using water-soluble white glue. Can be used either as a print-and-peel or a scaffolding method	Width: 200 µm; Height: 10 to 60 µm;	Low	1 h	Simplicity; Water-solubility of molds; Do not require a bonding step (scaffolding); Low-cost;	Low-resolution of molds	Low	Up to 3 times	[19]

3.6.1 Soft-lithography

Given the importance of what is considered the first rapid-prototyping tool (and gold standard) for the fabrication of PDMS-based microfluidic devices, we start this section briefly reviewing and discussing the conventional soft-lithography process [14] to give the readership a reference point for comparison with other tools, in terms of cost, turnaround times and method resolution.

In 1996, Xia *et al.* [146] used PDMS to replicate the patterns of micrometer structures fabricated using photolithography, such as diffraction gratings, which would be used as the elastomeric master for replica molding using other polymers, such as polyurethane. Based on this work, Delamarche *et al.* [147] built what might be considered the first PDMS-based microfluidic device in 1997, casting the elastomer on a commercially obtained master mold in silicon. In 1998, Duffy *et al.* [14] took another step in the development of microfluidic devices, and used photolithographic techniques developed by the Whitesides Group at Harvard University [148] to rapid-prototype master molds for PDMS-based microfluidic devices.

The mask fabrication process developed by the Whitesides group [14,148] uses a commercial printer that prints patterns on a transparency film. This low-cost patterned film is used as the contact photolithography mask [14,148], which is placed on top of a silicon surface coated with photoresist and exposed to radiation. After exposure, the photoresist is developed with the proper solvent system, and the photoresist goes through a second thermal treatment. The mold is then silanized by exposure with the silanizing agent

(Trichloro(1H,1H,2H,2H-perfluorooctyl)silane), which aids the PDMS stamp removal from the mold [90]. The mold fabrication process is depicted in Figure 3-10.

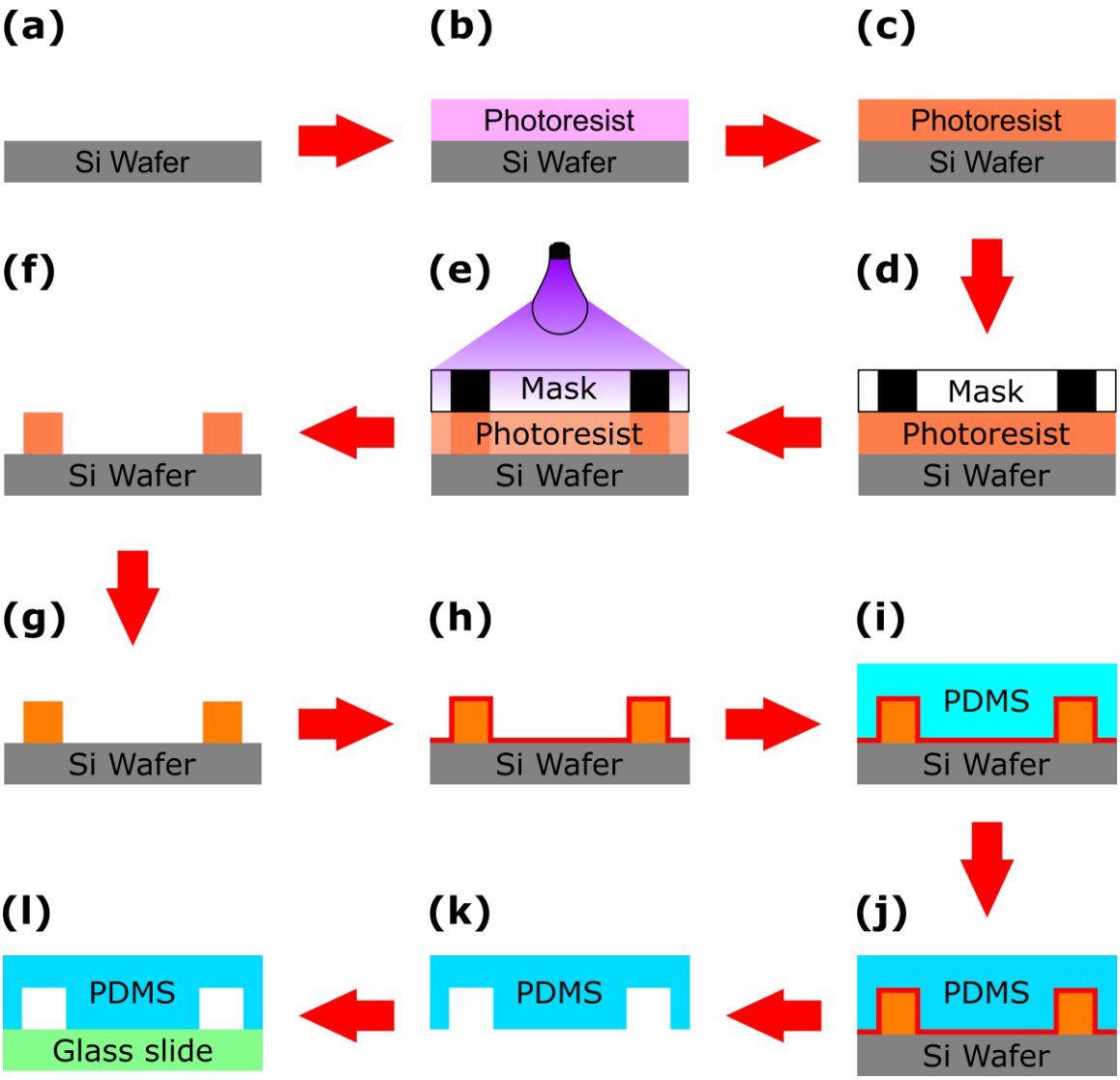

Figure 3-10 – Conventional soft-lithography mold fabrication process. (a) On top of a clean silicon wafer a (b) photoresist is spun. (c) The photoresist is soft-baked, and (d) the photomask is placed on top of the photoresist. (e) The photoresist is exposed to UV radiation, and (f) the excess of photoresist is developed. (g) The mold is hard baked and (h) silanized, being ready for use. (i) Fresh PDMS is poured onto the mold, (j) cured and (k) peeled off from the mold and (l) bonded to a substrate.

This rapid-prototyping master mold fabrication process using common printers can yield features with widths > 20 µm [14], and this low minimum feature size is the biggest advantage of this method. The quality of the printer and ink used impacts the mask and resulting device quality. Ink film density and coverage are highly important to the quality of the final device, as thin or spotty coverage can result in unwanted exposure of non-feature regions, increasing surface roughness and altering features themselves. The fabrication of masks is not confined to end-user printers, with some commercial polymer mask printers achieving [149] high-quality polymer masks, with features down to 10 µm. Further miniaturization can be achieved at the expense of higher resolution chrome masks and shorter wavelengths radiation [75,150], which are not readily available at most research facilities. Mold heights vary from 1 to 200 µm, depending on the photoresist used [14,90], and multi-height molds can be fabricated with this method [54], although the multiple photoresist spin coating processes, alignment steps and radiation exposures make this feature less attractive (Section 3.4.4 Multi-height molds).

The turnaround time to fabricate microfluidic devices using this method is ca. 24 h [14], which was a great advancement at the time (late 1990s), but not that impressive for today's standards, which has become a disadvantage of conventional soft-lithography. Another disadvantage is that the molds fabricated with this method cannot be used in conjunction with microwave thermal processing of PDMS [8,9], because the cured PDMS adheres to the silanizing agent in an irreversible manner. The biggest disadvantage of this method, however, is the need for cleanroom facilities to fabricate the master mold, expensive silicon wafer substrates and carcinogenic photoresist and silanizing agents [8,9].

Alternative methods [138–140] based on photolithography were created to alleviate the issues associated with the conventional method. Li *et al.* [138] borrowed another technique from the electronics industry, and used a Printed Circuit Board (PCB) to fabricate master molds for PDMS microfluidics. This strategy eliminates the need for cleanroom facilities, with a turnaround time of 3 h to fabricate molds and a minimum tested channel width of ~100 µm and height of 16 µm. The disadvantage of this method stems from the low quality of PDMS channels obtained. Features generated have increased surface roughness, due to the roughness of the supportive material of PCBs [138], *i.e.* the copper from boards could not be etched all the way down, requiring skilled operators to perform the etch in a reproducible manner. Another issue with this method, besides the generation of metal ion waste, is the isotropic etching profile of the PCB, which creates edges with low-resolution and round molds. This characteristic might be interesting for some valve-based applications [2,117], but limit the number of features that can be patterned in a mold.

Another photolithographic technique that does not require cleanroom facilities and also uses PCBs was presented by Lobo-Júnior *et al.* [139]. Instead of using photoresists such as SU-8 [14,90], these researchers used a polyvinyl acetate (PVAc) emulsion combined with a photoinitiator diazo sensitizer to act as photoresist, which also can be used on glass slides. This method has a turnaround time of 1.5 h to fabricate the relief molds, with a minimum tested channel width of 30 µm and heights ranging from 30 to 140 µm [139]. The biggest advantages of this method are the low-costs associated with it (cost of patterning photoresist: $0.05 per mold vs. $3.33 per mold using SU-8) and the water-based developing step of the photoresist, eliminating the use of organic solvents. Although the

authors claim that their method is greener in comparison with the commercial SU-8 photoresist [139], the combination of PVAC emulsion with the Diazo D photosensitizer makes the mixture harmful to health, which invalidates non-toxicity claims [139], and hence becomes a disadvantage of this technique.

In 2011, Scharnweber *et al.* [140] created a photolithographic method to prototype PDMS-based devices that does not require master molds. This technique uses direct UV irradiation (185 nm) to break polymer chains of cured PDMS, followed by a wet etching step using an ethanol and sodium hydroxide solution (1 M) (1:1 $_{(V/V)}$). This method generates PDMS channels with a minimum width in the range of 2 to 5 μm, and heights ranging from 3 to 10 μm, and it is capable of producing multi-height structures [140]. However, the disadvantages of this method include the need for chromium quartz masks, which are typically manufactured off-site and increase fabrication time and cost [14], as well as the 13 h process to fabricate the PDMS channels (12 h irradiation followed by 1 h wet etching), which is incongruent with the rapid turnaround times of rapid-prototyping ideals, evidencing an opportunity in the area.

3.6.2 Print-and-peel techniques

Print-and-peel (PAP) techniques are microfabrication methods that have been used to rapidly prototype master molds of PDMS-based microfluidic devices [151] outside cleanroom facilities. This non-lithographic set of tools forms relief molds by direct substrate patterning, either by laser-jet printing [15,16], wax-printing [8,17], xurography [9,18] or even solid-object printing [86]. PAP techniques enable design of microfluidic

devices in shorter times and at lower costs, aiding improvements in the interfacing between different unit operations on-chip, a challenge in the area [8]. Moreover, PAP also makes microfluidics, traditionally confined into expensive cleanroom facilities, available at low cost to research groups worldwide.

3.6.2.1 Laser-jet printing

The development of non-lithographic tools to rapid-prototype microfluidic devices in PDMS is almost anecdotal: In 2001, Tan *et al.* [152] reported in a short communication paper their method to rapidly fabricate PDMS-based microfluidic devices by photocopying a printed pattern on a transparency film. The reasoning behind not printing the patterns straight on the transparency film, instead of printing and then photocopying it, was because the resolution of the desktop printer was not good enough [152], and the pattern was then reduced 4 times while photocopying [153]. This method generates channel widths of 50 μm, and heights ranging from 8 to 14 μm [152].

It was only 4 years later, in 2005, that Bao *et al.* [15] presented the more straightforward method of printing the molds directly onto a transparency film. Using a HP 4050 printer, with a 1200 dpi resolution, the authors obtained channel widths of 60 μm, and heights of 10 μm [15]. Multiple printing steps increase the height of the channels (15 ± 2 μm [15]) and, in theory, allow for multi-height mold fabrication [16], although alignment between multiple precision printing cycles presents a challenge [16]. The turn-around times to fabricate molds using this technique is within minutes (17 printed sheets per minute), and is one of the biggest advantages of this method. Another advantage laser-

jet printing offers is the low-cost of the molds ($0.34 per page), making this method suitable for first iteration designs. The mold fabrication process by laser-jet printing is depicted in Figure 3-11.

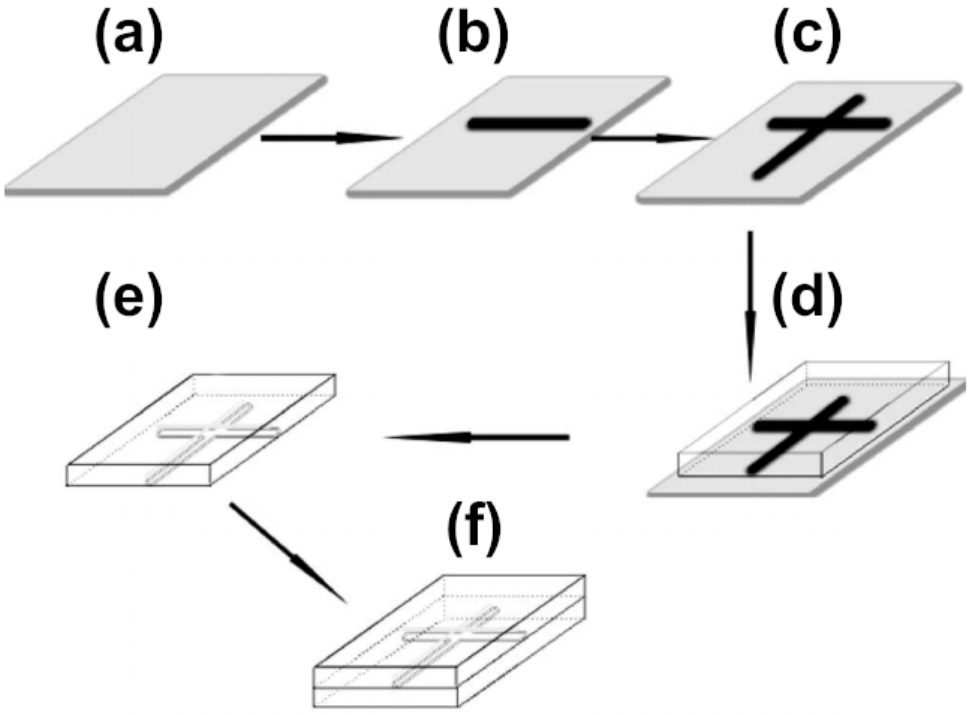

Figure 3-11 – Laser-jet printing fabrication of PDMS devices. (a) Clean transparency film. (b) Horizontal line printed on the transparency film using a laser printer. (c) Another horizontal line printed perpendicularly to the first one. (d) PDMS casting on top of the toner mold. (e) Patterned PDMS peeled off from the toner mold. (f) Patterned PDMS on top of a flat substrate. Reprinted from ref. [15]. Copyright 2005, with permission from Elsevier.

The disadvantages of this method include the lack of reusability of the molds due to mold degradation after PDMS casting [16] and the low aspect ratio of the channels

(height/width) that increases fluidic resistance and limits extensive fluidic manipulation [9].

To overcome the fluidic resistance issue, Grimes *et al.* [141] replaced the backing substrate from polyester transparency films to thermoplastic "Shrinky-Dinks" films, and printed the features using a conventional laser-jet printer. After shrinkage, mold heights were increased 400% from the printing step (initial height of 10 μm), creating channels 50 μm tall, 65 μm wide [141], with the potential for creating multi-height molds by multiple printing steps [141]. The 2 extra thermal treatments required in this technique (first thermal treatment to shrink the features, the second to re-flatten the mold) only increase mold fabrication turnaround times to 10 min, which is a versatile rapid-prototyping tool for the fabrication of PDMS-based microfluidic devices.

3.6.3 Wax printing

Wax printing is one of the most well-known manufacturing techniques for paper-based microfluidic devices [35,154], due to its inherent characteristics such as low-cost, simplicity and high throughput (24 printed sheets per minute) [112]. This method is also attractive to rapid-prototype master molds for PDMS-based microdevices [8,17].

Wax printing principles relies on the same functioning mechanism of piezoelectric inkjet printers [112]. Solid ink sticks are melted and transferred to the printhead, which sprays the molten wax droplets over the heated metal drum that is spinning, forming the mirrored version of the image being printed (Figure 3-12a). The mirrored image on the

drum is transferred to a sheet of paper when they are brought into contact with the aid of a transfer roller (Figure 3-12b), imprinting the figure in the proper orientation.

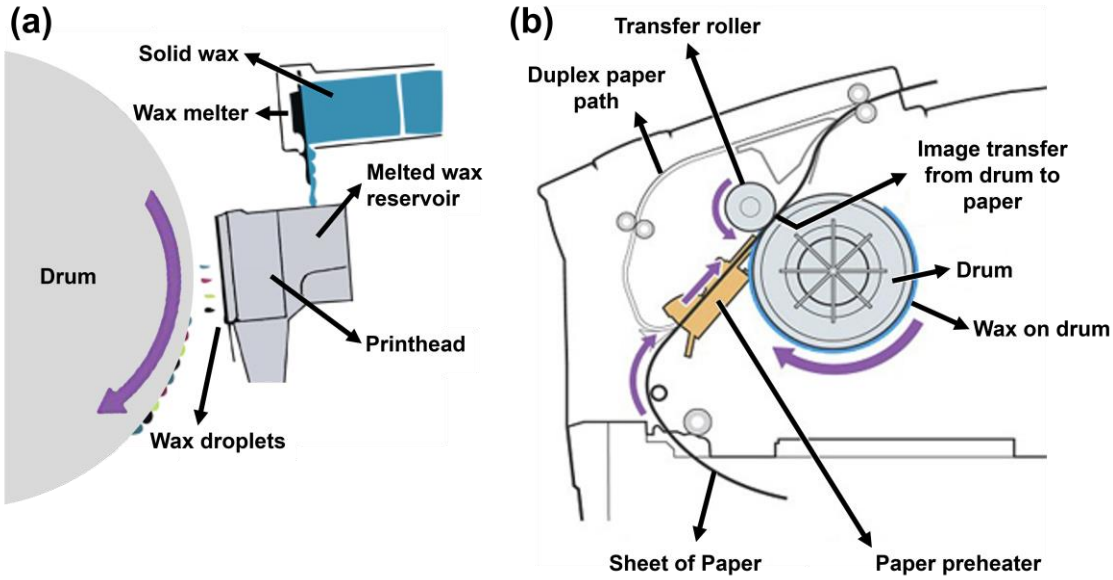

Figure 3-12 – Principles of functioning of a wax printer. (a) Formation of the negative of the image over the metal drum, using molten wax droplets. (b) Transference of the image from the metal drum to the paper surface. Reprinted (adapted) from ref. [155], with permission of IS&T: The Society for Imaging Science and Technology sole copyright owners of www.imaging.org.

Wax printing for PDMS-based microfluidics was first introduced in 2007 by Kaigala and coworkers [17] and advanced by our group in 2019 [8]. In its more advanced form, microfluidic devices are first designed (Figure 3-13a) and printed on a polyester transparency film using a wax printer (Figure 3-13b). The molds are then submitted to a thermal treatment in a convection oven (Figure 3-13c) to reflow the wax and smooth printed features [17]. Pre-degassed PDMS is poured on the mold (Figure 3-13d) and rapidly

cured in a microwave oven (Figure 3-13e) [8]. Individual devices are cut and holes are punched (Figure 3-13f). Then the device is either ready for gentle use applications, or bonded to a glass slide (Figure 3-13g-h), resulting in a final device (Figure 3-13i) capable of withstanding working pressures up to 300 kPa [8].

The minimum feature size created by wax printing is ca. 160 µm before reflowing (350 µm after thermal wax reflow), with a minimum separation between features of 200 µm (300 µm if thermal wax reflow is necessary) and a mold height of 13 µm [8], with low aspect ratio channels, resulting in devices with high fluidic resistance [9].

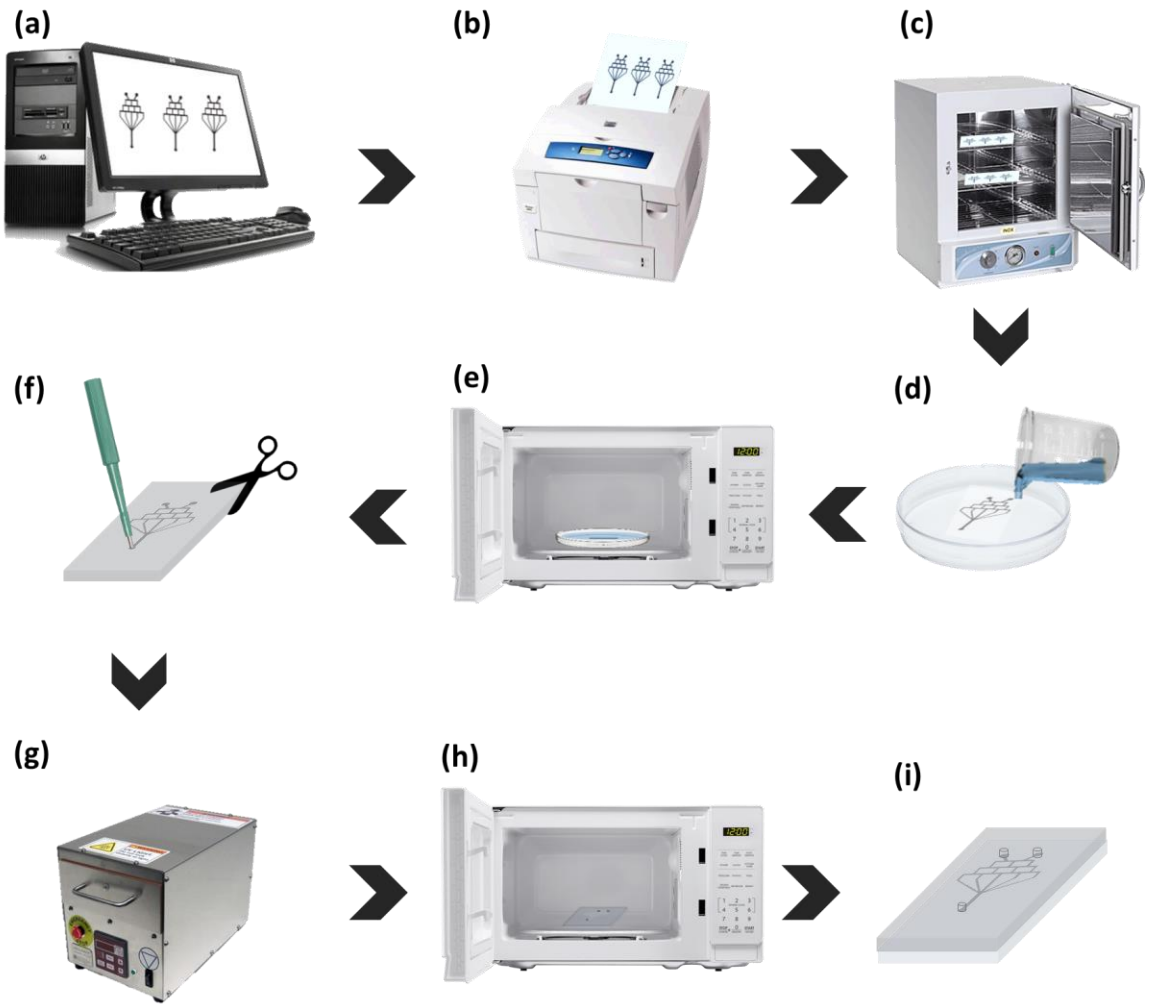

Figure 3-13 – Device fabrication steps using wax printing. (a) Device design. (b) Wax printing. (c) Wax reflow. (d) PDMS pouring. (e) PDMS curing. (f) Device cutting and hole punching. (g) Surface treatment. (h) Thermal annealing. (i) Final device. Reprinted from ref. [8]. Copyright 2019, with permission from Elsevier.

The main advantages of wax printing are the low-cost of each individual mold ($0.01 per mold), the low turnover time for mold fabrication (<2 min) and the compatibility with electrophoretic separations [8,17]. Among the disadvantages of this method are the high fluidic resistance of the channels [9], the lack of reusability of the molds and the low-curing temperature restriction imposed by the wax molds [9], which increases curing times

and therefore the manufacture time of a testable device. The biggest disadvantage of this method, however, is the discontinuation of the production of wax printers by Xerox™ [156], restricting the use of this technology to groups that own one of these machines, although some groups have developed their own wax printers [144], due to the potential of the technique.

3.6.4 Xurography

Xurography, or razor writing, was introduced in 2005 by Bartholomeusz *et al.* [18], as an alternative to conventional photolithographic processes, and it was improved by our group in 2019 [9]. First, a layer of adhesive tape is adhered to a flat backing substrate, taking care to not entrap any air bubbles in the mold. The substrate with the tape is then placed into the cutting plotter, which cuts the patterned features onto the tape. The cutting pressure of the plotter is regulated to prevent scoring the backing substrate during the process [18], especially when soft substrates like polyester transparency films are used as the support [9]. The excess tape is manually removed, leaving the mold on the substrate. The mold fabrication process is depicted in Figure 3-14.

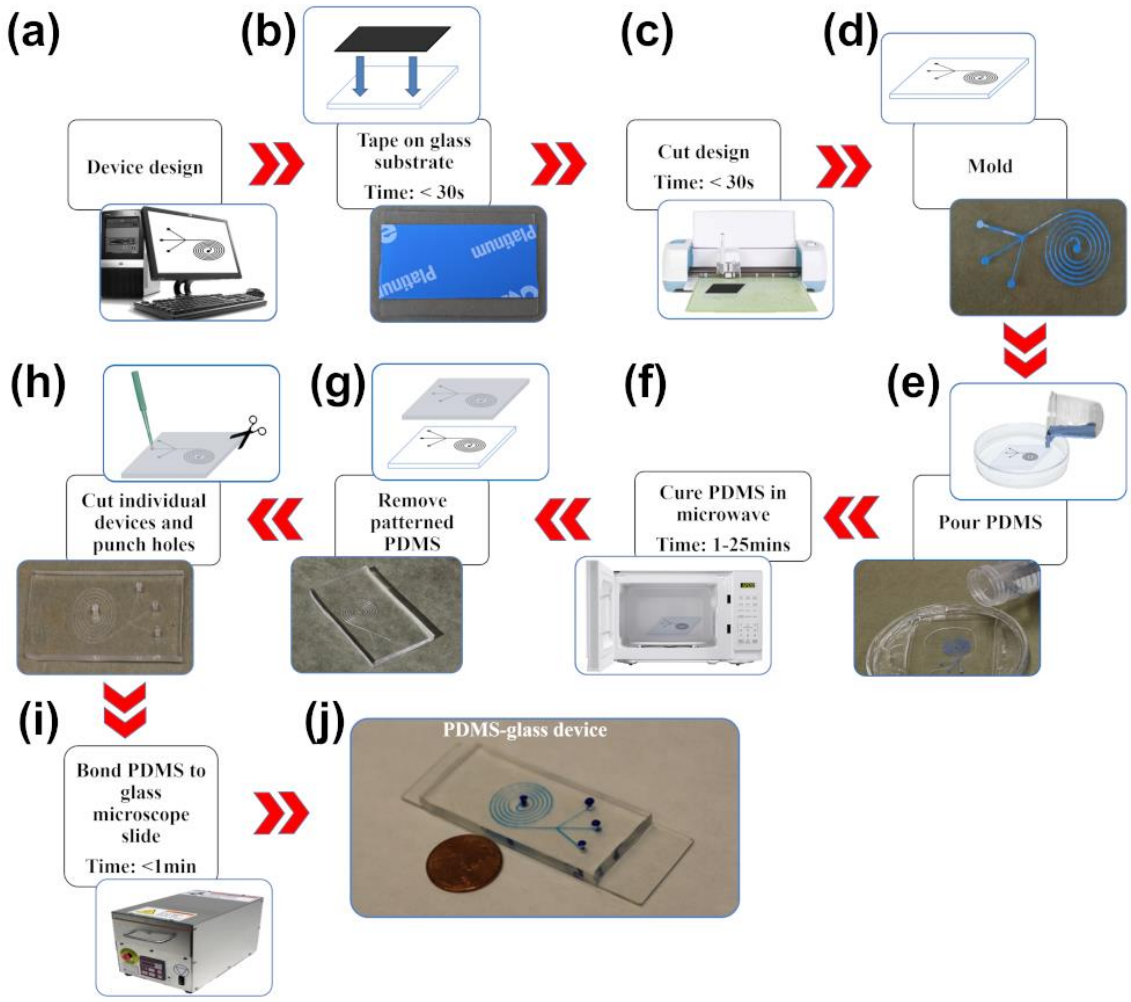

Figure 3-14 – PDMS device fabrication using xurography. (a) Device design. (b) Tape adhesion to a flat backing substrate. (c) Design cutting. (d) Peel off excess tape. (e) PDMS pouring. (f) PDMS curing. (g) Peel off patterned PDMS device from mold. (h) Device cutting and hole punching. (i) Device bonding. (j) Final device. Reprinted from ref. [9]. Copyright 2019, with permission from Elsevier.

This method generates PDMS channels with a minimum tested width of 32 µm [18], with variable heights [9,18]. The resolution of this method is dependent both on the tape being used and the cutter plotter. High resolution cutter plotters can be used [142], at the expense of increasing the start-up costs. The adhesive on the tape must be strong enough

to hold the smallest features onto the substrate while peeling the excess away, but cannot be so strong to the point it hinders its removal from the substrate.

The advantage of xurography, in comparison with other print-and-peel techniques, is the control over mold heights. Different channel heights can be achieved, either by the type of tape used [9,18], or by stacking layers of tape on top of each other [9]. In the latter case, the height of the PDMS channel is only limited by aspect ratio limitations of the final PDMS fluidic channels [75,90], and the minimum thickness of the tape substrate that can be obtained. Multi-height channels can be obtained using xurography, but the positioning of different layers of tape in specific regions of the substrate may require time and skill. Another advantage of xurography is its compatibility with microwave curing of PDMS [8,9], giving birth to the fastest rapid-prototyping method for fabrication of PDMS-based microfluidic devices (5 min to obtain a PDMS testable device - from design to testing) [9], depending on the tape used.

The disadvantages of xurography include the difficulty in removing very small features from the substrate without damaging the main mold. Bartholomeusz *et al.* [18] developed a 2-step process to aid in excess tape removal, by using an application tape to remove patterns from a release liner, before reapplying the cut designs to the final backing substrate. The drawbacks with this approach include the need for 2 extra steps and potential design warping during transfer, especially for malleable application tapes. Another disadvantage of xurography is the lack of scalability, due to the difficulty in automating excess tape removal.

An alternative xurography technique was proposed in 2015, by Cosson *et al.* [142]. Instead of using tape as the positive relief mold, only PDMS is used. PDMS is spun on top of an adhesive layer and cured, to create a thin film of the elastomer. This thin film is cut using a cutter plotter, and the small features are removed from the substrate, leaving behind features cut in thin PDMS film. A flat surface (either a PDMS slab or a glass slide) is plasma bonded to the PDMS, and cured for an hour at 80 ^{o}C. Once cured, the adhesive layer is removed from the thin film of PDMS, and another flat surface is bonded to the reverse side of the thin film, which creates enclosed PDMS channels [142]. This technique cannot reproducibly fabricate channels with features smaller than 100 µm [142], and it requires 3 thermal processing steps (1 hour each), substantially increasing turnaround times to obtain PDMS-based microdevices.

3.6.5 Solid-object printing

Although solid-object printing (3D printing) has been used mainly as a scaffolding technique to fabricate PDMS-based microfluidic devices (Section 3.6.6.2 3D-printing), its first mention in literature dates back to 2002, when McDonald and coworkers [86] first used a 3D printer as a PAP method, to fabricate positive relief master molds for PDMS channel fabrication.

The Fused Deposition Modeling (FDM) additive manufacturing technique is based on the deposition of a thermoplastic material by a printer head, which has 3 actuation directions (x,y, and z axes) [86,144]. Due to these 3 independent mechanisms, the printer has different resolutions depending on the axis in which it is printing [86], consequently

this also compromises the surface roughness of the molds – in this work, found to be~9 µm, before a reflow treatment to smooth out the features.

The advantage of this technique, as a PAP method, is the amenability to fabrication of multi-height molds, with turnaround times of 2 h [86]. The disadvantages of solid-object printing are the low-resolution of printed molds, with channels 250 µm wide and 500 µm tall [86], which is a direct result of limitations imposed by 3D printing technology. Additionally, the thermoplastic material used in 3D printing might contain amides, urethanes and other nitrogenated molecules [86], which might interfere with the curing of PDMS [87] (Section 3.3.1 PDMS Properties).

An advancement of 3D printing as a PAP method was presented by Comina and coworkers in 2014 [157], who further improved mold fabrication by using a different 3D printing technology. The use of stereolithography (SLA) and Digital Light Processing (DLP) techniques [144] allow molds to be printed with better resolution (50 µm wide channels [157]), at a fraction of the cost: A 3D printer in 2002 cost $50,000.00 [86], but only $2,000.00 in 2020 [158].

Chan *et al.* [87] improved the 3D stereolithography process even further, enabling the reuse of 3D relief mold networks by adjusting the printed mold geometry and PDMS peeling direction. This research enabled interlock PDMS channels to be ripped off and released from the mold [87], which can be reused. The ripped PDMS membrane is capable of self-healing after another curing step [87], meaning that channels will be sealed, resulting in a functional PDMS device, although there is a limitation on designs that can be achieved with this method [144].

3.6.6 Scaffolding techniques

Scaffolding, also known as sacrificial molding, are a series of techniques in which the molds are embedded in the structure – in this case, the cured PDMS – and are dissolved away from the matrix [132]. Scaffolding-removal methods are multi-step procedures that require *i)* the creation of the sacrificial molds, *ii)* the casting of the PDMS elastomer over the sacrificial mold and *iii)* the removal of the mold from the cured PDMS matrix by the use of a proper solvent system [19]. Sacrificial molding methods do not require bonding steps to enclose channels [143] (Section 3.5.1.4 Irreversible bonding), which is an advantage over PAP techniques. Many methods have been developed, including template embedding, 3D-printing, and the Green, Low-cost, User-friendly Elastomer method, discussed here in detail.

3.6.6.1 Template embedding

The first mention in literature regarding scaffolding for PDMS dates back to 2006, when Verma *et al.* [143] used Nylon threads embedded in a PDMS matrix to fabricate microchannels. After curing the PDMS, the authors removed the Nylon threads from the matrix by immersing the device in organic solvents (chloroform and triethylamine) [70] to swell the PDMS, followed by a small tension at one end of the thread [143]. The polymer block was de-swelled by drying the matrix at room temperature [143], however the authors did not provide any information on how the immersion in organic solvents impacted the final microfluidic channels features, in terms of dimensions or channel roughness. The PDMS device fabrication process by template embedding is depicted in Figure 3-15.

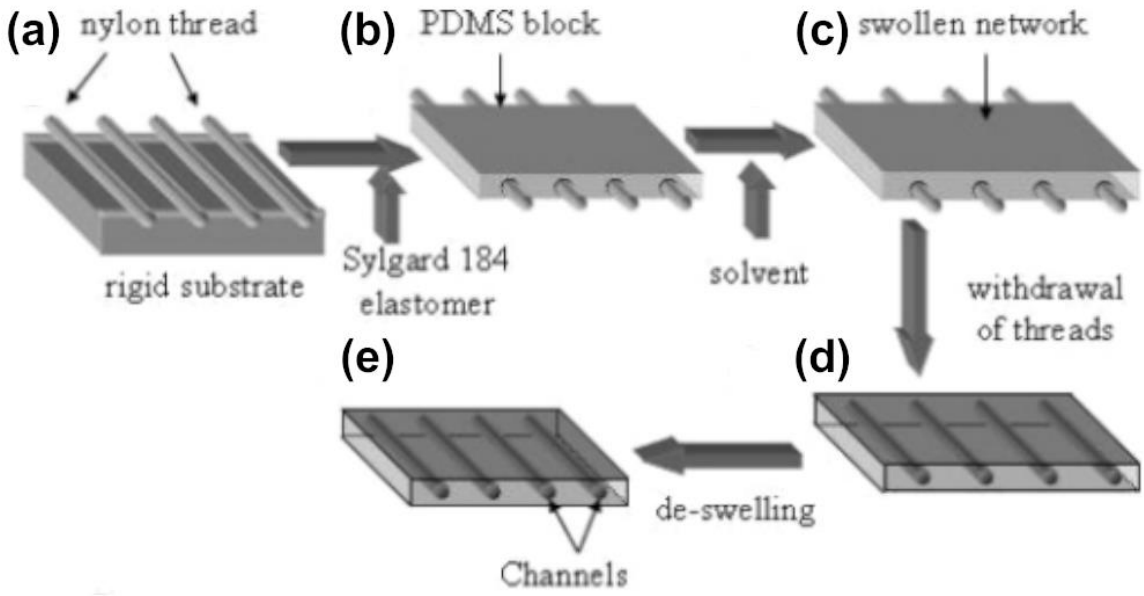

Figure 3-15 – PDMS device fabrication by template embedding. (a) Nylon threads placed on top of a thin layer of half-cured PDMS. (b) PDMS pouring on top of Nylon threads. (c) PDMS block immersion in organic solvent. (d) Nylon thread removal. (e) PDMS de-swelling by solvent evaporation at room temperature. Reprinted (adapted) with permission from ref. [143]. Copyright 2006, American Chemical Society.

The advantages of this method are the size of generated channels (50 to 250 μm), the simplicity of the patterning method, and the fabrication of round micrometric channels in PDMS, instead of the ubiquitous rectangular [14] or trapezoidal cross-sections [19]. However, disadvantages include the use of organic solvents to remove the mold from the PDMS matrix, which increases waste generation [19]; the lack of control of Nylon thread positioning to fabricate structures with the intended design; and the possibility of thread failure during removal, which leads to clogging of the channel and ruining the device. Although the functionality of devices fabricated with this method are very limited, it was the first demonstration of the scaffolding-removal concept, which boosted research in this area [19,131,132].

3.6.6.2 3D-printing

Even though 3D printing has been used as a PAP method to rapid-prototype PDMS devices since the early 2000's [86], the real potential of this additive manufacture process is the ability to fabricate truly three-dimensional networks, *i.e.* crossover features that do not touch [87]. Although the same result could be obtained by stacking 2D (planar) features [86], this underuses the system's capabilities, and increases the number of steps required to obtain the same final result. If one desires to print a 3D structure, but at the same time preserve the integrity of the PDMS device [87], it is necessary to remove the mold from within the elastomer matrix.

The current low cost of 3D printers (Section 3.6.5 Solid-object printing), along with the variety of materials that can now be printed [87,131,132,144], broadens the possibilities of what can be achieved in microfluidics. Even PDMS can now be 3D printed [159], although the need for a photoresist modifier and a photoinitiator modify the elastomer intrinsic properties, such as optical transparency and gas permeability [159].

3.6.6.2.1 Acrylonitrile Butadiene Styrene (ABS)

The first demonstration of a 3D microfluidic device printed using a 3D printer was performed by Saggiomo and Velders [132] in 2015. Using a conventional 3D printer and Acrylonitrile Butadiene Styrene (ABS) as the extruded scaffolding material, these researchers fabricated PDMS channels with diameters ranging from 90 to 500 µm, as well as multi-diameter channels [132]. The biggest contribution of their method was the

incorporation of several distinct functionalities in their proof-of-concept devices, such as a UV LED, a resistance element for selective heating, and even a solenoidal micro-coil to perform NMR spectroscopy in situ [132]. The PDMS scaffolding-removal process using ABS as the scaffolding material is depicted in Figure 3-16.

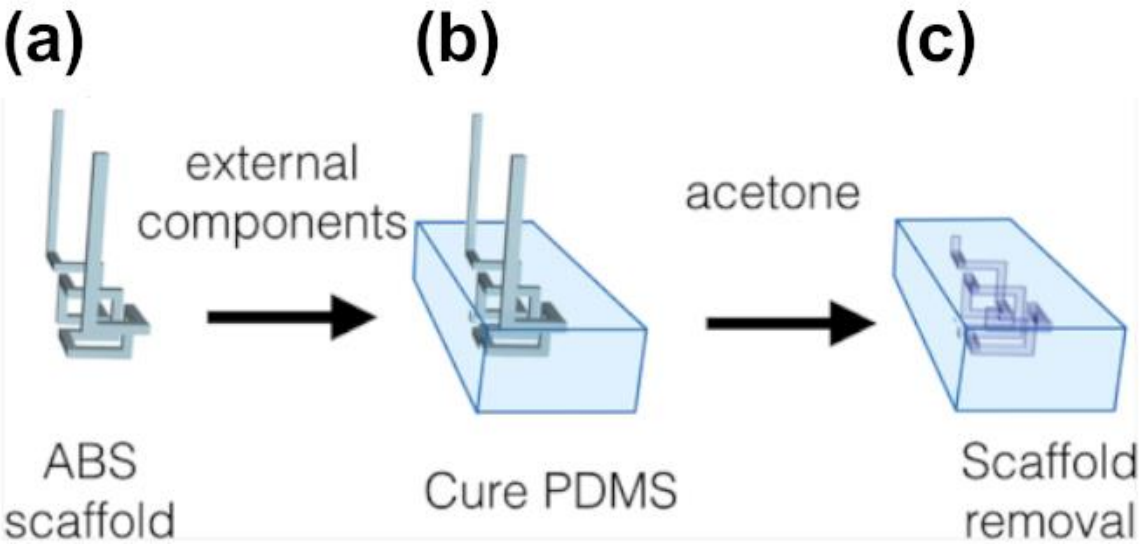

Figure 3-16 – PDMS device fabrication by scaffolding-removal using ABS. (a) The mold is 3D printed in ABS, and (b) PDMS is cast on top of it. After curing, (c) the ABS scaffold is removed by immersion in acetone (12 h). Reprinted from ref. [132]. Copyright 2015, with permission from Creative Commons, WILEY-VCH Verlag GmbH & Co.

The disadvantages of this method include a high surface roughness of the channels (mentioned by the authors, but not measured) [132], the use of organic solvents (acetone) to remove the scaffolding material from within the PDMS channels, which both swells the PDMS matrix [70] and generates more waste [19], and the length of time required to remove the ABS polymer from the PDMS channels (12 h) [70]. Also, this method likely

impacts PDMS curing near the 3D printed structure, due to the ABS composition, as discussed in Section 3.3.1 PDMS Properties. Although the 3D printing process can be performed in a couple hours, depending on the structure, the long scaffold removal process limits true rapid-prototyping [19], which is a drawback of this method. Also, if electronic components are being incorporated in the PDMS structure, the curing process must be performed at reduced temperature [70], which substantially increases the turnaround time of the fabrication process.

3.6.6.2.2 Wax

An alternative to using ABS as extruding material in Fused Deposition Modeling (FDM) is the use of wax, first presented in 2017 by Li *et al.* [144]. Wax has been used as a mold material for PDMS-based microfluidics since 2007 [17] (Section 3.6.3 Wax printing), so its use for 3D printing was a natural evolution in the application of this material. After casting PDMS on top of the mold, and curing it at 40 ^{o}C for 24 h, the wax was removed from within PDMS channels by an immersion in cyclohexane [70] for 10 min, followed by rinses with DI water [144].

When using wax as the sacrificial material, these researchers obtained channels 250 µm wide [144], with variable heights. The advantage of this method, as claimed by the authors, relies on the availability of wax, and its characteristic of being capable of being jetted after melted [144]. However, the disadvantages of this method make it impractical for several reasons: *i)* there is a need for a custom 3D printer which requires highly skilled personnel to design and build; *ii)* it uses cyclohexane, which generates organic solvent

waste [19] and swells the PDMS matrix [70]; *iii)* the wax molds are sensitive to high-temperatures, increasing the fabrication time for PDMS devices (although it seems that microwave processing is compatible with this method [8]); and *iv)* the fabrication time to obtain a testable device using this method is 48 h, less compatible with rapid-prototyping turnaround times [19].

3.6.6.2.3 Polyvinyl alcohol (PVA)

To alleviate some of the issues caused by the use of traditional FDM materials [132], Dahlberg *et al.* [131] proposed the use of poly(vinyl alcohol) (PVA) as the sacrificial material. The advantage of this approach is the water solubility of PVA, eliminating the need for organic solvents that swell PDMS [70], while also reducing the time required to remove the sacrificial material from within the elastomeric matrix [19]. Another advantage of this method is the ability of generating multi-height molds.

The average height of channels obtained by PVA 3D printing was 59 ± 6 μm, with a width of 298 ± 10 μm [131]. Disadvantages of this method include the special handling required for the PVA filaments, because of water uptake issues [131], and a turnaround time of 4 h to fabricate a testable device [131].

3.6.6.3 Green- Low-cost, User-friendly Elastomer – GLUE method

To overcome the shortcomings of other water-soluble scaffolding methods, Speller & Morbioli *et al.* [19] demonstrated in 2020 a green, low-cost, user-friendly, and elastomeric (GLUE) rapid-prototyping method to fabricate PDMS-based microfluidic devices. The GLUE method is the first method of its kind, because it can be used either as a Print-and-Peel method or as a scaffolding-removal method, using the same materials and the same methods [19].

This method uses water-soluble, non-toxic white glue as the patterning agent, eliminating the need for organic solvents [132,144], 3D printers [131,132,144] or UV exposure steps [139]. White glue is applied to a flat substrate, either by spin-coating or blade coating, and the glue is cured into a thin film on top of the flat substrate [19]. A laser cutter or a cutter plotter was utilized to cut patterns onto the thin film, and the excess glue film is removed [19]. If glass is used as the backing substrate, the mold can be reused after PDMS casting and curing (PAP method); if PDMS is used as the backing substrate, after fresh PDMS is cast and cured, the glue is washed from the channels with a warm Alconox solution (scaffold-removal method) [19]. The mold fabrication process is depicted in Figure 3-17.

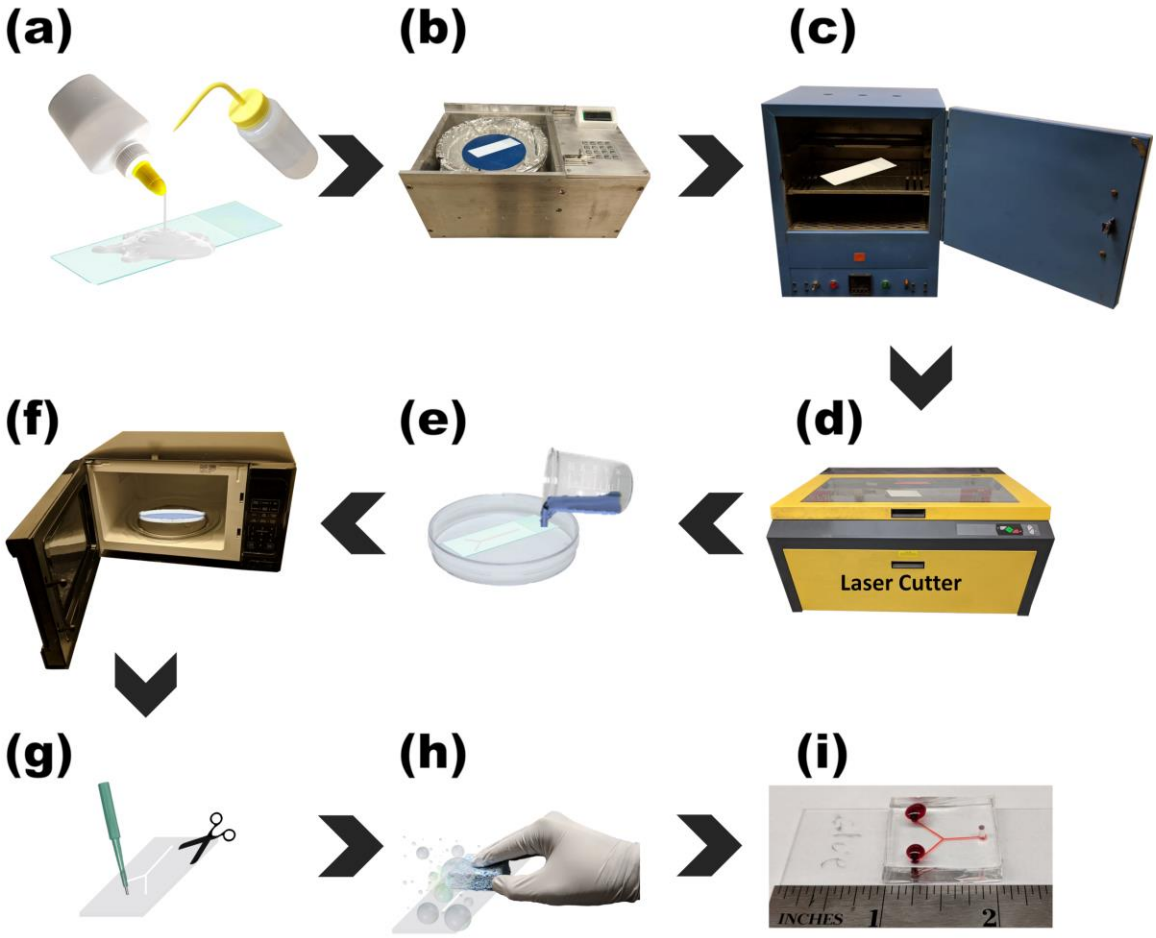

Figure 3-17 – PDMS device fabrication using the GLUE method. (a) Glue deposition on a flat substrate, wetted with isopropanol. (b) Glue spin coating process on top of the flat substrate. (c) Glue curing in the oven. (d) Design cutting using a laser cutter. (e) PDMS pouring. (f) PDMS curing. (g) Device cutting and hole punching. (h) Removal of the glue from within the PDMS channels. (i) Final device. Reprinted (adapted) with permission from ref. [19]. Copyright 2020, American Chemical Society.

This method generates 200 μm wide PDMS channels [19]. One of the biggest advantages of this method is the ability of generating multi-height molds (from 10 to 60 μm [19]), by using the etching function of the laser cutter, with the added advantage of intrinsic low-cost [19]. Typical turnaround times to fabricate testable PDMS-based

microdevices using this method are within 1-h, thanks to the compatibility of the glue molds with microwave thermal processing [8,19,118].

Disadvantages of the GLUE method include the need for a laser cutter if the ability to fabricate multi-height molds is desired [19] and temperature control to remove the glue from within PDMS channels, because PVA degrades and becomes insoluble at temperatures higher than 90 ^{o}C [19,131].

3.6.6.4 Liquid molding

Research into alternative methods to conventional soft-lithography [14] has led to a multitude of tools to fabricate microfluidic devices. In 2007, Chao *et al.* [145] presented an innovative scaffolding method to rapid-prototype PDMS microdevices using water-based molds. A mask containing the desired pattern is placed on top of a flat PDMS piece, and the system is exposed to an O_2 RF plasma [14], turning the exposed areas hydrophilic. The PDMS slab is placed in a solution of glycerol ($5\%_{(w/V)}$), which will stay on the hydrophilic areas. Fresh PDMS is then carefully poured on top of the PDMS slab and cured, forming the channels [145].

Alternatives to this method have been proposed in literature [160,161], but are based on the same liquid molding principle (term coined by Lu *et al.* [160]). This method is capable of generating PDMS channels from 100 to 1000 μm wide, with a minimum tested height of 40 μm [145].

The advantages of this method include the obvious use of water as the mold, completely eliminating the use of organic solvents [132,143], and it also eliminates bonding steps, by casting PDMS on PDMS [19]. The disadvantages of this method include the impossibility of fabricating multi-height structures and the need for longer curing times of PDMS (2 h at 60 ^{o}C). This method is also incompatible with microwave curing of PDMS [8,9]. The turnaround fabrication time for this method is around 2 h, with most of the time being used to cure the elastomer.

3.7 Concluding remarks

It has been over 30 years since micro total analytical systems (μTAS) were envisioned [1], and since its inception [7], the microfluidics field has matured [64] and it is now in its renaissance. Significant development has occurred in microfluidics over this period, expanding the field's capabilities and the applicability of lab-on-a-chip (LOC) devices. Much of this growth can be credited to the creation of rapid-prototyping tools, which accelerated the development of microfluidic devices from weeks to days [14] – and even minutes [8,9]. In this tutorial, we provided significant insights regarding each step of the development process of microfluidic devices and presented alternatives to each fabrication technique. Depending on the final goal, these methods can be combined to provide the desired results: If high-fidelity molds and reproducibility is sought, then conventional soft-lithography [14] is the method of choice; If speed is the requirement, then a combination of rapid-prototyping tools [8,9,15,18,19] with microwave curing of

PDMS [8,9] is recommended. If resources are scarce, then the use of office printers [15], egg-beaters [89] and room temperature curing of PDMS is advised.

The future of the microfluidics field relies on the universalization of this technology, which has been traditionally confined to expensive cleanroom facilities, but has been experiencing development to move beyond those confines. Rapid-prototyping tools are breaking these barriers, by lowering the costs associated with microfluidics research, and bringing microfluidic development to the benchtop. We hope that our tutorial review will help less experienced researchers, students, hobbyists and microfluidics enthusiasts worldwide by providing insights and practical tips on PDMS devices fabrication.

3.8 Acknowledgements

The funding agency CNPq (Science without borders, Grant No. 205453/2014-7) provided scholarship support (GGM). Research was supported by an appointment to NCS from the NASA Postdoctoral Program by the NASA Astrobiology Program, administered by Universities Space Research Association under contract with NASA. All work was done at Georgia Institute of Technology (Georgia Tech) with financial support from State of Georgia, USA.

CHAPTER 4. RAPID AND LOW-COST DEVELOPMENT OF MICROFLUIDIC DEVICES USING WAX PRINTING AND MICROWAVE TREATMENT

4.1 Abstract

Wax printing is a print-and-peel rapid prototyping technique (PAP) that enables rapid creation of master molds for miniaturized polydimethylsiloxane (PDMS) systems, circumventing the need for specialized microfabrication personnel and facilities. We have demonstrated wax printed molds with microwave thermal processing to cure PDMS (25 min) and thermally anneal PDMS to glass (30 min), representing one of the fastest non-lithographic methods for the fabrication of PDMS microfluidic structures to date. The smallest fabricated features are on the order of 350 μm wide and 5 μm tall. Three devices were fabricated using this technique, including a microfluidic gradient generator, a T-droplet generator, and a Y-channel microfluidic device, with performance comparable to literature devices fabricated via traditional photolithography. Direct comparison between Y-channel devices made with the new rapid prototyping technique and with standard photolithography showed similar laminar flow performance, and thus the feasibility of our

method. We have demonstrated device fabrication from design phase to testing within one hour, thus our innovative method significantly speeds up the development of microfluidic tools.

4.2 Introduction

The creation and development of microfluidic tools are essential for the attainment of micro total analytical systems (μTAS) [14] as envisioned by Manz *et al.* in 1990 [1]. These μTAS are attractive in multiple arenas including clinical research [3] and bioanalysis [53] due to their efficient sample and reagent consumption; environmental analysis [162] and on-site analysis in challenging environments [5] due to their small power usage and small footprint; and for the ability to conduct all sample handling steps on a single miniature, lightweight microdevice [14,151,163].

The fabrication of microfluidic devices using standard microelectronic fabrication techniques (photolithography and/or micromachining) with substrates such as glass or oxidized silicon (Si/SiO_2) requires highly specialized personnel and cleanroom facilities, culminating in a time-consuming and often costly process [14]. The advent of soft-lithography in the late 1990s and the use of polydimethylsiloxane (PDMS) substrates [14,150] stimulated rapid development in the area of microfluidics. This method enabled the completion of a fabrication cycle, from design to testing of microfluidic systems within 24 h [14,150]. The fabrication of SU-8 master molds for PDMS microdevices requires lithography and wet-etching processes (substrate cleaning, spin-coating, baking, photolithography, developing and surface treatment), placing a hard lower-limit of several

hours per fabrication cycle, while still requiring a cleanroom facility and trained professional personnel [151]. The development of a highly functional microdevice requires iterative system modifications and optimizations, further increasing the time-to-functional device required with complex photolithography [164]. However, the use of rapid prototyping techniques can enable faster development of μTAS at lower costs.

Rapid prototyping techniques are tools that can streamline the multiple parts of a production chain by reducing the time required for fabrication cycles, and are rapidly evolving in the field [59]. These tools have been used extensively in the aerospace and automotive industries [165], but due to their versatility and applicability they also have been employed in the direct manufacture of μTAS [166,167]. A diverse selection of techniques have been developed to fabricate master molds for PDMS microfluidic devices [151] as an alternative to photolithography. Print-and-peel (PAP) techniques like laser-jet printing [16], toner printing [15], solid-object printing [86] and wax-printing [17,79] do not require cleanroom facilities, and present as a common characteristic the direct deposition of patterning agent over a substrate surface, forming the positive relief of the master mold directly [151].

From these PAP techniques, wax printing has not been explored to the fullest of its capabilities. This fast-prototyping tool was first introduced in 2007 by Kaigala and coworkers [17], and has been extensively used in paper-based microfluidics [35,154] due to its high throughput (24 sheets per minute), low-cost and relative simplicity [112]. These characteristics are also beneficial for manufacture of wax-printed master molds for PDMS microdevices. As it was introduced, the PAP wax printing fabrication cycle produces microdevices within hours, with most of the fabrication time used to thermally cure the

PDMS (3 h, 60 ^{o}C). A relatively low curing temperature is required to avoid deformations of the wax patterns, which increases the curing time and processing time of this method. The optimization of the curing step is essential to improve the turn-around time from design to testing with fast-prototyping techniques.

Microwave processing can reduce the required curing time of thermosetting polymers [93] and is an alternative to conventional thermal treatments. The only mention of using microwave radiation for the fabrication of microdevices in PDMS appears in a conference abstract from 2008 by Gojo *et al.* [20], and to the best of our knowledge has never been explored in detail.

In this paper, we report a novel rapid prototyping method to manufacture microfluidic devices in PDMS, from design to testing within 1 hour, using a commercially available wax printer and a microwave oven. We first characterize the wax printed features on transparency films, followed by an evaluation of time and power settings of microwave processing on PDMS curing. We also compare thermal annealing treatments on irreversible glass-PDMS bond sealing of microdevices using a microwave and a conventional oven. Our results demonstrate that wax printing master mold fabrication with PDMS microwave processing gives rise to one of the fastest rapid prototyping tools in the microfluidics field, while also eliminating the need for cleanroom facilities and costly processes, which can significantly speed up the development of μTAS.

4.3 Materials & Methods

4.3.1 Reagents

Solid ink wax sticks were purchased from Xerox® (Rochester, NY), Arkwright polyester transparency films were purchased from Sihl® (Fiskeville, RI), sulfuric acid and isopropyl alcohol were purchased from VWR (Solon, OH), SYLGARD 184 silicone was purchased from Dow Corning® (Midland, MI), Corning™ Plain Microscope Slides were purchased from Fisher Scientific® (Agawam, MA). Food coloring dyes (McCormick®) and soybean oil (Crisco®) were purchased from a local grocery store. All reagents were used as received.

4.3.2 Wax Mold Fabrication

Wax patterns were designed using CorelDraw® X7 software (Figure 4-1a) and printed on a polyester transparency film using a Xerox Phaser 8580 wax printer (Figure 4-1b). After printing, the wax patterns were subjected to a thermal treatment (100 ^{o}C, 45 s) to reflow the wax and obtain smooth features (Figure 4-1c) [17].

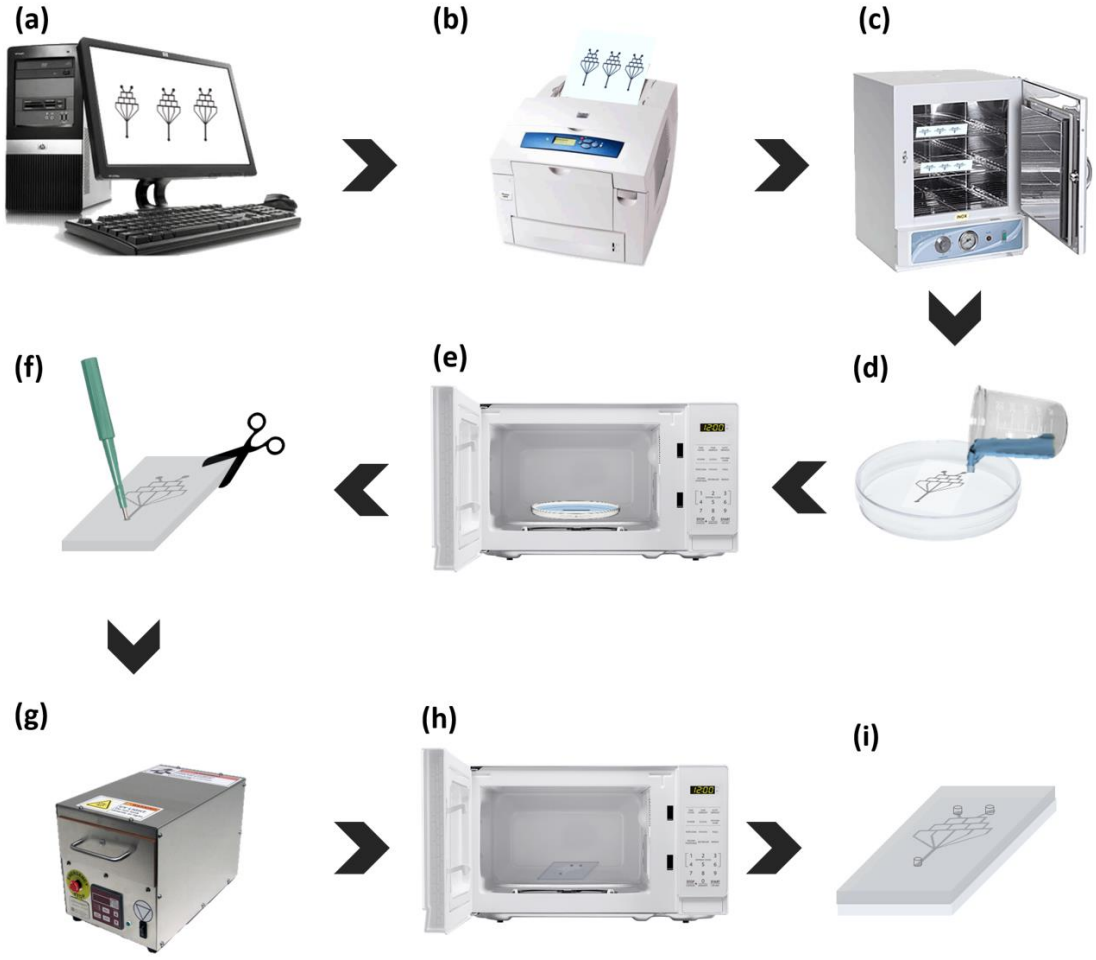

Figure 4-1 – Step-by-step fabrication of PDMS microfluidic devices using wax printing: (a) device design, (b) wax printing (< 1 min), (c) wax reflow (45 s), (d) pour degassed PDMS, (e) cure PDMS in microwave oven (25 min), (f) cut individual devices and hole punching ((< 1 min), (g) PDMS and glass slide cleaning and surface preparation in UVO cleaner (5 min), (h) chip thermal treatment after bonding (30 min) and (i) final device.

4.3.3 Device Fabrication

A mixture of PDMS prepolymer and curing agent (10:1 w/w ratio) was degassed under vacuum for 30 min and was cast against the wax mold (Figure 4-1d). The PDMS

was then cured in a commercial microwave oven (GE, model JES738WJ, 700 W) at ~140 W for 25 min (Figure 4-1e). Temperature measurements were taken with a Fluke 62 MAX IR non-contact thermometer. The patterned PDMS was peeled off the transparency mold and cleaned with isopropyl alcohol. Individual devices were cut from the PDMS and the reservoirs were created using biopsy punches (1.5 or 2 mm) (Figure 4-1f).

4.3.4 Sealing and Bonding

Glass slides were cleaned with concentrated sulfuric acid, rinsed thoroughly with deionized water and isopropyl alcohol, and dried in an oven at 150 ^{o}C. A clean glass slide and PDMS chip were inserted in a UVO-cleaner system Model No. 42 (Jelight, Irvine, CA), followed by a 5 min UV exposure. Both parts were brought into contact to create the irreversible glass-PDMS bond to seal the microdevice (Figure 4-1g). Bonded chips were thermally treated either in a conventional oven (2 h, 110 ^{o}C) with an aluminum heat spreader (~0.4 kg) over the chips, or in a commercial microwave oven at power setting level 2 (~140 W) for 30 min with a glass heat spreader (~0.4 kg) over the chips (Figure 4-1h), resulting in the final device (Figure 4-1i).

4.3.5 Ultimate Working Pressure Failure Mode Testing

A red food coloring dye test solution in DI water was pumped through patterned channels in the PDMS-glass chips using a syringe pump (kd Scientific, Legato® 180, Holliston, MA) with different flow rates (50 µL min^{-1} to 14 mL min^{-1}). Fluidic connections

were made using polyetheretherketone (PEEK) tubing (i.d. 1/32 in) and cut 10 µL Eppendorf pipette tips. A pressure sensor was placed at the end of the channel (LabSmith, 0800 uPS Pressure Sensor, Livermore, CA) and was connected to a microfluidic automation system (LabSmith, uProcess™ System, Livermore, CA). The setup is depicted in Figure B-1, Appendix B. Flow rates were increased to the maximum settings of the syringe pump / or until chips delaminated. PDMS-glass chips were designed with 1 cm channel length, 400 µm design width.

4.4 Results & Discussion

4.4.1 Wax Printing

4.4.1.1 Minimum Feature Size and Quality

According to the manufacturer [168], the Xerox Phaser 8580 wax printer has a printing resolution of 600x600 DPI (dots per inch) per color channel (combined 2400 DPI) [23], which would suggest a center-to-center spacing, and thus a minimum feature of approximately ~42 µm (25.4 mm / 600 DPI) [169]. Through printing testing, 490 DPI was the highest resolution achieved that did not introduce artifacts due to software or hardware (theoretical ~52 µm center-to-center spacing and maximum dot size - Figure B-2, Appendix B). While the center-to-center spacing is 52 µm as expected, the actual printed dot is nearly twice the size, overlapping half of the adjacent pixels (Figure B-2, Appendix B). The large dot size is likely due to the roller transfer step of the wax printer. Further as seen in Figure B-2a, Appendix B, when a designed line of 52 µm is sent to the printer, it

prints lines 3 times larger (163 ± 4 µm, vertical; 159 ± 3 µm, horizontal) than the designed size. This is due to the additional material added by overlapping adjacent dots and the extrusion of the wax material during the roller transfer step.

When lines with the minimum resolution are printed using other fast prototyping tools, such as a laser printer [15], they do not provide a continuous printed line like those observed in wax printing (Figure 4-2); instead, lines are disperse and irregular and cannot be used to provide functional channels [15]. Our findings are in agreement with the results presented by Wang *et al.* [169] and demonstrate the physical limitations of wax printing, for which the minimum feature size of printed lines is ca. 160 µm.

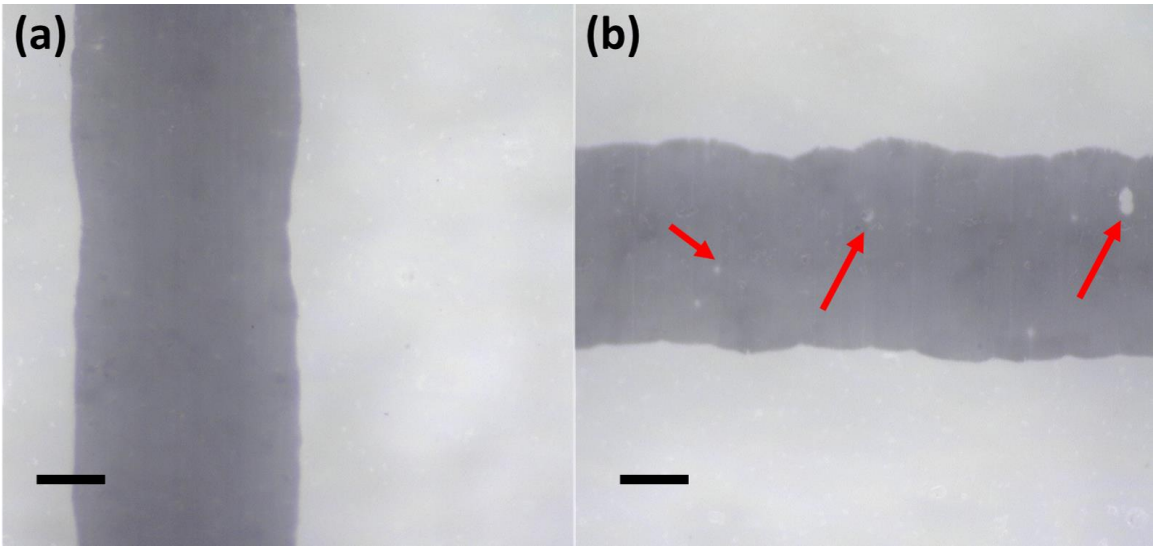

Figure 4-2 – Evaluation of the smallest width (10 µm design, 160 µm printed) of (a) vertical and (b) horizontal printed lines. The red arrows point small defects in the wax pattern. Scale bars are 50 µm.

Due to the basic functioning of the wax printer, vertical lines tend to be smoother than horizontal lines: in a vertical line, the molten wax is sprayed continuously on the

rolling metal drum using the same nozzle, while in a horizontal line it is necessary to actuate several nozzles simultaneously [44], which explains the rougher walls of horizontally printed lines in comparison to vertically printed lines (Figure 4-2, Figure B-3, Appendix B).

Channel roughness can alter performance in certain applications, including electrophoretic separations [17]. In Figure B-3d and f, Appendix B, thermal reflow treatment (100 ^{o}C, 45 s) of the wax molds is shown to remove the raster marks, producing smoother and more uniform channels (Figure 4-3d). The reflow temperature was chosen based on the melting point of the solid ink (100 ^{o}C) provided by the manufacturer [170]. Kaigala *et al.* [17] suggest a reflow period of 10 min, but we observe no significant roughness after a reflow period of 45 s (Figure B-3, Appendix B). Excessive heating of transparency films causes them to warp, which deforms the resulting PDMS device and prohibits proper sealing of the chip.

4.4.1.2 Evaluation of Wax-Printing Mold Fabrication

Figure 4-3 shows the minimum feature spacing without reflow (Figure 4-3a and c) and with reflow (Figure 4-3b and d). Horizontally printed lines were chosen for this study due to their lower resolution. As shown in Figure 4-3a, two horizontally printed parallel lines are completely separated when the separation distance is set to 200 μm (design). However, if thermal reflow is required, this separation distance will not be enough to maintain separation post-reflow (Figure 4-3b). When thermal reflow is necessary, the minimum separation distance between lines must be set to ≥ 300 μm (design, Figure 4-3d).

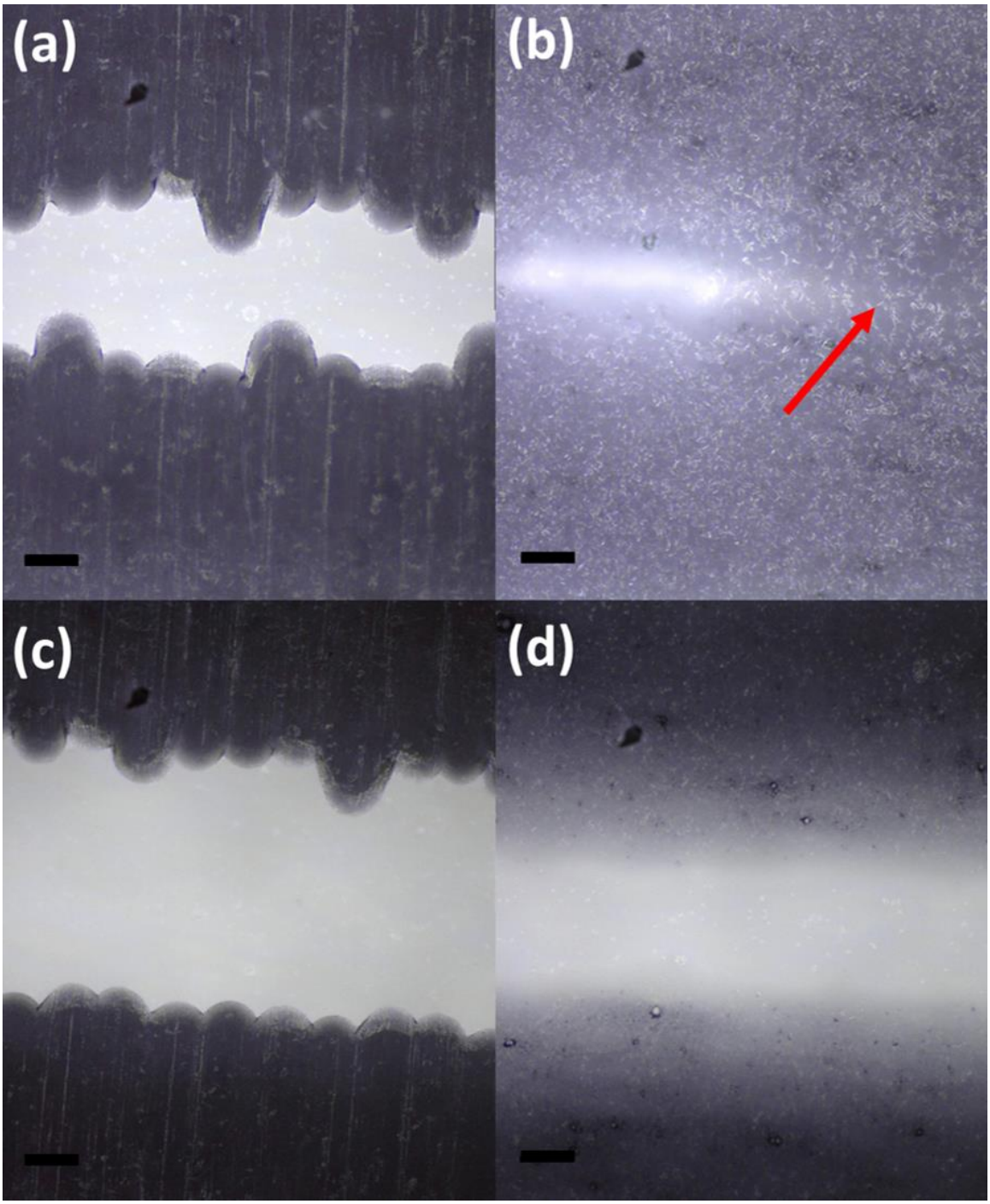

Figure 4-3 – Two horizontally printed lines (width: 250 µm design, 330 µm printed) separated by a design distance of 200 µm (a) before and (b) after thermal treatment (100 ºC, 45 s). The red arrow indicates the formation of a neck between the two printed lines after the thermal treatment. Two horizontally printed lines (250 µm, design) separated by a design distance of 300 µm (a) before and (b) after thermal treatment (100 ºC, 45 s). There is no contact between the lines. Scale bars are 50 µm.

The thermal reflow of the wax modifies the initially printed wax patterns width, height and aspect ratio. Figure 4-4 shows the characterization of these parameters before and after the thermal reflow treatment.

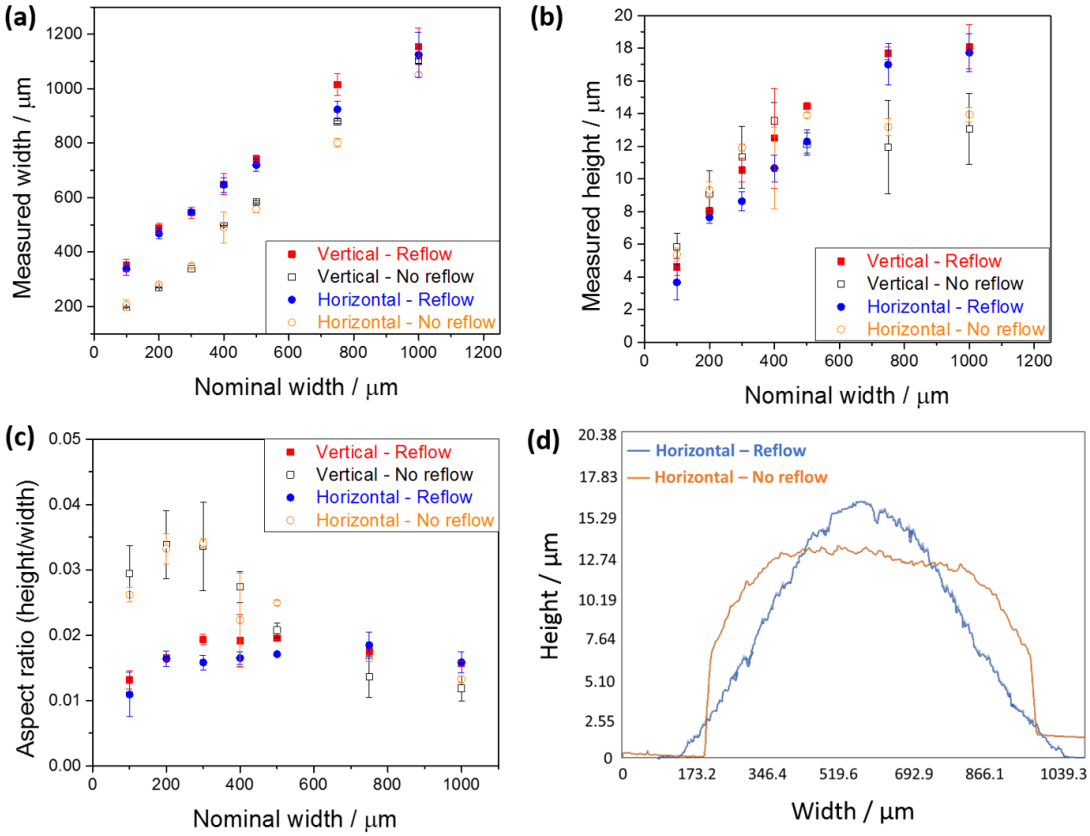

Figure 4-4 – Characterization of the wax printed molds before and after thermal reflow treatment. (a) Design line widths correlated with printed line widths. (b) Design line widths correlated with printed line heights. (c) Aspect ratio of positive relief wax molds. The values represent the average of three measurements ± 1 standard deviation. (d) Profile of the wax printed channels (axes not in the same scale).

The true width of the printed lines correlates linearly with the designed width (Figure 4-4a, r^2=0.99 for all the cases, Figure B-4 Appendix B) for both horizontal and vertical printing orientations. The better resolution for the vertically printed lines is observed by the intercept of the linear fit (Figure B-4c Appendix B). After thermal treatment, the vertical and the horizontal lines have the same dimensions (Figure B-4d Appendix B), showing that the difference in the printing mechanism does not generate a bias between horizontal and vertical channels of thermally treated wax molds.

The height of printed wax molds changes with the width of the printed lines (Figure 4-4b and Figure B-5, Appendix B) and the quality of printing (Figure B-7, Appendix B), reaching a plateau for design lines over 500 µm (Figure B-5), congruous with the results presented by Thomas *et al.* [151]. This causes the aspect ratio (height/width) of the thermally treated wax molds (Figure 4-4c and Figure B-6, Appendix B) to not change significantly for design lines with widths over 200 µm (ANOVA, C.I. 95%, Table B-1, Appendix B). The low aspect ratios inherent in this method lends it toward certain applications, like microchip capillary electrophoresis [17]; for instance, microchannels with small aspect ratios present higher electroosmotic flow (EOF) in comparison with channels with aspect ratios closer to unity [171].

One might expect that the use of shades of gray could provide pattern features with different heights [151] without affecting the width of the patterns (considering a straight vertical line), due to a more sparse deposition of black ink. Instead, the use of grayscale changes the width of the lines, due to the actuation of several nozzles overlaying cyan, magenta, and yellow (Figure B-8a to I, Appendix B). The use of grayscale is therefore not advantageous to decreasing the height of printed features.

4.4.2 PDMS Microwave Curing

Due to the temperature restrictions imposed by the wax molds, the first paper demonstrating PAP wax-printed molds [17] thermally cured PDMS devices in a conventional oven at a mild temperature of 60 ^{o}C for 3 h. To circumvent this limitation and enable this PAP process to be a truly fast-prototyping tool, we used microwave radiation to cure PDMS [20] on wax molds. When we used a conventional microwave oven for thermal treatment (power settings in Appendix B), degassed PDMS was cured in as little as 10 min (~350 W). We reached temperatures higher than 100 ^{o}C, which can distort wax molds, so lower power settings were also tested. At 70 W the temperature did not elevate above 60 ^{o}C, preserving the features of the wax molds, but required longer processing periods (50 min). A compromise between processing time and temperature was observed with microwave radiation ~140 W for 25 min, reaching average temperatures of 70 ^{o}C, 30 ^{o}C lower than the melting point of the solid ink (100 ^{o}C), preserving the patterns of the wax relief molds.

Conventional thermal processing of materials occurs by energy transfer due to thermal gradients from the surface to the bulk of the of the material being processed [93]. In contrast, microwave heating is due to energy conversion (radiant energy from electromagnetic radiation in the microwave region to thermal energy) [93]. Molecular dipoles align with the oscillating electric field applied to the system, and heat is generated throughout the volume of the material due to friction and agitation of these molecules every time the electric field is alternated [93,172]. The dipole moment of poly(dimethylsiloxane) increases with the size of its chains (0.949 D for a chain length of 3; 8.44 D for a chain length of 300),[173] and therefore should absorb more microwave radiation as chain length

increases. However, thermal effects might not be the only reason PDMS curing is accelerated under microwave irradiation. Microwave effects that are not purely thermal in nature (*i.e.* the increase of the pre-exponential factor A in Arrhenius law (Equation 7, Appendix B) and a decrease in the activation energy $\Delta G^{\ddagger}$) may explain the faster reaction rates in microwave-activated reactions [172,174]. As presented by Loupy *et al.* [175], solvent-free reactions are more prone to present microwave effects, and systems that react slower also tend to present a more pronounced microwave effect in comparison with faster reactions [174], which is observed in the present scenario. The PDMS curing reaction is solvent-free and is relatively slow (48 h to cure at room temperature). Our observations corroborate with a pronounced microwave effect, which could explain the accelerated curing of PDMS in a microwave oven. To the best of our knowledge, microwave-assisted catalytic olefin hydrosilylation with platinum-based catalysts has never been studied in detail, and even though it is beyond the scope of this paper to elucidate its mechanism, the authors strongly encourage research in this field due to our findings.

4.4.3 PDMS-Glass Microwave Assisted Thermal Annealing

Once cured, patterned PDMS is brought into contact with a rigid support (*e.g.* glass) to fabricate reversibly-sealed PDMS-glass hybrid devices [17]. This approach is the fastest method to create microdevices because it does not require additional fabrication steps, but great care must be taken during handling these devices due to the potential for delamination. The devices are limited to low-internal pressure and applications with relatively gentle handling and mild conditions. In cases where a more robust system is

required, an irreversible bond between PDMS-glass is desirable, and can be obtained either by plasma, corona or ultraviolet / ozone (UVO) treatment [81], often requiring a thermal annealing post-processing step [16]. This extra step increases processing time for fast-prototyping, making the optimization of the thermal processing relevant.

UVO-treated chips that received no thermal treatment delaminated (Figure 4-5) above internal pressures of 102 ± 50 kPa. UVO-treated chips thermally annealed in a conventional oven (2 h, 110 ^{o}C) and in a microwave oven (30 min, power setting level 2 (~140 W), average temperature of 60 ^{o}C) showed no statistical significant difference (*t*-test, C.I. 95%, Table B-3, Appendix B) in ultimate working pressure failure mode (Figure 4-5). Device integrity was preserved at all pressures tested, with devices withstanding pressures up to the maximum available to us of 305 ± 20 kPa and 275 ± 4 kPa, respectively. These devices demonstrated superior performance in comparison to chips that received no thermal treatment, and these results are evidence of the effectiveness of our microwave assisted thermal annealing of PDMS-glass bonding.

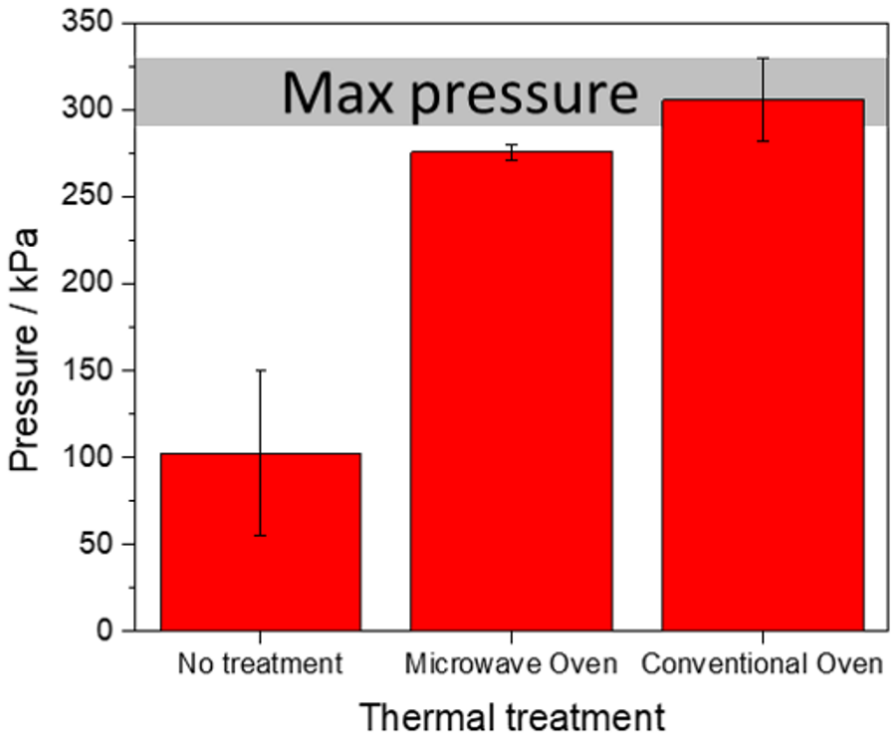

Figure 4-5 – Ultimate working pressure during failure mode testing. Chips with no thermal annealing treatment delaminated during testing, while chips submitted to microwave oven and conventional oven thermal annealing treatment preserved their integrity during the pressure tests. There is no significant statistical difference between measured pressures in chips submitted to the microwave oven and the conventional oven thermal treatments (t-test, C.I. 95%, Table B-3, Appendix B). The values represent the average of pressure measurements of three independent devices ± 1 standard deviation. The grey bar represents the range of pressures where the syringe pump would regularly stall.

Commercial microwave ovens have local fluctuation in applied electromagnetic field (hot spots and dead zones) [93], which explains some observed batch-to-batch variability, and also the observation that better results are obtained when articles rest following thermal annealing treatment.

PDMS-glass bonding occurs via a condensation reaction between a silanol group of the glass surface and a silanol group from the UVO-treated PDMS surface [176], and it has been shown that this reaction is highly accelerated under microwave heating in sol-gel processes [177,178], suggesting that a similar process may occur in our microwave assisted thermal annealing of PDMS-glass bonding.

4.4.4 Proof-of-Concept Devices

It is important to compare our innovative process to fabricate microfluidic devices with the conventional process (i.e. soft-lithography and laboratory oven) to show the feasibility of the method. A Y-channel PDMS microchip was cast using an SU-8 mold and a wax printed mold (design in Figure B-9c, Appendix B). As shown in Figure B-10, Appendix B, the same laminar flow regime can be seen in the SU-8 molded PDMS microchip (Figure B-10b, Appendix B) and in the wax-printed mold PDMS device (Figure B-10d, Appendix B), demonstrating that the fabrication method does not interfere with the performance of the microdevice.

The relatively small aspect ratio of the PDMS channels fabricated with wax printing make them ideal for electrophoretic separations [17], but the versatility of the method enables multiple fluidic applications. A microfluidic gradient generator was fabricated (Figure 4-6a, design Figure B-9a, Appendix B). Red and blue food dye test solutions in DI water were pumped into the gradient generator using a syringe pump, with a flow rate of 15 μL min^{-1}. Another microdevice created with this technology was a T-droplet generator (Figure 4-6b, design Figure B-9b, Appendix B). A blue dye testing solution in DI water

and soybean oil were pumped into T-droplet generator using a syringe pump with a flow rate of 6 µL min^{-1}.

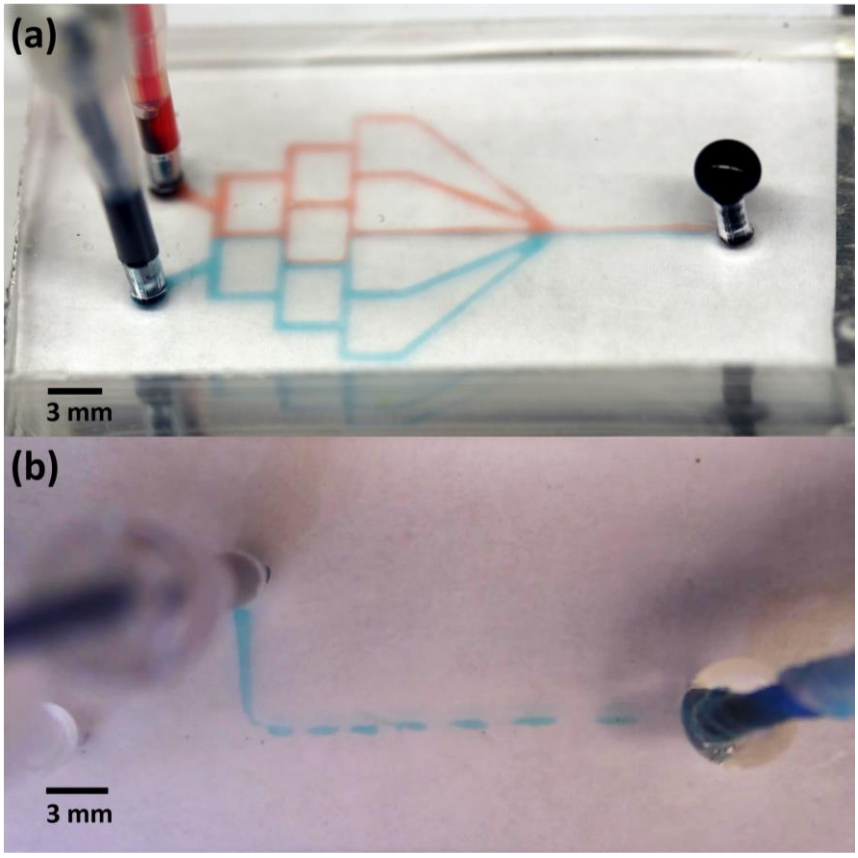

Figure 4-6 – Microfluidic devices generated by the wax printing fast prototyping technique. (a) A microfluidic gradient generator. (b) A T-droplet generator.

4.5 Conclusion

Rapid iterative design cycles, simplicity and low-cost are the main advantages of print-and-peel fast prototyping techniques, which make them attractive in the fabrication of master molds for miniaturized polydimethylsiloxane (PDMS) devices. Due to their

unique characteristics, wax printing master mold fabrication coupled with microwave thermal processing decreases manufacture time of PDMS microfluidic structures from design to testing within one hour, giving rise to one of the fastest rapid prototyping methods to date [179]. This work furthers the development of μTAS by providing a unique low-cost and ultra-rapid tool for iterative design. Our proof-of-concept devices for fluidic manipulation on chip demonstrate that our method has the potential to significantly enhance the creation of fully-integrated microfluidic tools in record time, while reducing costs associated with the development of this technology, making μTAS accessible to a more diverse development audience.

4.6 Acknowledgements

The funding agency CNPq (Grant No. 205453/2014-7) provided scholarship support (GGM). Research was supported by an appointment to NCS from the NASA Postdoctoral Program by the NASA Astrobiology Program, administered by Universities Space Research Association under contract with NASA. All work was done at Georgia Institute of Technology (Georgia Tech) with financial support from State of Georgia, USA. We gratefully acknowledge Julianna McNeice (Georgia Institute of Technology) for the photographs.

CHAPTER 5. CUTTING EDGE MICROFLUIDICS: XUROGRAPHY AND A MICROWAVE

Reprinted (adapted) with permission from "Cutting Edge Microfluidics: Xurography and a Microwave" by Nicholas C. Speller, Giorgio Gianini Morbioli, Michael E. Cato, Thomas P. Cantrell, Erin M. Leydon, Britney E. Schmidt and Amanda M. Stockton (2019) *Sensors and Actuators B: Chemical, v. 291, 250–256*.

5.1 Abstract

Microfluidic technologies enable precise fluidic manipulation at the microscale, with applications ranging from inexpensive medical diagnostics to automaton devices for extraterrestrial in situ analysis. However, development of microfluidic tools typically requires high-maintenance infrastructure and resource-intensive development processes, limiting their broad adoption. Furthermore, the development of effective microfluidic tools requires iterative design processes, multiplicatively increasing development time and cost. Rapid prototyping techniques minimize these expenses, accelerating development time and reducing manufacturing cost of microfluidic devices. Here we use the print-and-peel (PAP) technique of xurography to fabricate master molds in conjunction with microwave thermal processing of polydimethylsiloxane (PDMS) to rapidly fabricate PDMS-based microfluidics. Three types of tape (3M Blue Platinum, PVC and Kapton Tape) and three types of backing substrates (Soda lime glass, Silicon, Ceramic glass) were employed, enabling fabrication of microfluidic devices from design to device in as little as five

minutes. Minimum feature widths of ~200 μm and feature heights of ~60 μm were determined. Proof-of-concept devices made using these methods were employed for electrophoretic flow focusing applications. To the best of our knowledge this process represents the most rapid method for fabrication of PDMS microfluidics to date due to microwave thermal processing, enabling curing of PDMS in as little as 90 seconds. This work can significantly minimize device fabrication time and the start-up cost of fabrication infrastructure, enhancing efficiency and making microfluidics accessible to a broader user base.

5.2 Introduction

Microfluidics are the core of lab-on-a-chip (LOC) devices. These technologies handle and process nanoliter to microliter-scale fluidic volumes in structures with millimeter to micrometer characteristic length scales, where flow characteristics are dominated by low Reynolds numbers and high Stokes numbers [7]. Microfluidics have enabled precise fluidic manipulation at the microscale, leading to numerous applications ranging from clinical point-of-care diagnostics [180] to automaton devices for extraterrestrial in situ analyses [181]. Despite the demonstrated power of microfluidic tools in diverse fields [182], a majority of microfluidic technologies require trained personnel and intensive cleanroom facilities [183,184], placing resource-based limitations on technology development and adoption.

Traditionally, microfluidics have been fabricated using standard microelectromechanical systems (MEMS) fabrication processes developed in the silicon

industry to yield well-defined and reproducible features [18,183,184] including photolithography, chemical etching and thin film metallization of glass or silicon substrates. These multistep fabrication processes typically require expensive equipment, cleanroom facilities, characterization infrastructure, and days or weeks of highly trained person-hours per batch of typically a relatively small number of devices. This limits adoption of microfluidic technology development due to high start-up and operating cost [183]. Furthermore, glass- based and silicon-based processes are not conducive to rapid turnaround times, or to disposable devices (e.g. for medical applications) due to the associated material and fabrication costs [183,184]. Due to the need for rapid prototyping in both academic and commercial settings, researchers have investigated low-cost alternatives to glass and silicon photolithography, resulting in devices made of polymeric materials. Polymer-based microfluidics can have excellent biocompatibility, optical transparency, and other chemical and material properties. Low-cost fabrication methods for polymeric devices have been developed and include polydimethylsiloxane (PDMS) micromolding, laser ablation [185], hot embossing [186], micropowder blasting [187], micromilling [188], and stereolithography [189]. Recently, print-and-peel techniques, particularly xurography, have been adopted for fabricating microfluidic devices [18,190–198].

Xurography, first coined by Bartholomeusz in 2005 [18], is a technique that uses a cutting plotter to cut thin film polymer materials to directly create microfluidic channels, masks, or molds without requiring cleanroom facilities. Fabrication of 2-D and 3-D microfluidics have been demonstrated using this method [18,199,200], with the best cutting plotters capable of fabricating features down to 20 μm [18,200]. Xurography is

significantly faster than photolithography, and the most rapid xurography-based prototyping techniques utilizing pressure sensitive adhesive (PSA) substrates have enabled fabrication of functional devices from design on the order of minutes [200,201]. However, device fabrication times for xurography-based PDMS micromolding require considerably more time (1 to 24 h) [142,199]. Approximately 10% of microfluidic studies reported employ PDMS as the substrate (Figure C-1, Appendix C) due to ease of fabrication, low cost, biocompatibility, and excellent optical properties [183], indicating a need for rapid prototyping techniques that yield high quality PDMS devices.

Previously, we presented a wax-printing-based microwave-enabled method for rapid prototyping of PDMS devices [8]. The wax printing of molds coupled with microwave PDMS curing produces PDMS-based microdevices within an hour and is very fast when compared to other PDMS-based prototyping methods [199]. This method takes advantage of an accelerated PDMS curing time attributed to microwave effects and heat generation within the mass of the polymer [8,173]. However, wax printing results in features with low aspect ratio channels, creating channels with high fluidic resistance. This is disadvantageous for applications where relatively large volume fluidic throughput is needed. Furthermore, due to the use of wax as a patterning agent and transparency films as the mold substrate, only relatively low curing temperatures (60˚C) could be utilized in order to maintain micromold integrity [8]. Due to these limitations, the full potential of microwave processing to reduce the fabrication times of PDMS based devices could not be realized using wax-printed micromolds alone.

Here, we present an inexpensive and user-friendly ultra-rapid prototyping method for fabrication of PDMS devices using a cutting plotter, store-bought tape and a consumer-

grade microwave oven in order to circumvent the limitations of wax printing and accelerate the prototyping process. The cutting plotter is used to fabricate positive relief micromolds from the store-bought tape and microwave processing is utilized to cure the PDMS over the molds in as little as 90 seconds. We demonstrate the process using three different tapes (3M Blue Platinum, PVC Tape, and Kapton) in combination with three different substrates (glass, cellulose acetate transparency film, and silicon). We characterize plotter resolution by measuring resulting feature height and width. Finally, we fabricate and test proof of concept devices for electrokinetic focusing applications demonstrating devices fabricated via this method are of sufficiently high quality to be used in electrophoresis-based applications.

5.3 Materials & Methods

5.3.1 Materials

Sylgard 184 silicone (polydimethylsiloxane, PDMS) was purchased from Dow Corning® (Midland, MI). Corning™ plain microscope slides were purchased from Fisher Scientific® (Agawam, MA). Bright fluorescent polystyrene latex spheres (0.2 µm and 10 µm) were obtained from Magsphere Inc. (Pasadena, CA), Cricut Explore die–cutting machine/ cutter plotter (Provo Craft & Novelty, Inc. Spanish Fork, Utah) was obtained from Amazon. Write-on cellulose acetate transparency film was obtained from Staples (Framingham, MA). Scotch blue platinum painter's tape (3M, Maplewood, MN) was obtained from a local hardware store (Home Depot). Kapton and PVC tape were purchased

from McMaster-Carr (Elmhurst, IL). Labsmith SVM 430 microscope and Labsmith 6000D high voltage system were obtained from Labsmith (Livermore, CA).

5.3.2 Device Fabrication Process

5.3.2.1 Mold Fabrication

Microdevices were fabricated using the process shown in Figure 5-1. To fabricate the tape-based mold, the different varieties of tape (3M Blue Platinum, Kapton, and PVC) were adhered to a backing substrate with the aid of a flat edge, to avoid the entrapment of air bubbles. The backing substrate was comprised of either a cellulose acetate transparency film (CATF), glass microscope slide, or a silicon wafer. The tape-on-backing substrate was adhered to the Cricut cutting mat and premade CAD designs (AutoCAD) were cut into the tape layer using the Cricut cutter plotter. Subsequently, the tape-on-substrate was removed from the plotter and the excess tape was removed from the desired design by simply peeling away the excess with the aid of a scalpel.

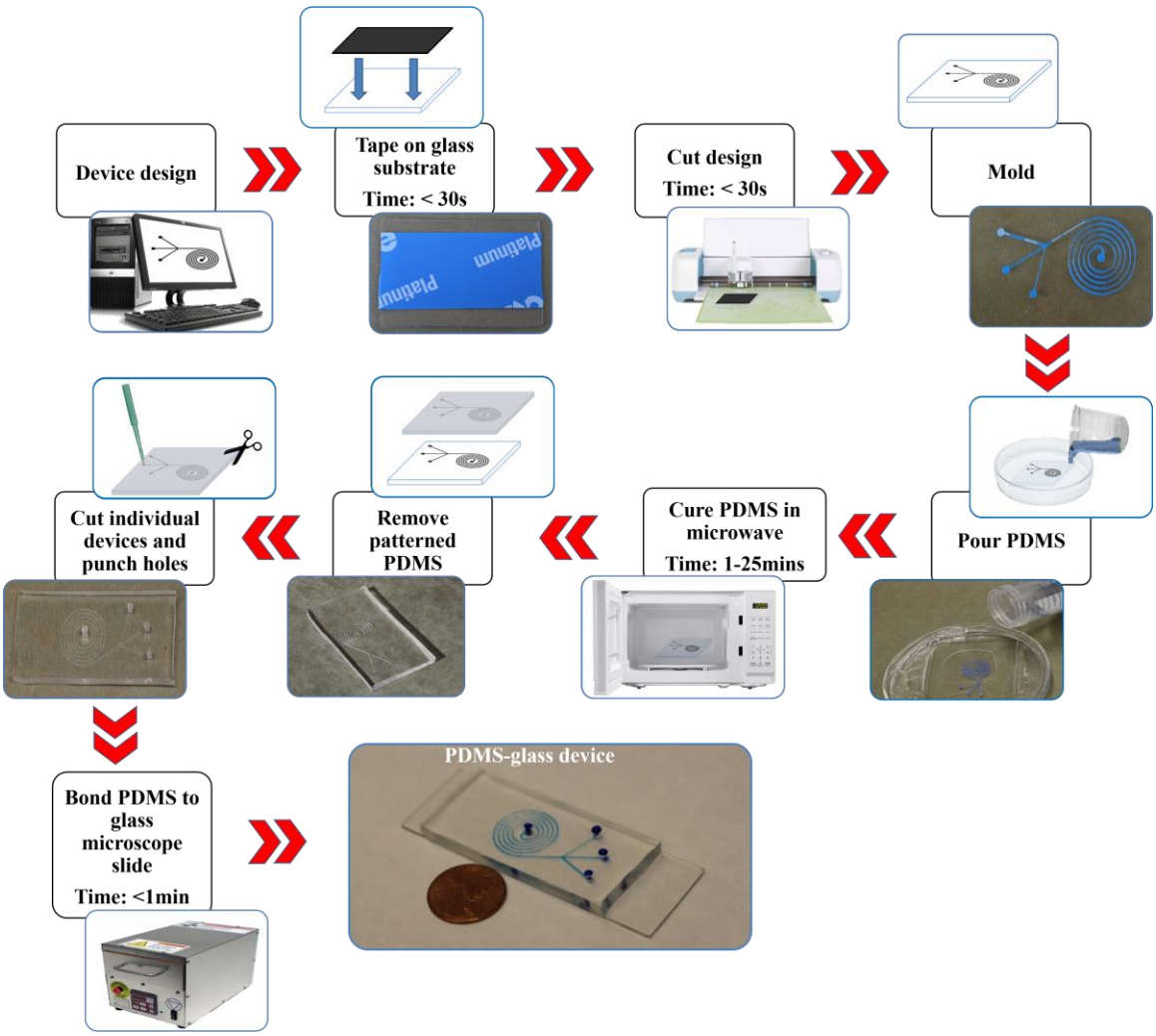

Figure 5-1 – Schematic of fabrication process.

5.3.2.2 PDMS Chip Fabrication

PDMS at 1:10 w/w ratio of curing agent to prepolymer was previously degassed in a vacuum chamber as reported previously [8] and poured over the tape design. PDMS was subsequently cured in a commercial microwave oven (GE, model JES738WJ, 700 W). Molds made with a CATF backing were cured for 25 min at power setting level 2 (~140 W). When a glass backing was used, molds were cured for 5 min at power setting HI (~700

W). Molds made with a silicon backing were cured for 3 min at power setting HI (~700 W). Molds made with a substrate sandwich were cured for 1.5 min at power setting HI (~700 W).

5.3.2.3 Chip Bonding

After the patterned, cured PDMS was removed from the design, wells were cut using a 2 mm diameter biopsy punch and the PDMS layer was bonded to glass slides to seal channels and make finished devices. For UVO bonding, the patterned PDMS and a glass slide were subjected to a 5-minute UVO exposure using a UVO-cleaner system Model No. 42 (Jelight, Irvine, CA). After 5 minutes, the two active surfaces of the glass and patterned PDMS were pressed together, completing the microfluidic device, and thermally annealed for a minimum of 15 minutes at 110 °C in an oven. For plasma bonding, devices were irreversibly bonded after a 60 second oxygen plasma exposure (Plasma Etch Model PE-25, Plasma Etch Inc, Carson City, NV) of the active surfaces of the patterned PDMS and glass slide. After the treatment, devices were pressed together, left to sit for 1 minute at room temperature, and could be used immediately thereafter.

5.3.3 Spiral Dielectrophoretic Focuser Fabrication

A spiral dielectrophoretic particulate focuser was designed using AutoCAD. The device is comprised of 5 loops where the inner diameter of the first loop is 4.5 mm. The device was designed to have channels with a width of 400 μm and a spacing between

consecutive loops of 600 µm. Total channel length from inlet, located in the middle of the spiral, to outlet is 173 mm. Fluorescent particles (10 µm) were utilized for visualizing particulate focusing within this device. A potential of -6000 V was applied from the inlet to the outlet, as shown in Figure C-2, Appendix C, using a custom-built power supply yielding an average electric field of ~ 350 V/cm throughout the device. The -6000 VDC variable power supply was built using a DC to high voltage DC module (XP Power, Sutter Creek, CA), and driven by a thermally compensated 5 V power source. Control input for the module was driven by a linear potentiometer adjusted by the user and output was measured by multimeter (Fluke Everett, WA). To apply the -6000 V potential to the device, the ground electrode was inserted into the inlet well and the high voltage electrode was inserted into the bottom outlet well. Videos were captured using Labsmith SVM 430 microscope (Labsmith Livermore, CA) (video recordings are available in the publisher's website).

5.3.4 Electrophoretic Focuser Fabrication

A symmetric six-channel electrophoretic focuser device was designed using AutoCAD. The device is comprised of 7 mm long inlet channel, with a 1 mm center separation. All channels were designed to be 400 µm in width. Fluorescent 200 nm polystyrene latex particles were used to visualize the flow focusing with 10 mM borate in all other channels. A Labsmith HVS448-6000D high voltage sequencer (Labsmith Inc. Livermore, CA) was used to apply potentials to inlet and outlet wells as depicted in Figure C-3, Appendix C. Potentials were applied to the top three wells with a ground in the desired

outlet well to facilitate flow switching. This design was chosen to enable sheath flow using the first three channels and flow switching using the second set of three channels. Flow switching was accomplished by grounding the desired well and floating the other outlet wells. In order to switch flow into respective outlet wells, a high voltage input signal was applied to the common (COM) pin of an OMRON relay, and the normally open (NO) and normally closed (NC) pins were attached to separate electrodes inserted into each well. The relay's solenoid was triggered by current buffering a square-wave output generated by an Agilent arbitrary signal generator with frequency manually adjusted by user.

5.4 Results & Discussion

5.4.1 Xurography Characterization

To determine the cutting resolution of the Cricut cutter plotter used in this study, straight channel molds were cut in horizontal and vertical orientations from Blue Platinum tape with channel widths ranging from 100 μm to 1 mm in 100 μm increments. Each channel was cut with 1 cm spacing between them and repeated 5 times to account for deviation caused by positioning on the cutting surface. Measurements of the channel width were taken at the top, center, and bottom of each channel. The average of these measurements for a given nominal channel width are plotted in Figure 5-2a, b, and c.

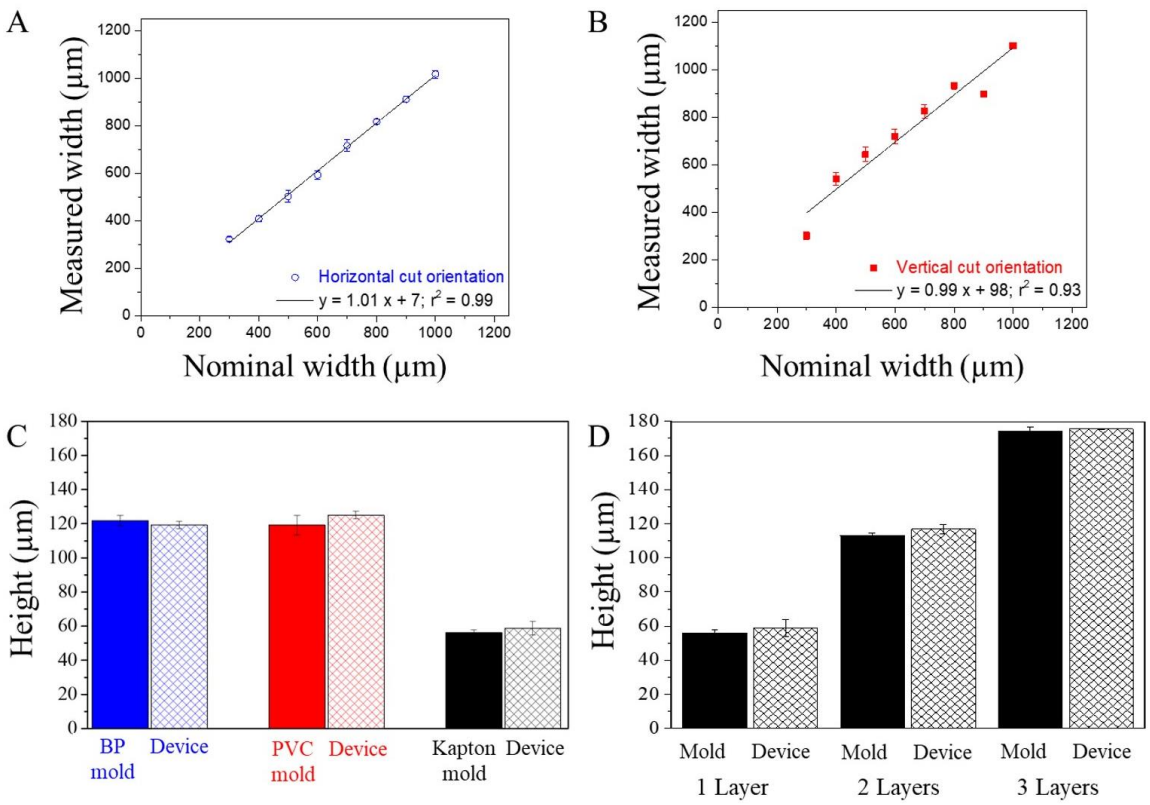

Figure 5-2 – Characterization of cut straight-channel tape molds and resulting devices. (a) Nominal channel widths compared with sticker cut channel widths cut on the horizontal axis of the cutter plotter. (b) Nominal channel widths compared with sticker cut channel widths cut on the vertical axis of the cutter plotter. (c) Comparison of tape mold height transfer to PDMS for three tape varieties. (d) Evaluation of multilayer Kapton tape molds and height transfer to PDMS. Values for channel width measurements represent the average of 5 measurements ± 1 standard deviation. Values for height measurements represent the average of 3 measurements ± 1 standard deviation.

The Cricut plotter used in this study has two separate positioning mechanisms for cutting designs: a belt drive to which the cutter head is mounted that provides horizontal displacement and a roller mechanism that provides vertical displacement of the substrate. The two positioning mechanisms have differential positioning precision, accuracy, and

resolution that lead to deviation from the desired design that is dependent upon the orientation of the cut. A statistically significant difference between the nominal and actual channel width on the order of 100 µm was seen for the channels cut in the vertical orientation (C.I. 95%, Table C-1, Appendix C). Horizontally cut channels were found to exhibit no statistically significant difference between the nominal and actual channel widths (C.I. 95%, Table C-1, Appendix C). The smallest feature cut in the horizontal orientation with this cutting plotter was nominally 200 µm using horizontally oriented channels, in agreement with cut limits observed with other plotters used xurography studies [201]. Cutting plotters with higher positioning accuracy and precision have been shown to have minimum feature sizes on the order of 10 µm, with the associated increase in expense associated with these plotters [142,202].

Heights of channels cut from three different tape varieties are show in Figure 5-2c, where heights were measured for 400 µm-wide nominal mold channel width cut from 3M Blue Platinum tape, Kapton tape and PVC tape and their corresponding PDMS channels. PVC tape with reported manufacture thickness of 152 µm yields channel heights on the order of 120 µm, while Kapton tape with a reported manufactures thickness of 63.5 µm yields channels on the order of 60 µm. Channels with aspect ratio (height to width) of 1:6.6 and 1:3.3 were created. The height of channels cut with the cutter plotter is determined by the thickness of the tape used for the mold or by the number of layers applied to the substrate. Hence channel height and ultimately the aspect ratio of final features can be easily altered by selecting tapes with desired thicknesses or by stacking layers of a tape with a specific thickness, (Figure 5-2d) a notable advantage of this rapid prototyping method.

It is important for fabrication methods to have control over the degree of surface roughness within channels. Controlled or minimal surface roughness are required in some applications (i.e. capillary electrophoresis) and can be attained with the proper choice of materials. Surface roughness of the PDMS channels created from the molds is directly dependent upon the surface roughness of the tape material. Images of the 400 μm nominal horizontal channels of each tape variety and their corresponding PDMS channel casting are shown in Figure 5-3. Tapes with rougher surfaces such as the Blue platinum and PVC tape tested here produce PDMS channels with correspondingly rough surfaces and hence a much lower degree of optical transparency as shown in Figure 5-3. In contrast, Kapton which is a characteristically smooth tape produces PDMS channels with minimal surface roughness and channels with a high degree of optical transparency. Kapton tape generates the smoothest side walls as well, as compared to other tapes.

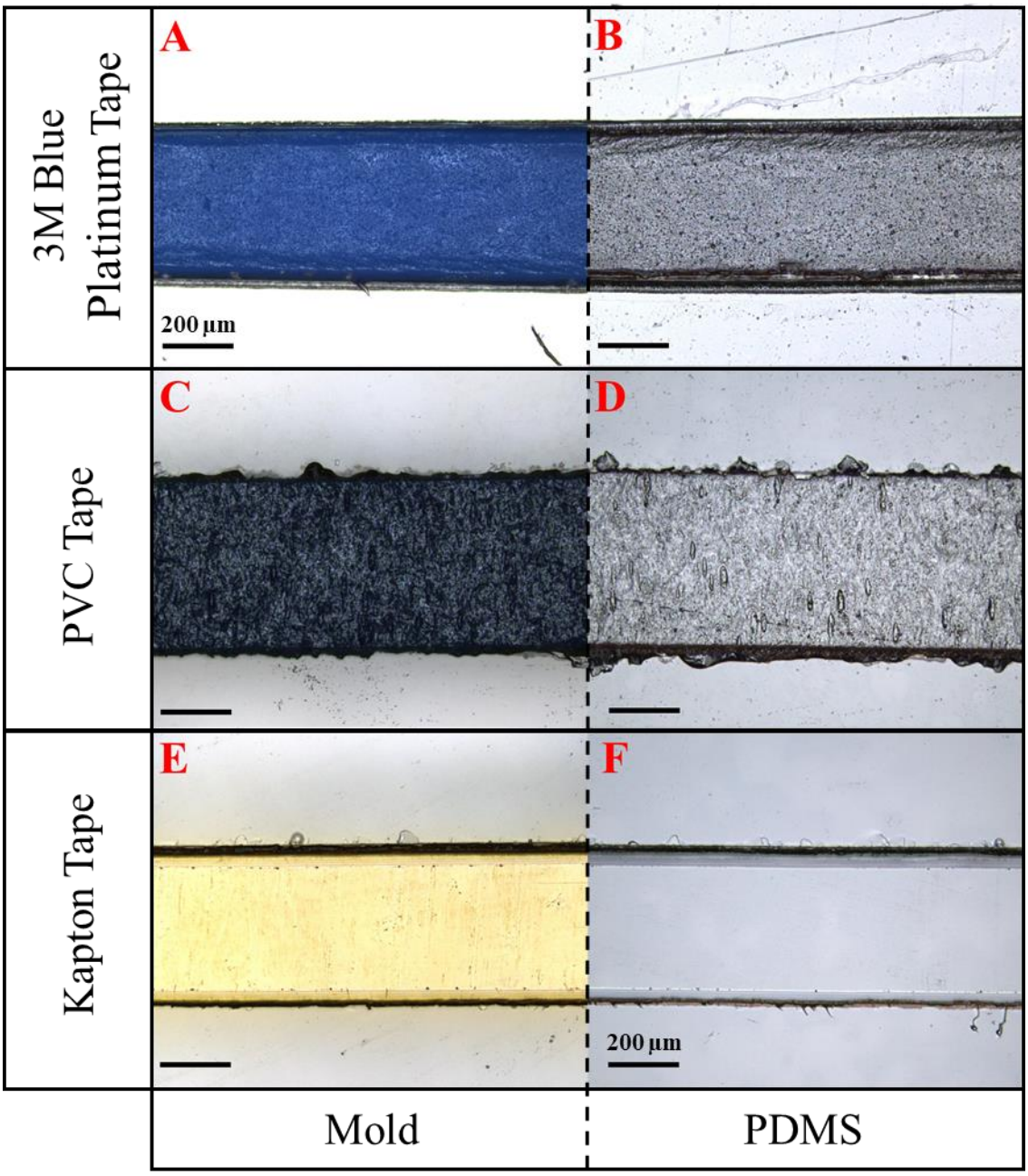

Figure 5-3 – Micrographs for print-and-peel xurography method with a mold nominal channel width of 400 µm. (a) 3M Platinum Blue tape mold. (b) PDMS channel casted on 3M Platinum Blue tape mold. (c) PVC tape mold. (d) PDMS channel casted on PVC tape mold. (e) Kapton tape mold. (f) PDMS channel casted on Kapton tape mold. Scale bars are 200 µm.

5.4.2 Rapid microwave curing of PDMS

The longest step in PDMS rapid prototyping methods is typically the time required to cure PDMS. Previously, we demonstrated that microwave processing of PDMS leads to accelerated curing times (25 minutes) [8], however microwave processing was limited to 20% microwave power (700 Watt max) due to properties of the mold and substrate materials [8]. Thermally stable polymer tapes such as PVC tape (165 °C) and Kapton tape (700 °C), coupled with a thermally stable backing layer like glass or silicon which can withstand higher temperatures, enable higher microwave power to be used during curing, thus decreasing curing time. Table 5-1 shows the curing times and temperatures of multiple PDMS curing methods including those developed within this study. Devices made with these methods are shown in Appendix C.

Table 5-1 – Curing times and surface temperatures of PDMS and substrates using conventional and microwave methods (100% power at 700 Watt)

Methods	Substrate	Curing Time	Temperature (Set Point)	PDMS Surface Temperature	Substrate Surface Temperature	Top Sandwich Substrate Surface Temperature	Bottom Sandwich Substrate Surface Temperature	Ref.
No Heat Treatment	--	48 h	25 ˚C	--	--	--	--	[203]
Conventional Oven	--	2 h	65 ˚C	--	--	--	--	[110]
Microwave	Wax PTF	25 min	--	70 ˚C	--	--	--	[8]
	CATF	25 min	--	70 ˚C	70 ˚C	--	--	*
	Borosilicate Glass	5 min	--	80 °C	71 °C	--	--	*
	Silicon Wafer	3 min	--	86 °C	132 °C	--	114 °C	*
	Ceramic Glass	3 min	--	92 °C	204 °C	115 °C	--	*
	Substrate Sandwich	1.5 min		88 °C	--	--	--	*

* New to this work

While microwave radiation absorbance by PDMS dominates the curing process, there is contribution from thermal conduction when the backing substrate exhibits heating due to high microwave absorptivity [93]. The two substrates tested that exhibit higher microwave absorbance are silicon and ceramic glass and enabled shorter PDMS curing times (3 min for each) reaching higher temperatures (132 °C and 204 °C respectively) than soda lime glass, which enabled PDMS curing in 5 min, reaching 71 °C. Interestingly, even though the ceramic glass exhibits a higher surface temperature, curing time is not significantly decreased compared to the silicon wafer. The PDMS cures from the substrate-surface up resulting in a diminished rate of conduction-based curing with time due to the diminishing thermal gradient thus, the last one minute of curing is dominated by direct interaction of microwaves with PDMS rather than by convection from the substrate. Consistent with this observation, PDMS curing time can be reduced by increasing thermally-conductive contact with microwave absorbing substrates, for example, by sandwiching the PDMS between two substrates as depicted in Figure C-4, Appendix C. PDMS cured in 1.5 minutes using this method, whether sandwiching the PDMS mold between two silicon wafers or between a silicon wafer and a ceramic glass panel. This is the fastest curing time reported for PDMS in literature.

5.4.3 Spiral Dielectrophoretic Focuser

As proof-of-concept of this fabrication method, a spiral dielectrophoretic focuser was fabricated (Figure 5-4). The tape mold of the spiral dielectrophoretic focuser cut on a CATF backing is photographed in Figure 5-4a, and b shows a photograph of the final PDMS

device. The device was designed to have channels with a width of 400 μm and spacing between consecutive loops of 600 μm. Dimensions of the channels of the final device were measured to have an average width of 492 ± 17 μm and the spacing between consecutive loops of 534 ± 19 μm. The 5-loop design was chosen to allow the 10 μm particles to spend more time translating through the non-uniform electric field, which enhances the focusing in relatively large channel widths [204]. Furthermore, 10 mM borate buffer was utilized to enhance the focusing effect since it was reported that higher buffer concentration enhances focusing [204], but buffer concentrations greater than 10 mM were avoided to minimize the impact of Joule heating which causes problematic generation of bubbles within the channel. The surfactant TWEEN 20 was added to the borate solution at a 1% concentration to negate particle-particle and particle channel surface interactions. The extended length of the channel was chosen to account for the breakdown distance required for the 6000 V potential estimated to achieve focusing in the device. The continuously curving path of the spiral causes the particles to experience a non-uniform electric field with a region of high electric field at the inner wall of the channel and low electric field at the outer wall [204]. Translation of particles through these electric fields is governed by the differential polarizability of the particles and the background solution [204–207]. The polystyrene latex particles are less polarizable than the borate buffer, causing them to experience negative dielectrophoretic force and thus migrate towards the region of lower electric field at the outer wall of the channel.

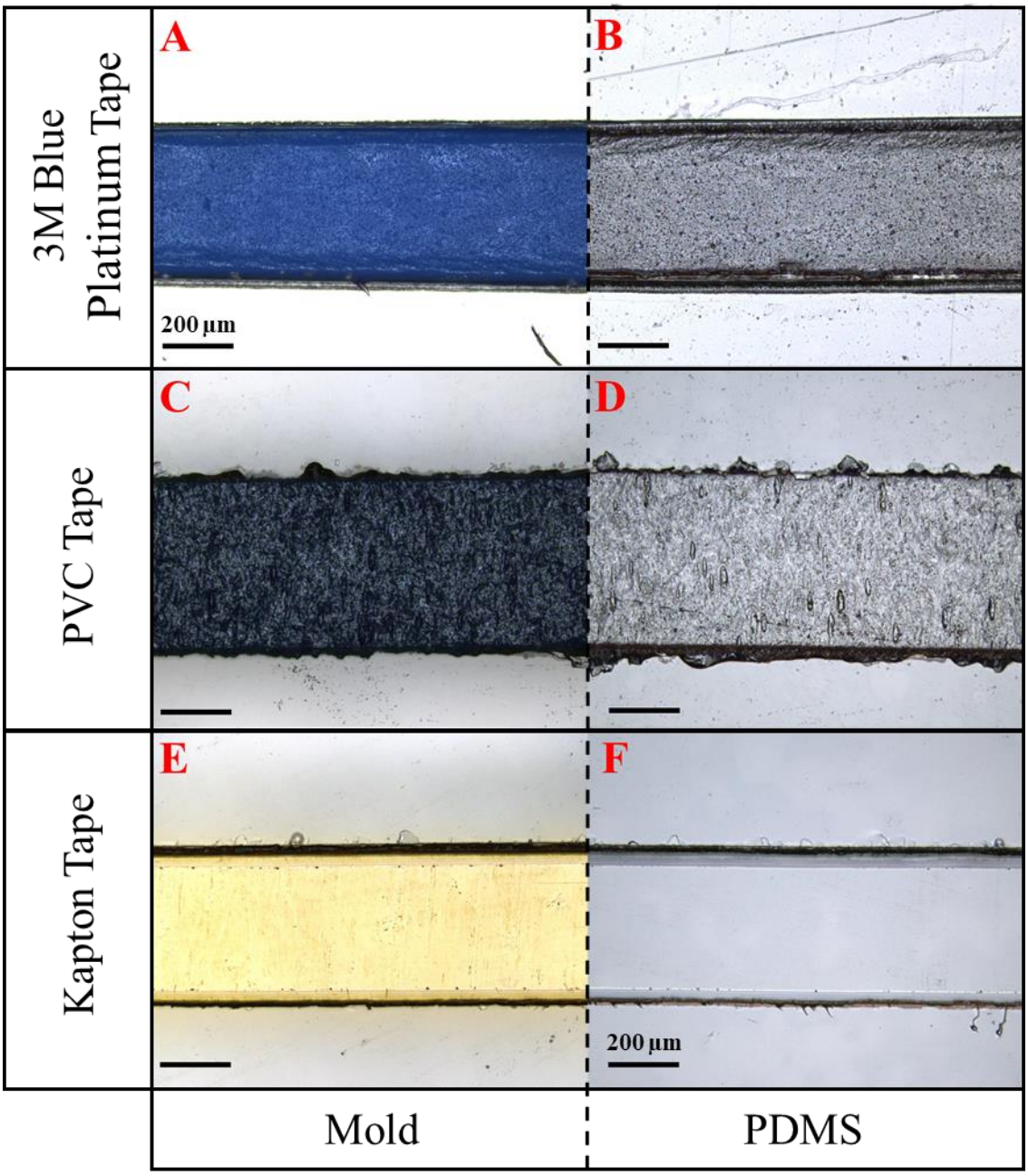

Figure 5-4 – Spiral dielectophoretic focuser images of A) the tape design cut by the sticker printer on a CATF and B) the final PDMS device filled with 5mM methylene blue.

Focusing of the 10 µm particles was observed as depicted in Figure 5-5. Particles initially entered the device from the inlet well with a random distribution across the channel (Figure 5-5a). However, upon travel through each successive loop, particles began to align by loop 2 (Figure 5-5c) and by loop 3 translate away from the inner wall of the channel towards the outer wall (Figure 5-5D). After travelling into the 5th loop of the spiral, particles focus into a single linear region following the contour of the outer wall as observed in Figure 5-5f. Videos of particle movement in the 1st, 3rd, and 5th loops are available in the publisher's website.

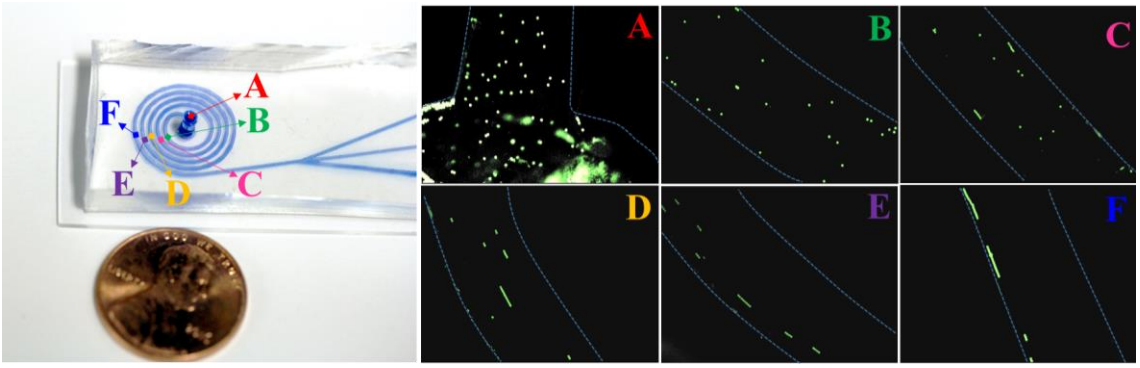

Figure 5-5 – Images of particle motion in a spiral dielectrophoretic focuser in (a) inlet well and entrance to the channel, (b) first loop, (c) second loop, (d) third loop, (e) fourth loop, and (f) fifth loop.

5.4.4 Electrophoretic Focuser

As a further proof-of-concept, a multi-T electrophoretic flow focuser was fabricated. A photograph of the tape mold of the electrophoretic focuser cut on a CATF backing is shown in Figure 5-6a, and Figure 5-6b shows the final PDMS device. The symmetric 6-

inlet device was designed to have channel widths of 400 µm and the average channel width of the final device in the horizontal direction was measured to be 495 ± 32 µm and 552 ± 46 µm in the vertical direction. The symmetric 6-inlet design was chosen to enable sheath flow using the first three channels and flow switching using the second set of three channels. Electrophoretic force is used to migrate the 200 nm polystyrene latex particles from the sample inlet towards a chosen outlet channel. The polymerization process of polystyrene nanospheres causes them to exhibit a slight negative surface charge in solution, enabling electromigration of polystyrene nanoparticles using electrophoretic force [208]. When the particles migrate out of the sample channel and into the first intersection, they are pinched by the electric field applied to the sheath wells. This causes the trajectory of the particles to deflect into a narrower flow profile.

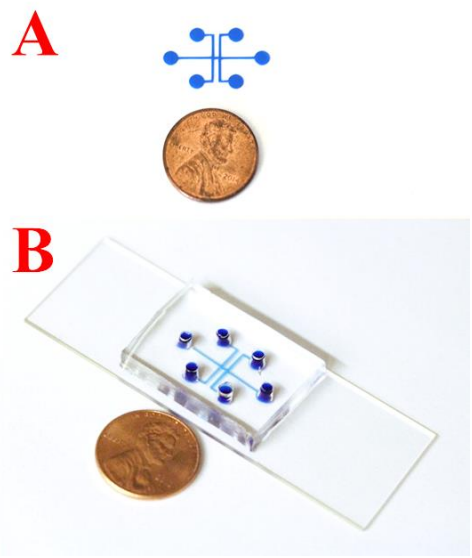

Figure 5-6 – Electrophoretic focuser images of (a) the tape design cut by the sticker printer on a CATF and (b) the final PDMS device filled with 5mM methylene blue.

Flow focusing of the nanospheres, as shown in Figure 5-7, is dependent upon the ratio of the potential applied to the sheath wells versus the potential applied to the sample well, where higher ratios yield narrower sample flow profiles. Still-frames from videos of each flow focusing condition are shown in Figure 5-7 and videos of flow focusing are available in the publisher's website. Potentials were applied as denoted in Table C-3, Appendix C to generate the flow focusing conditions depicted in Figure 5-7. At a 1:1 ratio, i.e. -200 V applied to sheath inlets and – 200 V applied to the sample inlet, a less focused (145 ± 4 µm wide) sample stream is obtained at that spans approximately one-third ($1/3^{rd}$) of the channel. When a larger 1.3:1 ratio, i.e. -260 V applied to sheath inlets and -200 V applied to the sample inlet, the sample stream is much more focused (19 ± 4 µm wide) and spans approximately one twenty seventh ($1/27^{th}$) of the channel. At the conditions tested, it was empirically observed that a ratio higher than 1.3 impedes sample flow.

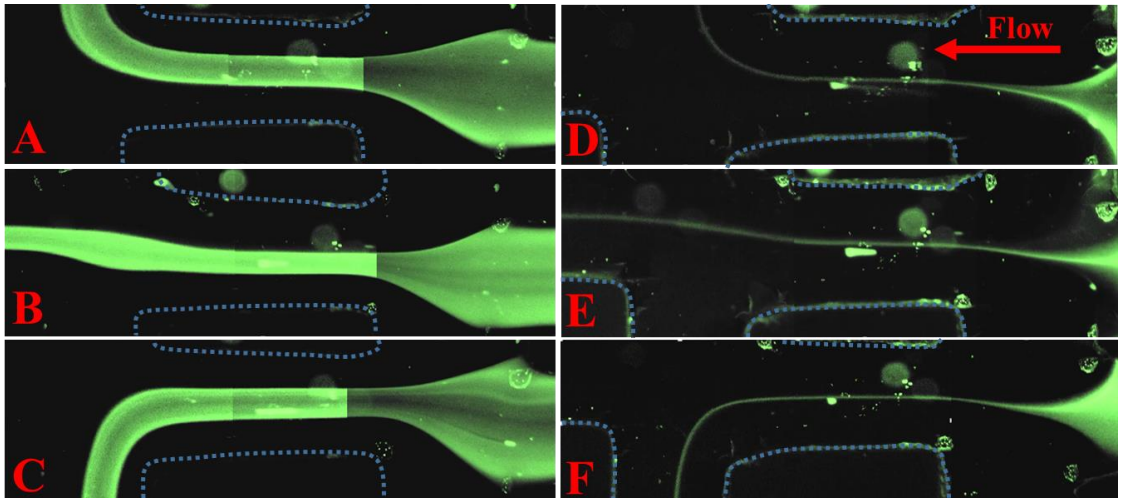

Figure 5-7 – Still-frames from videos of electrophoretic flow focusing at two different sheath flow ratios and flow switching with 200 nm polystyrene latex particles. (a) 1:1 sheath flow/ sample ratio with top output selected. (b) 1:1 sheath flow/ sample ratio with middle output selected selection. (c) 1:1 sheath flow/ sample ratio with bottom

output selected. (d) 1.3:1 sheath flow/ sample ratio with top output selected. (e) 1.3:1 sheath flow/ sample ratio with middle output selected. (f) 1.3:1 sheath flow/ sample ratio with bottom output selected. Blue dotted lines are shown to help visualize channel walls. Color variation is due to image stitching from video still frames with different saturation levels automatically compensated for by the video recording software.

5.5 Conclusion

A novel bench-top method for rapid prototyping of PDMS-based microfluidic chips using xurography in combination with microwave curing was demonstrated and characterized. This method significantly reduces time and monetary costs associated with microfluidic fabrication, uses inexpensive non-toxic materials, and avoids the use of cleanroom infrastructure. This method is ultra-rapid, producing high quality electrophoresis-grade PDMS-based devices (from CAD to complete microfluidic device) in less than 5 minutes. The most rapid PDMS curing was obtained in 90 seconds. This method represents the fastest fabrication process for PDMS microdevices to date. Electrokinetic focusing devices were demonstrated as a proof of concept, proving the utility of this fabrication method for applications with stringent quality requirements like electrophoresis. Consumable cost of this method is as low as $0.66 per device and startup cost is as low as ~ $300 (cost break down depicted in Table C-4 to Table C-6, Appendix C). Ultimately, this method has the potential to revolutionize PDMS-based microfluidic fabrication by yielding inexpensive microfluidic development at unforeseen speeds, firmly placing microfluidic development capabilities within the reach of researchers, classrooms and even hobbyists worldwide.

5.6 Acknowledgements

This research was supported by a fellowship appointment to NCS from the NASA Postdoctoral Program by the NASA Astrobiology Program, administered by Universities Space Research Association under contract with NASA, funding to NCS from NASA PSTAR program grant NNX16AL07G to PI B.E. Schmidt, as well as the Georgia Institute of Technology (Georgia Tech) and the State of Georgia, USA. The CNPq funding agency provided support via scholarship to GGM (Grant No. 205453/2014-7). We gratefully acknowledge Dr. Mina Georgieva (Georgia Institute of Technology) for her assistance with the statistics as well as Julianna McNeice for assistance with revisions. This work was performed in part at the Georgia Tech Institute for Electronics and Nanotechnology, a member of the National Nanotechnology Coordinated Infrastructure (NNCI), which is supported by the National Science Foundation (Grant ECCS-1542174).

CHAPTER 6. GREEN LOW-COST USER-FRIENDLY ELASTOMERIC (GLUE) MICROFLUIDICS – MAKING MICROFABRICATION CHILD'S PLAY

6.1 Abstract

Micro total analysis systems (μTAS) are highly attractive across numerous fields including science, engineering and medicine due to their portability, low power use and efficient sample and reagent consumption. Development of fully-functional microfluidic devices is based on iterative design and testing of multiple prototype microdevices, and the use of hazardous conventional microfabrication methods makes this iterative process resource-intensive and prohibitive for many users worldwide. Rapid prototyping techniques can alleviate these issues, enabling accelerated development of microfluidic structures at reduced costs, making this technology available to a broader user base, from classrooms to researchers in laboratories with limited resources. Here, we present a Green, Low-cost, User-friendly and Elastomeric (GLUE) rapid-prototyping method to fabricate custom master molds for polydimethylsiloxane (PDMS) based microfluidic devices, using an application of water-soluble poly(vinyl) acetate (PVAc) glue. The smallest features of

the molds are on the order of 80 µm wide, with tunable height control from 10 to 60 µm. This method is capable of fabricating three-dimensional features. As a proof-of-concept, several microfluidic devices ranging from a droplet generator to a lifting gate pneumatic microfluidic processor were fabricated to demonstrate the versatility and applicability of our method. To the best of our knowledge, this is the first rapid-prototyping process that can be used either as a Print-and-Peel method or as a scaffolding technique using the same process and patterning material. The simplicity and inexpensive nature of this application of PVAc glue can significantly improve the development of integrated µTAS devices, while also making microfluidics greener and accessible to researchers with limited resources and little to no experience in the field.

6.2 Introduction

The automation of all steps during chemical analysis (*i.e.* sampling, sample transport, sample pretreatment, separation and detection) in a single compact device has been envisioned since the 1990s, when Manz *et al.* first introduced the concept of miniaturized total analytical systems (µTAS) [1]. The development of these lab-on-a-chip (LOC) systems was boosted by the advancement of the microfluidics field [7], leading to applications ranging from genetic analysis [209] to field-deployable autonomous systems for in situ analysis [5,210]. The widespread use of microfluidic tools across multiple fields, however, has not yet become a reality [7] due to the resource-intensive facilities required to develop this technology [9].

Conventional microfluidic fabrication processes rely on standard microelectromechanical systems (MEMS) fabrication techniques [10] including photolithography, micromachining and chemical etching [10]; and on substrates of the silicon industry such as glass and oxidized silicon (Si/SiO_2) [8,9]. These time-consuming multistep procedures require highly trained personnel, specialized equipment and expensive cleanroom facilities, increasing the costs of microfluidic technology development [8,9].

A diverse selection of techniques were created to circumvent some of the characteristic issues of conventional manufacturing processes [211], with emphasis on the soft-lithography method created by the Whitesides Group in the late 1990s [14]. This method, in conjunction with the broad adoption of polymers such as polydimethylsiloxane (PDMS) [9], enabled the full development of microdevices within 24 h [14,75], considerably improving the fabrication turnaround times of microfluidic structures. However, the downside of these methods is the reliance on fabrication of master molds based on the carcinogenic SU-8 photoresist [14], which requires cleanroom facilities and trained personnel to perform lithographic and wet-etching processes [151,212]. These processes are inefficient, still incompatible with the iterative process that is microfluidic device development [8,164] and do not comply with the principles of green chemistry [98].

Rapid-prototyping methods to fabricate master molds for PDMS microfluidics have been created as alternatives to expensive photolithographic SU-8 mold production [151], enabling the development of μTAS at faster rates, reduced cost [8], and lower environmental impact. Print-and-Peel (PAP) techniques such as wax-printing [8,17], xurography [9,18] and laser-printing [16] are the most straightforward mold fabrication

methods, due to the direct deposition of the patterning agent on the substrate to create the positive relief mold [8,151]. Scaffold-removal mold fabrication methods [131,132], on the other hand, are multi-step procedures, where *1)* a sacrificial mold is generated, *2)* polymer is cured over the mold and *3)* the mold is dissolved by the use of an appropriate solvent system. These strategies do not require expensive cleanrooms to fabricate molds [8,9] and can be used by people with little to no experience in microfluidics, which is ideal for exploratory studies.

One of the first reported scaffold-removal fabrication processes produced of PDMS-based devices using 3D-printed acrylonitrile butadiene styrene (ABS) as the sacrificial material with acetone as the scaffold-removal solvent [132]. However, this approach has limitations, including: *1)* the use of an organic solvent to remove the scaffold generates chemical waste; *2)* the time required to dissolve the ABS mold in acetone (12 h) is quite long and prohibits truly rapid prototyping; *3)* the chemical incompatibility of PDMS and acetone causes swelling of the PDMS [70]; and *4)* the need for a high resolution 3-D printer may require a high initial investment.

To address some of these issues, Dahlberg *et al.* [131] developed a method to 3D print water-soluble poly(vinyl) alcohol (PVA) as the sacrificial material. The use of PVA eliminates the requirement for organic solvents to remove the scaffold material from the PDMS matrix, while reducing the time required to remove the sacrificial materials embedded in the devices (from 12 h to 2.5 h) [131]. However, this method still requires a high resolution 3-D printer, which increases the startup and operating costs of the process [9]. It is also worth mentioning that special care must be taken with the PVA printing filament, which must be dry-stored due to environmental water uptake, impacting the final

dimensions of the printed mold [131]. These limitations demonstrate the need for an improved water-soluble patterning technique.

The use of white glue as the material for microfluidic scaffolds and molds is attractive owing to intrinsic characteristics, including low-cost ($28 / gallon) and non-toxicity [213], which contrast greatly with toxic photoresists used in resource-intensive cleanroom environments [14]. The water-solubility of white glue also avoids the generation of organic solvent waste [213], in compliance with the principles of green chemistry [98]. These desirable properties of glue are due to its composition, reported elsewhere as a poly(vinyl acetate) (PVAc) emulsion [213].

Here, we present a Green, Low-cost, User-friendly and Elastomeric (GLUE) rapid-prototyping method to fabricate master molds for PDMS-based microfluidic devices, using water-soluble non-toxic white glue as the patterning material. The uniqueness of our method stems from several key innovations, specifically: *1)* the first direct use of a water-soluble PVAc emulsion, which does not require a UV exposure step to generate molds [139]; *2)* it does not require a 3D printer to fabricate molds [131,132]; *3)* it is, to the best of our knowledge, the first tested rapid-prototyping technique that can be used either as a Print-and-Peel method or as a scaffolding process, using the same patterning material and fabrication process; *4)* it has the ability to create multi-height molds in a single step, avoiding the use of multiple masks and time-consuming mask alignment steps, which are required in conventional lithographic processes [214]; *5)* it is compatible with microwave thermal processing of PDMS [8,9], unlike molds fabricated using conventional soft-lithography [14]; and *6)* the inherent low-cost of materials, comparatively green reagents, and equipment used in our innovative method, which provides microfluidic access to

researchers across the globe. All these characteristics make this method the only one of its kind.

In this paper, we characterize the unique aspects of our process and demonstrate its capabilities by fabricating PDMS-based microfluidic devices. These devices include diverse designs and applications, such as a Y-channel device, a droplet generator, a pneumatic pump and a microfluidic processor. The patterning agent was characterized using FTIR and ESI-MS. Two different methods, spin-coating and blade-coating techniques were demonstrated for fabrication of glue thin films with variable heights and these films were characterized using laser confocal microscopy. Subsequently, laser cutter resolution was characterized by measuring height and width of cut glue molds, and the utility of the raster function of the laser cutter was explored to fabricate multi-height glue molds in a single step. Mold reusability was evaluated by examining mold height and surface roughness. Finally, the use of glue films as molds and scaffolding materials were evaluated via fabrication of functional microfluidic devices, demonstrating the simplicity and utility of the GLUE method.

6.3 Materials & Methods

6.3.1 Reagents

Isopropyl alcohol and Alconox® Powder Detergent were purchased from VWR (Solon, OH); SYLGARD 184 silicone was purchased from Dow Corning® (Midland, MI). Corning™ plain microscope slides were purchased from Fisher Scientific® (Agawam,

MA). Food coloring dyes (McCormick®), water-soluble glue (Elmers Glue®) and soybean oil (Crisco®) were purchased from a local grocery store. PVC tape was purchased from McMaster-Carr (Elmhurst, IL). All reagents were used as received.

6.3.2 Mold Fabrication

6.3.2.1 Spin Coating

The water-soluble glue was deposited on a previously cleaned plain surface that was wetted using isopropanol (either a glass slide or a cured PDMS flat slab, Figure 6-1a). The glue was spun on the substrate using a spin coater (Figure 6-1b) with speeds varying from 900 rpm to 2400 rpm, in 300 rpm increments. After being deposited on the plain substrate, the water-soluble glue was cured in an oven for 10 min at 60 ^{o}C (Figure 6-1c) to form a thin film. For taller mold fabrication, the glue was deposited on the substrate, spun and cured before an additional layer was applied to the substrate.

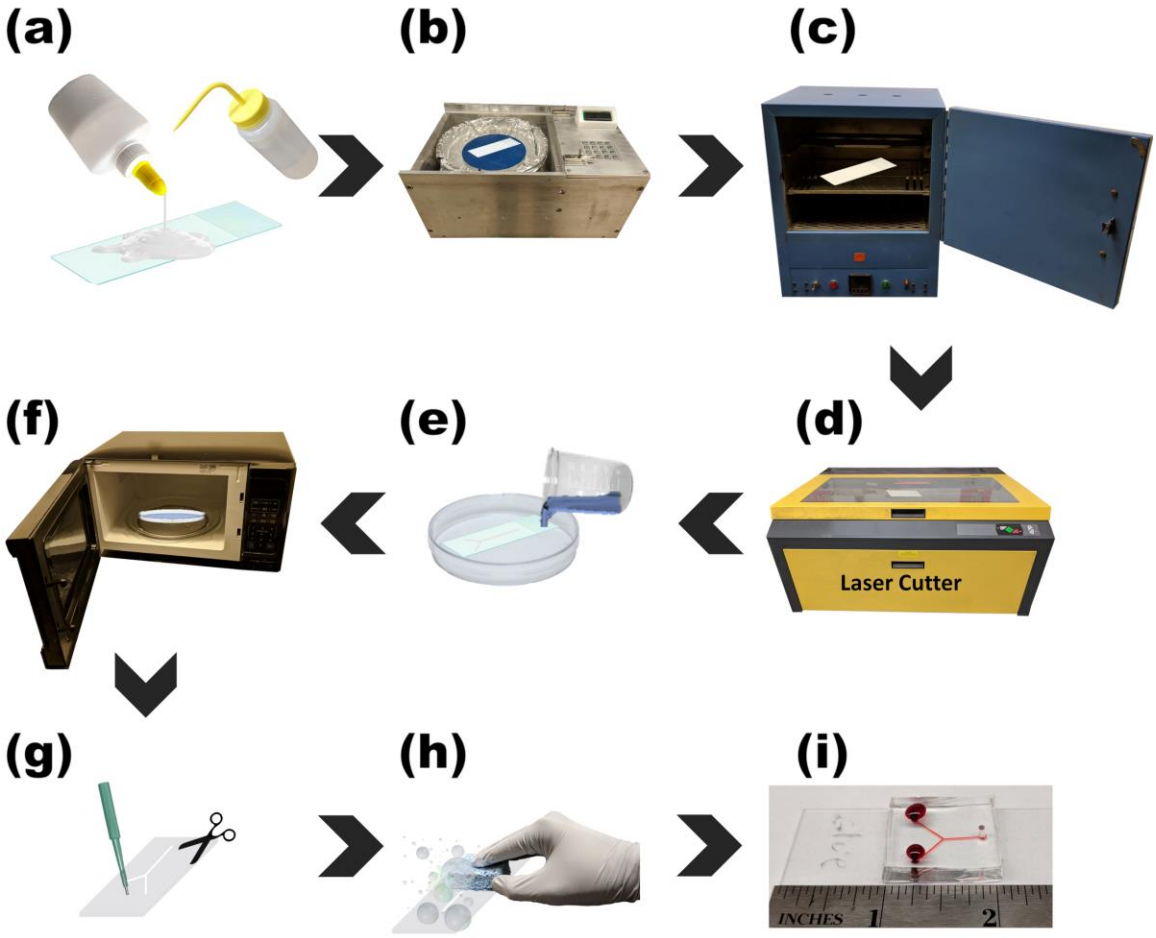

Figure 6-1 – Step-by-step fabrication of PDMS-based microfluidic devices using water-soluble glue scaffolding: (a) water-soluble glue deposition on a flat substrate with isopropanol wetting the substrate surface, (b) spin coating of the substrate with water-soluble glue, (c) curing glue in an oven, (d) pattern cutting using a laser cutter, (e) degassed PDMS pouring on the mold, (f) PDMS curing in microwave oven, (g) individual devices cutting and hole punching, (h) glue mold removal and (i) final functional device.

6.3.2.2 Lowest-Cost Mold Fabrication Method – Blade Coating

Glass slides and PDMS slabs were cleaned with an Alconox® solution, rinsed thoroughly with isopropanol and dried with lint-free Texwipes (Kernersville, NC) prior to use. PVC tape was adhered to the clean substrate with the aid of a flat edge tool (Figure D-

1a, Appendix D), which avoided tape wrinkles and the entrapment of air bubbles under the tape [9]. Squares were cut into the tape layer (Figure D-1b, Appendix D) using a Cricut Explore die–cutting machine / cutter plotter (Provo Craft & Novelty, Inc. Spanish Fork, Utah) and removed from the substrate with the aid of a scalpel (Figure D-1c, Appendix D) [9], leaving a tape border ~1 cm wide on the glass slide.

Water-soluble glue was deposited close to the tape edge (Figure D-1d, Appendix D) and was spread on the substrate surface with the aid of a flat edge tool, which was touching the tape edges but not the substrate (blade coating, Figure D-1e, Appendix D).The system was placed in an oven for 10 min at 60 ^{o}C to cure the glue (Figure D-1f, Appendix D). Taller molds were created by stacking multiple layers of tape on the glass substrate. For each additional layer of tape added to the mold, the curing time of the glue on the mold was increased 5 min to account for the extra glue added (15 min for 2 layers of tape, 20 min for 3 layers of tape).

6.3.2.3 Mold Cutting

If glass slides are used as substrate, a cutter plotter [9] (Figure D-2, Appendix D, Y channel and droplet generator) or laser cutter can be used to cut the molds; however, if PDMS is the substrate of choice, then the laser cutter method is required. Microfluidic device molds were designed using AutoCAD® software and cut into the previously prepared glue thin films using a CO_2 laser cutter (Universal VLS 6.60 CO_2 laser cutter, Figure 6-1d). Laser cutter settings were as follows for vector cuts of a single layer glue thin film: 10% laser power (PWR), 85% laser speed (SPD) and 1000 PPI resolution. For each

additional glue layer on the mold, the laser power was raised 5% to cut the desired pattern (2 layers, laser power: 15%; 3 layers, laser power: 20%). The excess water-soluble glue of the thin film was removed from the substrate with the aid of a scalpel, leaving the desired glue pattern adhered to the substrate. For multi-height mold fabrication, the glue on the substrate was etched using the raster engraving function of the laser cutter. To obtain variable heights on the glue mold, the laser power was kept at 12.5%, and the laser speed was varied from 40% to 70%, in 5% increments.

6.3.3 Device Fabrication

Two distinct methods were utilized to demonstrate versatility of the GLUE method for fabrication of single or multilayer microfluidic devices: 1) A non-bonding method which employs zero external bonding steps (i.e. ultraviolet ozone (UVO) or plasma surface treatment prior to putting surfaces in contact) [8,9] during device fabrication and 2) a bonding method which employs plasma cleaning prior to device bonding.

6.3.3.1 GLUE Non-Bonding Method

As a first step, a glue thin-film was prepared on a PDMS substrate as described in the Blade Coating section. Then the thin film was laser cut (20% PWR 85% SPD) and the excess glue film was removed to reveal the patterned glue mold. A mixture of PDMS prepolymer and curing agent (10:1 w/w ratio) which was previously degassed under vacuum [8], was cast on top of glue molds (Figure 6-1e) which were prepared on the PDMS

substrate. The PDMS was then cured either in a commercial microwave oven (GE, model JES738WJ, 700 W) at ~700 W for 5 min (Figure 6-1f) [8,9] or in a conventional convection oven for 3 h at 60 ^{o}C [17]. Individual devices were cut from the PDMS and fluidic access was enabled using biopsy punches (Figure 6-1g). After exposing the water-soluble glue inside the channels, the device was sonicated in a ultrasonic water bath (FALC LABSONIC LBS 1 - H3, Italy) with a warm Alconox® solution (60 ^{o}C) for an amount of time dependent on the device design to remove the glue scaffold from the PDMS channels (Figure 6-1h). Channels were flushed with DI water prior to use. If the glue pattern is deposited on a PDMS substrate, then no further processing is required, and the device is ready for use (Figure 6-1i).

6.3.3.2 GLUE Bonding Method

As a first step, a glue thin film was prepared on a glass substrate as described in the Blade Coating section. Then the thin film was either laser etched (20% PWR 85% SPD) or cut with a cutter plotter, and the excess glue film was removed to reveal the patterned glue mold. A mixture of PDMS prepolymer and curing agent (10:1 w/w ratio) that was previously degassed under vacuum [8] was cast on top of glue molds as depicted in Figure 6-1e. PDMS was cured as described in the GLUE Nonbonding Method section and then the PDMS membrane containing the pattern was peeled off the mold, and fluidic access was enabled using biopsy punches as depicted in Figure 6-1g. The patterned layer was subsequently washed with water and IPA, dried, and bonded to glass or PDMS using either

UVO or plasma bonding [8,9,68]. Glue molds created on glass substrates using the bonding method can be reused.

6.3.3.3 Proof-of-Concept Devices Fabrication

To demonstrate the versatility and applicability of the GLUE method, diverse proof-of-concept devices were designed and fabricated. Such devices comprise a Y-channel laminar flow device (Figure D-2a, Appendix D), a droplet generator (Figure D-2b, Appendix D), a pneumatic pump [119] (Figure D-3, protocol in Appendix D) and a microfluidic processor (Figure D-5, Appendix D).

6.4 Results & Discussion

6.4.1 Glue Characterization

The exact composition of Elmer's white glue is proprietary, as presented on the manufacturer's website [215]; however, spectrometric and spectral analysis (ESI-MS, Figure D-14, Table D-1 and ATR-FTIR, Figure D-15, Appendix D) suggests that this material is primarily composed of poly(vinyl acetate) and poly(vinyl alcohol). Poly(vinyl alcohol) (PVA) acts as a surfactant for poly(vinyl acetate) (PVAc) emulsions and is incorporated in the PVAc film [216]. This PVA incorporation is likely what confers solubility in water to the cured PVAc film because PVAc by itself is insoluble in water [217]. While both PVA and PVAc have been used separately as materials for molds in

microfluidic applications [131,139], only PVA has been used as a scaffold material [131], and PVAc has not been used as either a scaffolding material or a print-and-peel substrate. The use of the emulsion of the two (white glue) is new to this work.

6.4.2 Mold Characterization

6.4.2.1 Mold Cutting

Glue molds spun at different speeds were cut into crosses with channel widths ranging from 100 µm to 1000 µm, in 100 µm increments. These glue patterns were characterized using an Olympus® LEXT OLS4000 laser confocal microscope (Figure 6-2), to determine: *i)* the vertical (Figure 6-3a) and horizontal (Figure 6-3b) cutting resolution of the laser cutter, and *ii)* the height of the glue molds at different spin speeds (Figure 6-3c). The laser confocal microscope was also used to characterize glue molds that received multiple glue depositions (each layer of glue was spun at 2100 rpm) as well as to characterize PDMS channels generated from cast of these molds (taller molds, Figure 6-3d).

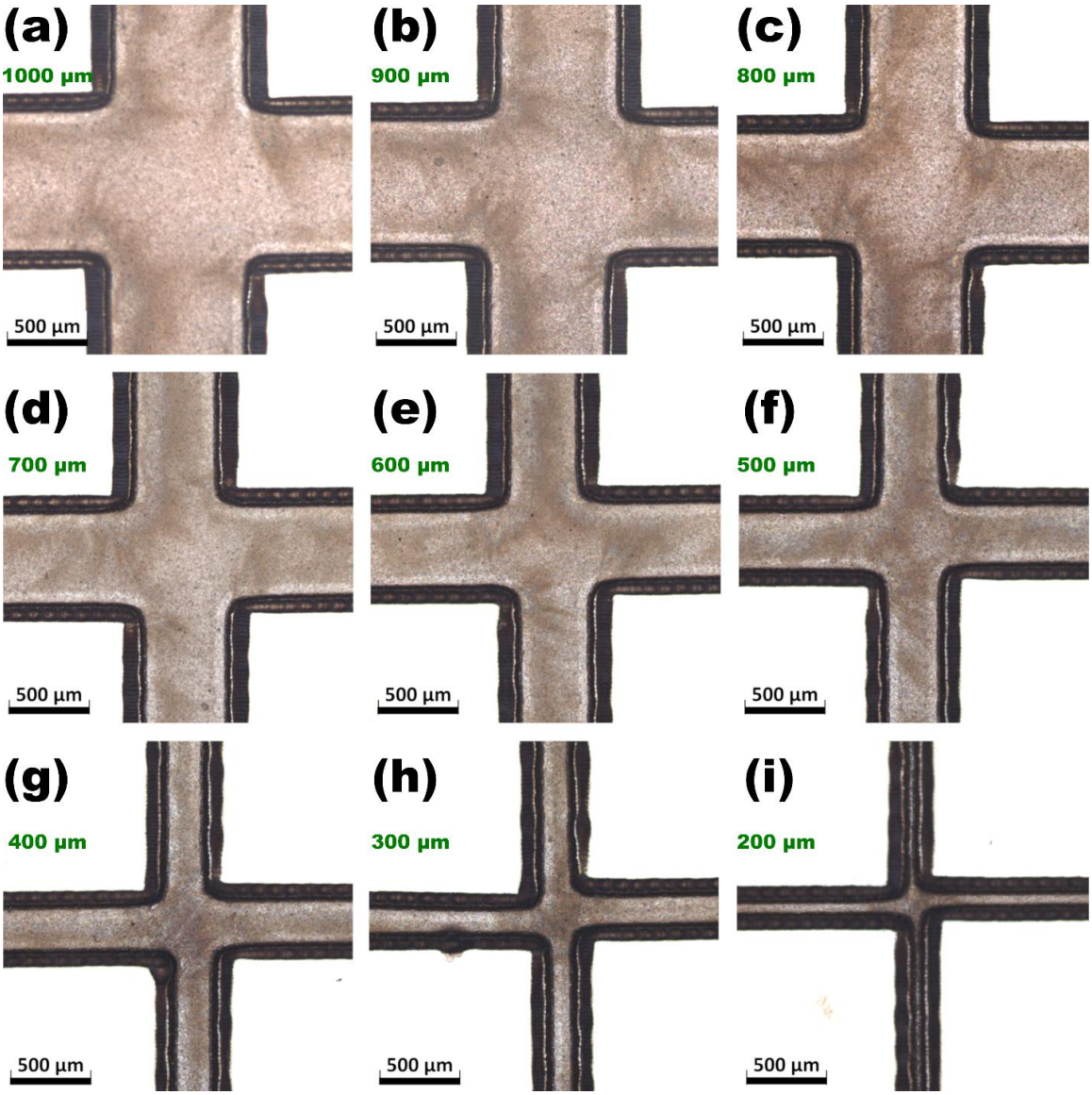

Figure 6-2 – Confocal micrographs of glue molds on PDMS cut into crosses with a laser cutter. Channel width designed to (a) 1000 µm, (b) 900 µm, (c) 800 µm, (d) 700 µm, (e) 600 µm, (f) 500 µm, (g) 400 µm, (h) 300 µm, and (i) 200 µm. The micrograph of the cross with 100 µm channel width is depicted in Figure D-16, Appendix D.

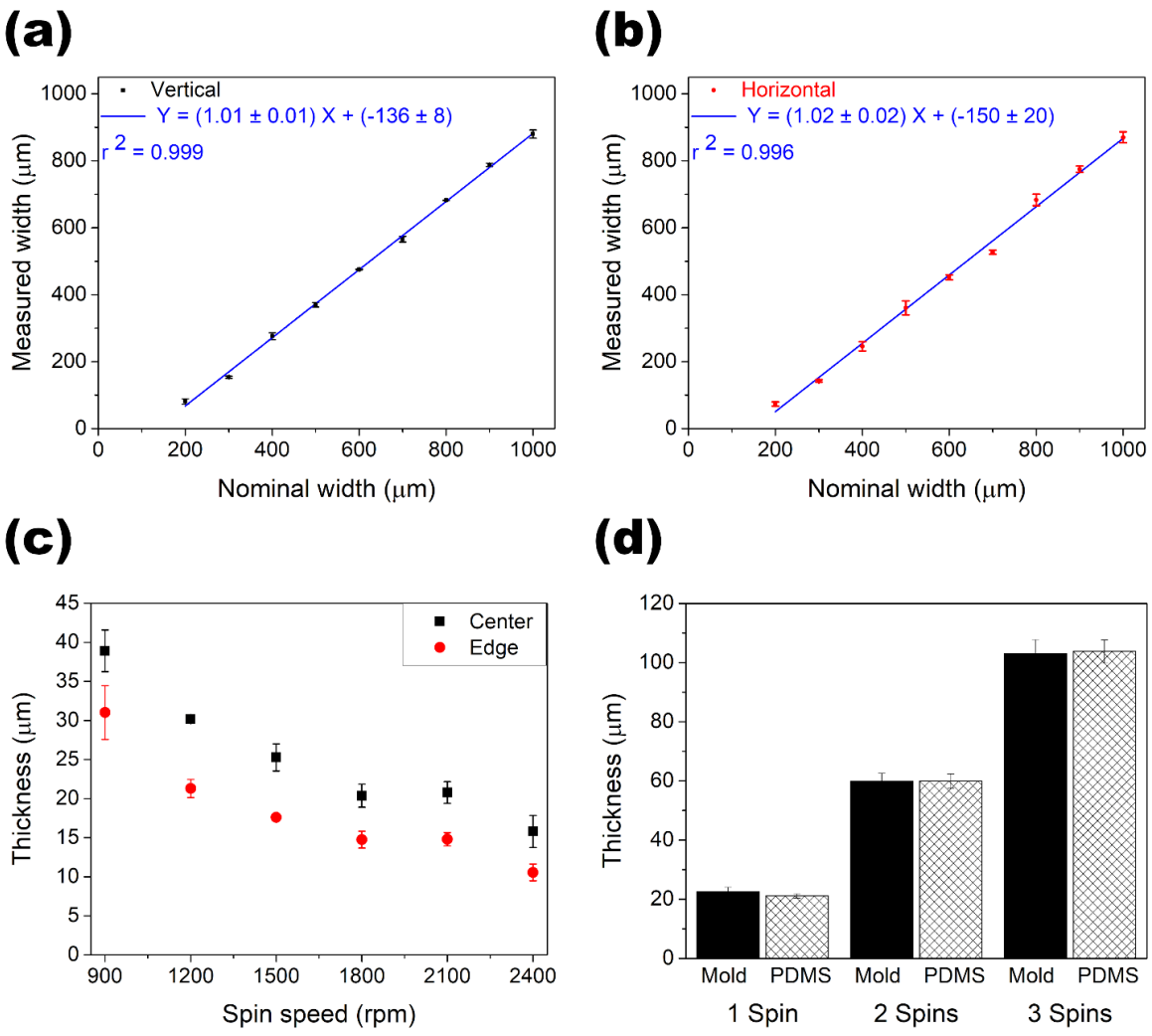

Figure 6-3 – Characterization of glue molds. Designed channel widths correlated with cut channel widths in (a) vertical cut orientation and (b) horizontal cut orientation. (c) Film thickness of glue molds spun on glass substrates at different speeds in the spin coater. (d) Film thickness for multiple glue applications on a glass substrate (all applications were performed at 2100 rpm) and height transfer to PDMS. The values in all plots represent the average of 3 measurements ± 1 standard deviation.

The measured width of the laser cut molds correlates linearly with the designed width for both vertical (Figure 6-3a, r^2=0.999) and horizontal (Figure 6-3b, r^2=0.996) cut orientations. There is not enough evidence to suggest a statistically significant difference between the vertical and horizontal cut orientations (*z*-test, confidence interval (C.I.) 95%,

Table D-2, Appendix D); there is, however, a statistically significant difference between the measured and nominal widths on the order of 100 μm (C.I. 95%, Table D-3, Appendix D). The smallest feature cut tested had a nominal width of 100 μm (Figure D-16, Appendix D), generating a channel width of 24 ± 9 μm in the horizontal orientation (vertical belt mechanism of the laser cutter), but as the nominal width was close to the laser cutter offset, it did not cut channels in the vertical orientation (horizontal belt mechanism of the laser cutter), ablating the glue off the substrate in that orientation (Figure D-16, Appendix D). Therefore, the devices designed for testing had minimum channel designs at least 200 μm wide.

The cutter plotter used in this work was characterized in a previous work [9], reaching minimum features of 300 μm wide. The cutter plotter method can only be used to cut designs on glue molds when glass is used as the backing substrate. When PDMS is used as the backing material, the blade of the cutter cuts through the glue thin film and reaches the PDMS under it. The flexible nature of PDMS allows the blade to drag the glue film from its original position and detach it from the substrate, precluding correct mold cutting. The laser cutter method does not present this issue and can be used in conjunction with either glass or PDMS backing substrates.

6.4.2.2 Spin Coating

The first method investigated to create glue thin films on substrate surfaces was spin coating. The thickness of glue films varies with the square root of the rotational speed of the spin coater chuck (Equation 8), reaching a plateau for values over 2100 rpm (Figure

6-3c). Spin speeds below 900 rpm were not capable of spreading the glue on the substrates (glass and PDMS) for the tested conditions, and therefore were not studied. There is a film thickness difference ~5 μm between the center and the edges of the glue film (Figure 6-3c), owing to the relatively high viscosity of this material (2850 ± 50 cP, Table D-4, Appendix D), which impacts the spin coating process [218]. The wettability of the substrate also affects the spin coating process [219] and, therefore, the thickness of the film spun on it. Glue films spun on glass are ~7 μm thicker than glue films spun on PDMS (Figure D-17, Appendix D) for the same experimental conditions owing to the lower water-glass contact angle ($\theta_{water\text{-}glass} = 20^o$), in comparison with the water-PDMS contact angle ($\theta_{water\text{-}PDMS} = 109^o$) [220].

The height of glue molds, and therefore the depth of the PDMS channels cast on them (Figure 6-3d, Table D-5, Appendix D), also changes with the number of glue applications spun on the substrate (Figure 6-3d), showing the versatility of this method.

6.4.2.3 Lowest-Cost Method

To enhance simplicity and reduce cost of glue film fabrication, a blade coating method was employed as described in the Blade Coating section and characterized. In this method, the thickness of glue films is directly related to the number of layers of tape adhered to substrate to create the tape border. The tape border defines the thickness and size of the final glue membrane (Figure D-18a, Appendix D), because it creates the reservoir that is filled with glue. For each layer of tape added to the substrate, the height of the glue membrane increases 18.4 ± 0.8 μm (Figure D-19, Appendix D), but the films did

not present a change in the surface roughness (Figure D-18b, Appendix D). There is no statistically significant difference between the surface roughness of glue molds fabricated using multiple layers of tape using the blade coating method and glue molds fabricated using multiple depositions of glue using the spin coating method (ANOVA, C.I. 95%, Table D-6, Appendix D). Notably, the thickness of glue films made using the blade coating method does not depend on the substrate used (Figure D-20 and Table D-7, Appendix D), which is an advantage over the spin coating method.

As an alternative approach, we tested an inverse xurography method [9], in which the desired design was cut into the tape on glass and removed from the mold, leaving a tape stencil on the glass substrate (Figure D-21c, Appendix D). Glue was applied to the mold (Figure D-21d, Appendix D), spread on the glass slide with the aid of a flat edge tool (Figure D-21e, Appendix D), and it was cured in an oven for 10 min at 60 ^{o}C (Figure D-21f, Appendix D). After curing, the tape was carefully removed from the glass substrate (Figure D-21g, Appendix D), leaving the glue pattern on the glass slide (Figure D-21h, Appendix D). This approach, however, does not generate homogeneous molds, owing to: *1)* air entrapment in the glue film at the tape edges (Figure D-22b,d,f, Appendix D) and *2)* bulging of the glue molds, the latter becoming more pronounced for taller molds (Figure D-22c,e, Appendix D). Because of our findings, the inverse xurography method was not further explored.

6.4.2.4 Multi-Height Molds

To assess the amenability of our method to fabrication of multi-height molds, the raster engraving function of the laser cutter was explored. The raster engraving function of the laser cutter machine enables the fabrication of glue molds with variable heights (Figure 6-4a), to be fabricated from a uniform thin film in a single step. However, there is a tradeoff between the fabrication of multi-height molds and the surface roughness of the mold: the use of the raster engraving function increases the surface roughness of the glue films, as quantified by the root-mean-square (RMS) of laser confocal profiles (Figure 6-4b). Surface roughness is on the order of approximately 3-5 microns for raster-etched regions as compared to the 2-micron surface roughness observed for the innate film. For 40% SPD, at 12.5% PWR, the glue is completely ablated from the substrate, which explains the lower surface roughness than the native glue film. For faster SPDs (45% to 70%), there is no statistical difference between the surface roughness of the films etched by the laser (Table D-8, Appendix D). The ablated surfaces presented an increased surface roughness when compared with the native glue film (Figure 6-4b, Table D-9, Appendix D).

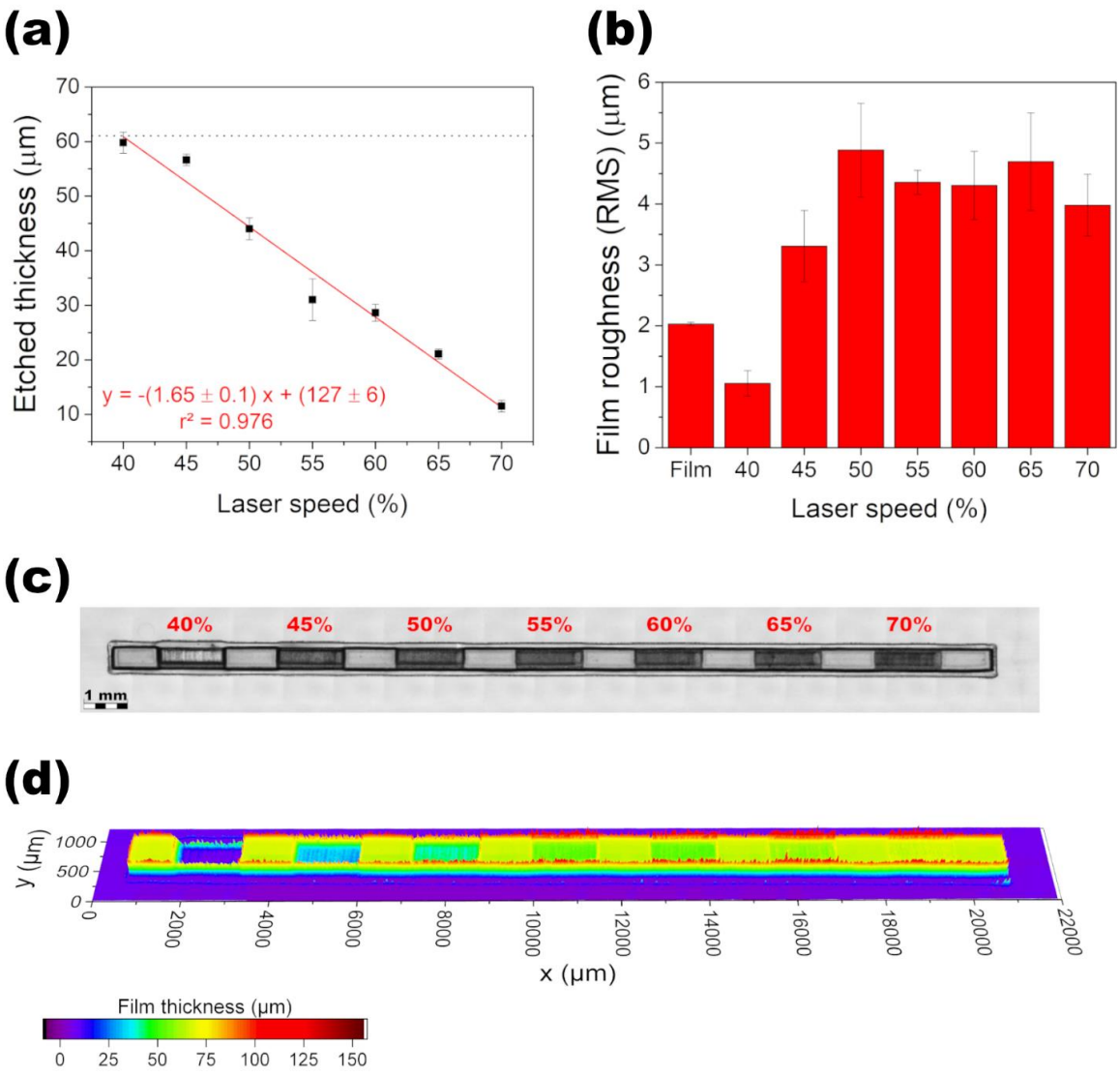

Figure 6-4 – Characterization of glue mold thickness after raster engraving. (a) Glue mold etched thickness as a function of laser speed. For each 10% decrease in laser speed the glue mold is etched ~16 µm further, accordingly to the best fit regression. The red line represents the linear regression of the data, and the dashed line represents the film thickness before etching. (b) Glue film surface roughness in terms of root-mean-square of laser confocal profiles. The values in all plots represent the average of 3 measurements ± 1 standard deviation. Glue molds were prepared using 3 layers of tape. Laser cutter settings were as follows: 12.5% laser power and 1000 PPI resolution, with variable speeds. (c) Laser confocal micrograph of a multi-height glue channel etched at different laser speeds in different positions. Laser speeds are showed in the picture. (d) Surface plot of the multi-height glue channel presented in (c). Film thicknesses thicker than 65 µm are due to optical aberrations of the laser measurement.

The fabrication of multi-height molds using conventional photolithography would require sequential spins of toxic photoresist on the substrate, baking and exposure steps, as well as the use of different masks and time-consuming mask alignment steps [214]. One of the biggest advantages of our method in comparison with other microfabrication procedures [9,14,17], is the ability to fabricate multi-height channels in a single step (Figure 6-4c,d), with no alignment required. Furthermore, by tuning the laser settings, virtually any mold thickness is achievable (between the height of the original glue film thickness and the bottom of the substrate), showing the versatility of our method. This is particularly promising for fabrication of microdevices with three dimensional features.

6.4.2.5 Mold Reusability

Despite the low-cost associated with the fabrication of individual molds ($0.52 / mold, Table D-10, Appendix D), mold reusability was evaluated in terms of mold height and surface roughness using the root-mean-square (RMS) of the laser confocal profiles of the glue molds (Figure 6-5). Due to excellent adhesion of the glue to a clean glass substrate, glue molds can be reused at least three times with no deterioration of features (further uses were not evaluated). There was no appreciable change in either mold height (Table D-11, Appendix D) or surface roughness (Table D-12, Appendix D) after 3 casts, demonstrating the robustness of this method.

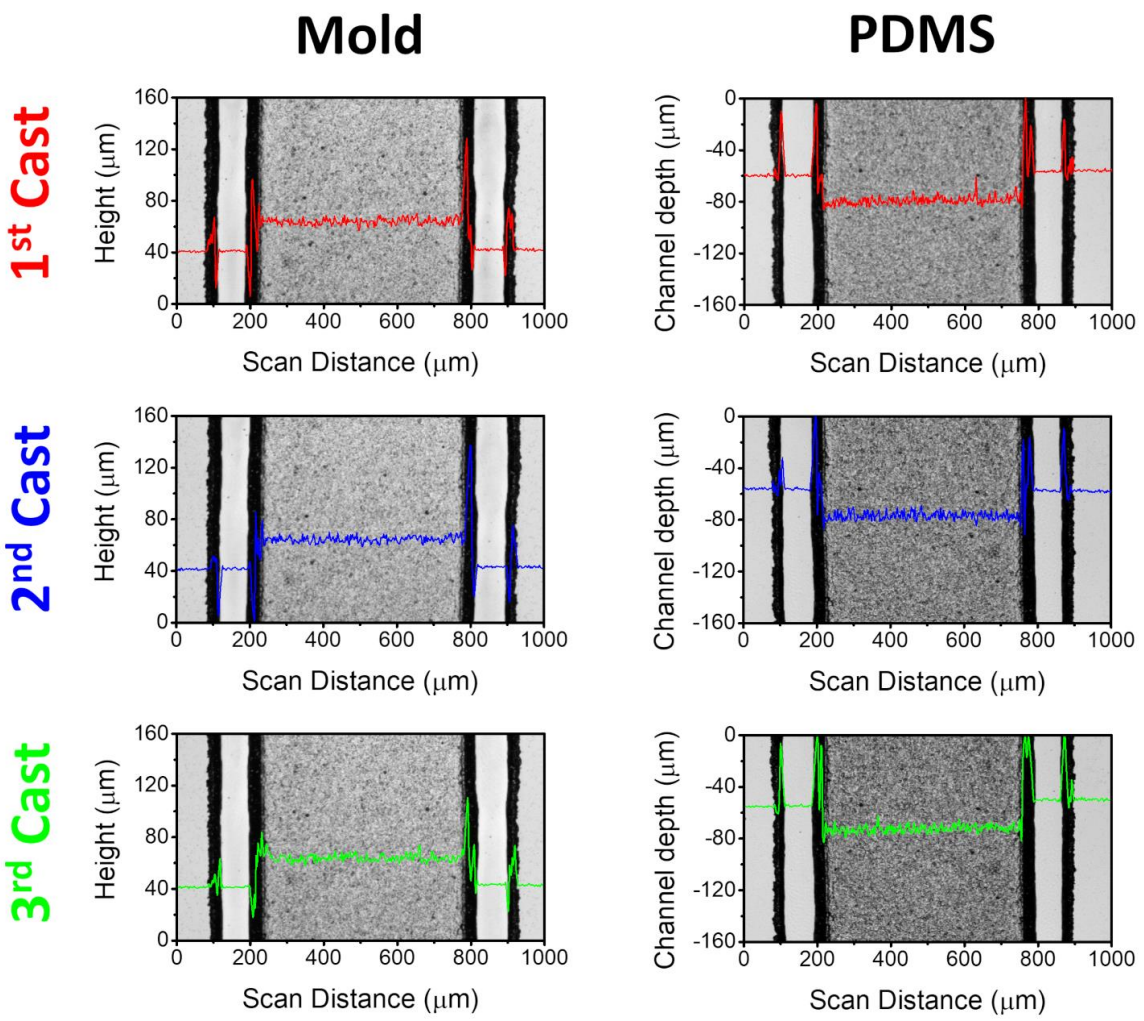

Figure 6-5 – Characterization of glue mold reusability. The laser confocal micrograph used for each measurement is depicted in the back of each plot. After each measurement, fresh PDMS was poured over the same mold and cured in a microwave oven. The average height and surface roughness of the features are: First cast: mold height = 22 ± 2 µm, mold rms = 1.9 ± 0.2 µm; PDMS channel depth = 21.2 ± 0.7 µm, PDMS rms = 2.22 ± 0.04 µm. Second cast: mold height = 21.4 ± 0.7 µm, mold rms = 1.84 ± 0.04 µm; PDMS channel depth = 21 ± 2 µm, PDMS rms = 2.47 ± 0.04 µm. Third cast: mold height = 21 ± 2 µm, mold rms = 2.0 ± 0.2 µm; PDMS channel depth = 20 ± 1 µm, PDMS rms = 2.2 ± 0.1 µm. The values represent the average of 3 measurements ± 1 standard deviation.

6.4.2.6 Channel Cleaning

When the glue film is deposited on PDMS to act as a scaffold for the channels, it is necessary to remove the glue enclosed into the channels after casting PDMS on them. Earlier work that utilized PVA-only scaffolding found that sonication with water alone required an extended time (150 min) to completely remove PVA in a typical device (height: 160 µm; width: 700 µm; length: 20 mm) [131]. To circumvent this issue, we combined sonication with the use of a warm (60 ^{o}C) Alconox solution (anionic surfactant) which aids in solubilization of PVAc and PVA [221], the majority components of the glue utilized here, to remove the glue scaffold from PDMS channels. This strategy enabled cleaning of PDMS channels with relatively high fluidic resistance (height: 51 ± 9 µm; width: 439 ± 9 µm; length: 10 mm) within 30 min, showing the efficiency of our approach. An increase in temperature did not provide better results: when the temperature was set to 90 ^{o}C, the PVA in the film started decomposing, becoming insoluble in water [221] and clogging the channel.

The cleaning time of scaffolded microdevices depends on: *1)* the design of the device, with lower times for devices with lower fluidic resistance; and *2)* if the channels are open in both ends (fluidic access to both inlet(s) and outlet(s)) or if the device contains only an inlet, without outlets, in which case the required time to clean the channels increases.

The biggest advantage of scaffolding methods is the elimination of the PDMS-substrate bonding step [14]. Scaffolding allows for the fabrication of microfluidic structures with larger blueprints, which would require large plasma cleaners that may not

be readily available; moreover, it also makes microfluidics more affordable for researchers without access to the conventional infrastructure required for microfabrication.

6.4.2.7 Scaffolding: PDMS-PDMS Devices

An essential component of multilayer soft lithography [117] is the integration and bonding of multiple layers of elastomer [127]. The most common approach is oxidation of PDMS surfaces with oxygen plasma [117,127], which are irreversibly bonded upon contact, leading to the obvious disadvantage of little room for error and thus misalignment [127]. Another common strategy is 'off-ratio bonding', in which individual layers are partially cured before bonding via a second thermal treatment to fully cure the polymer [83,127]. The biggest drawback of off-ratio method is that it requires the layers use different prepolymer to curing agent ratios, leading to different mechanical and optical properties of the individual layers [127]. Our method avoids the issues of both these methods, as it avoids the use of oxygen plasma and uses the well-established 10:1 ratio for all individual layers.

When making PDMS-PDMS devices using glue scaffolding, the laser cutter can ablate some of the PDMS substrate (Figure 6-6a), as well as creating valleys around the mold (Figure 6-6b). Pouring fresh PDMS on these molds fills these indentations (Figure 6-6c), creating a perfectly sealed channel (Figure 6-6d) after curing.

Using our microchip working pressure testing setup (Figure D-7, Appendix D), we tested the maximum working pressure that PDMS-PDMS devices fabricated using our

scaffolding-removal method could withstand. Devices with a hydrodynamic resistance of $(2 \pm 1) \times 10^{12}$ Pa s m^{-3} can withstand a working pressure of 170 ± 30 kPa at a flow rate of 14.2 mL min^{-1} without bursting (Figure D-23,Table D-13, Appendix D). That was the maximum flow rate setting of our syringe pump. Our results agree with the results presented by Lai *et al.* [127], and the advantage of our method stems from the fact that fresh PDMS was poured on a fully cured PDMS slab containing the glue mold, instead of a partially cured elastomeric membrane layer [127].

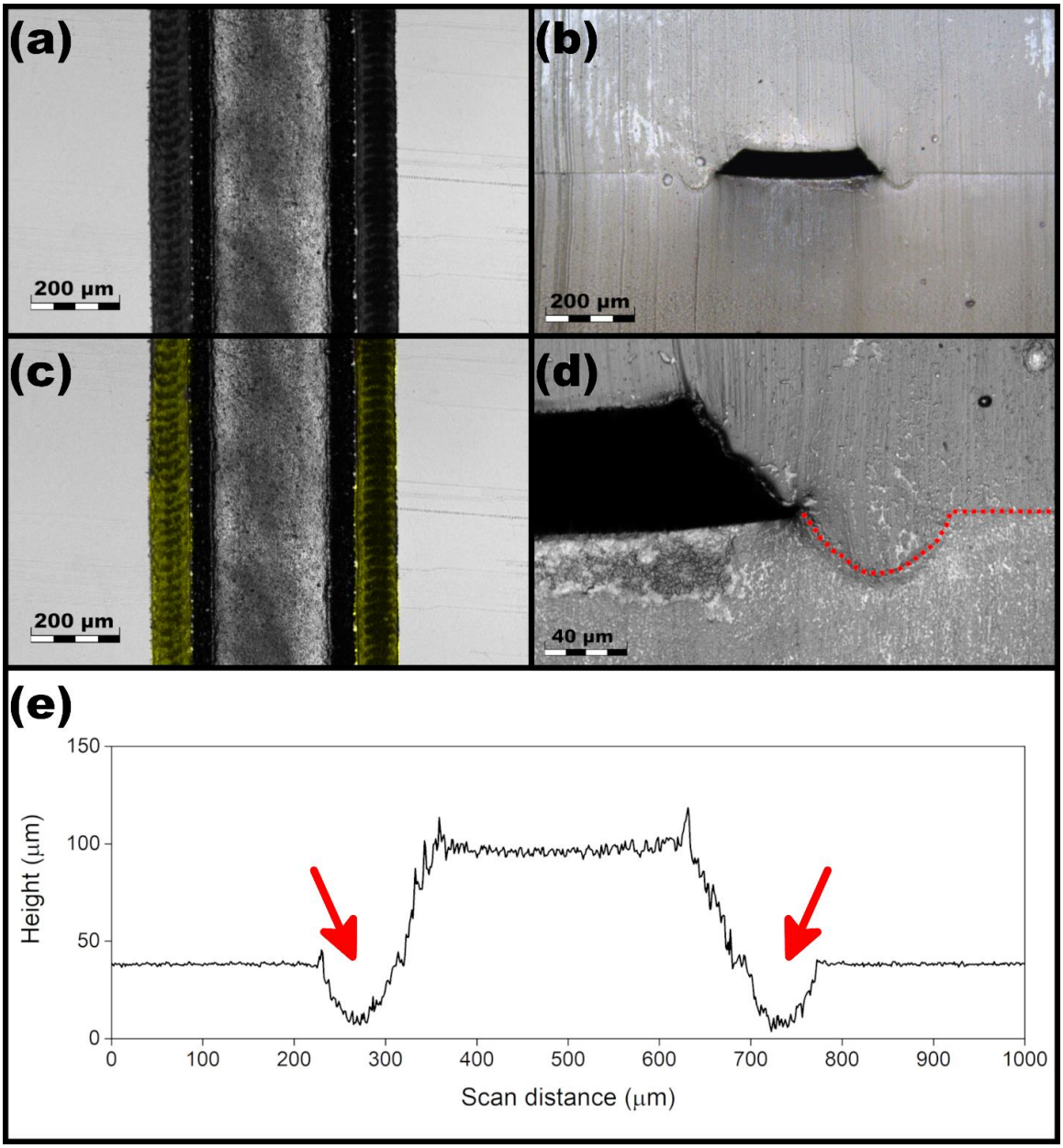

Figure 6-6 – Glue mold fabricated on a PDMS substrate. (a) Confocal micrograph of the glue channel cut on PDMS. (b) Laser confocal micrograph of a cross-section of a channel that was fabricated using the scaffolding-removal method. (c) Highlighted in yellow, PDMS ablated during the mold cutting process. (d) Interfacial zone between the PDMS slab containing the glue mold and the PDMS that was cured over the mold. The interface is marked with a red dotted line to ease visualization. (e) Profile of the glue mold. The red arrows indicate the indentation on the PDMS generated during the laser cutting process.

6.4.3 Proof-of-Concept Devices

To demonstrate the capability of this innovative use of white glue material in this method, we fabricated and tested microfluidic devices to perform common unit operations on chip, including a Y-channel laminar flow generator, a T-droplet generator, and even more complex multilayer structures, such as 3-valve normally open pneumatic pump and a 2x2 pneumatic lifting gate microfluidic processor.

6.4.3.1 Y-Channel Laminar Flow Generator

One of the characteristics of solutions in microchannels is laminar flow, which occurs at low Reynolds numbers [9], enables solutions to be combined with diffusional rather than turbulent mixing, and leads to many of the unique powers of microfluidics [11]. The most basic laminar flow generator combines 2 streams of solutions into a single stream using a Y-channel configuration, representing the simplest approach to observe laminar flow in a microdevice. Using Y-channel microchips, we compared PDMS-glass devices fabricated using a conventional SU-8 mold with devices fabricated using our innovative GLUE method by observing their ability to generate laminar flow (Figure 6-7a and in video recordings available in the publisher's website). The mold and microdevice used in this experiment are depicted in Figure D-2a and c, Appendix D.

It was possible to observe the interfacial region between water and black dye solution infused in both the SU-8 and glue devices, which demonstrates the lack of turbulent flow. Higher water flow rates displace the interfacial region from the middle of the microchannel towards wall of the microchannel. The color difference of the dye solutions in SU-8 and glue devices is due to the different channel heights (SU-8 mold: 70 μm tall, 500 μm wide; Glue mold: 17.7 ± 0.4 μm tall, 415 ± 3 μm wide), which changes the optical density [8].

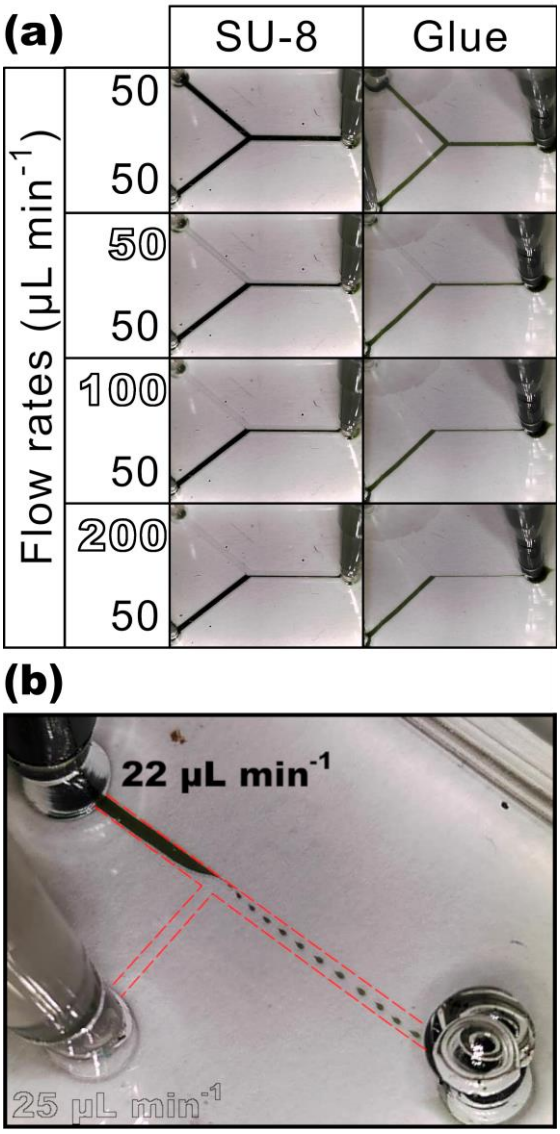

Figure 6-7 – Proof-of-concept microfluidic devices. (a) Y-channel laminar flow generator. On the left, a PDMS device cast on a SU-8 mold. On the right, a PDMS device cast on a glue mold. The devices fabricated by both methods exhibit laminar flow, evidenced by the lack of mixing at the interfacial region. Depicted in the figure are the flow rates of the solutions infused in each inlet using syringe pumps. Solid numbers represent the flow rate of a black dye solution, and outlined numbers represent the flow rate of DI water. (b) T-droplet generator. On the top left, a black dye solution in DI water pumped with a rate of 22 µL min^{-1}. On the bottom left, soybean oil pumped with a rate of 25 µL min^{-1}. Red lines are a visual aid to show channel wall positions.

6.4.3.2 T-Droplet Generator

The generation and manipulation of droplets is another characteristic application of microfluidics [7], with numerous examples in the biomedical field [222]. Droplet generator devices can have different geometries, but the most basic format uses a T-channel configuration, in which the continuous phase disrupts the flow of the disperse phase. Figure 6-7b presents a T-droplet generator with a continuous phase composed of soybean oil (infused at a rate of 25 μL min^{-1}) and a disperse phase composed of black dye in DI water (infused at a rate of 22 μL min^{-1}). The mold and microdevice used in this experiment are depicted in Figure D-2b and d, Appendix D.

6.4.3.3 Fluidic Handling Devices

A core requirement for development of μTAS is fluidic manipulation on chip, which is comprised of steps of fluid transport, i.e. routing and mixing in a programable and automated fashion [5]. The use of a series of monolithic microvalves can perform these tasks, but the fabrication of these devices using conventional methods typically requires multiple photo masks and photoresist application steps, as well as expensive cleanroom architecture [5]. However, using our GLUE method it is possible to build complex multilayer devices capable of performing all relevant fluidic manipulation steps on chip at a fraction of the cost and time required for use of conventional tools, besides not requiring the use of toxic reagents.

6.4.3.4 Fluidic Handling Devices

A core requirement for development of μTAS is fluidic manipulation on chip, which is comprised of steps of fluid transport, i.e. routing and mixing in a programable and automated fashion [5].

6.4.3.4.1 Pneumatic Pump

To demonstrate the simplicity of our method for fabrication of functional multilayer microfluidic devices, a 3-valve normally-open pneumatically actuated pump capable of fluidic transfer was fabricated utilizing a variation of the non-bonding method described in the GLUE Nonbonding Method section and depicted in Figure D-4, Appendix D. This method requires neither expensive cleanroom architecture nor bonding techniques, yet enables fabrication of a multilayer functional microfluidic pump. This is the first demonstration of such a feature with an inexpensive, cleanroom-free, water soluble, scaffolding method reported in literature. The pump design is comprised by three layers: a fluidic layer, a membrane layer, and a pneumatic layer. The design of the pneumatic pump is depicted in Figure D-3, Appendix D. Figure D-24, Appendix D, depicts the double chamber pumping routine, while Figure D-8, Appendix D represents the respective opening and closing valve sequence used in this experiment. Figure 6-8 depicts the effect valve actuation time has on pumping rate, agreeing with the results presented by Stockton *et al.* [119] using pumps fabricated by conventional tools. A range of pumping rates (64 ± 3 μL min^{-1} to 32 ± 3 μL min^{-1}) were achieved over the range of wait times (25 ms to 200 ms) tested, as demonstrated in Figure 6-8b.

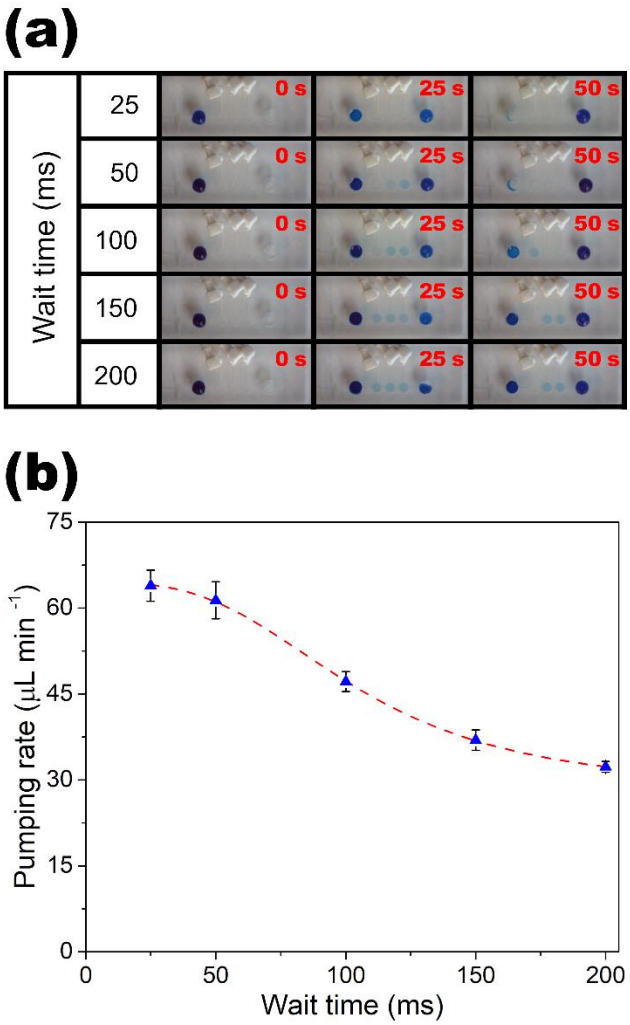

Figure 6-8 – 3-valve normally-open pneumatic pump. (a) Time-lapse images of pumping cycles using different wait times. (b) Plot of pumping rate vs. valve wait time. Error bars represent the standard deviation of 3 replicate measurements. The red dashed line is a guide for the eyes and does not represent a best fit curve.

6.4.3.4.2 Pneumatic Lifting Gate Microfluidic Processor

To demonstrate the intricacy and complexity that our method can achieve for fabrication of microfluidic devices, a lifting gate pneumatic processor was fabricated, and automated mixing was demonstrated (Figure 6-9). Pneumatic processors are powerful tools

for fluidic routing and capable of performing all types of metering and mixing operations needed to perform analyses on-chip [5]. The processor design utilized here comprised of a 2x2 configuration with 8 lifting gate valves, 4 I/O wells and a multilayer construction (fluidic layer, pneumatic layer and membrane layer). The design of the microfluidic processor is depicted in Figure D-5, Appendix D. Fabrication of the lifting gate processor demonstrated here was accomplished utilizing a variation of the GLUE-bonding method and depicted in Figure D-6, Appendix D.

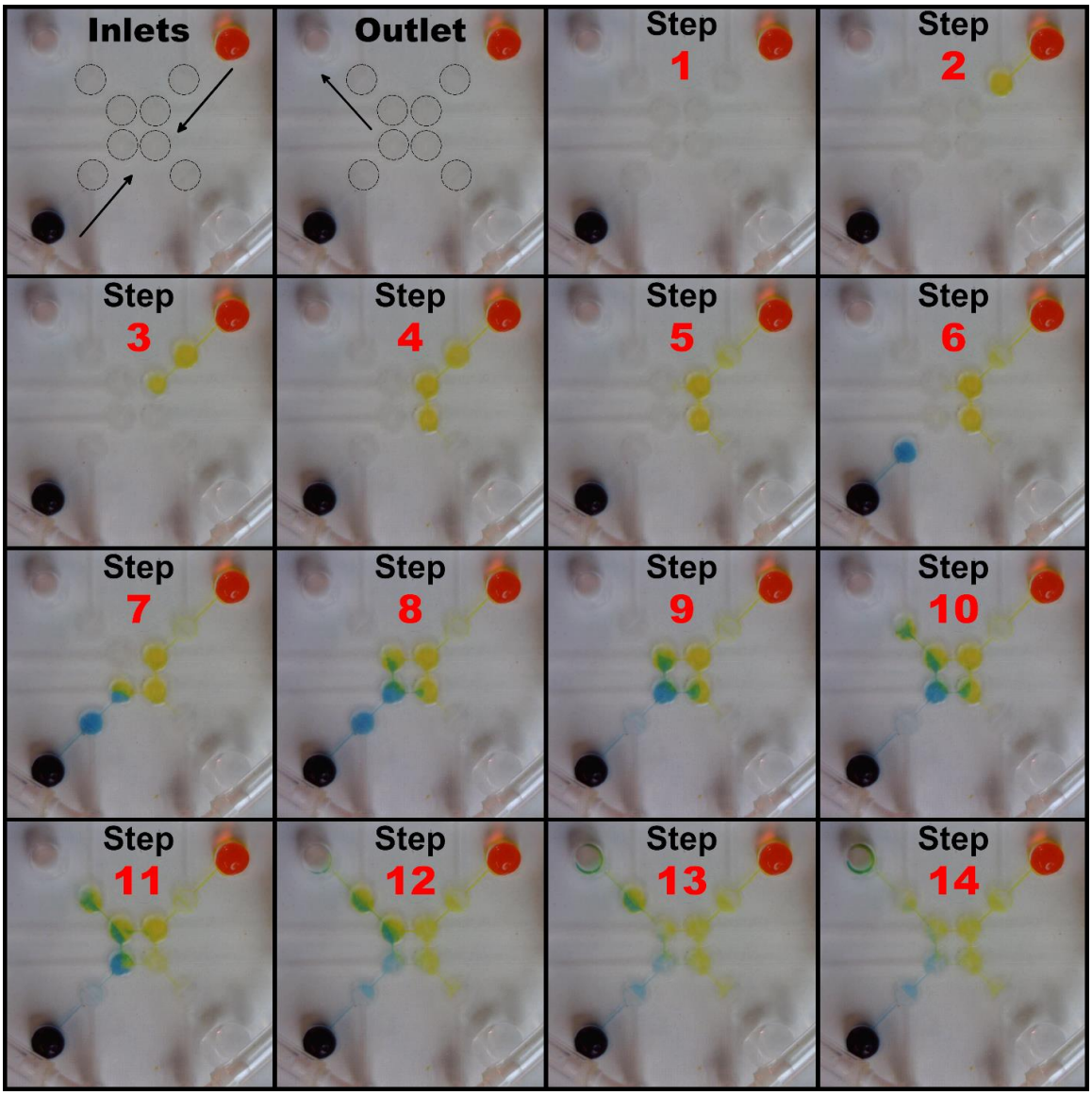

Figure 6-9 – 2x2 microfluidic processor used to perform a mixing routine. A blue dye solution and a yellow dye solution are transported, mixed and routed towards an outlet reservoir, generating a green mixture.

Functionality of the fabricated lifting gate processor was demonstrated by mixing yellow and blue dyes to create a green mixture. The fluidic manipulation schematics of the mixing routine and the respective opening and closing valve sequences used in this experiment are depicted in Figure D-9 and Figure D-10, Appendix D, while the fluidic

manipulation schematics of the cleaning routine and the respective opening and closing valve sequences used in this experiment are depicted in Figure D-11 and Figure D-12, Appendix D. The processor exhibited no leakage as evidenced by Figure 6-9 and Figure D-13, Appendix D, and video recordings available in the publisher's website, demonstrating optimal sealing function of the lifting gate valves, and a pumping rate of 90 ± 6 µL min^{-1} was achieved when filling the central processor for a 50 ms wait time.

6.5 Conclusion

The need for green and accessible tools to boost microfluidics development gave rise to our unique Print-and-Peel and scaffold-removal method to fast-prototype PDMS-based microfluidic devices. This bench-top technique uses white glue as the patterning agent to fabricate water-soluble master molds and was demonstrated and characterized, yielding minimum tested feature widths of 200 µm, with tunable heights. Another advantage of this unique patterning process is the amenability of the GLUE method for fabricating multi-height molds in a single step. The fabrication of such multi-height devices can boost the investigation of the development of neurons *in vitro* [96], without requiring mask alignment steps or sequential spins of hazardous chemicals to fabricate microfluidic molds. Furthermore, when used as a scaffolding method, the GLUE method eliminates the need for any bonding steps. The proof-of-concept devices fabricated with our process demonstrates the potential of this technology to create fully integrated µTAS. With an estimated cost of $0.52 per mold (Table D-10, Appendix D), this green and low-cost method does not require the use of toxic reagents nor cleanroom facilities. Our results

demonstrate that the GLUE process eliminates most barriers imposed by conventional microfabrication methods, giving researchers in resource-limited areas access to a powerful tool that will accelerate the development of fully functional μTAS. The simplicity and ingenuity of this method is such that it is child's play in comparison to the amount of rigor and difficulty required using conventional photolithographic fabrication techniques in cleanroom facilities. The intrinsic low-cost of the GLUE method coupled with the use of non-toxic materials enables its use as an educational tool to teach microfluidics, in settings such as grade school classrooms or to provide microfluidic access to hobbyists worldwide.

6.6 Acknowledgements

The funding agency CNPq (Science without borders, Grant No. 205453/2014-7) provided scholarship support (GGM). Research was supported by an appointment to NCS from the NASA Postdoctoral Program by the NASA Astrobiology Program, administered by Universities Space Research Association under contract with NASA. All work was done at Georgia Institute of Technology (Georgia Tech) with financial support from State of Georgia, USA. This work was performed in part at the Georgia Tech Institute for Electronics and Nanotechnology, a member of the National Nanotechnology Coordinated Infrastructure (NNCI), which is supported by the National Science Foundation (Grant ECCS-1542174). The authors would like to thank the Materials Innovation and Learning Laboratory at the School of Materials Science and Engineering at the Georgia Institute of Technology. We gratefully acknowledge Dr. Mina Georgieva (Georgia Institute of

Technology) for her assistance with the statistics, and Mr. David Bostwick (Georgia Institute of Technology) for his assistance with the mass spectrometric measurements.

CHAPTER 7. AN AUTOMATED LOW-COST MODULAR PLATFORM FOR VERSATILE MICROFLUIDIC DEVICE TESTING AND DEVELOPMENT

Reprinted (adapted) from "An Automated Low-Cost Modular Platform for Versatile Microfluidic Device Testing and Development" by Giorgio Gianini Morbioli, Nicholas C. Speller, Michael E. Cato and Amanda M. Stockton (2020). To be submitted to *Lab on a Chip*.

7.1 Abstract

The development of functional microfluidic devices requires multiple iterations of the design, fabrication and testing of an initial concept. Much attention in the literature has been given to improve the design of microdevices, and several rapid-prototyping techniques have been created to fabricate microfluidic structures in the past decade. However, little attention has been given to the testing phase of this iterative process, which is as crucial as the other steps. Testing results "make or break" a concept, therefore making it perhaps the most important phase in design iteration. Conventional approaches to test microdevices typically require fixed mounts as testbeds, which are usually machined in hard substrates and do not allow for rapid modifications. This, in turn, limits alterations in the design of microfluidic devices, imposing an unnecessary constraint in the iterative development cycle. To alleviate these issues, we present here a new approach to test microfluidic devices by using modules. The modular system contains hardware that can be

rapid-prototyped, if needed, speeding up the testing of devices without imposing restrictions on the design of devices. Another innovation presented here is the creation of an open-source automated computer application to automate fluidic manipulations in Programmable Microfluidic Arrays (PMAs), which also aids in the testing of microfluidic devices. This application, written in Python, only requires from the user the positioning of reservoirs containing reagents, their mixing ratios and the output reservoir. This work decreases the development time and resources required to make functional microfluidic devices, at lower costs, which is an advancement on conventional approaches.

7.2 Introduction

In the early 1990s, Manz *et al.* [1] first presented the concept of miniaturized total chemical analysis systems (μTAS): systems capable of performing macroscale analytical processes, but in an integrated microstructure [1]. This ideal microsystem would perform all analytical steps in an automated fashion, with a better performance than conventional macroscale tools [1], due to intrinsic characteristics of miniaturization that include low reagent and sample consumption, and therefore low waste generation [8,9,19], lightweight and portability [54], with improved separation performance [1]. These appealing characteristics make these miniaturized analytical devices attractive to multiple areas, including bioanalytical chemistry [53], clinical chemistry [3] and separation science [54,55], among many others.

Although these Lab-on-a-Chip (LOC) devices present many advantages over conventional macroscale systems, they are not widely adopted yet [7]. In 2006, George

Whitesides posed this question: “Why is every biochemistry laboratory not littered with ‘labs on chips’?” [7]. One response is the machinery required to operate these devices, meaning that instead of labs-on-a-chip, we end up with chips-in-a-lab, at significant economic costs. The development of fully functional microfluidic devices, core to the attainment of true μTAS, is expensive in nature [14].

Microfluidic devices initially were fabricated on glass or silicon substrates using conventional fabrication methods borrowed from the electronics and microelectromechanical systems (MEMS) industries [9,10], such as micromachining, etching and photolithography. These microfabrication techniques require multiple steps to be completed, which are performed by skilled professionals in high-maintenance cleanroom environments [9], which leads to the high-costs associated with the development of this technology. Alternative methods to fabricate microfluidic devices can alleviate most of the issues associated with the use of conventional fabrication techniques, with special emphasis on fast-prototyping tools [223]. Rapid-prototyping methods have been used extensively in other technological fields, such as the automotive and the aerospace engineering sectors [165], but have carved their way into the microfluidics field in the past two decades [223].

The first ‘rapid-prototyping’ methods to fabricate microfluidic devices reported in literature date back to the late 1990’s, when the Whitesides Group at Harvard University first reported what came to be known as soft-lithography [14], which resulted in the popularization of the now ubiquitous poly(dimethyl siloxane) – PDMS [223]. Since then, rapid prototyping of PDMS-based devices has led to device fabrication turnaround times

as low as 5 min [9], with molds created by wax printing [8], xurography [9] and the Green, Low-cost, User-friendly Elastomeric (GLUE) method [19].

The prototyping of microfluidic devices is only one of the steps in the development of functional microfluidic devices, which is an iterative process requiring: *i)* the design of the structure, *ii)* the fabrication of the device, and *iii)* the testing of the fabricated prototype [223]. Much of the work dealing with the development of microfluidic devices has been focused on device fabrication [8,9,15,17,19,131,142], but less attention has been given to the other steps, particularly the testing phase. The testing phase is the litmus test for the functionality of a device: if the device does not fulfil its requirements, then iterations become necessary until the desired outcome is achieved. Alterations in the microfluidic device design are the first modifications to be performed in this iterative process, but there is a disconnect between the design of the device itself and the testbed used during the testing phase.

The most common testing mounts are machined and drilled in hard substrates [224], requiring a skilled person to operate fabrication machinery, and require several hours or days for fabrication. Once fabricated, these rugged systems can be used to test several devices. However, conventional manifold assemblies are chip-specific, due to the positioning of pneumatic and fluidic connections, limiting the use of the testing system. This adds time and cost to the development of microfluidic devices if major alterations are needed, because of the need to modify or rebuild monolithic structures. Ideally, manifold design would not interfere with the design of the microfluidic chip, and therefore allow for rapid modifications. This is particularly true when fast-prototyping methods to fabricate

PDMS chips are used, in which the manufacture time of devices are within the one-hour range [8,9,19].

Simple devices structures, such as a 2-inlet gradient generator or Y-channels [8], do not require complex mounts to be tested. More complex structures, however, would require multiple connections with external equipment [122], increasing the complexity of the testbed design. This is the case for Programmable Microfluidic Arrays (PMAs), also known as microfluidic processors [5]. PMAs are multilayered devices containing microfluidic valving components, capable of performing different fluidic operations on-chip, including pumping, mixing, dilution and delivery [225]. The automation of these fluidic operations is what makes sample handling on-chip possible [225]. Monolithic elastomeric microfluidic valves are the heart of PMAs. They are fabricated by sandwiching a flexible elastomer membrane between two surfaces, with fluidic and pneumatic features. The positioning of features is system dependent, depending on if the valves are normally-open, normally close or lifting-gate structures [181,225]. When three (or more) valves are connected, it is possible to actuate them in sequence, forming a peristaltic pump [225], making fluidic manipulations on-chip possible [225]. To operate microvalves, the use of external support system are required, like solenoid valves for pneumatically actuated systems [119,181], or pistons, for hydraulically actuated systems [118].

PMAs expand the use of microfluidic devices in different arenas, such as genetic analysis [226] or clinical chemistry [227], but they lend their true power to field-deployable remote analytical systems, like the autonomous Mars Organic Analyzer [5]. One of the shortcomings of PMAs, however, is the need for the manual coding of valves, in terms of

‘open-close-wait’ instructions [224]. A more rugged approach is the automation of the routines, with minimal inputs from the user.

In this paper, we present a modular approach to alleviate problems in the testing of microdevices, integrating the steps of the iterative development process of microfluidic devices. We first present the advantages a modular system present over a conventional testbed. We also present a low-cost alternative to use active pumping components on-chip operated by solenoid valves, by substituting commercial Data Acquisition systems (DAQs) for an Arduino microcontroller, for a fraction of the price. Finally, we present an automated computer application to automate programming of fluidic routines in programmable microfluidic arrays. Our innovative approach improves the development of microfluidic devices by enabling a rapid testing of devices and automating PMAs programming and reprogramming. The low-cost of the components, coupled with an open-source code to operate fluidic devices gives students and researchers worldwide access to the microfluidics field, which was once confined into expensive cleanroom environments [9,19].

7.3 Materials & Methods

7.3.1 Materials

PVC tape, acrylic sheets, PVC clear tubing (i.d. 1/8” and 1/16“), 304 stainless steel round tubes, and Tygon® tubing were purchased from McMaster-Carr (Elmhurst, IL). 12 V vacuum pumps (Karlsson Robotics, Tequesta, FL) and 1/5 HP air compressor (China)

were obtained from Amazon. Arduino® MEGA microcontroller board was purchased from Arduino (Italy). Resistors, transistors, LEDs, capacitors, breadboards and jumper wires were purchased from Digi-Key electronics (Thief River Falls, MN). Solenoid valves and face mounts were purchased from The Lee Company (Westbrook, CT). Epoxy glue (Gorilla Glue, Cincinnati, OH) and water-soluble glue (Elmers Glue®) were purchased from a local retailer.

7.3.2 Reagents

Isopropyl alcohol and Alconox® Powder Detergent were purchased from VWR (Solon, OH); SYLGARD 184 silicone was purchased from Dow Corning® (Midland, MI). Corning™ plain microscope slides were purchased from Fisher Scientific® (Agawam, MA). Food coloring dyes (McCormick®) were purchased from a local grocery store. All reagents were used as received.

7.3.3 Manifold fabrication

A manifold to comport rapid-prototyped microfluidic devices was designed in SolidWorks® (Figure 7-1, blueprints in SI). The polymeric main body and the base were machined in Delrin® acetal rods using a Harrison M300 lathe, and the polymeric pneumatic connection was laser cut in an acrylic sheet (1/8 inch thick) using a Universal VLS 6.60 CO_2 laser cutter. Stainless steel tubes (outer diameter: 1.73 mm; wall thickness: 0.178 mm)

were cut in tubes of length ~1.2 cm and glued to the cut acrylic sheet using an epoxy glue, which enables the sealing between the PDMS microchip and the pneumatic connectors.

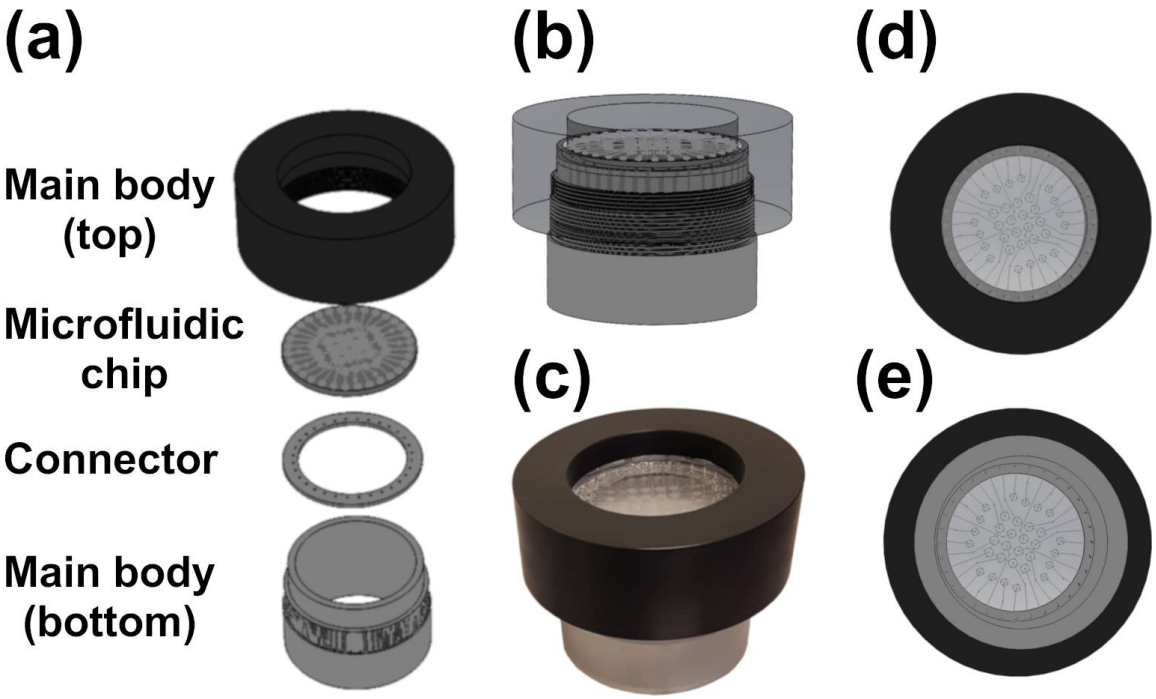

Figure 7-1 – Microfluidic manifold to house rapid-prototyped microfluidic devices. (a) Manifold modular components in an exploded view. (b) Solid model of assembled modular system (side view). (c) Photograph of assembled modular system (side view). (d) Solid model of assembled modular system (top view). (e) Solid model of assembled modular system (bottom view).

7.3.4 Electronic circuit to operate solenoid valves

An electronic circuit to operate the solenoid valves and their housing were designed in SolidWorks® (Figure 7-2). The electronic components were soldered into a protoboard (circuit in SI) and the housing parts were laser cut in an acrylic sheet (1/4 inch thick) using a Universal VLS 6.60 CO_2 laser cutter. The solenoid valves were screwed into the face

mounts, soldered into the breadboard and the whole stack was placed inside the acrylic housing. An Arduino microcontroller board was placed on the bottom of the housing, and each solenoid was connected to a different pin on the board (Table E-1).

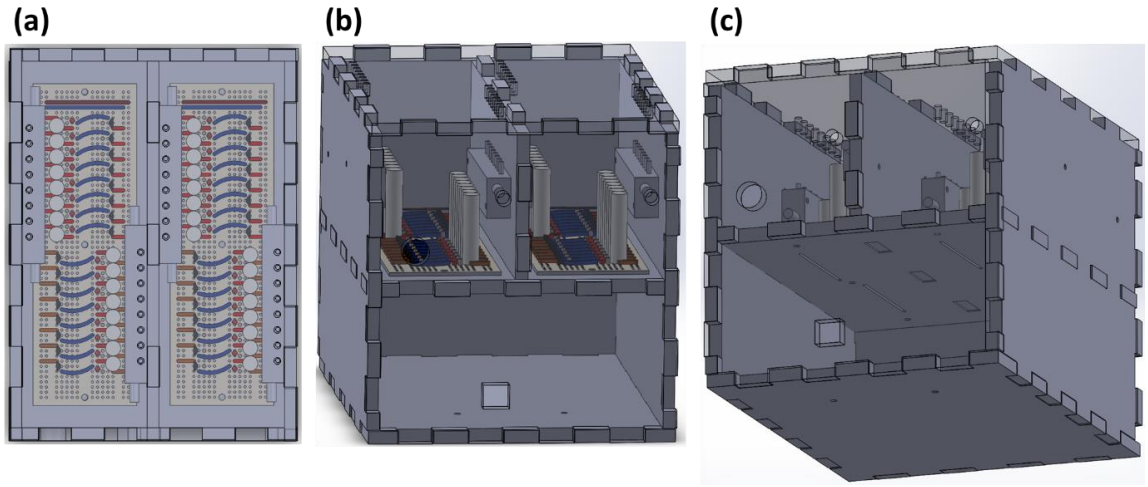

Figure 7-2 – Electronic circuit and its housing to operate the solenoid valves. (a) Top view of the housing with the protoboards and the solenoid valves. (b) Isometric view of the housing, with emphasis on the bottom, which stores the Arduino microcontroller board. (c) Isometric view of the housing, showing holes for connections of the solenoid manifolds to vacuum tubing.

7.3.5 Program to automate fluidic manipulation

A program to automatically generate fluidic operations on chip was written in Python (code available in GitHub). This program accepts as parameters: *i)* the input reservoirs and *ii)* the volume of fluid from the input reservoirs, in terms of number of valves used (Figure 7-3a); *iii)* the output reservoir (Figure 7-3b); *iv)* the valves to be avoided – if

any (Figure 7-3c), and *v)* the wait time between valve actuation between steps (Figure 7-3d).

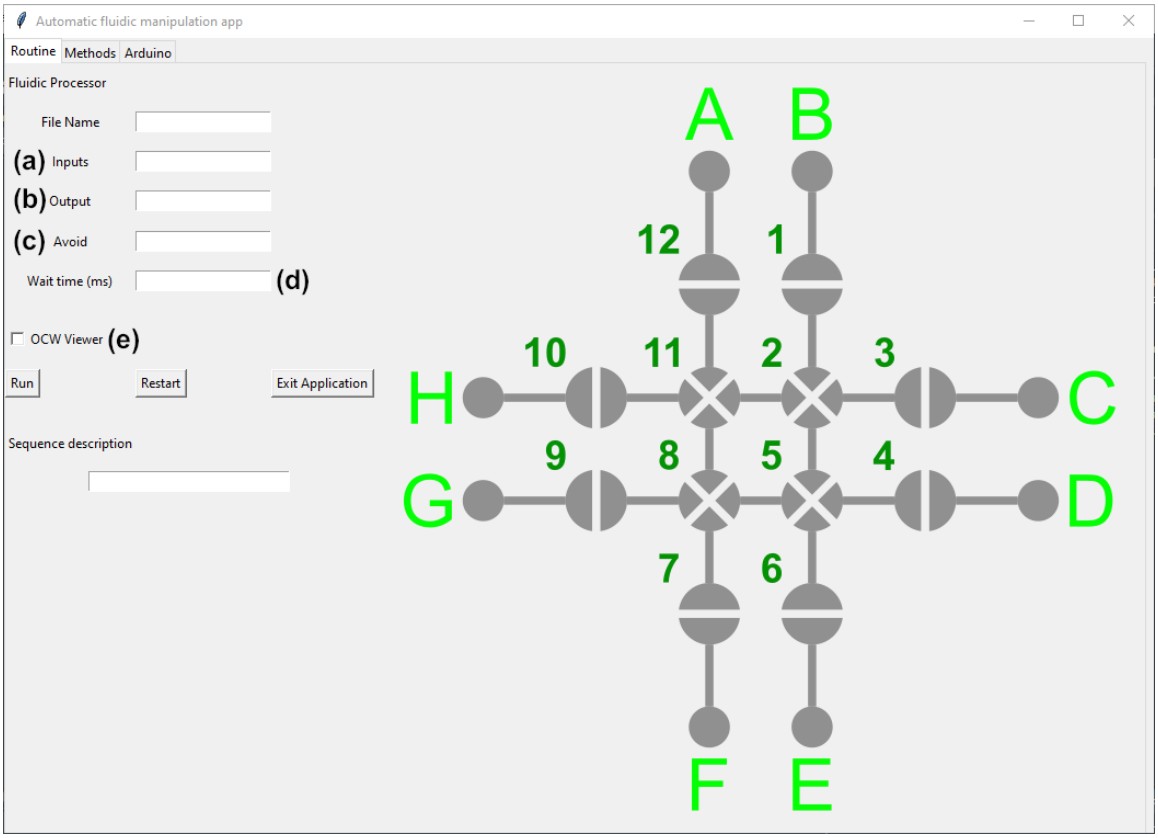

Figure 7-3 – Fluidic Manipulation App initial screen, at the Routine tab. (a) Input reservoirs and the number of valves used. (b) Output reservoir. (c) Valves to be avoided (if any). (d) Wait time in ms. (e) OCW Viewer option.

This program returns a list of commands to open, wait and close (OCW) solenoid valves that can be read by an OCW composer or viewer [228]. The OCW viewer generates a visualization of the routine and enables the combination of different routines, and can be enabled or disabled (Figure 7-3e). The generated string of commands for the process can

be read in a conventional LabView system [224], but here is read by custom code (SI) for the Arduino microcontroller. If needed, the Python code can be easily altered by the user, to include other functionalities that are system-specific, being another advantage of this open source code approach.

7.3.6 PDMS microfluidic device fabrication

7.3.6.1 Mold fabrication

The molds for the fluidic and pneumatic layers were fabricated using the Green, Low-cost, User-friendly Elastomeric (GLUE) rapid-prototyping method [19]. Briefly, glass slides were cleaned using an Alconox® solution, rinsed with isopropyl alcohol and dried with lint-free Texwipes (Kernersville, NC). Three layers of PVC tape were adhered to the clean glass substrate, and a 40 cm x 70 cm square was cut on the tape, removed from the substrate with the aid of a scalpel, leaving a tape border on the glass slide. Water-soluble glue was then deposited at the edge of the tape, and using a flat edge tool, the glue spread on the glass substrate. The glue was cured in an oven at 60 ^{o}C for 15 min [19].

A mold for a 2x2 Programmable Microfluidic Array was designed using AutoCAD® software (design available in the SI), and cut into the previously prepared glue thin films using a CO_2 laser cutter (Universal VLS 6.60 CO_2 laser) [19]. The thin film was laser cut (20% PWR 85% SPD), and the lifting gate feature of the molds were laser etched into the glue mold (12.5% PWR 40% SPD), in the gate regions of the valves. Glue excess was

peeled off from the mold with the aid of a scalpel, leaving the relief mold on the glass substrate.

7.3.6.2 Chip fabrication

A mixture of degassed PDMS (10 : 1 w/w ratio of prepolymer to curing agent) was cast against the relief mold [8,9,19]. The mixture was cured in in a conventional convection oven for 3 h at 60 ºC. The lifting gate thin membrane of PDMS (~200 µm thick) was bonded to a flat PDMS slab, via plasma treatment (1 min, Plasma Etch Model PE-25, Plasma Etch Inc, NV). For the fluidic layer, a dab of glue was applied to each feature in which a permanent bond was not desired, prior to plasma exposure [19]. The pneumatic actuation layer was then aligned by eye with the fluidic layer and bonded, forming the sandwich structure depicted in the SI.

7.3.7 Manifold Assembling

The microfluidic chip is placed into the polymeric main body of the testing system, and the polymeric pneumatic connector is attached to it. The lip in the top main body holds the stack together when the bottom main body is screwed to it (Figure 7-1), enabling air tight contact between the microfluidic chip and the connector. If the design of the device is smaller than the distance to the lips of the top main body, a second acrylic piece is used to keep the stack together. When PDMS is used as the microchip material, it also acts as a gasket, sealing connections [122]. Tygon® tubing connects to each individual port of the

connector to a solenoid valve in the electronics housing. Four 12 V vacuum pumps provide vacuum for the solenoid valves in the system. The solenoid valves can be independently actuated by the Arduino microcontroller board.

7.4 Results & Discussion

7.4.1 Modular manifold

The main advantage of the modular manifold is that it can be used with different microchips: If for any reason the microfluidic chip must be redesigned, only the polymeric pneumatic layer must be modified, instead of the whole system. The major components of the manifold are represented in Figure 7-1. The upper main body contains a tapped hole, by which the pneumatic and fluidic connections can be made, and a threaded base is used to hold the whole stack together when the lower main body is attached to it. The polymeric pneumatic connector is not bonded to the main body, as represented in Figure 7-1. The lip on the upper main body prevents features from falling from the stack.

The microfluidic chip is then aligned with the holes in the polymeric pneumatic connector, and sealing is made by the pressure applied by the polymeric bottom piece screwed into the polymeric main body (Figure 7-1b). The advantages of this approach include: *i)* the minimization of the number of screws used to keep layers together (from one screw in each corner of the main body to "one" – the bottom itself); *ii)* the more homogeneous pressure applied to the microchip, which improves the sealing, because just "one screw" is used, which is parallel to the surface of the microchip [13], and *iii)* the

correct adjustment of the stack height to the microchip used, without the need for external PDMS pieces to “shim” the height of the chip, which also contributes for a better sealing of the pneumatic connections.

The use of a connector base to ‘plug-and-play’ the microchip to the testing mount it is preferable to the use of loose hoses. The torque exerted by twisted hoses at the microfluidic device can cause delamination of its layers, rendering the device unusable. When attaching tubing to a rigid base, such as the one depicted in Figure 7-4, any tension in the hosing are contained by the rigid base, and not transferred to the device, maintaining its structural integrity. The connector base is made of acrylic material because it is a material compatible with rapid-prototyping tools, such as laser cutting, and it presents good interfacing with PDMS [229]. Also, it is the only part of the whole stack that would need to be modified in case of the design alterations to the microfluidic device. It is possible to laser cut this part in minutes, allowing for rapid changes in the system, as depicted in Figure 7-4.

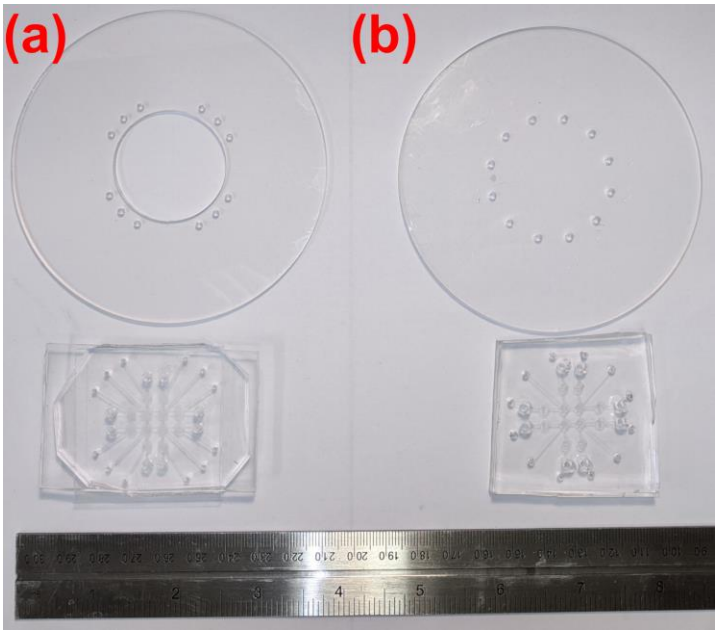

Figure 7-4 – Acrylic connectors with different designs. (a) Connector for a 2x2 PMA in which pneumatic connections were divided in quadrants. (b) Connector for a 2x2 PMA in which pneumatic connections were equally spaced.

Modular testbeds are the most compatible approach for use in conjunction with rapid-prototyping methods to fabricate microfluidic devices [223], eliminating the apparent disconnection between the use of prototyping tools that are capable of fabricating a device within minutes [9] and the use of fixed testing mounts that do not allow for rapid device modification.

7.4.2 Automatic Fluidic Manipulation Application

Programmable Microfluidic Arrays are intended for general purpose usage, rather than a particular single application [181]. This situation is analogous to a Central Processing Unit (CPU) versus an Application-Specific Integrated Circuit (ASIC) in the

microelectronics field: CPUs are fast, but ASICs are faster, when performing the same task. However, CPUs are more versatile, and can perform multiple different tasks, while ASICs are limited to their intended purpose [230]. Therefore, PMAs should be programmable and reprogrammable in a more efficient way, rather than manually coded [224], evidencing the need for automation.

The Automatic Fluidic Manipulation Application was written in Python, because it is a free, open-source object-oriented programming language [231], with a simple syntax for beginners, and it is a computer language that has been growing in popularity in the scientific community [232]. The open-source code, made available to the community through GitHub, enables researchers to modify the code as needed, accordingly to their needs and specific systems. The automated application is based on the Dijkstra's algorithm [233], and is described in detail in the Supplementary Information material. To use the Application with different device designs, the user updates the dictionaries regarding feature positioning, as described in the SI. Figure 7-5 brings the Application main window for Programmable Microfluidic Arrays with different configurations (2x2, 3x3 and 4x4).

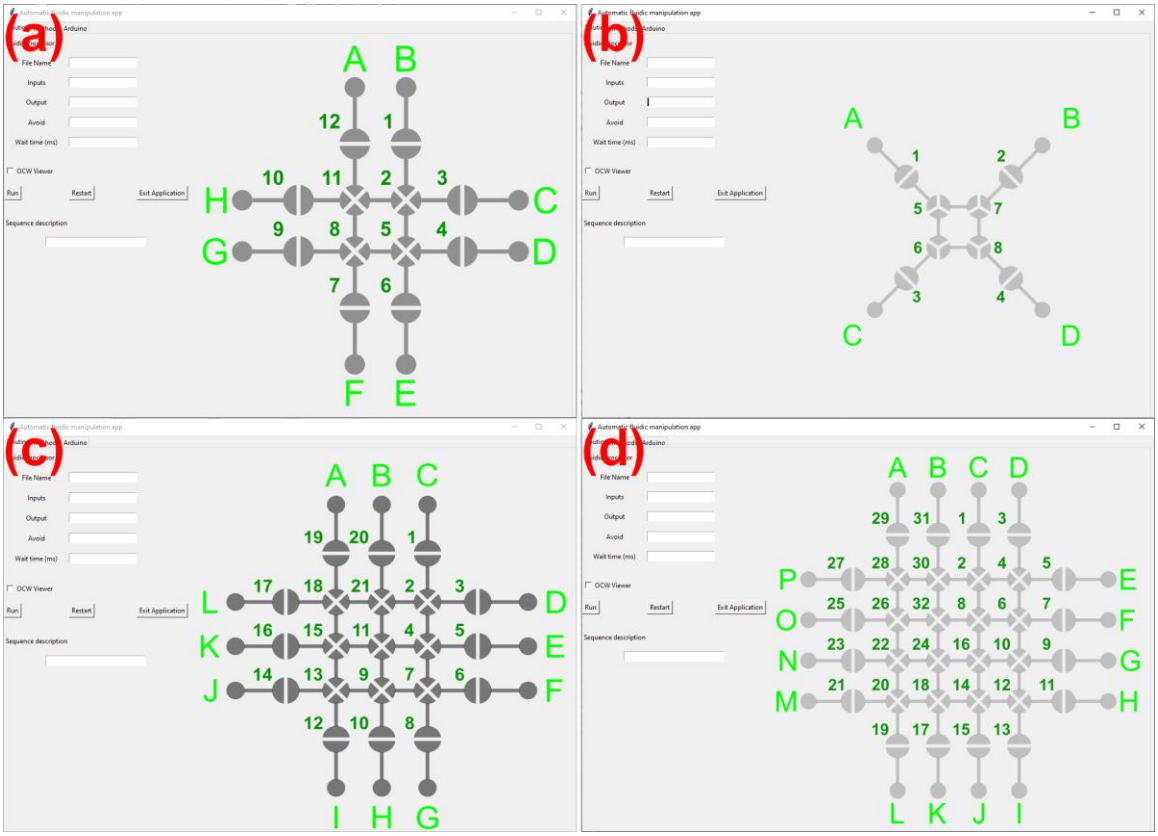

Figure 7-5 – Fluidic Manipulation App initial screen for Programmable Microfluidic Arrays in a (a) 2x2 configuration, (b) 2x2 configuration with only one inlet per processor valve, (c) 3x3 configuration, and (d) 4x4 configuration.

Another characteristic of the Automatic Fluidic Manipulation App is that individual routines can be combined to generate a method, which are defined here as a combination of individual fluidic manipulation steps. An example of a routine would be the combination of two reagents, routed to an outlet reservoir, followed by the washing of the PMA.

When a method is created, it generates a string of commands that can be either used in conventional LabView-operated systems [224], or used with our Arduino-operated system. The Automatic Fluidic Manipulation App was written to operate the Arduino directly from the Python console, with no need to change languages from Python to C++.

This was done by using the PyFirmata library in the Python code and the Firmata protocol in the Arduino.

7.4.3 Proof-of-Concept device operation

To demonstrate the functionality of the modular testing system and the Automatic Fluidic Manipulation App, we fabricated and tested a 2x2 pneumatic lifting gate Programmable Microfluidic Array (design and device in SI), with twelve lifting gate valves and eight input/output wells. The devices were operated with a vacuum of -75 kPa, to open the valves, and an air pressure of 70 kPa to seal the valves. A simple routine of mixing black and red dye was performed (Figure 7-6) to demonstrate the functionality of the modular system, automated computer application and Arduino-operated solenoid valves.

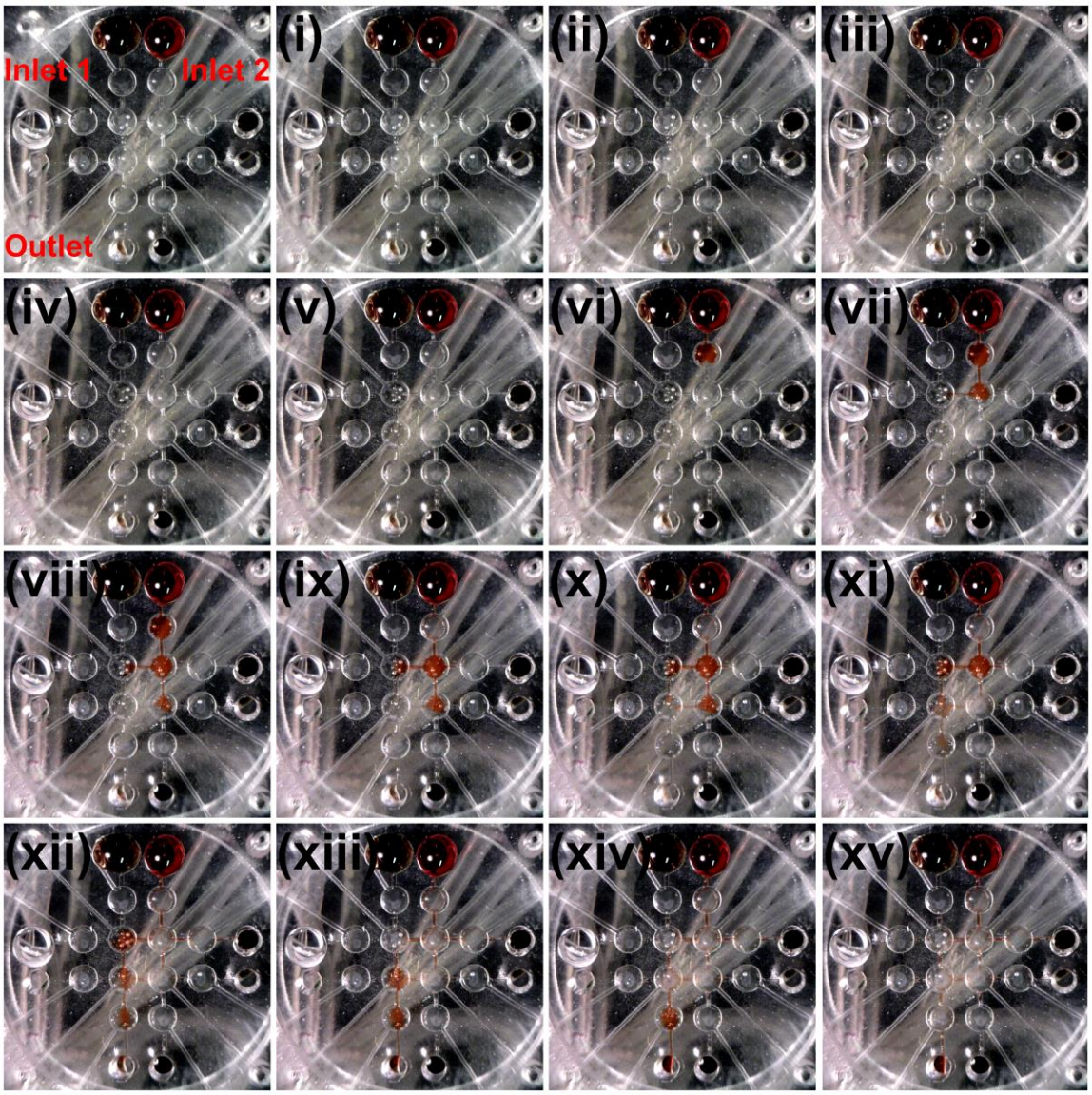

Figure 7-6 – A 2x2 Programmable Microfluidic Array fabricated using the GLUE method, tested using the modular mount and operated by solenoids controlled by an Arduino, automated by the Automatic Fluidic Manipulation App. Black and Red dyes were mixed and transported towards an outlet.

7.5 Conclusion

The need to improve the testing step of the iterative microfluidic device development process gave rise to our innovative approach. This low-cost modular system is

advantageous for versatile testing of microfluidic devices, when compared with fixed machined mounts. The use of parts that can be rapidly prototyped, in conjunction with machined parts brings the best of the two worlds together: the ruggedness of the machined hard substrates with the speed and versatility of the rapid-prototyped parts. The modular approach makes a significant contribution to the field, because the testbed design does not interfere with the design of the microfluidic device design, as opposed to what happens when using system-specific testing mounts. Our approach is also in alignment with the use of rapid-prototyping tools to fabricate PDMS-based microdevices, with turnaround times within the one-hour range [8,9,19].

Another improvement in the testing phase of the development of microfluidic devices is the use of a low-cost approach to operate pneumatically actuated Programmable Microfluidic Arrays. We developed a system to operate solenoid valves using an Arduino microcontroller, instead of conventional commercial DAQs, for a fraction of the cost (Table E-3, SI).

Finally, and most importantly, we created an automated computer application capable of automatically perform fluidic manipulations on-chip, which has been one of the biggest shortcomings in PMAs field. Our computer application expands the programmable and reprogrammable capabilities of Programmable Microfluidic Arrays, without the need for manual coding of valves, with minimal input from the end user. This breakthrough application will expand the userbase of PMAs, and will improve the capabilities of field-deployable autonomous systems [234], making them more rugged and truly autonomous.

The versatility of the modular approach, the low-cost of the components to operate the system, and the open-source code to operate microfluidic devices improves the iterative process of developing microdevices, by ameliorating the issues of the often-neglected testing phase. Our new approach is a step forward towards the popularization of microfluidics, once restricted to those with access to cleanroom environments. This research enables the use of this technology as an educational tool to people interested in the field, providing microfluidics access to students, hobbyists and researchers worldwide.

7.6 Acknowledgements

The funding agency CNPq (Science without borders, Grant No. 205453/2014-7) provided scholarship support (GGM). Research was supported by an appointment to NCS from the NASA Postdoctoral Program by the NASA Astrobiology Program, administered by Universities Space Research Association under contract with NASA. All work was done at Georgia Institute of Technology (Georgia Tech) with financial support from State of Georgia, USA. This work was performed in part at the Georgia Tech Institute for Electronics and Nanotechnology, a member of the National Nanotechnology Coordinated Infrastructure (NNCI), which is supported by the National Science Foundation (Grant ECCS-1542174). We gratefully acknowledge Dr. Timur Tankayev (Georgia Institute of Technology) for his assistance with the code. We acknowledge UCB Space Science lab for uncited and unpublished code.

CHAPTER 8. CONCLUSIONS AND PROSPECTS

8.1 Recapitulation

The development of microfluidic devices is comprised of *i)* the design of a microfluidic structure, *ii)* the fabrication of the designed device, and *iii)* the testing of the fabricated microdevice. The development of fully functional microfluidic devices, however, is an iterative process, meaning that the steps described in *i), ii)* and *iii)* are often repeated until a desired microdevice performance is obtained. The iterative nature of this process increases time and, hence cost associated with the development of microfluidic technology. Improvements in each step of this iterative development process can diminish these resource costs and enable significant advancements in the microfluidics field.

The design of microfluidic devices is primordial to their function. Microfluidic devices, in a very similar fashion to computer programs, perform as they were designed and fabricated, which do not necessarily correspond to the task they were envisioned for. This is because microscale systems behave differently than their macroscale counterparts, and the physics of fluid manipulation at the microscale is usually is non-intuitive to the non-expert. Mixing, for example, is slow with the diffusion of species in laminar flow, rather than rapid with a turbulent stream, unless active microfluidic mixing is introduced by device design and operation [235]. Viscous forces play a significantly bigger role than inertial forces in these microsystems, described by the Stokes equation for low Reynolds numbers ($Re << 1$) [7] Some other complications that might arise during the design stage of microdevices are related with the combination of different unit operations on-chip (*e.g.* microfluidic mixer, gradient generator, droplet generator), which still remain a challenge

in the field [236], even for experienced designers and users. The use of rapid-prototyping tools aids in the design of microfluidic devices, because it can quickly demonstrate the flaws arising from a bad design.

The first “rapid-prototyping” fabrication of microdevices was demonstrated in the seminal work of the Whitesides group at Harvard on soft-lithography [14], which profoundly changed the microfluidics field. This method changed materials, methods and requirements to fabricate microfluidic devices. PDMS instead of hard substrates [10], replica molding instead of etching / machining [10], and turnaround times within hours [14] instead of days [10] made the micro total analytical systems (μTAS) envisioned by Manz *et al.* [1] more attainable, demonstrating the significance of fast-prototyping tools to the field.

Since the development of soft-lithography as a rapid-prototyping tool to fabricate PDMS-based microfluidic devices [14], several alternative prototyping tools that do not require cleanroom environments emerged in the literature [8,9,16,19,131]. The characterization of each new technique becomes necessary to enable a fair comparison between the rapid-prototyping tools, namely: *i)* materials requirement and their toxicity; *ii)* method resolution, in terms of minimum width and height attainable; *iii)* start-up costs; *iv)* turnaround times; *v)* multi-height molds fabrication capabilities, and *vi)* mold degradation or reusability.

Testing also plays a big role in the development of functional microdevices. Although less attention has been given to the testing step in counterpart to design and fabrication, this step is the make-or-break point for a device: if it does not perform as it

expected, another iteration cycle is required. The problems arising from current device testing approaches are: *i)* testbeds with fixed connections (either actuation or fluidic lines), limiting the alterations of the design of the device to enable the reuse of the testbed; *ii)* manual programming of routines, in the case of active pumping elements on-chip, which can be laborious depending on the complexity of the design; and *iii)* costs associated with testing equipment and the software required to operate the hardware.

In the work described in this thesis, alternatives to the conventional workflow to develop microfluidic devices were proposed. The main goal of this thesis was to create rapid-prototyping techniques to reduce turnaround times, costs and infrastructure requirements associated with the development of microfluidic tools, from the design stage to the testbed, making microfluidics available to researchers, hobbyists and students worldwide.

8.2 Rational Design of Microfluidic Devices

8.2.1 Conclusions

In Chapter 2, I discussed the role of fluidic resistance in 3-dimensional microfluidic paper-based analytical devices (3D-µPADs). Starting with a sample multiplexer design available in literature [25] (1 inlet, 16 outlets), I demonstrated that the fluidic resistance of each channel for each individual layer of the 3D device plays an important role for sample dispersion through the device. By rationally designing microfluidic devices, I showed that it is possible to remove sample dispersion bias in devices, which in turn removes the bias

of colorimetric results of enzymatic assays supported on the cellulosic matrix – the most common application of µPADs. Another advancement of this study was the creation of a new assembling method for 3D-µPADs using magnets, creating an evenly distributed force to keep the layers in contact throughout the duration of the assay.

8.2.2 Prospects

Sample multiplexers, as the one discussed in this work, are useful to both enable multiple tests of the same sample for several markers (clinical triage), and the creation of either external or standard addition calibration curves on-chip. The advantage of the use of these curves is quantitative or semi-quantitative results, as opposed to qualitative readouts [237]. Early attempts to create standard addition calibration curves on-chip [37] demonstrated the need for external parameters, which defeats the purpose of obtaining the calibration curve while the sample is assayed. This suggests an opportunity in the field: using sample multiplexers with dried assay reagents on the detection layer and dried standards in another layer, making it possible to obtain a standard addition calibration curve on-chip at the moment of the analysis, applying a single drop of sample at the inlet. This is no simple task: past efforts demonstrated that the non-linearity of the detector response still requires unusual 2^{nd}, 3^{rd} and even 4^{th} order polynomial fits to estimate the concentration of the analyte of interest in the original sample [238]. An approach that might improve the results would involve the combination of redox indicators, using the well-established linear regression at the linear region of the calibration curve, away from the zone of signal saturation.

8.3 Rapid and Low-Cost Development of Microfluidic Devices Using Wax Printing and Microwave Treatment

8.3.1 Conclusions

In Chapter 4, I presented the first rapid-prototyping tool I developed using wax printing to generate the relief structures for PDMS replica molding and using microwave treatment to accelerate PDMS curing. These technologies existed separately [17,20], but their coupling generated one of the fastest fabrication methods for PDMS-based microfluidic devices available in literature, curing PDMS in 25 min instead of 3 h in a conventional oven. This study also demonstrated the feasibility of PDMS-glass bond annealing using microwave treatment in 30 min, as an alternative to the conventional 2-h thermal annealing treatment in a convection oven after plasma bonding. This work demonstrated that wax printing can be used to fabricate structures to perform different unit operations on-chip in proof-of-concept devices including gradient generators and droplet generators. It is worth mentioning that the wax printing method is best for applications that do not require high-pressure driven fluidic manipulation on chip, such as microchip capillary electrophoresis [17], given the low aspect ratio of channels (height / width), which increases fluidic resistance of the structure as a whole.

8.3.2 Prospects

The work presented in Chapter 4 was the seed for the other projects related with the creation of rapid-prototyping tools presented in this thesis. The other developed techniques did not suffer from the drawbacks of the wax printing method, such as *i)* limitations regarding curing temperatures of PDMS, *ii)* low aspect ratio of channels (height / width),

and *iii)* the impossibility of changing the height of the molds, owing to the printing method itself. The biggest disadvantage of this method, however, is the discontinuation of wax printers by the Xerox corporation®, the company which owns the technology. This means that research that relies on wax printing will be confined to groups that already own a wax printer, or to groups that are capable of developing their own printing technology [144] – which is an even smaller niche than the research groups owning the commercial technology. Given the current scenario, I foresee a shrinkage in the utilization of this technology, in comparison to the use of other available tools.

8.4 Cutting Edge Microfluidics: Xurography and a Microwave

8.4.1 Conclusions

In Chapter 5, we developed an improved method to rapid-prototype PDMS-based microfluidic devices. Instead of using wax printing to create the relief molds, a cutter plotter was used to cut designs on tape – a method called xurography. The advantage of this method, in comparison with wax printing, is due to factors that include: *i)* decreased thermal limitations on PDMS curing imposed by the molds; *ii)* mold height tunability by changing the type of tape used or by layer-stacking, which *iii)* removes fluidic resistance restrictions imposed by low-aspect ratio channels. One of the biggest advantages of this rapid-prototyping tool is the low start-up costs associated with it, which are as low as $300 depending on the resolution of the plotter.

8.4.2 Prospects

The work presented in Chapter 5 truly gives researchers worldwide access to microfluidics, owing to the low-cost of the method itself and its start-up and the relaxation of requirements of conventional soft-lithography. It does not require cleanroom environments nor experts to operate expensive instrumentation. Besides basic research on microfluidics, this rapid-prototyping tool also has the potential to help healthcare providers in resource-poor locations, by manufacturing *in situ* point-of-care testing tools, such as immunodiagnostic assays on-chip [239] or to aid other biological sample preparation steps, such as using a spiral inertial microfluidics separator to concentrate analytes of interest from a whole biological sample [3]. Hobbyists and students worldwide also benefit from this technology, which can be used to teach the physics of microfluidics.

8.5 Green Low-Cost User-Friendly Elastomeric (GLUE) Microfluidics – Making Microfabrication Child's Play

8.5.1 Conclusions

In Chapter 6, we developed a method to fabricate PDMS-based microfluidic devices that is unique in the fact that this is the first tested fabrication method that, using the same materials and methods, can be used either as a Print-and-Peel (PAP) or as a scaffolding-removal technique. If used as a PAP technique, molds can be reused to generate several PDMS devices, which further lowers fabrication costs. If used as a scaffolding-removal technique, then no bonding steps are required to seal the device, and devices with larger

blueprints can be obtained. One of the biggest advantages of this method, however, is the fabrication of multi-height molds in a single step, using the laser cutter raster-engraving function. This feature eliminates cumbersome mask alignment steps, diminishing costs of the fabrication of different masks and speeding up turnaround times to obtain multi-height channels. The simplicity of the method, the low-cost of the reagents and their non-toxicity, and its versatility makes this technique ideal for beginners in the microfluidics field, but also an ideal exploratory tool for more experienced researchers.

8.5.2 Prospects

The work presented in Chapter 6 is another innovative tool that can give people access to microfluidics, which was traditionally confined into cleanroom environments. Like xurography (and wax printing, to a small extent), the use of rapid-prototyping tools will help popularize microfluidics, by enabling more people hands-on experience with this technology.

The use of non-toxic white glue as the scaffolding material might be used to encapsulate materials into PDMS-based microchannels, which can be used to further functionalize microchannels surface after PDMS curing or to encapsulate reagents into specific sections of a microdevice, for example. The proof-of-concept devices showed in this work demonstrate only a fraction of the capabilities of this technique which we hope will boost research in microfluidics and μTAS.

8.6 An Automated Low-Cost Modular Platform for Versatile Microfluidic Device Testing and

8.6.1 Conclusions

In Chapter 7, I developed strategies to improve testing of microfluidic devices. First, I proposed a modular approach as an alternative to conventional fixed mounts, commonly used to test microfluidic devices. The advantage of the modular approach is that parts of the mount can be rapid-prototyped, bringing versatility and ease of fabrication allied with the ruggedness of machined parts of the rest of the mount. Another innovation of this work was the creation of a cost-effective Arduino-based system to control solenoid valves, used to operate Programmable Microfluidic Arrays (PMAs). The biggest innovation brought by this work, however, was the creation of an automated computer application to automate programming of fluidic routines in programmable microfluidic arrays, requiring from the user minimal inputs, unlocking the true programming and reprogramming capabilities of PMAs.

8.6.2 Prospects

The work presented in Chapter 7 gives researchers worldwide access to Programmable Microfluidic Arrays, by eliminating costs associated with hardware and software needed to operate such systems. The automated code to automate fluidic operations on-chip, which can be personalized based on the user's needs, can be integrated with other functions (*e.g.* detection), to give rise to true miniaturized total chemical analysis

systems. These approaches to improve testing of microfluidic devices will definitely improve research in Programmable Microfluidic Arrays and μTAS.

8.7 The Future of Microfluidics

When in its infancy, the microfluidics field borrowed fabrication tools from the microelectronics industry [10], so it is not illogical to draw a parallel between the fields. As technology has evolved, electronic microdevices became more ubiquitous and more accessible – nowadays, more than half of the global population has access to the internet via mobile devices [240]. There is no reason to expect that microfluidics will be different, and that this technology will also be ubiquitous in the future. To quote George Whitesides: "the advantages microfluidics offers are too compelling to let pass" [7].

The most successful commercial product using microfluidic technology still is the inkjet printer [241] (and curiously enough, it came full circle when inkjet printers began to be used to fabricate microfluidic devices [242]). Other microfluidics-based products are becoming more popular, but mostly technologies are still confined within laboratory walls [243]. The creation of new rapid-prototyping tools, allied with improved approaches to design and test microfluidic devices, will reduce the costs and increase the speed of with the development of this technology. This will make microfluidics more attractive to be used in tasks that currently are being performed by their macroscale counterparts. The creation of other commercially available microfluidic devices will aid in the popularization of this technology, in the same fashion computers moved from laboratory to the hands of the general population.

I am grateful for the opportunity to contribute with the field, by creating tools that can put microfluidics in the hands of researchers, hobbyists, students and anyone with curiosity in science around the globe.

APPENDIX A. SUPPLEMENTARY INFORMATION OF CHAPTER 2: RATIONAL DESIGN OF MICROFLUIDIC DEVICES

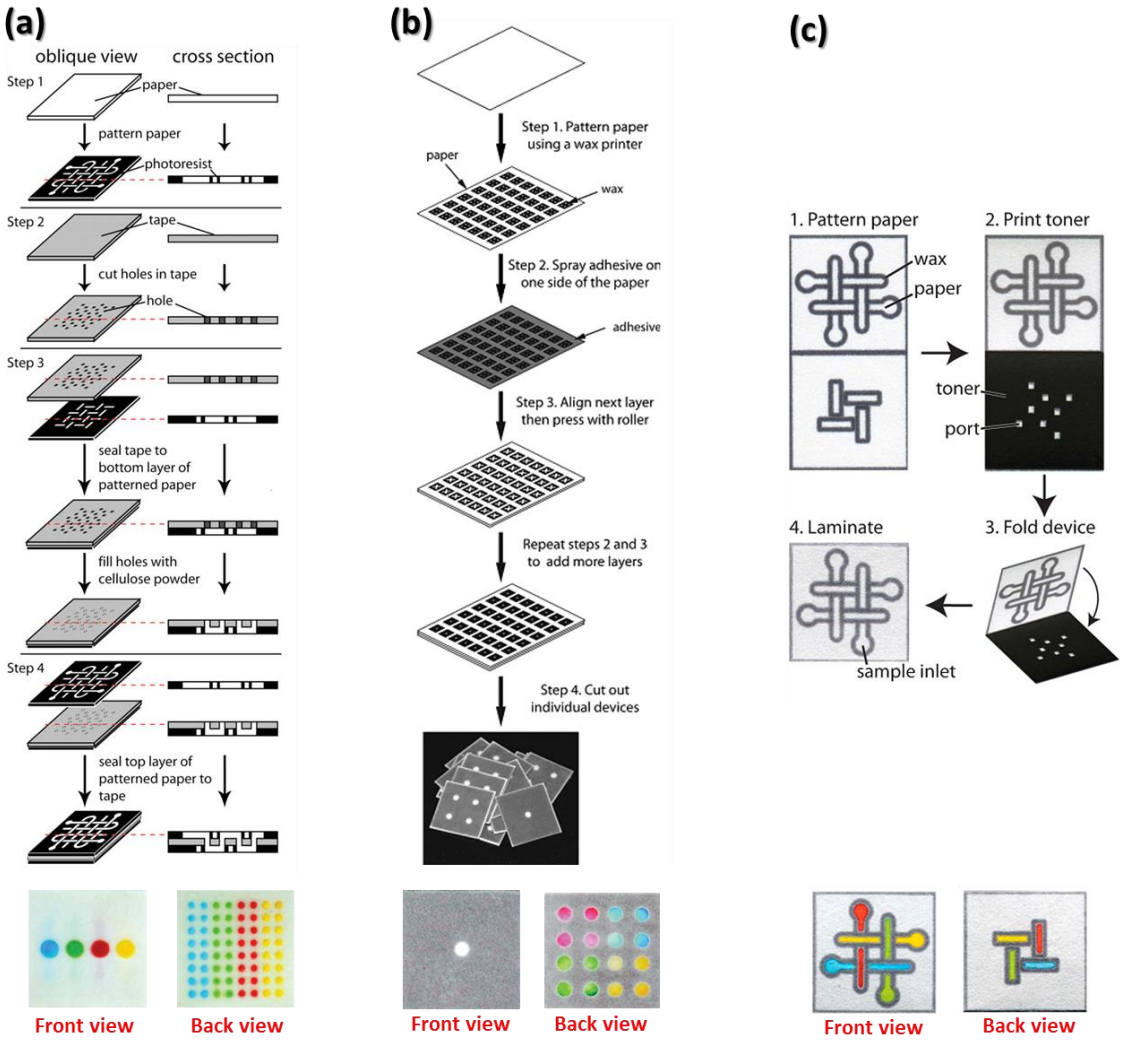

Figure A-1 – Irreversible methods for layer assembly. (a) Layers assembled using tape and cellulose powder. Adapted with permission from ref. [26]. Copyright (2008) National Academy of Sciences. (b) Layers glued together using adhesive spray. Adapted from ref. [25] with permission of The Royal Society of Chemistry. (c) Layers assembled together using toner and lamination. Adapted from ref. [46] with permission of The Royal Society of Chemistry.

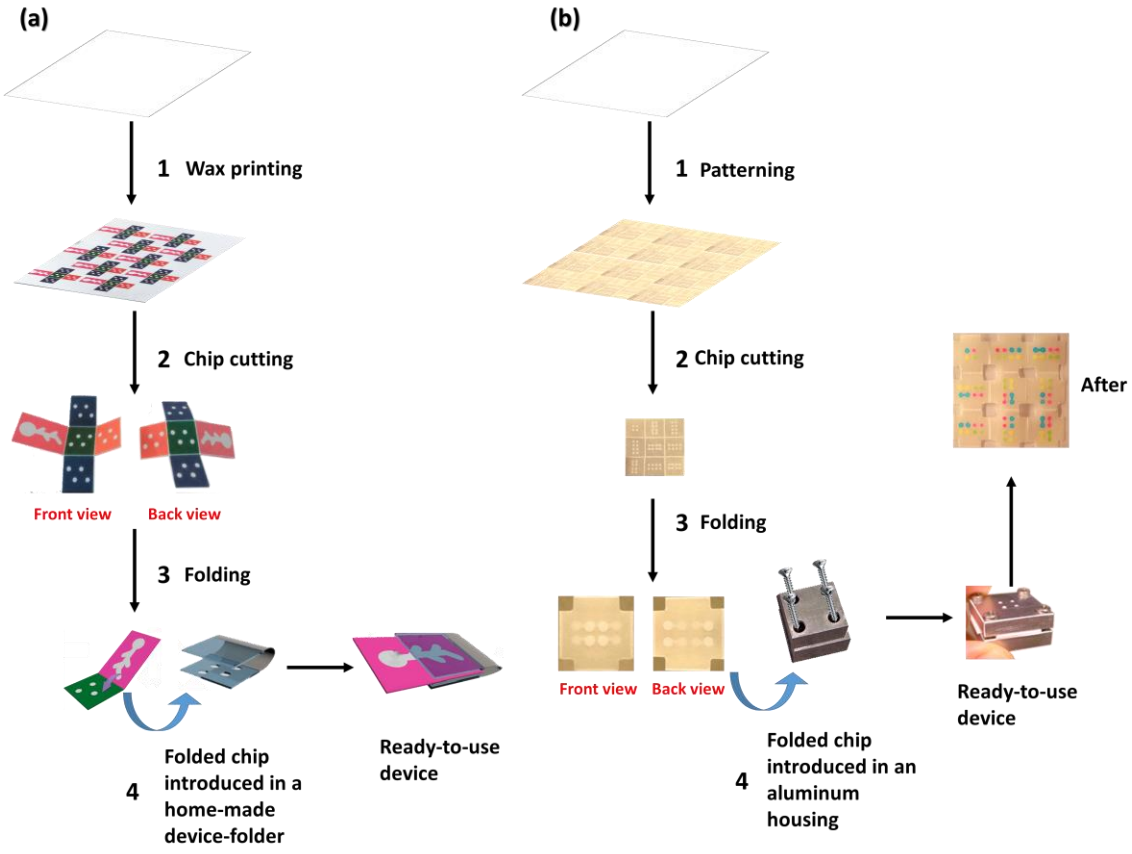

Figure A-2 – Reversible methods for layer assembly in origami paper-based devices. (a) Layers held together using an external device-folder. Adapted from ref. [23] with permission of The Royal Society of Chemistry. (b) Layers held together using an external aluminum housing and screws. Adapted with permission from ref. [29]. Copyright (2011) American Chemical Society.

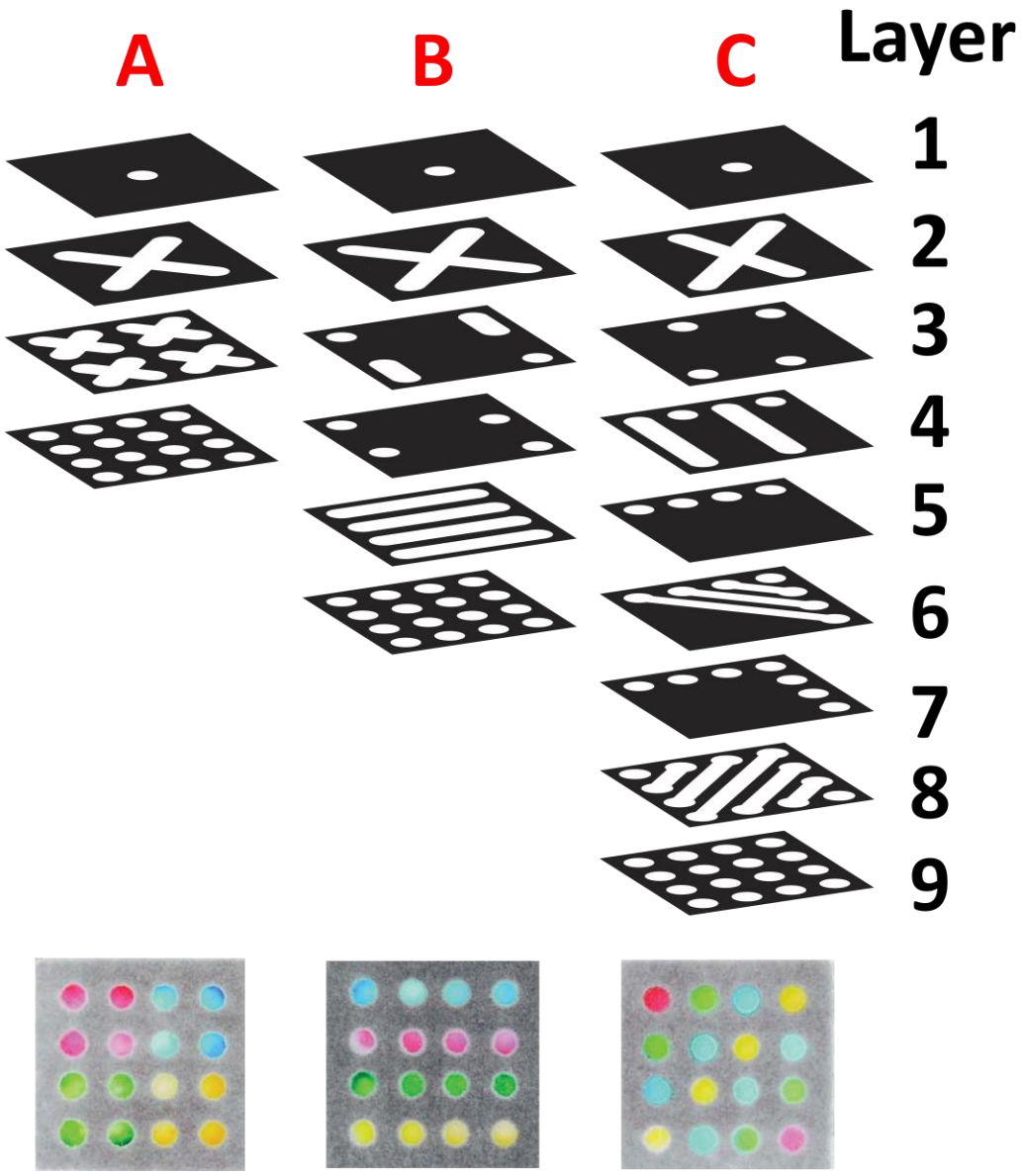

Figure A-3 – Distinct designs of 3D-µPADs and their respective fluidic dispersion patterns on the bottom layer. For the first Design A (4 layers total), dyes were spotted on layer no. 3. For the Design B (6 layers total) dyes were spotted on layer no. 4. For the Design C (9 layers total) dyes were spotted on layer no. 3. Adapted from ref. [25] with permission of The Royal Society of Chemistry.

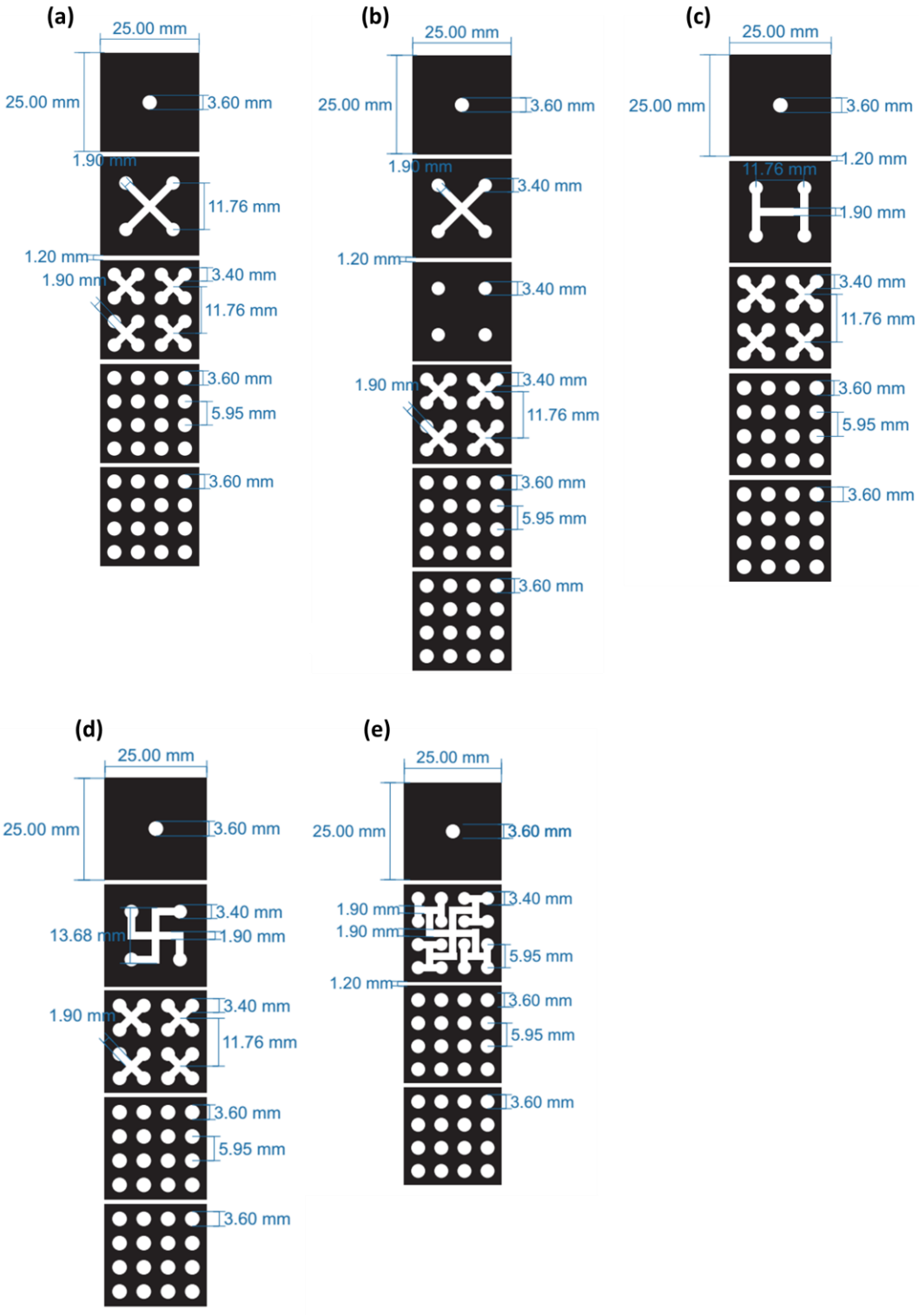

Figure A-4 – Specifications of the designs used in this work. (a) First evaluated design. (b) Second evaluated design. (c) Third evaluated design. (d) Fourth evaluated design. (a) Optimized design.

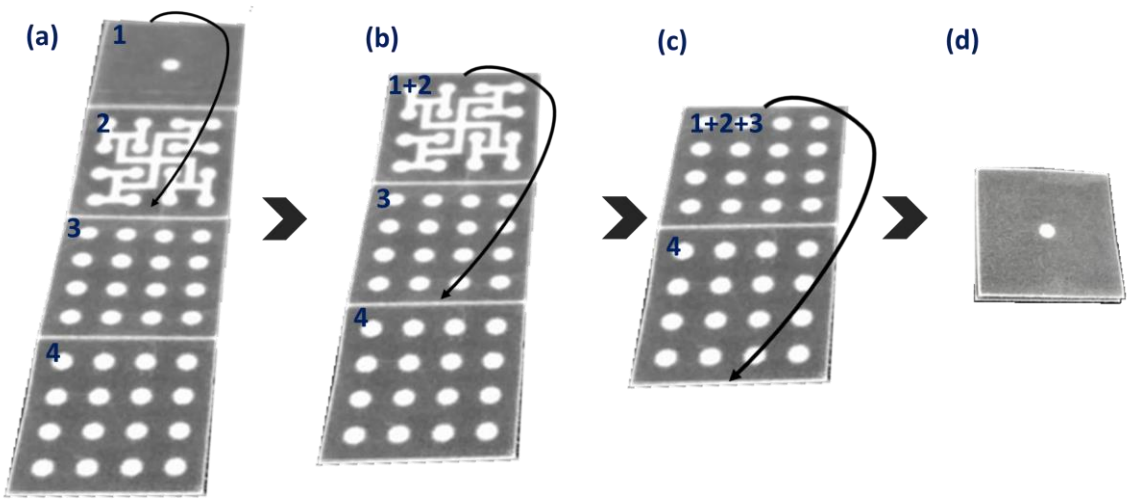

Figure A-5 – Folding instructions for the origami paper-based microchip devices. (a) The edges of the first and second layers are brought into contact, being aligned and folded. (b) The edges of the first and second layers (together) are brought into contact with the edges of the third layer, being aligned and folded. (c) The edges of the first, second and third layers (together) are brought into contact with the edges of the forth layer, being aligned and folded. (d) Origami paper-based microchip device completely folded (25 x 25 mm).

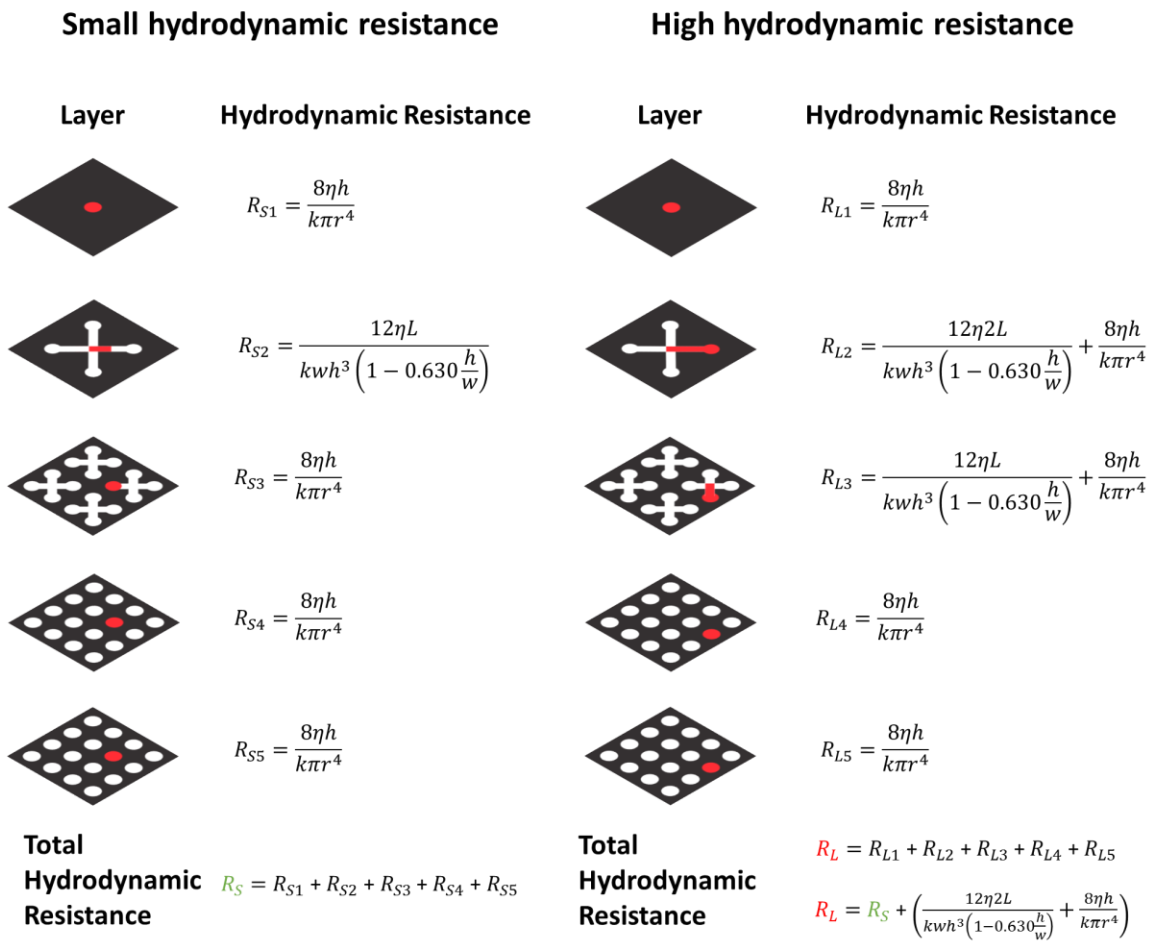

Figure A-6 – Hydrodynamic resistance in each layer of the original model design [25]. The path to the central spots presents a smaller hydrodynamic resistance than the path to the peripheral spots, explaining the observed bias.

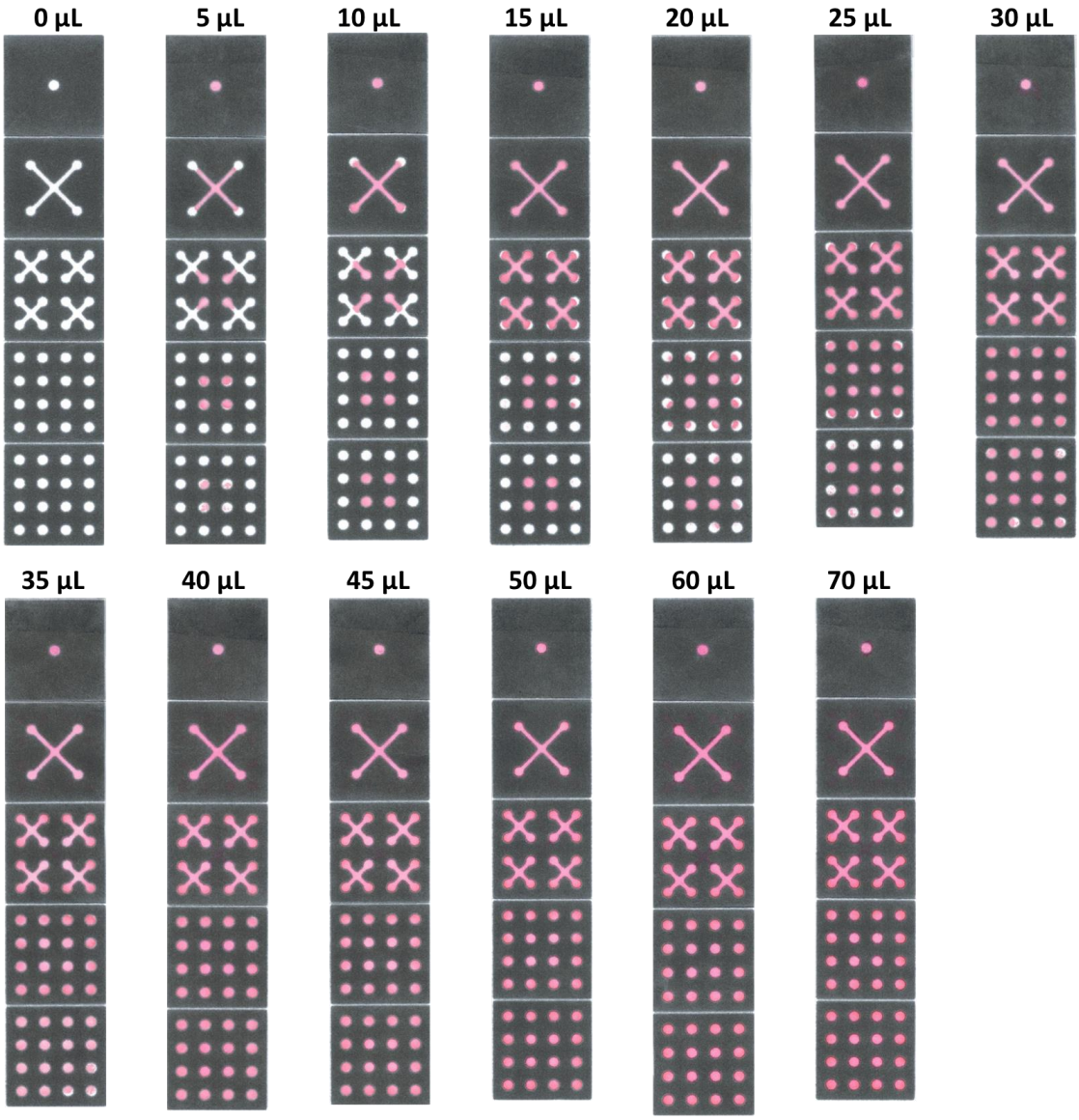

Figure A-7 – Original digitalization of the first paper-based microchip design evaluated in this study (ref. [25]).

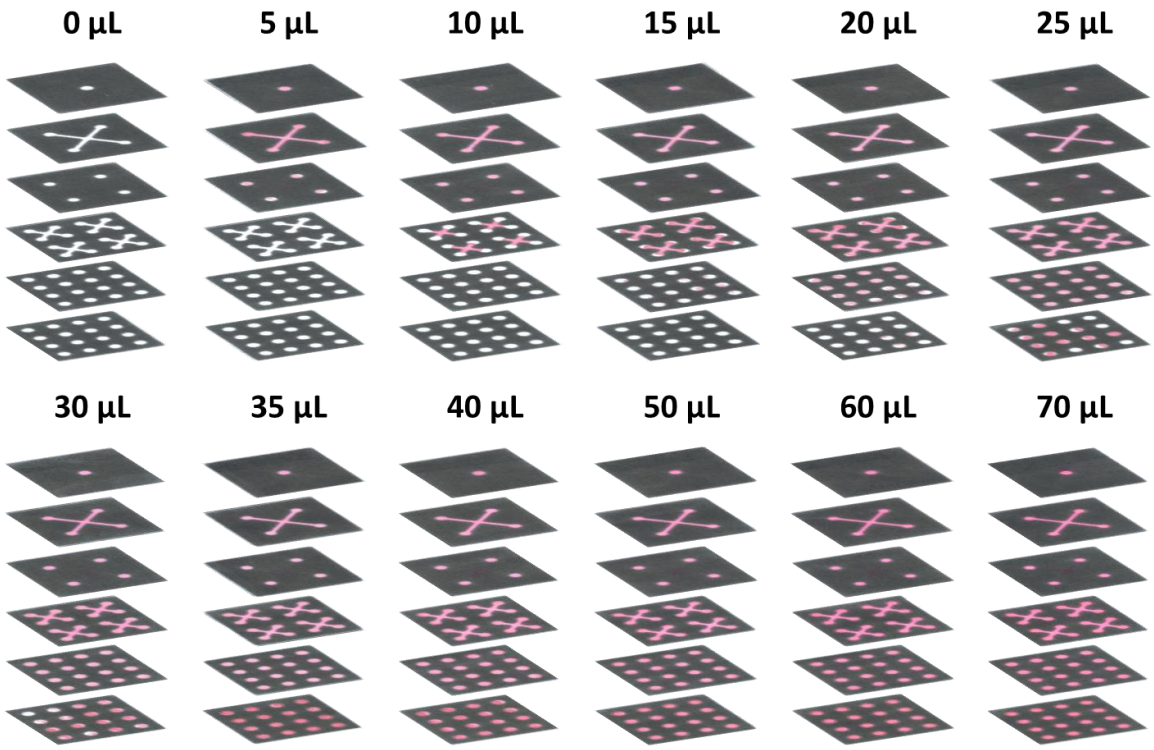

Figure A-8 – Exploded view of the second paper-based microchip design evaluated in this study. This chip design presents an extra layer in comparison with the original model (ref. [25]).

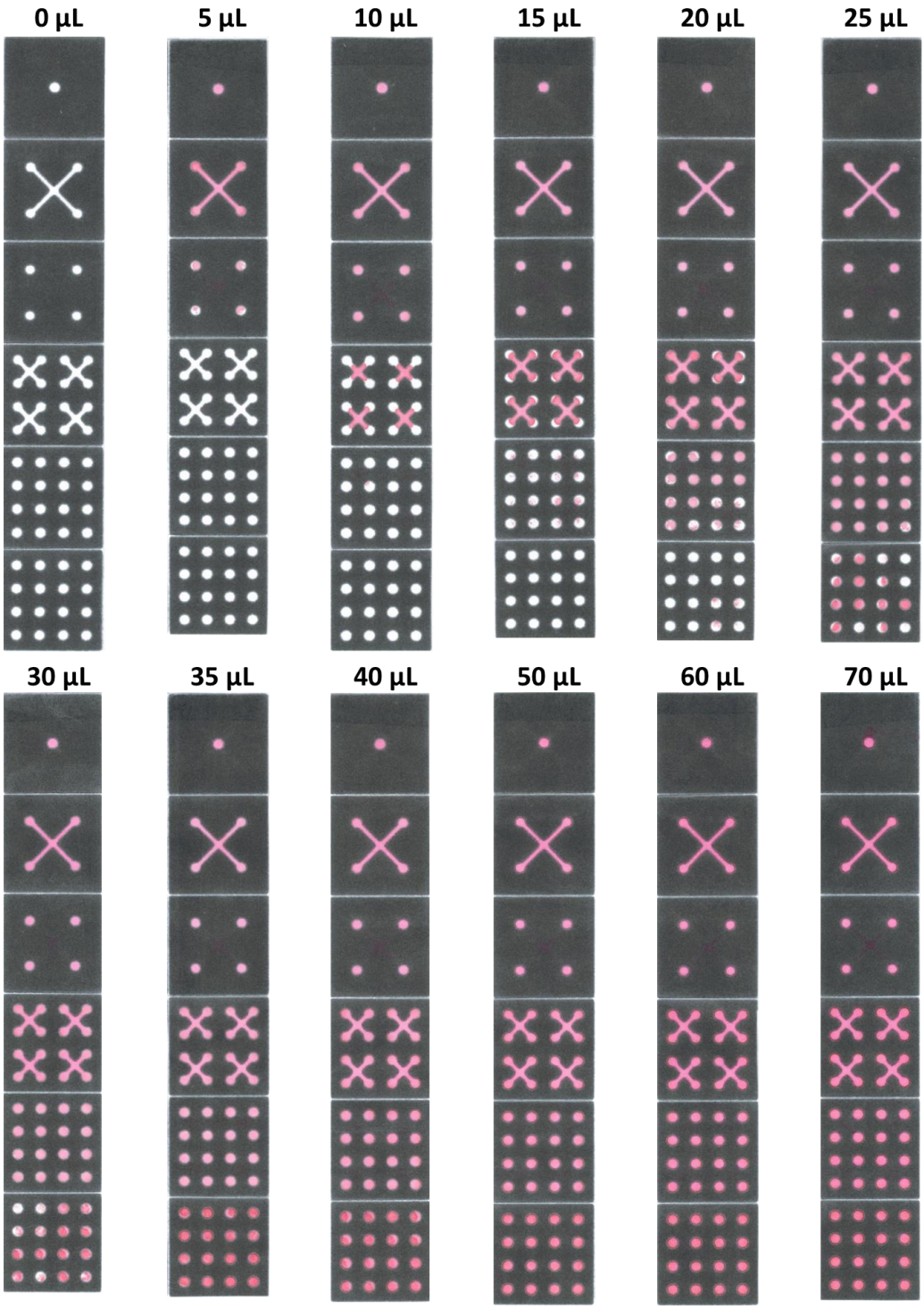

Figure A-9 – Original digitalization of the second paper-based microchip design evaluated in this study. This chip design presents an extra layer in comparison with the original model (ref. [25]).

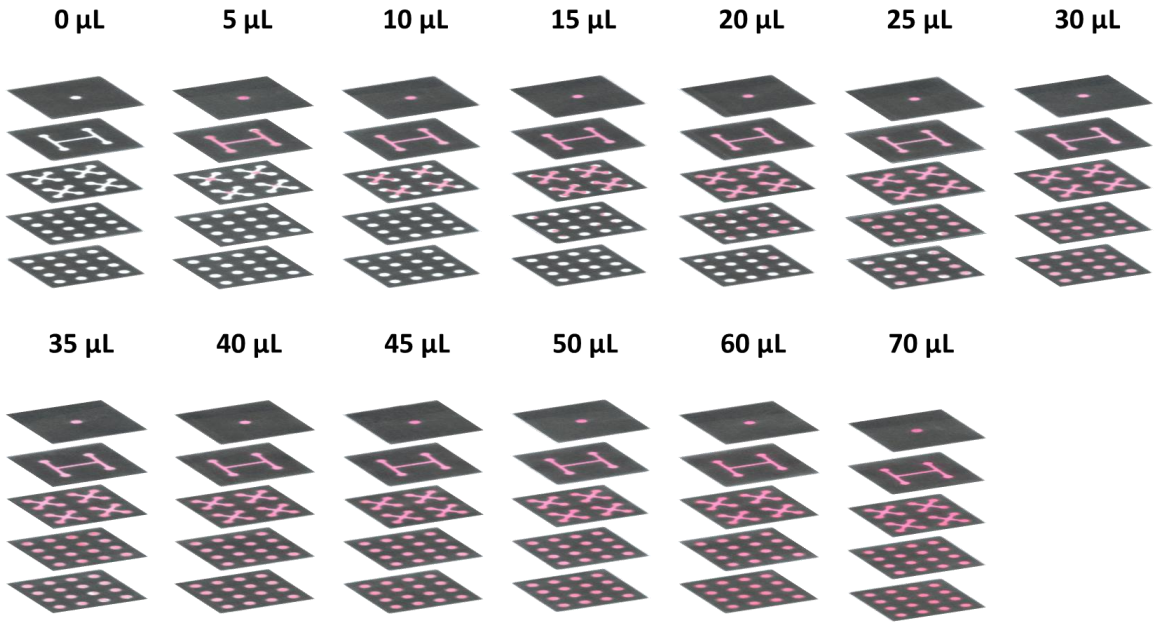

Figure A-10 – Exploded view of the third evaluated paper-based microchip design.

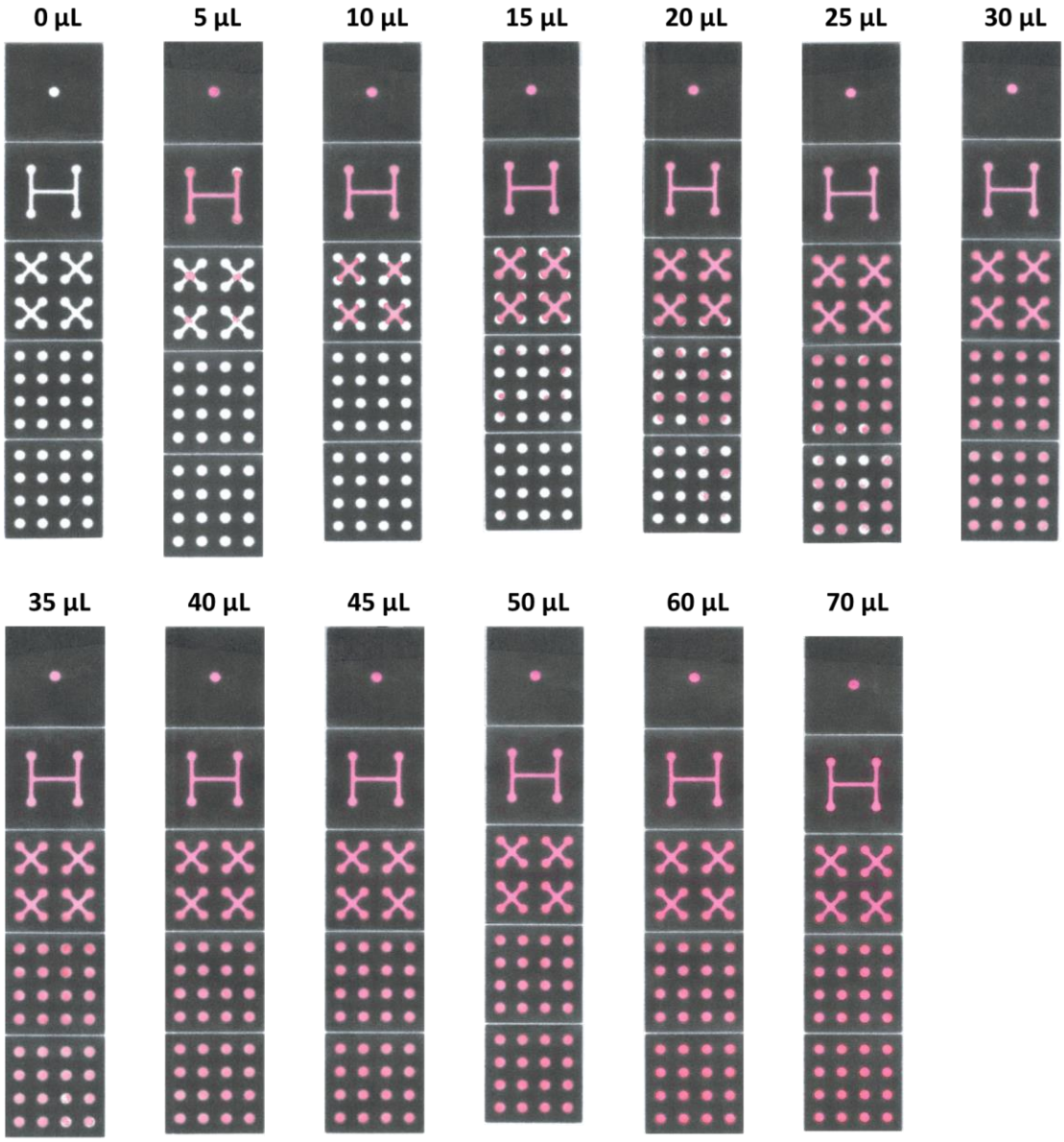

Figure A-11 – Original digitalization of the third evaluated paper-based microchip design.

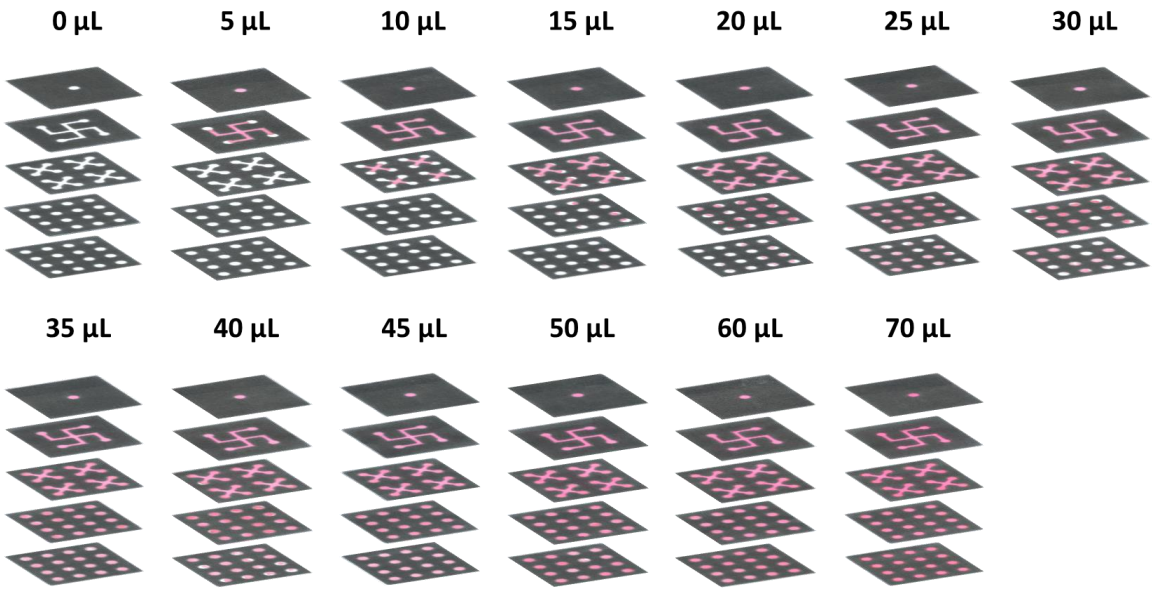

Figure A-12 – Exploded view of the fourth evaluated paper-based microchip design.

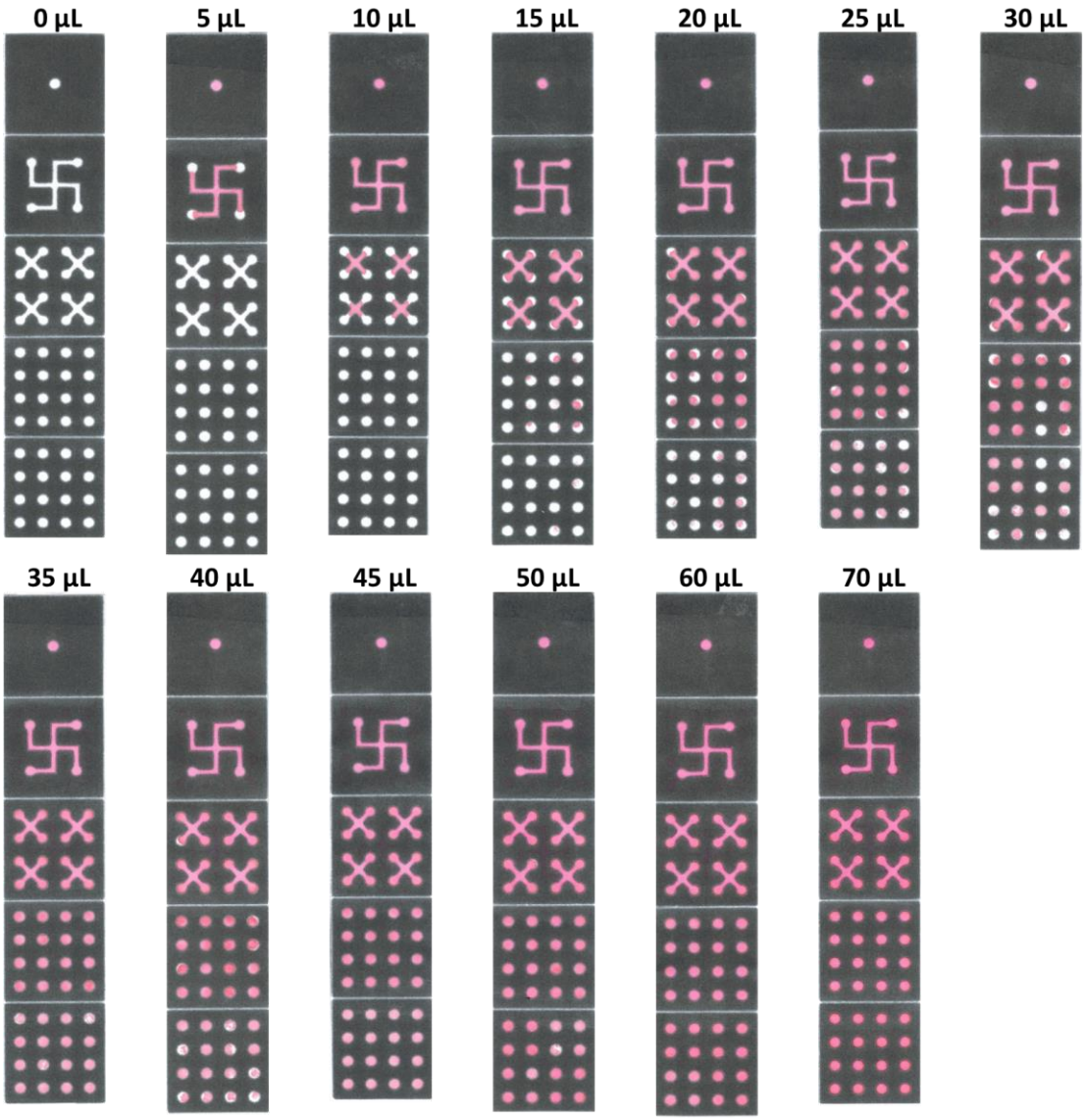

Figure A-13 – Original digitalization of the fourth evaluated paper-based microchip design.

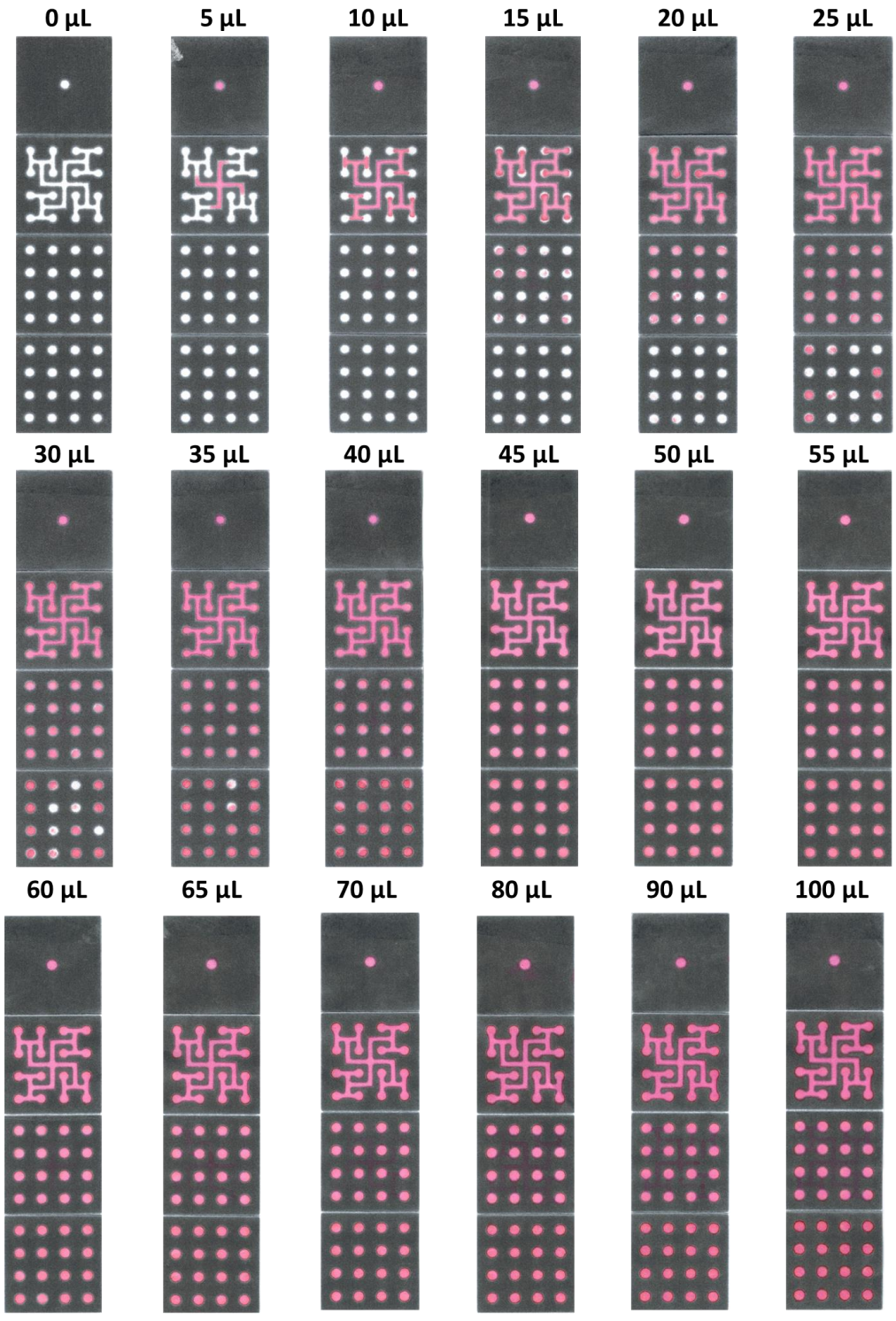

Figure A-14 – Original digitalization of the Optimized paper-based microchip design.

A.1 Enzymatic Assay

To test whether the design of the paper-based device impacts and biases results, we performed an enzymatic assay using the glucose oxidase / peroxidase system as a model [37]. This assay is based on two coupled enzymatic reactions: the glucose oxidase enzyme oxidizes the glucose in the presence of oxygen and water, generating gluconolactone and hydrogen peroxide (Equation 5). The peroxidase catalyzes the oxidation of the redox indicator (ABTS → $ABTS^{\cdot+}$) and the reduction of the hydrogen peroxide to water (Equation 6) [37]. The oxidized form of this redox indicator is a blue-greenish product that is detected at the bottom layer of the device.

$$C_6H_{12}O_6 + H_2O + O_2 \xrightarrow{Glucose\ Oxidase} C_6H_{12}O_7 + H_2O_2 \quad (5)$$

$$H_2O_2 + ABTS \xrightarrow{Horseradish\ Peroxidase} ABTS^{\cdot+} + H_2O \quad (6)$$

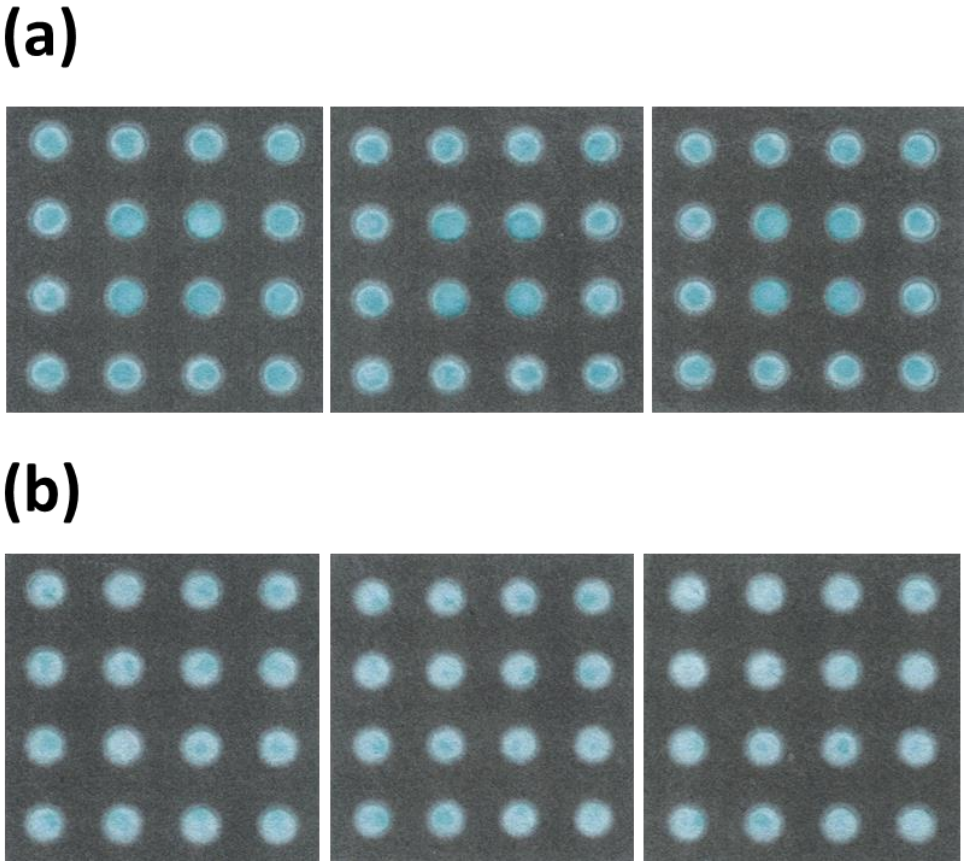

Figure A-15 – Digitalized outputs of the colorimetric glucose assay without change in contrast. (a) Original design. (b) Optimized design.

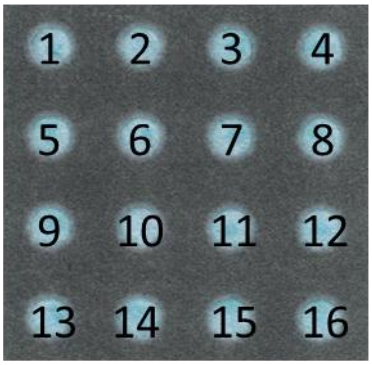

Figure A-16 – Example of digitalized assay showing the spot numbers.

Table A-1 – Data used to create the histograms of Figure 2-4 for the glucose assay and the *t*-Test of Table A-2. The experiments were run in triplicate

	Mean Pixel Intensity for the glucose bioassay / A.U.					
Spot #	**Original design**			**Optimized design**		
1	91.67	92.33	88.67	87.00	80.33	77.67
2	92.67	94.00	92.00	86.67	81.67	81.00
3	94.67	90.00	93.67	89.67	83.33	83.00
4	92.33	95.00	94.00	87.00	85.67	84.67
5	89.33	91.67	87.00	86.67	78.33	74.33
6	99.00	99.67	101.00	85.00	77.67	79.33
7	91.00	99.67	102.00	87.00	81.33	84.67
8	96.33	94.00	91.67	83.33	83.33	81.00
9	87.67	94.33	90.67	87.67	83.67	81.67
10	99.67	102.00	101.67	81.00	84.00	83.00
11	101.00	101.33	102.67	84.67	80.67	88.33
12	93.33	91.33	89.67	83.00	80.00	82.67
13	92.00	88.33	92.00	86.00	85.67	81.33
14	94.67	91.67	91.00	87.00	87.67	87.00
15	90.33	90.33	91.67	83.67	79.00	84.00
16	94.33	95.33	94.33	83.67	78.67	82.00

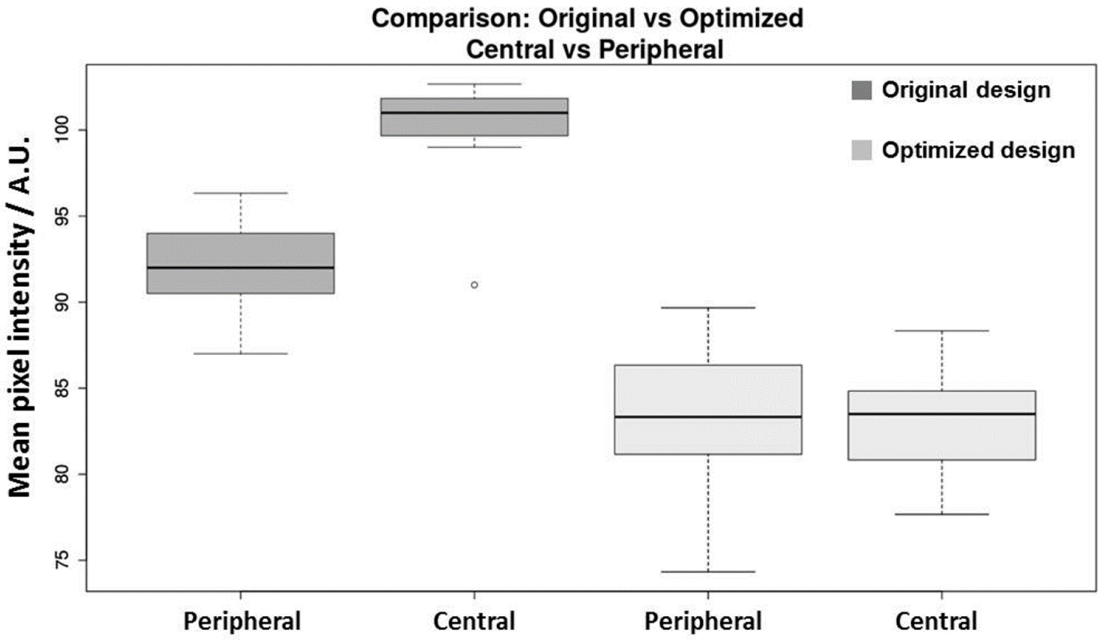

Figure A-17 – Box-and-whisker plot for the peripheral and central spots of the original and optimized designs. This plot depicts the difference between the medians of central and peripheral spots in the original design (statistically significant (*t*-test, C.I. 95%)) and between the medians of central and peripheral spots in the optimized design (difference not statistically significant (*t*-test, C.I. 95%)). There is a larger variance in the colorimetric outputs of the optimized design, indicating that the reaction did not proceed to completion. The circle at the central spots of the original design depicts an outlier.

Table A-2 – *t*-Test analysis for two samples, assuming equal variance in the population. As it is possible to observe, for the optimized design the null hypothesis is true ($t_{calc}<t_{crit}$), showing that there is no statistical difference between the color in central and peripheral spots. For the original design, the null hypothesis is false ($t_{calc}>t_{crit}$), and there is statistical difference between the color of central and peripheral spots

		Original design			**Optimized design**	
***t*-Test: Two-Sample Assuming Equal Variances**		***Peripheral Spots***	***Central spots***		***Peripheral spots***	***Central spots***
Mean		92.06	100.06		83.31	83.06
Variance		5.17	9.45		11.31	9.92
Observations		36	12		36	12
Pooled Variance		6.19			10.98	
Hypothesized Mean Difference		0			0	
df		46			46	
t Stat		-9.65			0.226	
P(T<=t) one-tail		6.31 E-13			0.411	
t Critical one-tail		1.68			1.68	
P(T<=t) two-tail		1.26 E-12			0.822	
t Critical two-tail		2.01			2.01	

A.2 Increased Sample Volume and Time of Reaction

To test how the reaction time and the sample volume affects colorimetric output results, we performed the enzymatic assays using the optimized device, changing the sample volume (65 and 80 µL) and the reactional times (10 and 20 min), as depicted in Figure A-18.

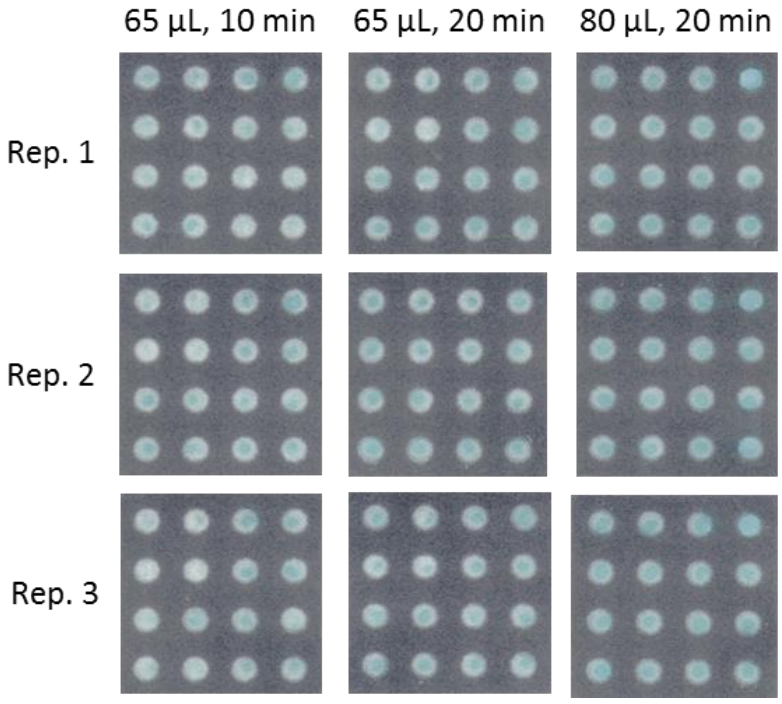

Figure A-18 – Digitalized outputs of the colorimetric glucose assay without change in contrast for the optimized design. The assay conditions (volume and reactional times) are indicated in the figure. The glucose standard solution concentration was 2.0 mmol L^{-1}.

Table A-3 – Data obtained for the glucose assay with different sample volumes and different reactional times, using the device with optimized design (Figure A-17). The experiments were run in triplicate

Mean Pixel Intensity for the glucose bioassay / A.U.										
Spot #	**65 µL, 10 min (control)**				**65 µL, 20 min**				**80 µL, 20 min**	
1	88.33	72.00	79.33		77.00	90.67	91.33		95.67	96.33	87.67
2	85.00	71.33	78.67		75.33	87.00	86.67		93.67	96.00	89.00
3	88.67	85.33	91.33		86.00	86.67	92.00		95.00	97.67	91.00
4	91.00	86.33	86.33		84.00	89.67	96.33		91.33	93.00	84.00
5	81.33	64.67	74.33		70.67	89.00	81.67		87.00	91.67	84.00
6	81.00	66.00	74.00		68.67	85.33	81.00		88.33	92.33	83.00
7	84.00	78.67	88.00		82.00	85.00	87.67		91.67	93.67	83.33
8	81.00	79.00	86.33		87.00	85.00	88.00		89.00	93.67	81.33
9	80.33	80.00	78.67		81.67	89.33	85.67		89.67	93.00	84.33
10	79.33	76.33	88.33		78.00	87.00	89.33		88.67	87.67	81.33
11	76.33	73.00	88.00		82.67	87.67	84.67		91.67	92.00	85.00
12	79.00	72.33	80.00		81.33	86.67	88.00		87.00	90.00	86.33
13	80.33	80.67	79.00		85.67	89.67	91.67		89.00	92.67	84.00
14	81.33	76.00	78.67		85.67	89.00	91.33		94.67	89.00	83.33
15	79.00	74.67	86.67		87.33	90.33	86.00		94.00	95.33	84.67
16	79.33	74.33	87.00		82.00	92.67	85.33		94.33	92.67	85.67

[Glucose] = 2.0 mmol L^{-1}

We observed that an increase both in the reaction time and in the sample volume present a statistically significant increase in the colorimetric output, with a decrease in the variance (Table A-4), due to a higher homogeneity of the color developed in the spots. This result suggests that this approach can be used to improve the LOD and LOQ of the method via addition of larger volumes of sample containing lower concentrations of the analyte of interest.

Table A-4 – One-way ANOVA tests comparing the results presented in Table A-3, using the device with optimized design. Both the increase in reaction time and sample volume present a statistically significant increase in the colorimetric signal ($F_{calc}>F_{crit}$). A decrease in the standard deviation with the increase in reaction time and sample volume due to more homogeneous results is also observed

SUMMARY					
Groups	*Count*	*Sum*	*Average*	*Variance*	*Standard deviation*
65 µL, 10 min	48	3850.67	80.22	37.03	6.1
65 µL, 20 min	48	4112.33	85.67	28.28	5.3
80 µL, 20 min	48	4305.33	89.69	19.51	4.4

One-way ANOVA between 65 µL, 10 min and 65 µL, 20 min						
Source of Variation	*SS*	*df*	*MoS*	*F*	*P-value*	F_{crit}
Between groups	713.22	1	713.22	21.84	9.87E-06	3.94
Within groups	3069.74	94	32.66			
Total	3782.96	95				

One-way ANOVA between 65 µL, 10 min and 80 µL, 20 min						
Source of Variation	*SS*	*df*	*MoS*	*F*	*P-value*	F_{crit}
Between groups	2153.35	1	2153.35	76.16	9.32E-14	3.94
Within groups	2657.59	94	28.27			
Total	4810.94	95				

One-way ANOVA between 65 µL, 20 min and 80 µL, 20 min						
Source of Variation	*SS*	*df*	*MoS*	*F*	*P-value*	F_{crit}
Between groups	388.01	1	388.01	16.24	1.13E-04	3.94
Within groups	2246.29	94	23.9			
Total	2634.3	95				

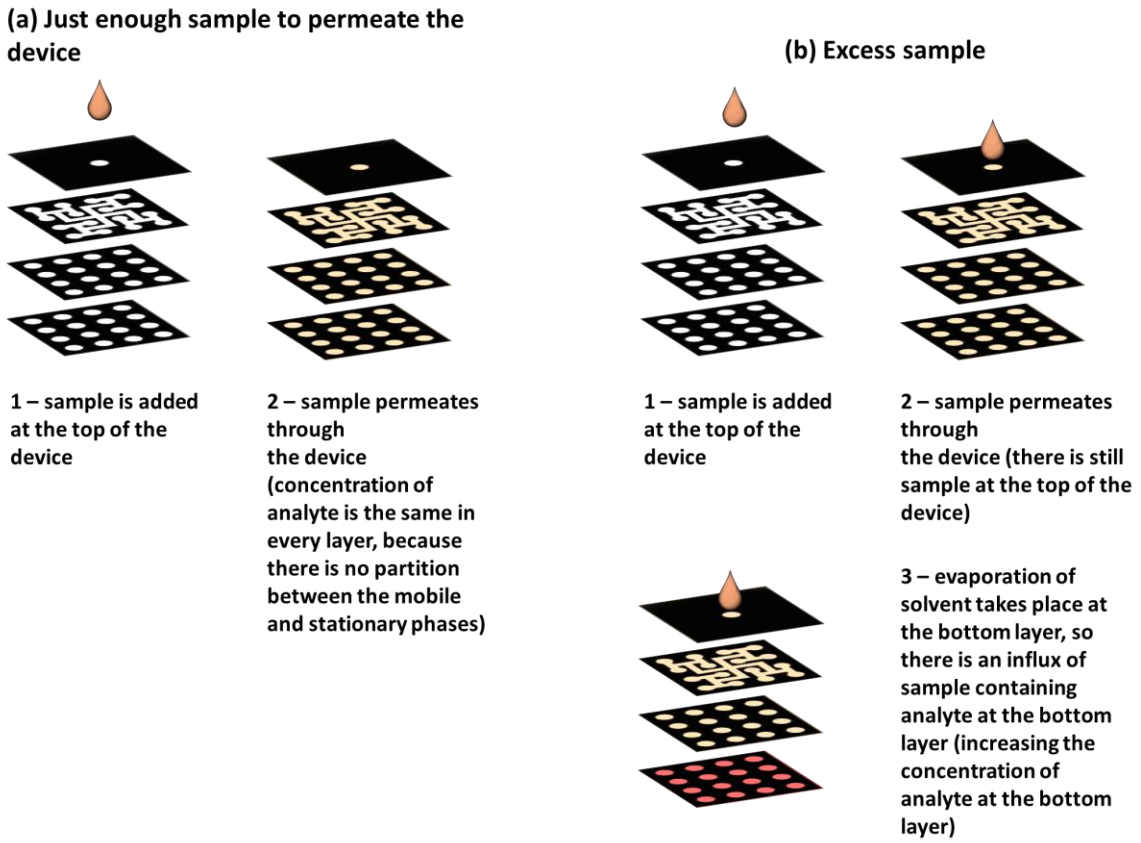

Figure A-19 – Schematics of the concentration process when an excess of sample is introduced to the 3D-µPADs. (a) When just enough sample is introduced in the device, the sample will permeate through the structure, so all layers will present the same concentration of analyte (because there is no interaction between cellulose and the analyte, as demonstrated in Figure A-21). (b) When an excess of sample is introduced in the device, the sample will permeate through the device as well, and all layers will contain the same concentration of analyte. However, the bottom layer of the device is open, in contact with air, enabling solvent evaporation. Then, more sample (and therefore more analyte) is transported towards the bottom layer, which already contains analyte, explaining the higher concentration of analyte at the bottom layer.

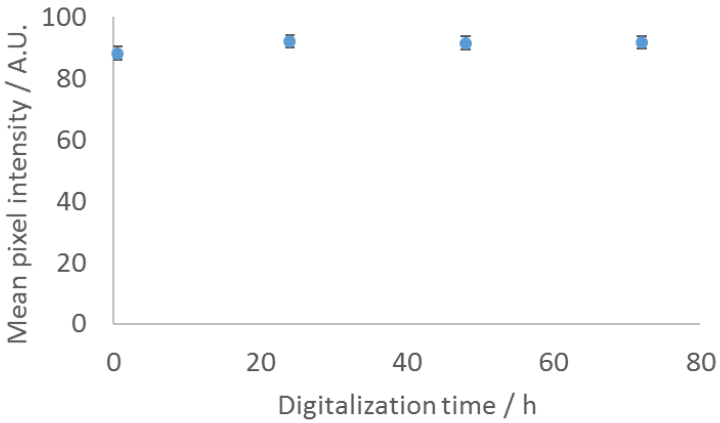

Figure A-20 – Signal stability test for the colorimetric glucose assay. 65 µL of a 2 mmol L^{-1} glucose standard was applied at the top of the optimized design device, and the reaction proceeded for 20 min. Digitalization of the devices were performed after: 30 min, 24 h, 48 h and 72 h.

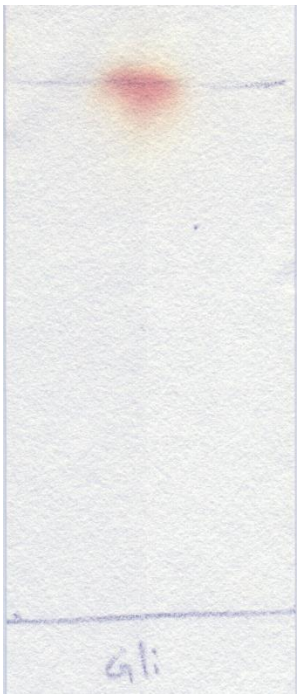

Figure A-21 – Paper chromatography of glucose with a retention factor of 1 (Rf = 1), showing that there is no adsorption of the analyte on the paper support. The glucose solution was spotted at the bottom line and dried in air before the elution was

performed with deionized water (solvent line marked with the top line). The paper plate was revealed by spraying a solution containing glucose oxidase, peroxidase and potassium iodide, to avoid further elution of the glucose. There is no partitioning mechanism between the glucose in the aqueous matrix (mobile phase) and in the water adsorbed on the cellulose (stationary phase), because both mobile and stationary phases are water. Adapted from ref. [44] with permission.

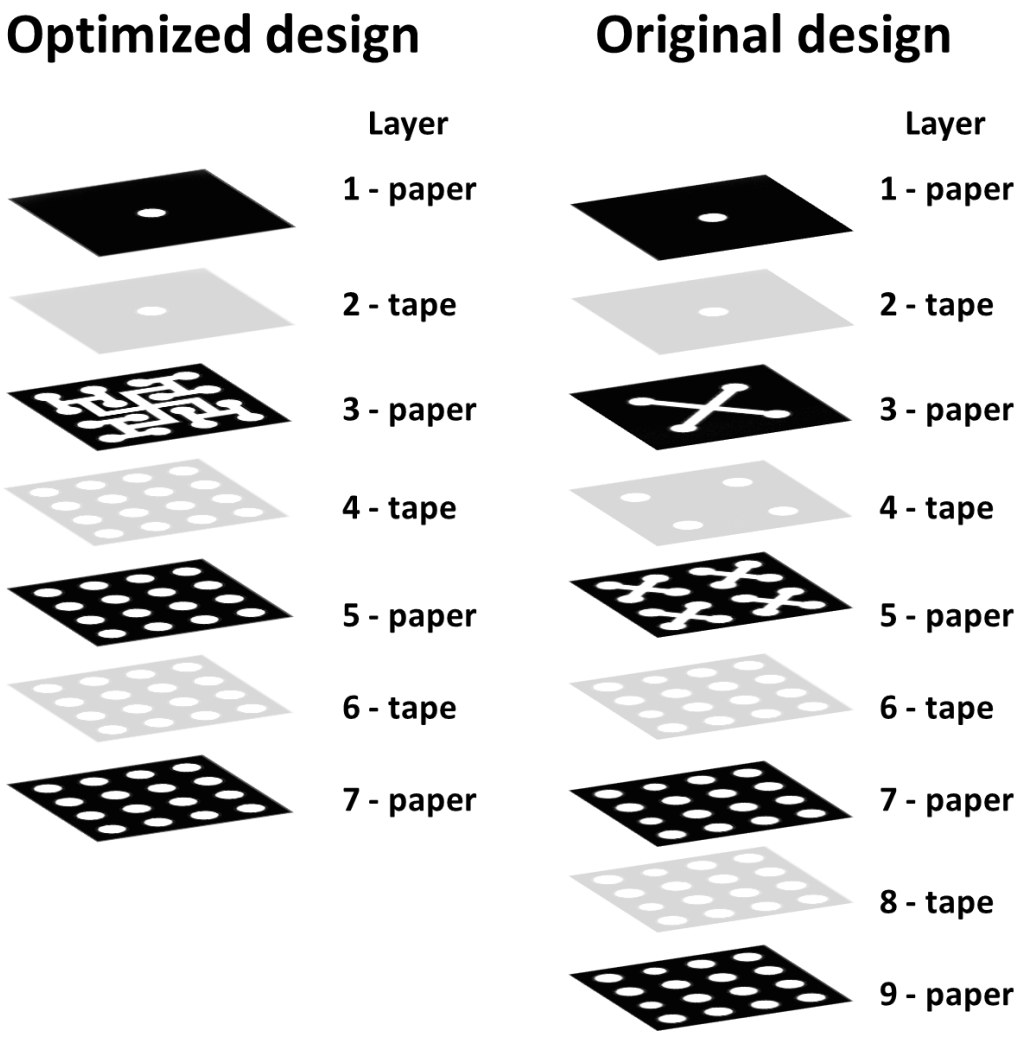

Figure A-22 – Representation of 3D-µPADs with the optimized (left) and original (right) designs, using double-tape layer for assembly [26]. The original design requires 2 more layers than the optimized design, which shows that the rational design of the layers benefit 3D-µPADs in general, independent of the layer-assembly method.

APPENDIX B. SUPPLEMENTARY INFORMATION OF CHAPTER 4: RAPID AND LOW-COST DEVELOPMENT OF MICROFLUIDIC DEVICES USING WAX PRINTING AND MW TREATMENT

B.1 Ultimate Working Pressure Failure Mode Testing

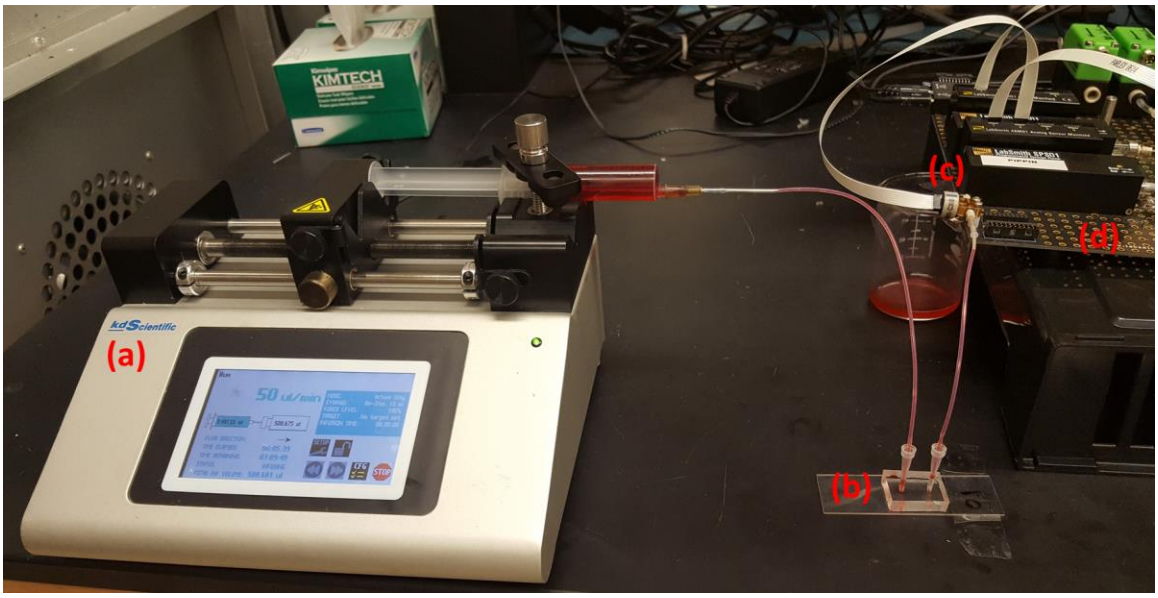

Figure B-1 – Photograph of the experimental setup for chip working pressure testing. (a) Syringe pump. (b) PDMS-glass hybrid microchip (1-cm long, nominal width: 400 µm). (c) Fluidic pressure sensor (d) Microfluidic automation system.

B.2 Printer Resolution

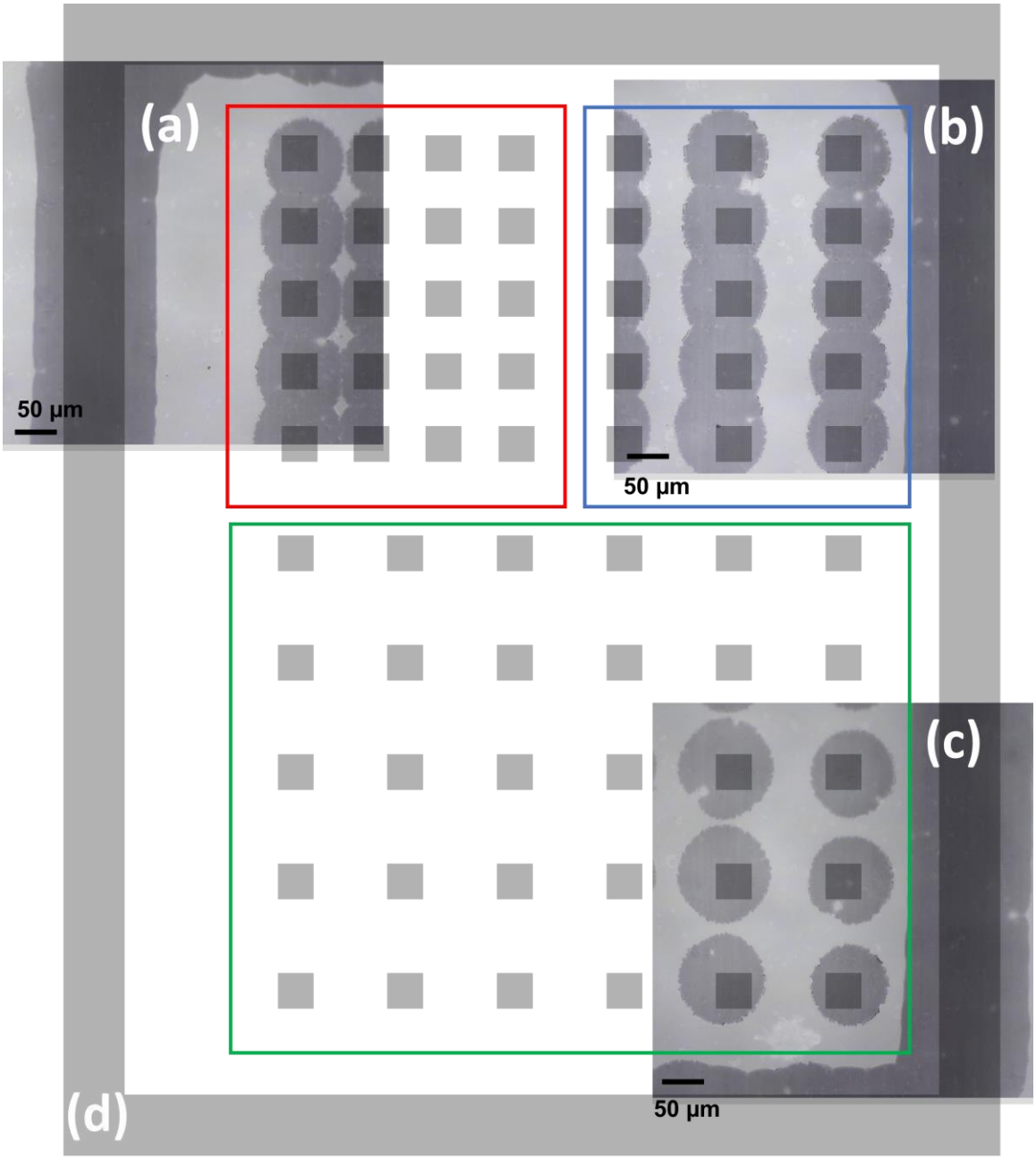

Figure B-2 – Evaluation of printer resolution. (a) 1 pixel wide vertical line, no spacing between vertical pixels (b) Pixels separated by 1 pixel of distance horizontally and 1 pixel of distance vertically. (b) Pixels separated by 2 pixels of distance horizontally and 1 pixel of distance vertically. (c) Pixels separated by 2 pixels of distance horizontally and 2 pixels of distance vertically. (d) A single pixel-wide box surrounds the patterned pixels. Scale bars are 50 µm.

A transparent pattern of square pixels surrounded by a single pixel-wide box is overlaid on the actual microscope images of the wax printed features in Figure B-2. The red box encompasses pixels separated by one pixel of distance, in the vertical and horizontal directions. The blue box encompasses pixels separated by one pixel of distance in the horizontal direction and two pixels of distance in both the vertical. The green box encompasses pixels separated by two pixels of distance, in the vertical and horizontal directions.

The real printing resolution of the Xerox Phaser 8580 wax printer is 600x600 DPI. The pixel pattern overlaid in Figure B-2 was designed at 490 pixels per inch (PPI) and printed at 490 DPI, to print all the designed pixels at the correct scale. 490 DPI was chosen as this was the highest resolution that reliably printed features without artifacts due to software or hardware issue. Given a 490 DPI resolution, the anticipated center-to-center spacing, and thus the maximum dot size would be roughly ~52 μm (25.4 mm / 490 DPI). However, while the center-to-center spacing is 52 μm as expected, the actual printed dot is nearly twice the size (103 ± 8 μm), overlapping half of the adjacent pixels (Figure B-2). This is difference is likely due to the roller transfer step of the wax printer extruding the dot onto the printed substrate.

When adjacent pixels are designed alternating between black pixel and white pixels (Figure B-2b), the printed dots corresponding to the black pixels take up about half of the neighboring adjacent pixels (empty space) and thus there is some contact between the adjacent printed black pixels (dots). When there is no separation between the pixels (as in the border of Figure B-2a), the excess material from the overlapping dots is extruded by the roller transfer step of the printer resulting in an increased printed line width. Thus, while

the size of individually printed pixels is 103 ± 8 µm, the size of a line with a width of one pixel is 163 ± 4 µm, vertical or 159 ± 3 µm, horizontal. For comparison purposes, a mask fabricated with a high-resolution printer for soft-lithography can generate channels around 20 µm, while for submicron resolution a chrome photomask is usually required (at higher costs) [91].

B.3 Vertical versus horizontal printing

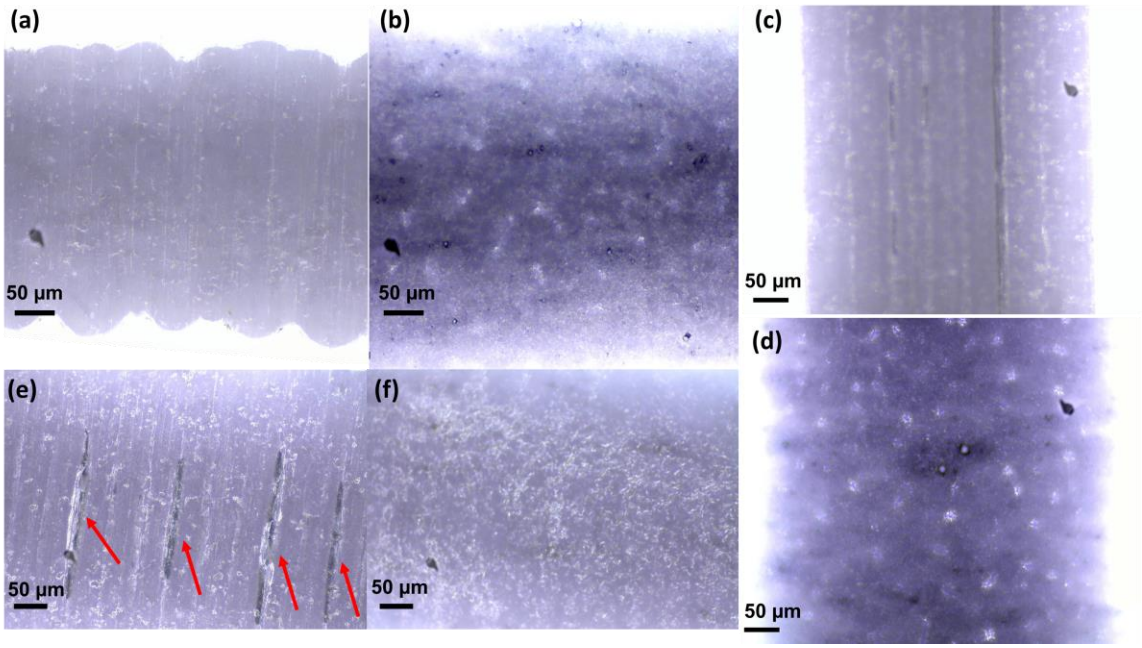

Figure B-3 – Evaluation of horizontally printed features (nominal size: 250 µm) (a) before and (b) after thermal treatment and vertically printed features (c) before and (d) after thermal treatment (100 ºC, 45 s). (e) Details of raster marks on wax patterns before thermal treatment. (f) Smooth wax patterns after thermal treatment. Scale bars are 50 µm.

B.4 Characterization of Wax Molds

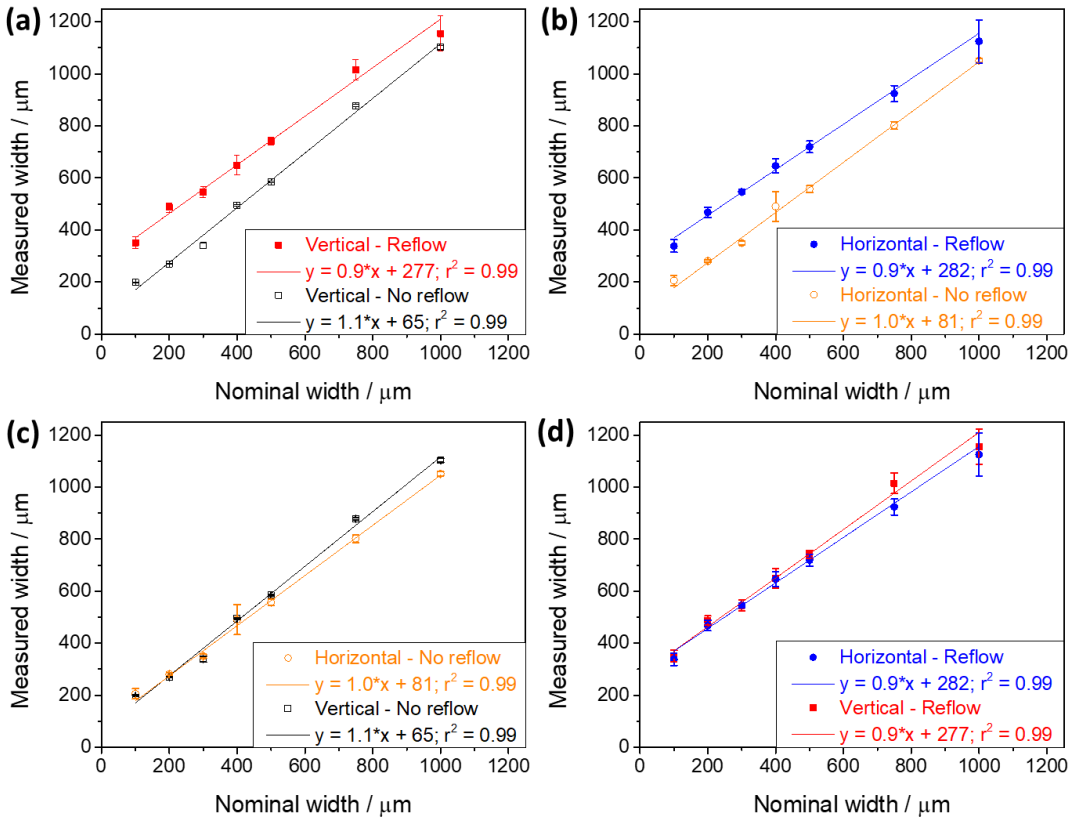

Figure B-4 – Characterization of the wax printed molds. (a) Nominal line widths compared with printed line widths in a vertical orientation. (a) Nominal line widths compared with printed line widths in a horizontal orientation. (c) Nominal line widths compared with printed line widths before thermal reflow treatment. (d) Nominal line widths compared with printed line widths after thermal reflow treatment. The values represent the average of three measurements ± 1 standard deviation.

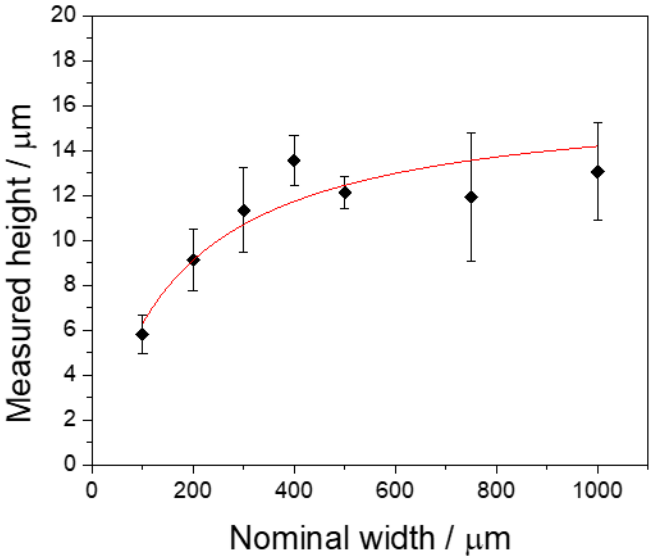

Figure B-5 – Nominal line widths compared with printed line heights in a vertical orientation before thermal reflow treatment, using photo printing quality. The red line between experimental points is a guide to the eyes and does not represent a best fit curve. The values represent the average of three measurements ± 1 standard deviation.

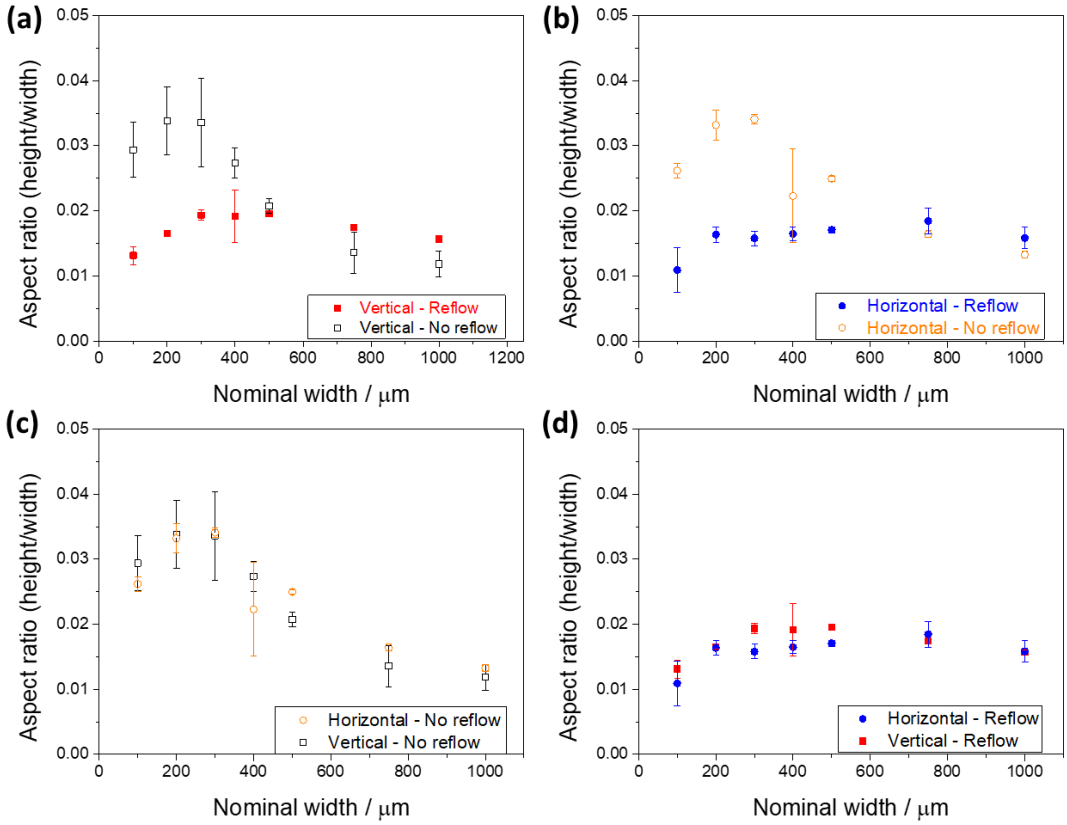

Figure B-6 – Characterization of the wax printed molds. (a) Aspect ratio of molds printed in a vertical orientation. (b) Aspect ratio of molds printed in a horizontal orientation. (c) Aspect ratio of wax molds before thermal reflow treatment. (d) Aspect ratio of wax molds after thermal reflow treatment. The values represent the average of three measurements ± 1 standard deviation.

Table B-1 – One-way ANOVA tests comparing the aspect ratio (height/width) of molds printed in vertical and horizontal orientations after thermal reflow treatment. Both printing orientations did not show a statistically significant difference for nominal lines over 200 µm ($F_{calc}<F_{crit}$)

One-way ANOVA – Vertical printing						
Source of Variation	*SS*	*df*	*MoS*	*F*	*P-value*	F_{crit}
Between groups	1.48E-05	5	2.96E-06	1.72	0.206	3.11
Within groups	2.07E-05	12	1.72E-06			
Total	3.55E-05	17				

One-way ANOVA – Horizontal printing						
Source of Variation	*SS*	*df*	*MoS*	*F*	*P-value*	F_{crit}
Between groups	4.00E-05	5	7.99E-06	2.8	0.0667	3.11
Within groups	3.42E-05	12	2.85E-06			
Total	7.42E-05	17				

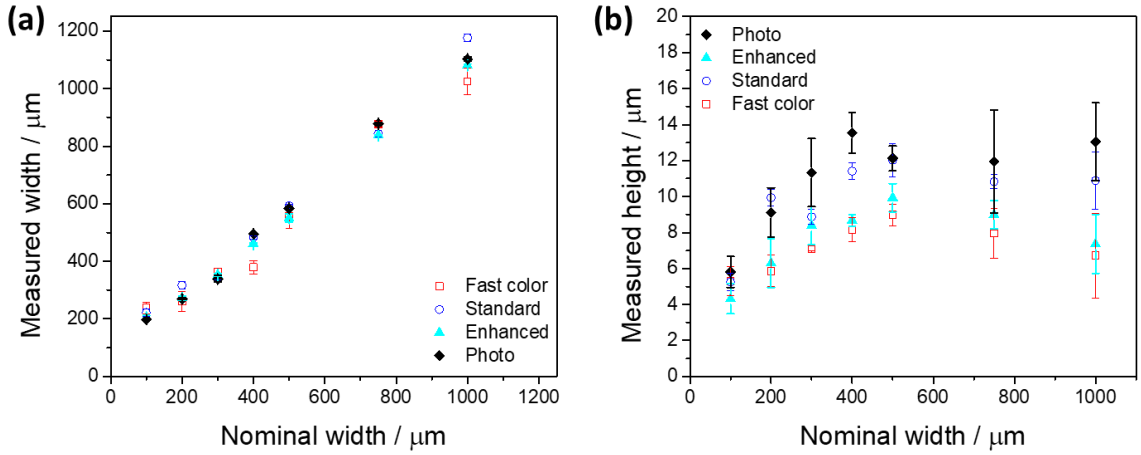

Figure B-7 – Characterization of the wax molds printed with different printing qualities. (a) Nominal line widths compared with printed line widths in a vertical orientation. (b) Nominal line widths compared with printed line heights in a vertical orientation. The values represent the average of three measurements ± 1 standard deviation.

B.5 Grayscale Usage

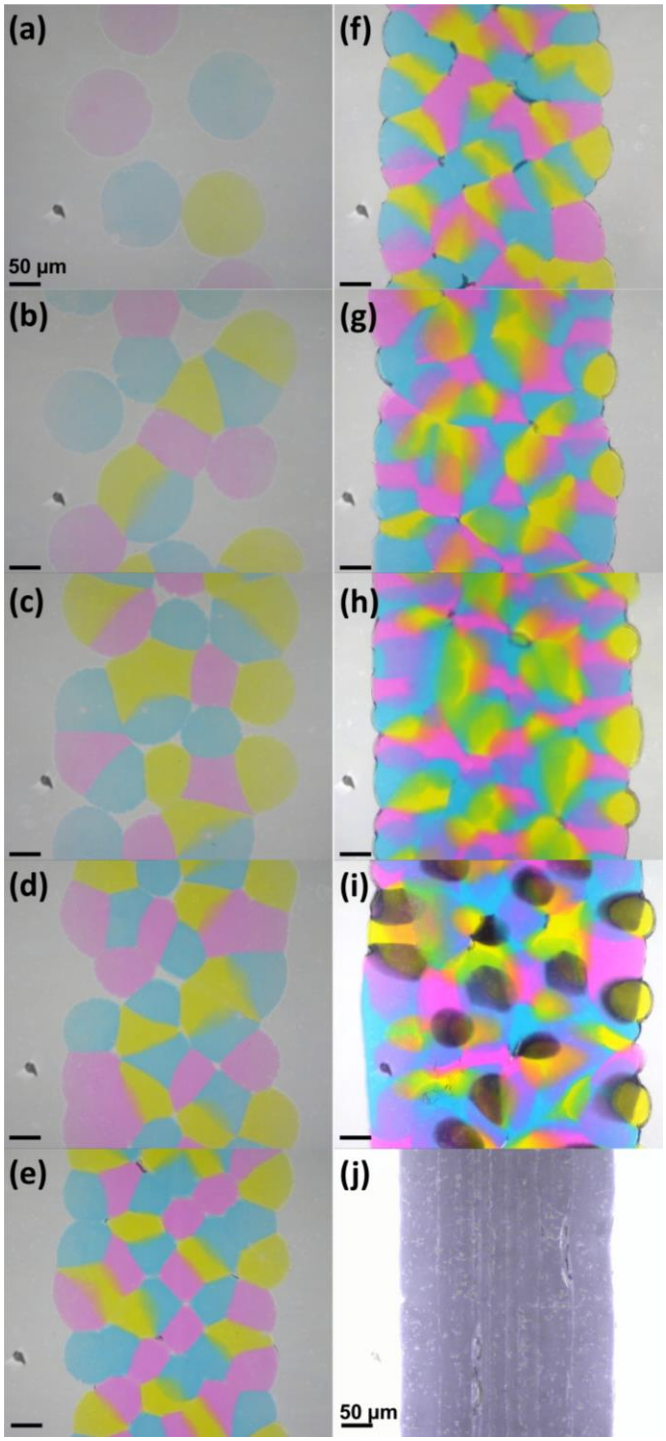

Figure B-8 – Vertically printed features (nominal size: 250 µm) printed in shades of gray in the CMYK color space (a) K 10, (b) K 20, (c) K 30, (d) K 40, (e) K 50, (f) K 60, (g) K 70, (h) K 80, (i) K 90 and (j) K 100. Scale bars are 50 µm.

As can be seen in Figure B-8, the shades of gray are composed of a mixture of the different solid inks (cyan, magenta, yellow and eventually black - Figure B-8i) being applied together using different nozzles, in a similar fashion as the horizontal printing (Figure B-2a), which in turn also modifies the width of the patterns. The use of shades of gray below K 50 does not generate useful patterns, due to the high number of voids in the printed structure. When K value reaches 100 (black in CMYK space color), the printer prints the vertical pattern continuously, using the same nozzles, which explains the shape of the line in Figure B-8j.

B.6 Multiple Printing Steps and Mold Reusability

While the PAP rapid prototyping technique toner printing [15,16] allows for changes in pattern heights by printing over the same transparency film repeatedly, this multiple printing approach to increase channel height cannot be used in conjunction with wax printing due to the principles of operation of this technology. The wax patterns on the surface of the transparency film melt when in contact with the printer's hot metal drum, hindering the transfer of the new wax layer onto the previously deposited one. It also leaves wax smudges on the metal drum that affect future printings, and therefore is also not recommended.

In principle, molds created by wax printing could be reusable, but in practice this is untenable. As demonstrated by Vullev *et al.* [16], the reuse of fast-prototyped molds increases the surface roughness of PDMS channels, which is detrimental for applications like capillary electrophoresis. [17] Also, fast-prototyping techniques enables low-cost

fabrication of the molds (~$0.01, Table B-2) within minutes, minimizing the need for reusability.

Table B-2 – Fabrication costs using wax printing

Material	Pages	Price ($)	Cost per page ($)
Transparency film [a]	50	15.79	0.32
Solid ink [b]	8600 [c]	179.99	0.02
		Total cost per page	0.34
		Devices per page [d]	24
		Cost per mold	**0.01**

[a] https://www.staples.com/Apollo-Transparency-Film-for-Laser-Printers-Letter-Clear-8-1-2-x-11-50-Pack/product_829903 - Access on 11/21/2018.
[b] https://www.shop.xerox.com/supplies-accessories/8580-config-hc - Access on 11/21/2018.
[c] Each pack of solid ink can print up to 8600 pages.

B.7 Ultimate Working Pressure Failure Mode Testing

Table B-3 – *t*-tests comparing the efficacy of thermal treatments on pressure testing for bonded PDMS-glass hybrid chips. The conventional oven treatment and the microwave thermal reannealing pressure tests did not show a statistically significant difference ($t_{calc}<t_{crit}$), but both thermal treatments showed a statistically significant difference ($t_{calc}>t_{crit}$) in comparison with no thermal treatment

	Pair		Pair		Pair	
	Nothing	*Oven*	*Nothing*	*Microwave*	*Oven*	*Microwave*
Average	102.2	305.3	102.2	275.3	305.3	275.3
Variance	2235	575.1	2235	16.6	575.1	16.6
Number of observations	3	3	3	3	3	3
Pearson correlation	-0.4472		-0.7612		-0.2397	
Hypothesis test for difference of means	0		0		0	
df	2		2		2	
Stat t	-5.689		-5.944		2.057	
P(T<=t) one-tailed	0.01477		0.01358		0.08799	
t_{crit} one-tailed	2.92		2.92		2.92	
P(T<=t) two-tailed	0.02954		0.02716		0.176	
t_{crit} two-tailed	4.303		4.303		4.303	

B.8 Microwave Power Settings

The power of the commercial microwave oven used in this study (GE, model JES738WJ, 700 W) could be tuned in 10% increments, from ~70 W to ~700 W. The power setting 20 (~140 W) presented the best results in this study, preserving the features of the wax printed molds.

B.9 Arrhenius Law

$$k = \mathrm{A}\exp\left(\frac{-\Delta \mathrm{G}^{\ddagger}}{RT}\right) \tag{7}$$

k is the rate constant;

A is the pre-exponential factor;

$\Delta G^{\ddagger}$ is the activation energy

R is the universal gas constant

T is the temperature.

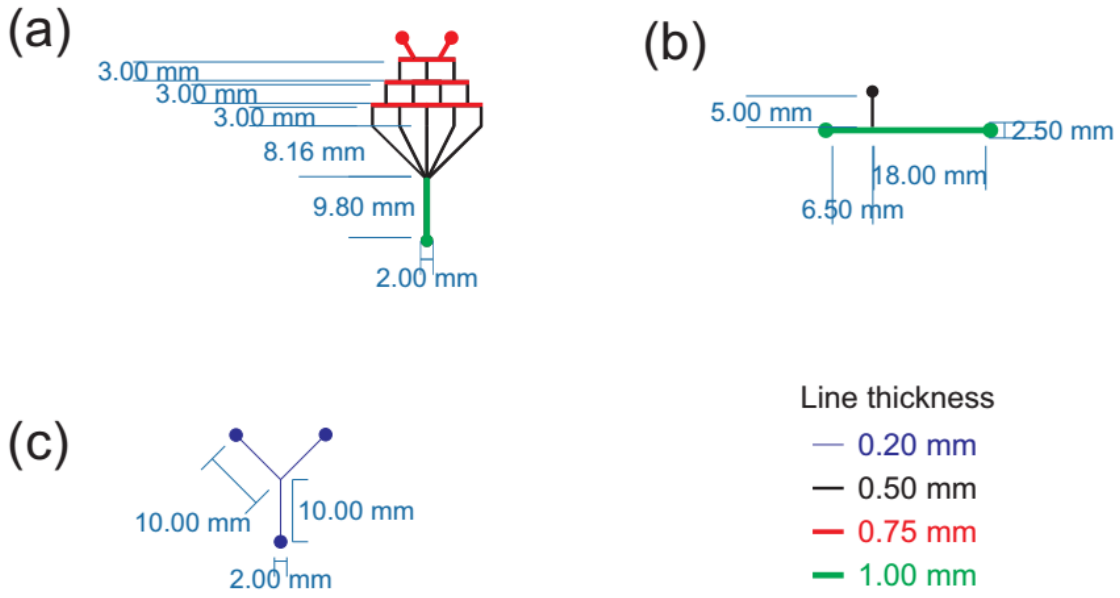

Figure B-9 – Design of microfluidic devices used as Proof-of-Concept devices. (a) Microfluidic gradient generator. (b) T-droplet generator. (c) Y-channel.

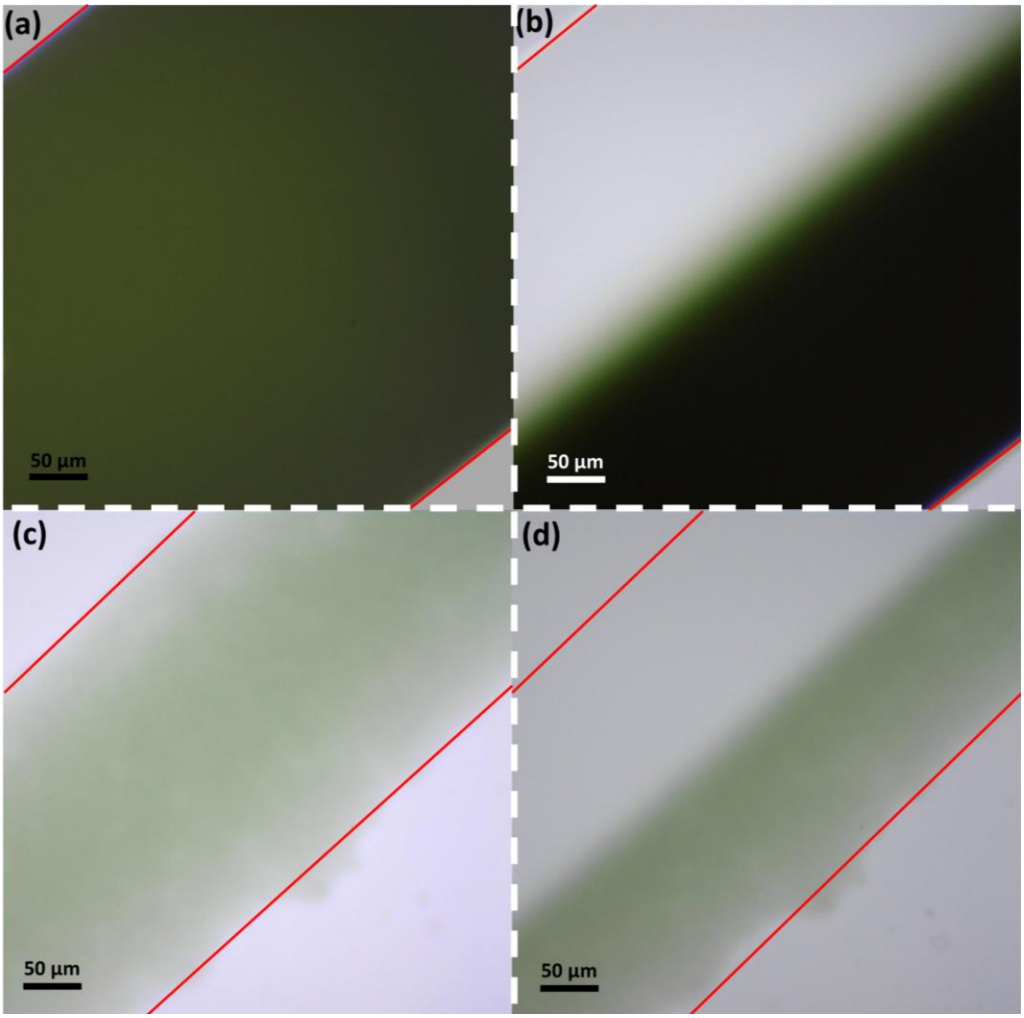

Figure B-10 – Comparison between the performance of Y-channel PDMS microchips to achieve laminar flow. (a) PDMS microchip cast on a mold fabricated using soft-lithography, filled with green dye by both inlets, and (b) with DI water in the upper inlet and green dye in the bottom inlet. (c) PDMS microchip casted on a mold fabricated using wax-printing, filled with green dye by both inlets, and (d) with DI water in the upper inlet and green dye in the bottom inlet. Both devices present laminar flow (noticed by the lack of mixing at the interface of the solutions), demonstrating the versatility of the fast-prototyping method. Flow provided by a syringe pump (flow: 20 µL/min). Soft-lithography mold specifications: 70 µm tall, 500 µm wide. Each channel was 1 cm long. Wax-printed mold specifications: 9 ± 1 µm tall, 490 ± 20 µm wide. Each channel was 1 cm long. Red lines in the micrographs are a visual aid to show channels' walls position. Color differences between (a) and (b); and (c) and (d) are due to contrast differences. Color differences between wax-printed and soft-lithography cast PDMS chips are due to differences between the height of the channel (taller channels present a higher optical density).

APPENDIX C. SUPPLEMENTARY INFORMATION OF CHAPTER 5: CUTTING EDGE MICROFLUIDICS: XUROGRAPHY AND A MICROWAVE

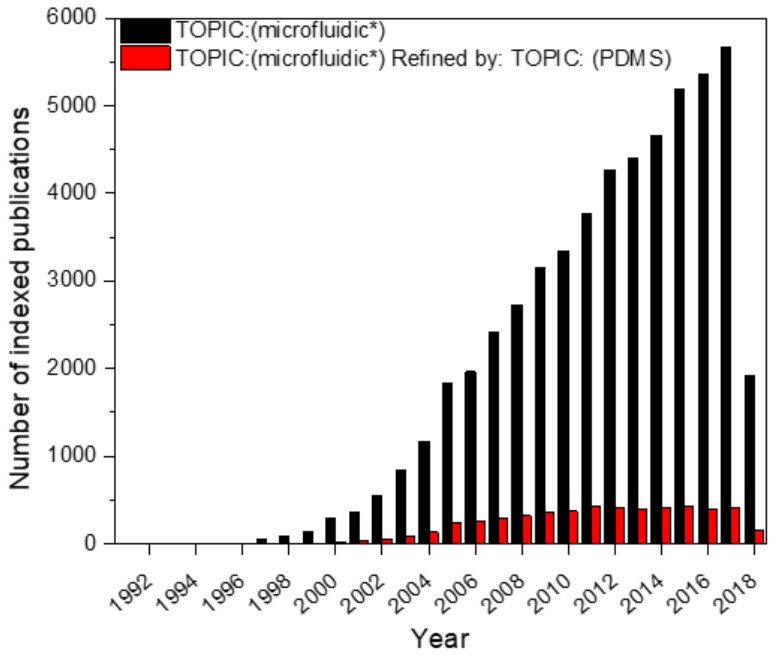

Figure C-1 – Number of indexed publications in microfluidics, retrieved from Web of Science 05/18/2018. Indices: SCI-EXPANDED, SSCI, A&HCI, CPCI-S, CPCI-SSH, BKCI-S, BKCI-SSH, ESCI, CCR-EXPANDED, IC. In black: TOPIC:(microfluidic*). In red: TOPIC:(microfluidic*) Refined by: TOPIC: (PDMS). Timespan: All years.

Table C-1 – Calculated parameters from linear regression of the fit to the data from the vertical cutting orientation and horizontal cutting orientation, with a confidence interval (C.I.) of 95%*

	Vertical		Horizontal	
r^2	0.935		0.994	
Confidence interval	2.50%	97.50%	2.50%	97.50%
Intercept / μm	39.1	157.9	-10.9	23.9
Slope / A.U.	0.907	1.08	0.98	1.03

* Obtained using R package.

Table C-2 – Statistical hypothesis *t*-tests comparing the height of the tape molds and the height of PDMS channels casted on its respective tape mold (confidence interval (CI): 95%). The null hypothesis states that there is no significant statistical difference between the height of tape molds and the PDMS channels casted on its respective mold and any differences between them are due to chance. There is not enough evidence to reject the null hypothesis ($t_{calc} < t_{crit}$ and p-value > p CI)

	3M Blue Platinum		PVC		Kapton	
	Tape	*PDMS*	*Tape*	*PDMS*	*Tape*	*PDMS*
Average	122	119	119	125	56	59
Variance	13	7	48	7	4	24
Number of observations	3	3	3	3	3	3
Pearson correlation	10		28		14	
Hypothesis test for difference of means	0		0		0	
df	4		4		4	
t calc	1.035		-1.381		-0.868	
P(T<=t) one-tailed	0.18		0.12		0.217	
t_{crit} one-tailed	2.132		2.132		2.132	
P(T<=t) two-tailed	0.359		0.239		0.435	
t_{crit} two-tailed	2.776		2.776		2.776	

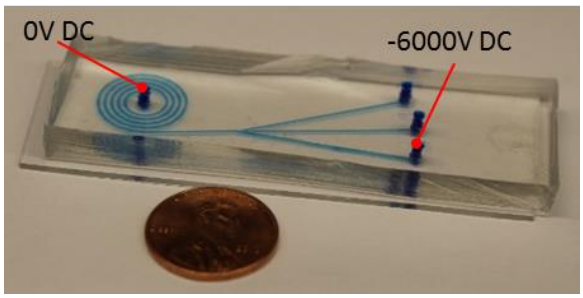

Figure C-2 – Schematic of applied potentials for the spiral dielectrophoretic focuser.

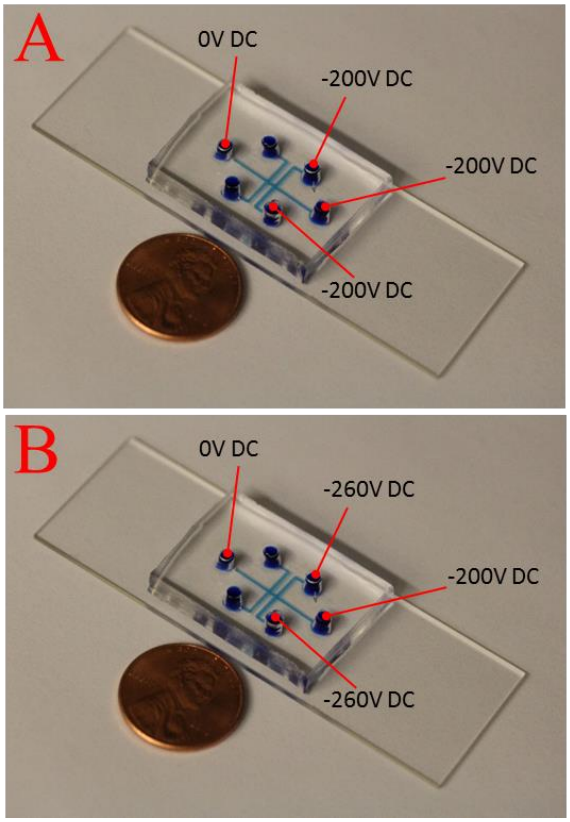

Figure C-3 – Schematic of applied potentials for the electrophoretic focuser that yield a wide (a) and narrow (b) sheath flow stream focused to the middle outlet.

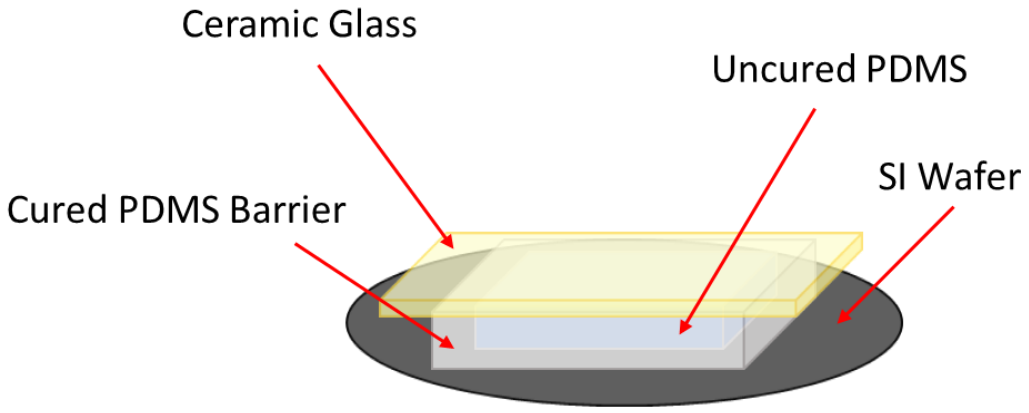

Figure C-4 – Experimental setup that enables curing of PDMS is 1.5 minutes.

C.1 Device Fabrication Examples and Notes on Fabrication Methods

Devices fabricated using the 5-minute curing on a glass backing substrate, 3-minute curing on a silicon backing substrate, and 1.5-minute curing in a substrate sandwich are shown in Figures S5- S7. The 3-minute silicon and 1.5-minute substrate sandwich-enabled curing methods can exhibit minor localized defects due to elevated temperatures causing expansion of trapped gases below the tape of the mold which are mitigated by achieving optimal lamination. Additionally, silicon-adhesive Kapton tape (<260 ˚C) exhibits fewer defects than acrylic-adhesive based Kapton tape (<140 ˚C) in these processes due to greater thermal stability of the adhesive. The 5-minute glass process has mild thermal conditions and does not exhibit any deformation, representing the best compromise between speed and quality while also employing the lowest cost materials.

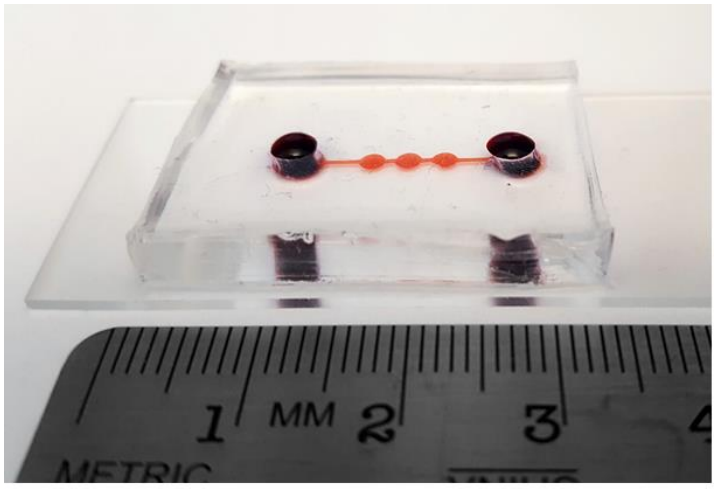

Figure C-5 – Proof-of-concept microdevice fabricated within 5 minutes using the substrate sandwich 1.5 min PDMS curing method with a Kapton tape mold.

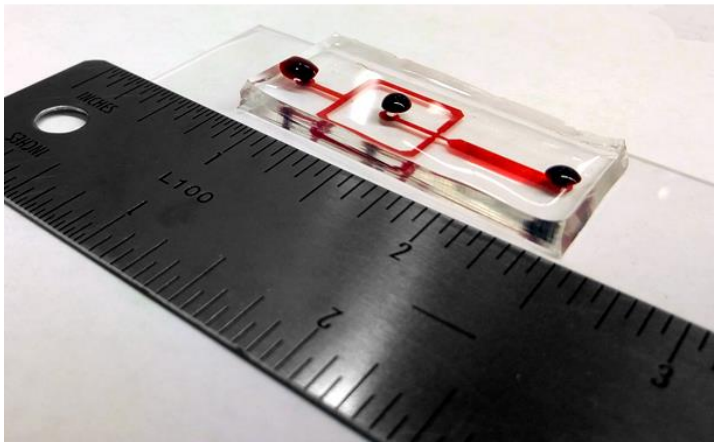

Figure C-6 – Proof-of-concept microdevice fabricated using the silicon wafer curing method (3 minute PDMS curing) with Kapton tape mold.

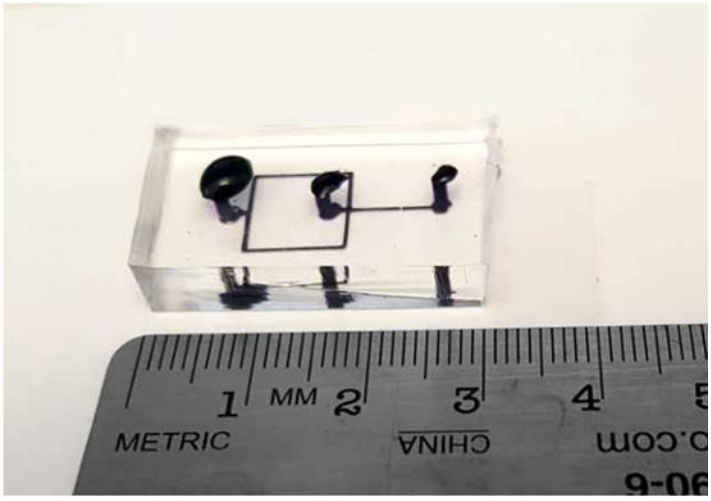

Figure C-7 – Proof-of-concept microdevice fabricated using the 5-min PDMS curing glass method (5 minute PDMS curing) with Kapton tape mold.

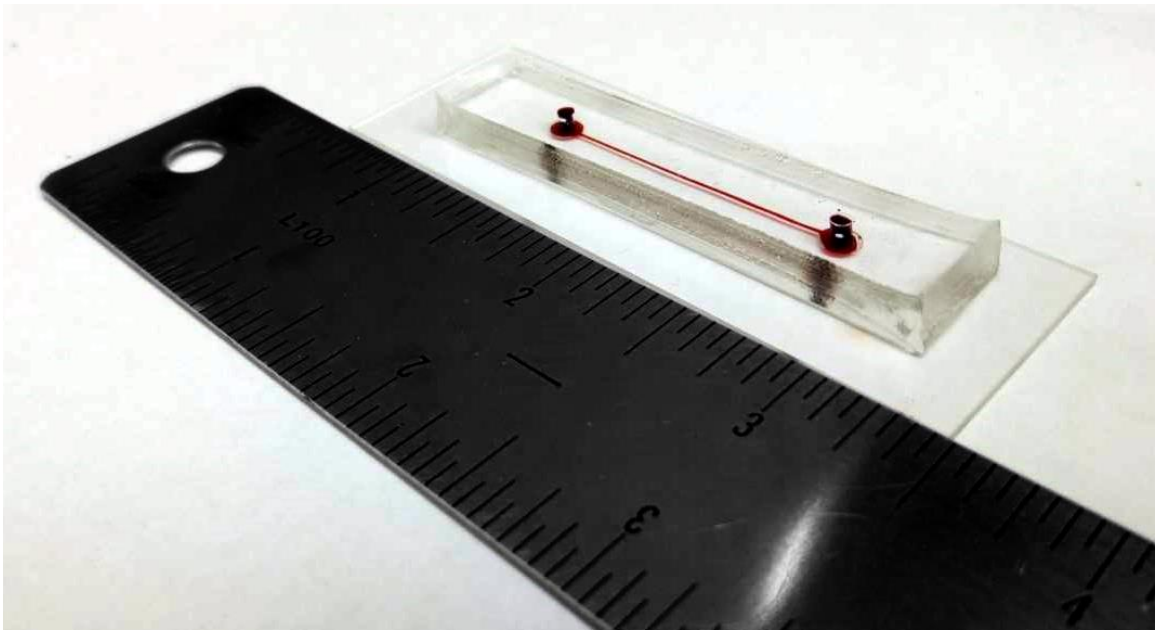

Figure C-8 – Proof-of-concept microdevice fabricated using the 5 minute PDMS on glass curing method with a PVC tape mold and sealed using only surface adhesion (no plasma pre-treatment).

Table C-3 – Electrical biases for electrophoretic flow focusing

	Outlet bias (Volts DC) in each channel					
Image	Top Right	Mid Right	Bot Right	Top Left	Mid Left	Bot Left
A	-200	-200	-200	0	Float	Float
B	-200	-200	-200	Float	0	Float
C	-200	-200	-200	Float	Float	0
D	-260	-200	-260	0	Float	Float
E	-260	-200	-260	Float	0	Float
F	-260	-200	-260	Float	Float	0

C.2 Fabrication and Prototyping Lab Instrumentation Costs

Table C-4 – Material Cost per Device

Material	Cost Per Device ($)	Consumable	Reusable
Kapton Tape *	0.20	X	
PVC Tape *	0.01	X	
3M Blue Platinum Tape *	0.03	X	
Glass Microscope Slides	0.17		X
PDMS **	0.49	X	

* Assumes 3 inch x 1 inch strip of tape to cover the entire microscope slide
** Assumes 7 g of PDMS at a cost of $0.07 / g

Table C-5 – Microfluidic Prototyping Lab Instrumentation Cost Used This Study

Instrument	Cost ($)
Cricut Cutter Plotter	180.00
Vacuum	1,953.00
Plasma Cleaner	5,900.00
700-Watt Microwave	50.00
Vacuum Chamber	75.00

Thermal annealing [122], simple surface adhesion (Figure C-8) [17], or clamped based pressure sealing [122] could be used in place of plasma bonding to reversibly seal microdevices for low fluidic pressure applications reducing lab start-up cost to ~ $2500 (using the equipment employed in this study). Finally, a lab set up cost of ~ $300 could be achieved by replacing the lab grade vacuum pump with a simple 12V vacuum for degassing PDMS (Table C-6).

Table C-6 – Lowest Cost Microfluidics Prototyping Lab Instrumentation Estimate

Instrument	Cost ($)
Cricut Cutter Plotter	180.00
Vacuum	15.00
Plasma Cleaner	--
700-Watt Microwave	50.00
Vacuum Chamber	75.00

APPENDIX D. SUPPLEMENTARY INFORMATION OF CHAPTER 6: GREEN LOW-COST USER-FRIENDLY ELASTOMERIC (GLUE) MICROFLUIDICS

D.1 Low-Cost Mold Fabrication Method – Blade Coating

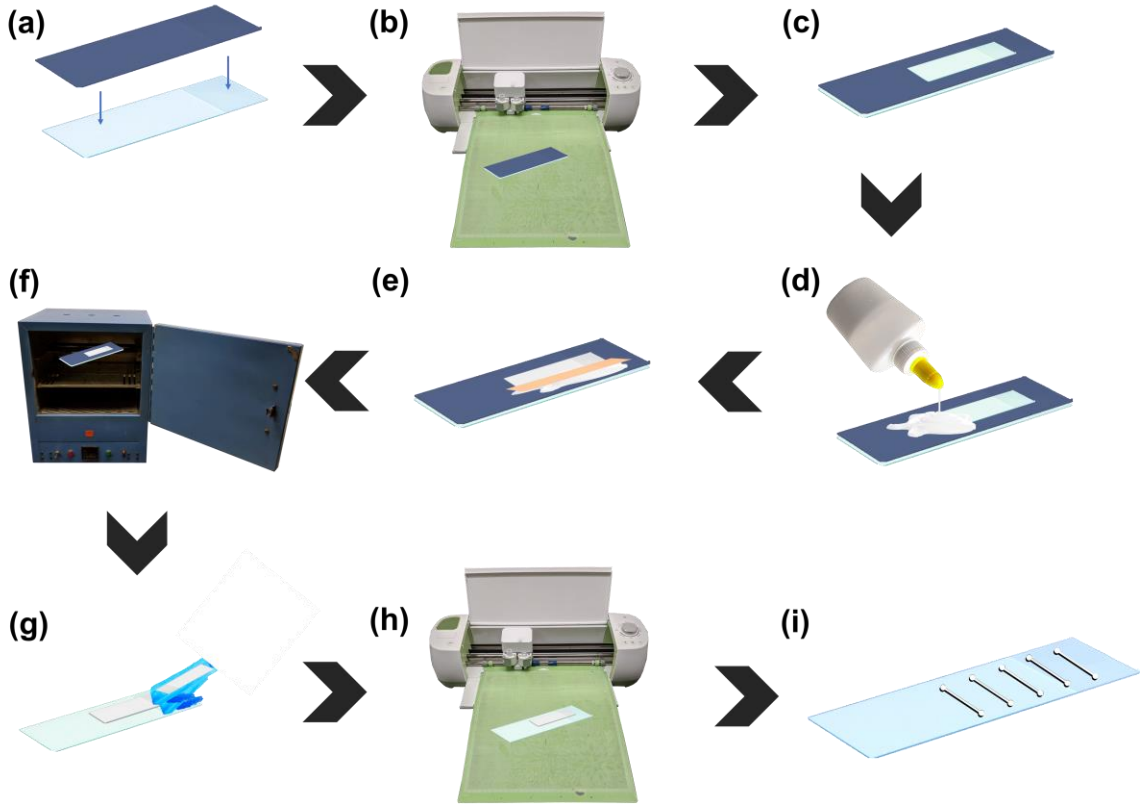

Figure D-1 – Step-by-step fabrication of PDMS-based microfluidic devices using the blade coating method. (a) PVC tape adhesion to a glass backing substrate. (b) Rectangle cutting on tape using a cutting plotter to create a glue reservoir. (c) Remove of the 'internal' rectangle, leaving the tape border on the backing substrate. (d) Water-soluble glue deposition on the edges of the tape of the mold. (e) Glue spreading onto the mold using a flat edge tool. (f) Glue curing in an oven. (g) Tape removal to expose the glue film. (h) CAD designs cutting on the glue film using a cutting plotter. (i) Glue mold.

D.2 Mold Cutting – Cutter Plotter

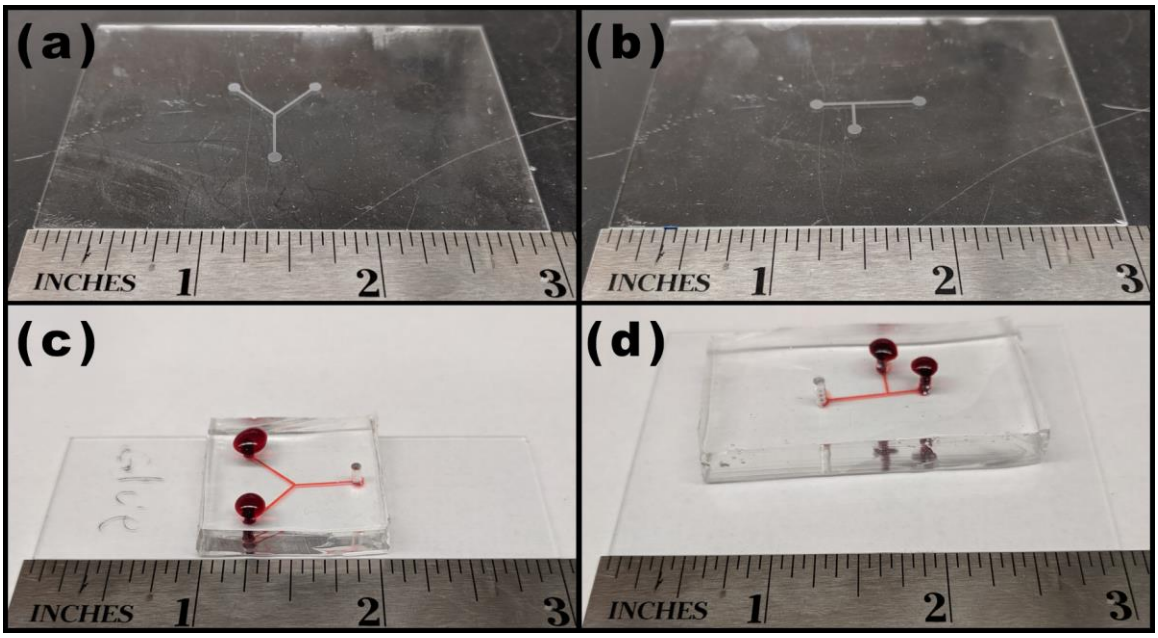

Figure D-2 – Proof-of-concept devices fabricated using the glue method and cut using the cutter plotter. (a) Glue mold of a Y-channel laminar flow generator (17.7 ± 0.4 µm tall, 415 ± 3 µm wide). (b) Glue mold of a T-droplet generator (18.3 ± 0.4 µm tall, 510 ± 20 µm wide). (c) PDMS-glass device of a Y-channel laminar flow generator filled with red dye. (d) PDMS-glass device of a T-droplet generator filled with red dye.

D.3 Proof-of-Concept Devices

D.3.1 3-Valve Normally Open Pneumatic Pump Fabrication

Briefly, the pump was designed in AutoCAD (Figure D-3) and the fluidic layer was laser etched into a freshly prepared glue thin film on a PDMS substrate to create a glue mold on the PDMS substrate (Figure D-4). A tape border was applied to the substrate and freshly degassed PDMS was squeegeed across the glue mold surface and cured during 30 min at 60 ^{o}C, creating a thin elastomer membrane (231 ± 2 µm), as depicted in Figure D-

4. Subsequently, another glue thin film was prepared on the cured PDMS membrane layer as described previously, and the pattern was repeated to create the pneumatic layer (Figure D-4). Degassed PDMS was cast over the pneumatic layer, cured, and fluidic access wells were cut into the pneumatic and fluidic layers. The complete, multilayer monolithic pneumatic pump was then sonicated as described in the GLUE Nonbonding section to remove residual glue. Normally open valves were chosen for this process to increase the rate of glue removal from the final device.

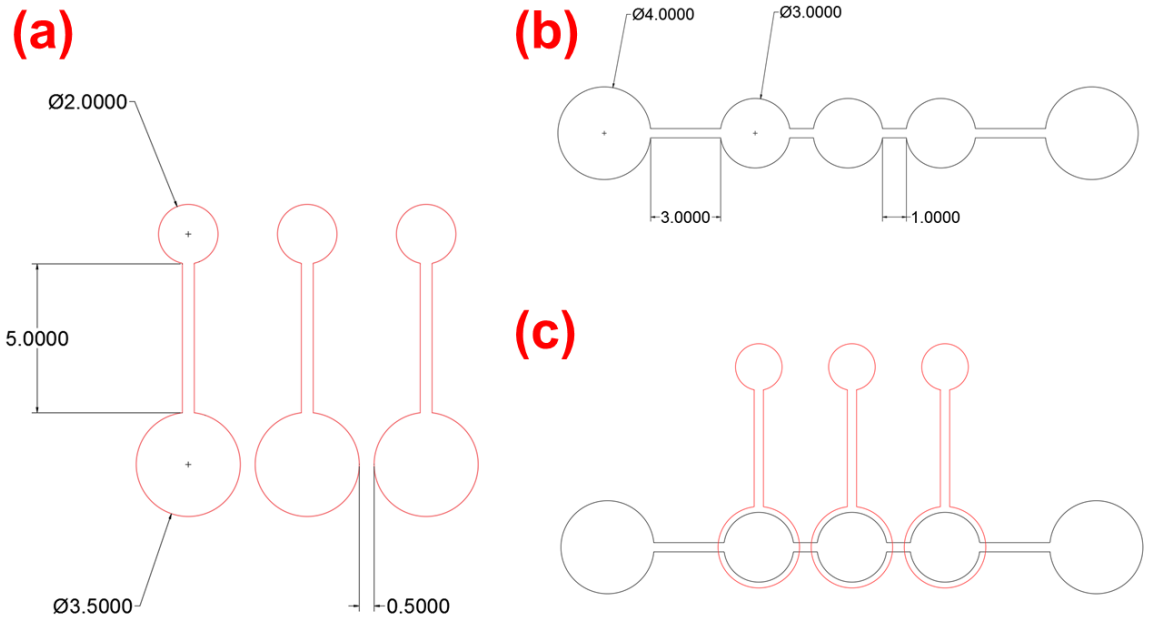

Figure D-3 – Design of a 3-valve normally open pneumatic pump. (a) Pneumatic layer design and dimensions. (b) Fluidic layer design and dimensions. (c) Layers aligned. All dimensions are in mm.

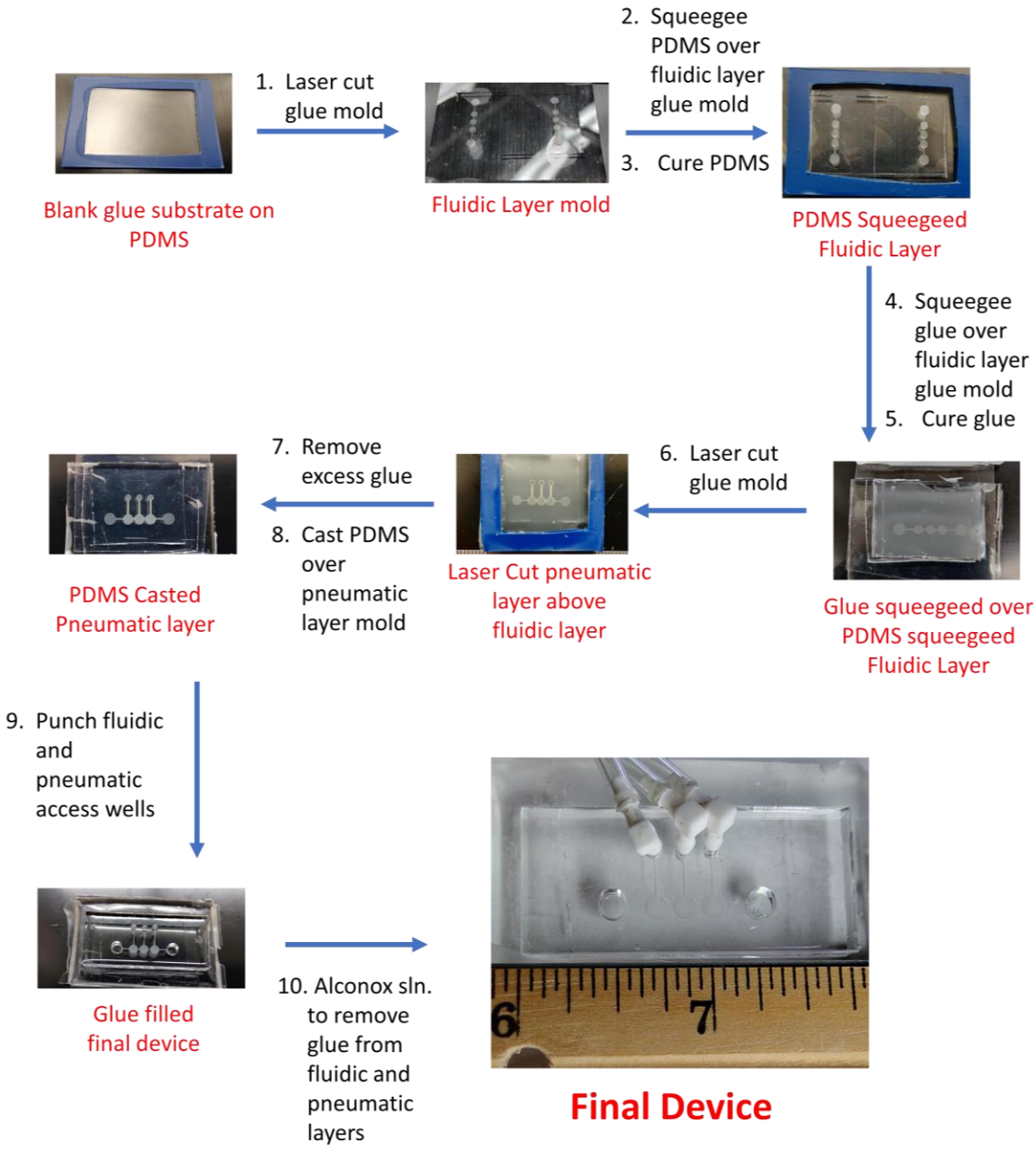

Figure D-4 – Fabrication steps of a 3-valve normally open pneumatic pump.

D.3.2 Pneumatic Lifting Gate Microfluidic Processor Fabrication

Briefly, the pump was designed in AutoCAD (Figure D-5), and a glue thin-film was freshly prepared on a glass substrate (Figure D-6). The fluidic layer pattern was vector cut (20% PWR 85% SPD) from the glue thin film while lifting gate feature molds were raster etched (12.5% PWR 40% SPD) into the valve regions of the fluidic layer (Figure D-6), all during the same laser cutting step. A tape border was applied to the substrate and freshly degassed PDMS was squeegeed across the glue mold surface and cured (Figure D-6). This created a thin membrane layer (231 ± 2 μm) containing the fluidic channels and perfectly aligned 3-dimensional lifting gate features as depicted in Figure D-6, in a single, simple reproducible step. Another glue thin-film on a glass substrate was prepared and the pattern for the pneumatic layer was laser cut and the excess from the glue film was removed. PDMS was cast over the pneumatic layer mold, cured and fluidic and pneumatic access wells were cut using a biopsy punch. The pneumatic layer was aligned by eye and bonded to the thin film fluidic layer prepared in the previous step. Then, fluidic access wells were cut into the film layer. The monolith containing the pneumatic layer and thin film layer was then removed, and a small drop of glue was applied to each of the lifting gate features and cured to prevent bonding of the lifting gate features in the final step. Finally, the PDMS monolith was plasma bonded to a glass slide to seal the fluidic layer yielding the final device. Alconox solution was cycled through the device using the mixing routine to remove excess glue from the lifting gate features.

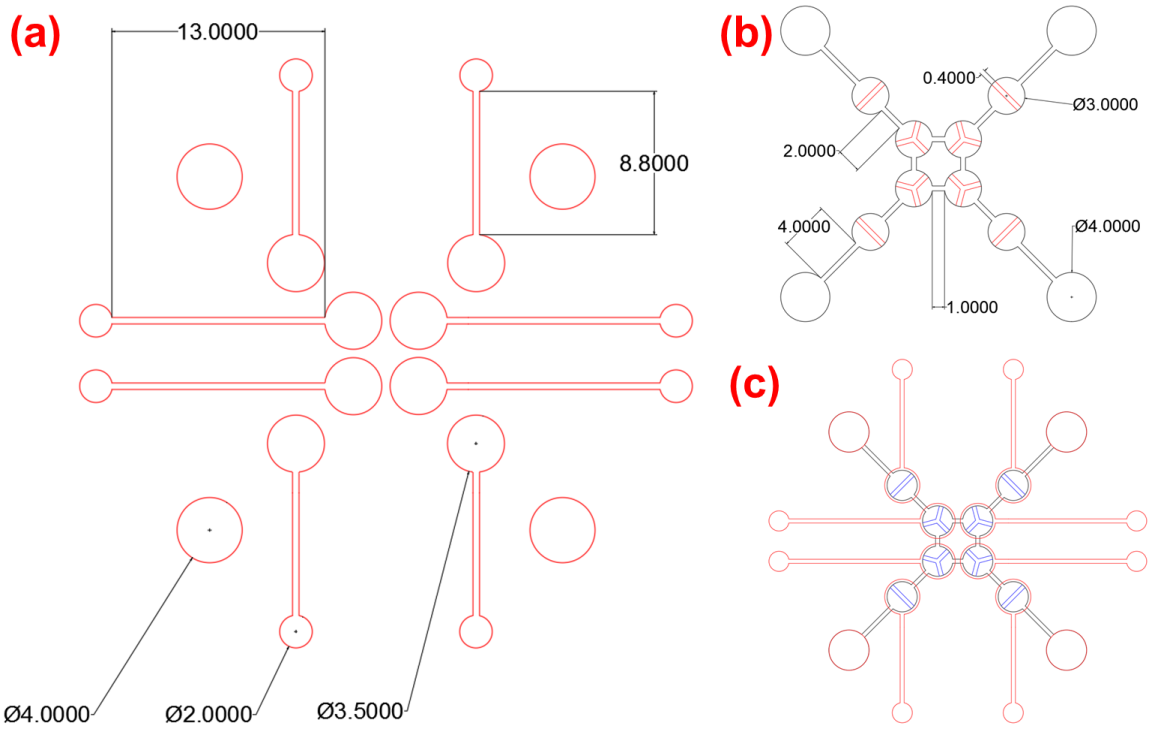

Figure D-5 – Design of a pneumatic lifting gate microfluidic processor. (a) Pneumatic layer design and dimensions. (b) Fluidic layer design and dimensions. (c) Layers aligned. All dimensions are in mm.

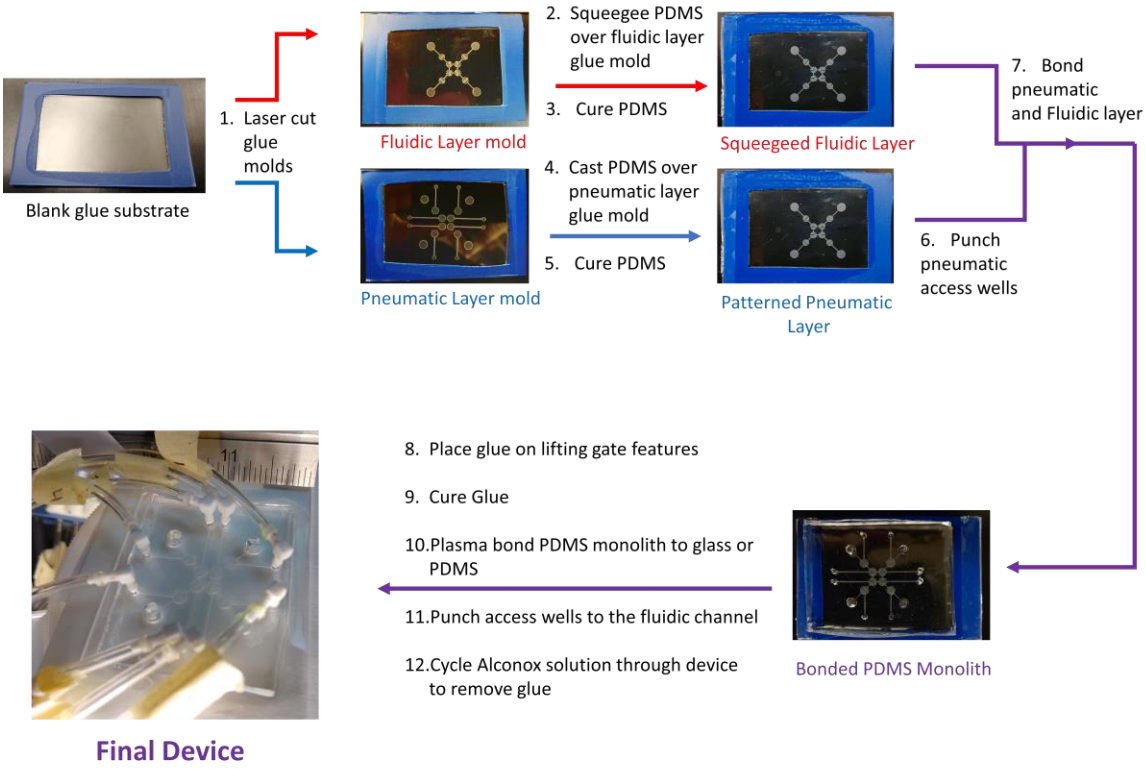

Figure D-6 – Fabrication steps of a pneumatic lifting gate microfluidic processor.

D.4 Device testing

D.4.1 Microchip Working Pressure Testing

To test the mechanical resistance of scaffolded PDMS devices, glue molds were fabricated on freshly cast PDMS slabs (4 mm thick) using the blade coating method using 3 layers of PVC tape. CAD designs were cut into the glue molds using the laser cutter, and degassed PDMS was cast onto these molds. After curing (conventional oven, 3 h, 60 ^{o}C), PDMS devices were sonicated with a warm soap solution to remove the glue from the channels, as described in the fabrication section in the main manuscript. Microchannels were designed to be 1-cm long and 600 µm wide.

Using a syringe pump (kd Scientific, Legato® 180, Holliston, MA), DI water was infused through the microchips with different flow rates (100 µL min^{-1}, 200 µL min^{-1}, 300 µL min^{-1}, 400 µL min^{-1}, 500 µL min^{-1}, 750 µL min^{-1}, 1 mL min^{-1}, 5 mL min^{-1}, 10 mL min^{-1} and 14.2 mL min^{-1}), for 30 s per rate. A pressure sensor (LabSmith, 0800 uPS Pressure Sensor, Livermore, CA) was placed at the beginning of the microchannel, and it was connected to a microfluidic automation datalogging system (LabSmith, uProcess™ System, Livermore, CA) connected to a computer. The pressure testing system is shown in Figure D-7.

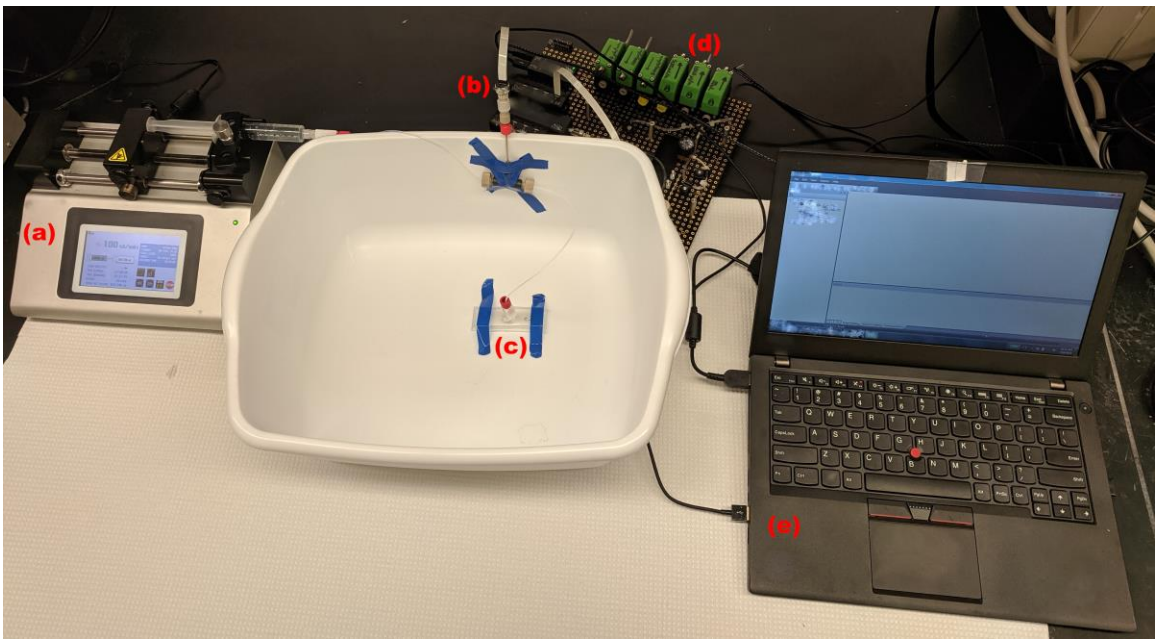

Figure D-7 – Photograph of the experimental setup for microchip working pressure testing. (a) Syringe pump (kd Scientific, Legato® 180, Holliston, MA). (b) Fluidic pressure sensor (LabSmith, 0800 uPS Pressure Sensor, Livermore, CA). (c) PDMS-PDMS microchip. (d) Microfluidic automation system (LabSmith, uProcess™ System, Livermore, CA). (e) Computer.

D.4.2 Y-Channel Laminar Flow Generator

Y-channel devices were designed using AutoCAD and were fabricated according to the procedure described in the Device Fabrication section, using the sticker cutter to cut the glue films (Figure D-2a and c). One inlet was infused using a black dye solution in DI water, and the second inlet was infused with DI water. Two syringe pumps (kd Scientific, Legato® 180, Holliston, MA) were used to provide different flow rates for each inlet of the Y-channel device (50 µL min^{-1}, 100 µL min^{-1} and 200 µL min^{-1}). The pumping of solutions was recorded using a digital microscope (AD-413MT-FVW Series Digital Microscope, DinoLite, Torrance, CA).

D.4.3 Droplet Generator

A T-droplet generator device was designed using AutoCAD and was fabricated according to the procedure described in the fabrication section of the main text, using the sticker cutter to cut the glue films (Figure D-2b and d). Using a syringe pump, a black dye testing solution in DI water was infused at one inlet of the device, with a rate of 22 µL min^{-1}, and soybean oil was infused at the other inlet, with a rate of 25 µL min^{-1}. The droplet generation was recorded using a digital microscope.

D.4.4 3-Valve Normally Open Pneumatic Pump

A LabView program was used to actuate a bank of solenoid valves, which were connected to a vacuum and a N_2 pressure line [119]. Each valve of the pneumatic pump was connected to a solenoid valve of the bank and was actuated individually. Different wait times for each step in the pumping routine were used (25 ms, 50 ms, 100 ms, 150 ms and 200 ms), yielding different pumping rates. The pumping routine is depicted in Figure D-8. A blue dye solution in DI water was used as the testing solution to enable visualization. The pumping of solutions was timed and recorded using a digital microscope.

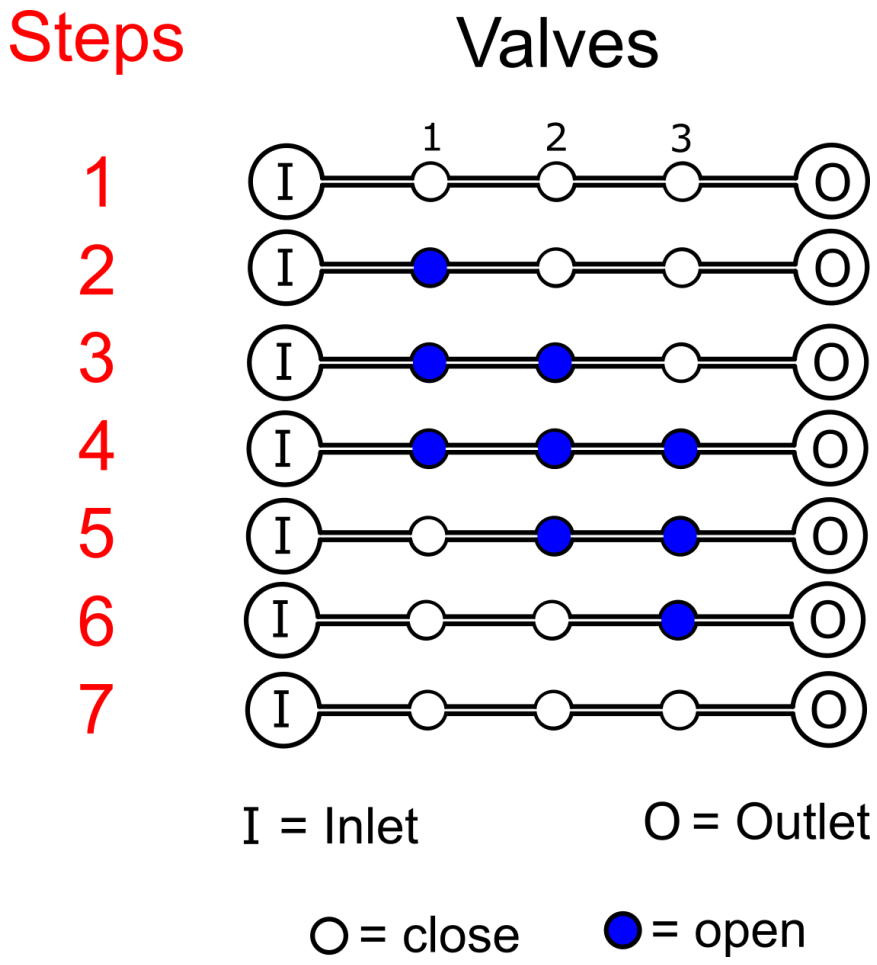

Figure D-8 – Valve opening and closing routine of the 3-valve normally open pneumatic pump.

D.4.5 Pneumatic Lifting Gate Microfluidic Processor

A custom LabView program was used to actuate the solenoid valves [119], a blue dye solution in one inlet and a yellow dye solution in a second inlet were combined using the microfluidic processor, generating a green dye mixture at the outlet. The dye mixing routine is shown in Figure D-9, and the opening and closing valve sequence is depicted in Figure D-10. The valves of the processor were cleaned using DI water (Figure D-11), which was added to a third inlet of the processor. The opening and closing valve sequence are depicted in Figure D-12. Figure D-13 shows still frame pictures of the cleaning process. The dye mixture and cleaning routines were recorded using a digital microscope.

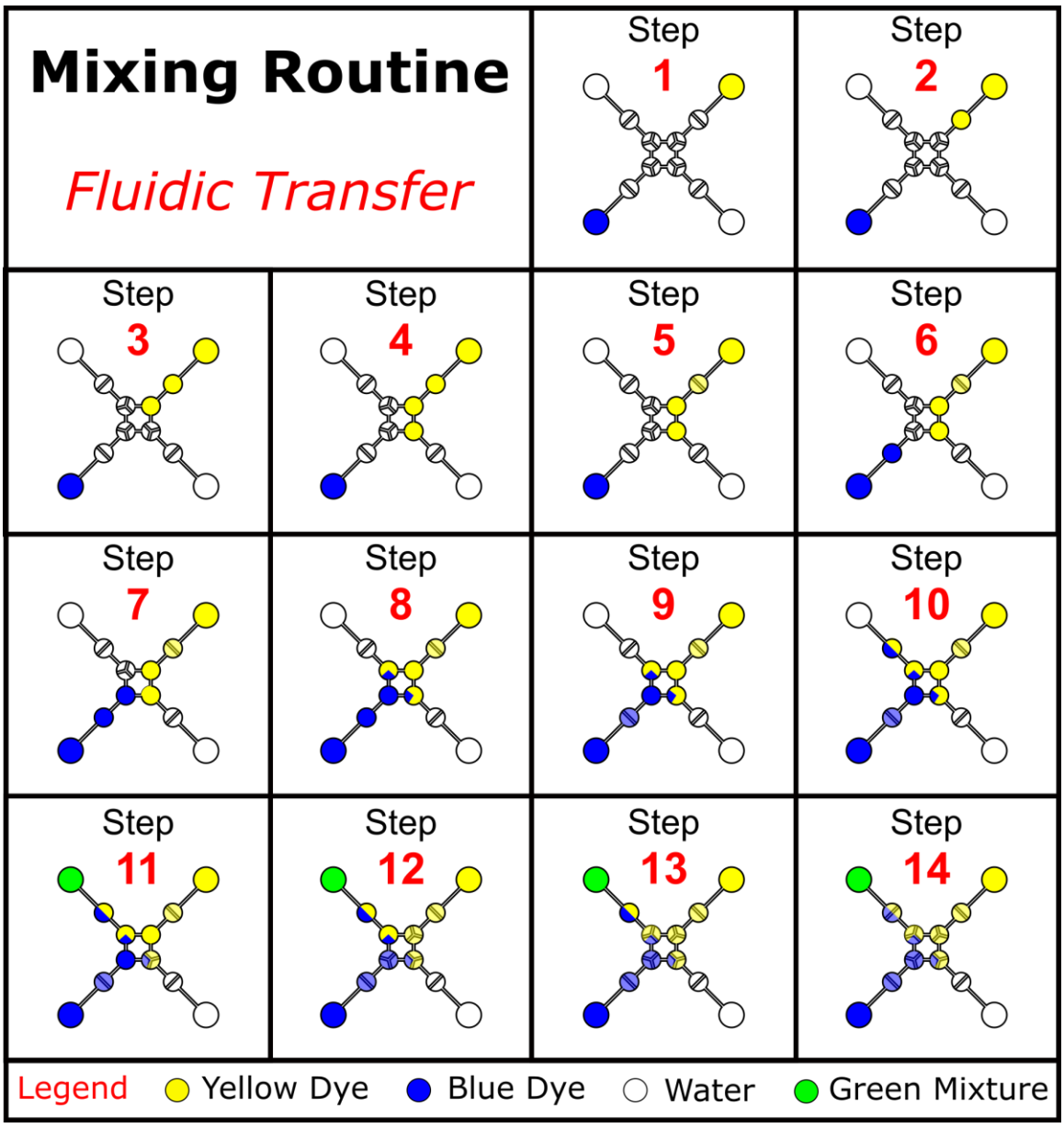

Figure D-9 – Schematics of the dye mixing routine used in the fluidic processor.

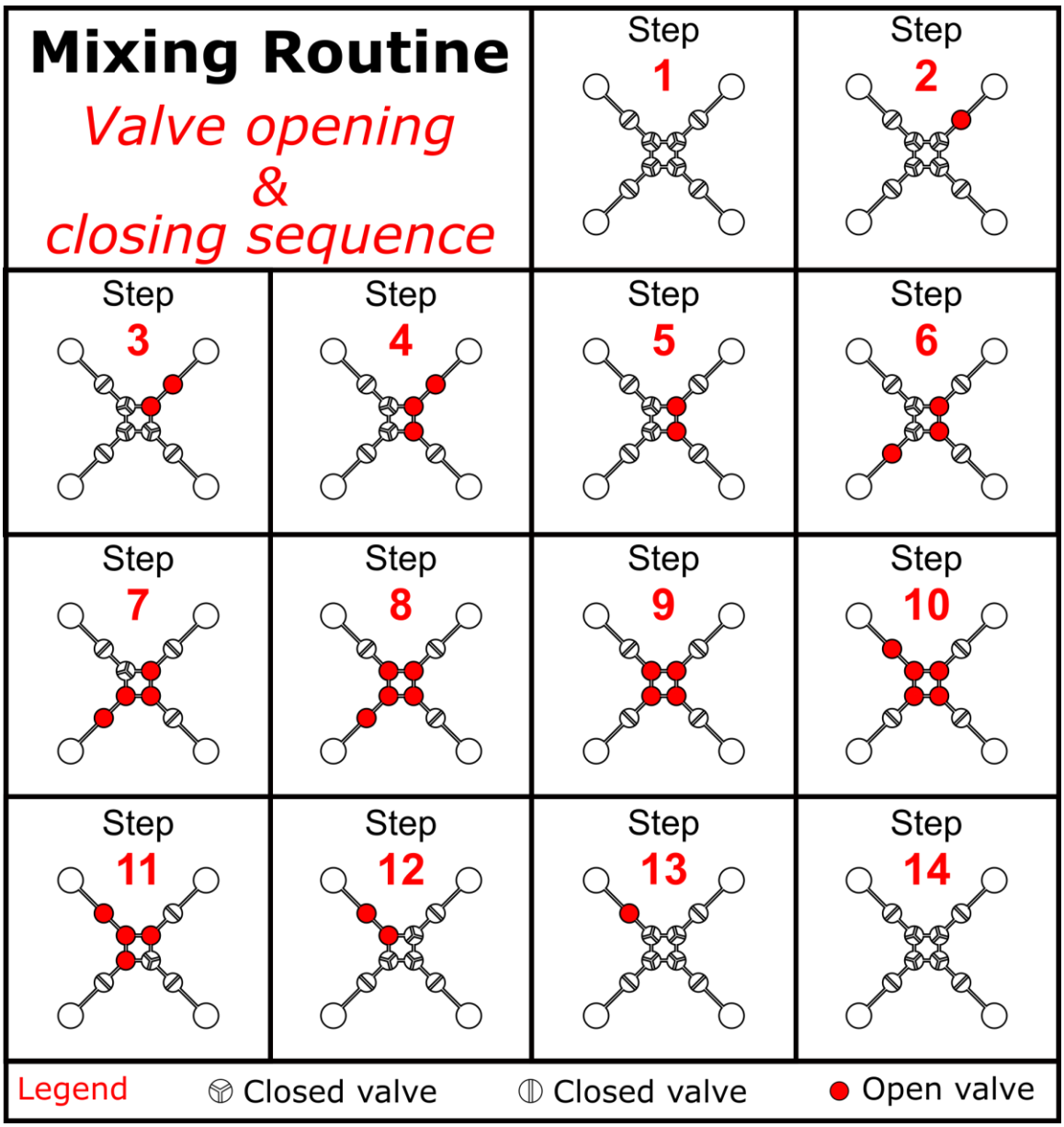

Figure D-10 – Schematics of the opening and closing valve sequence used for the mixing routine depicted in Figure D-9.

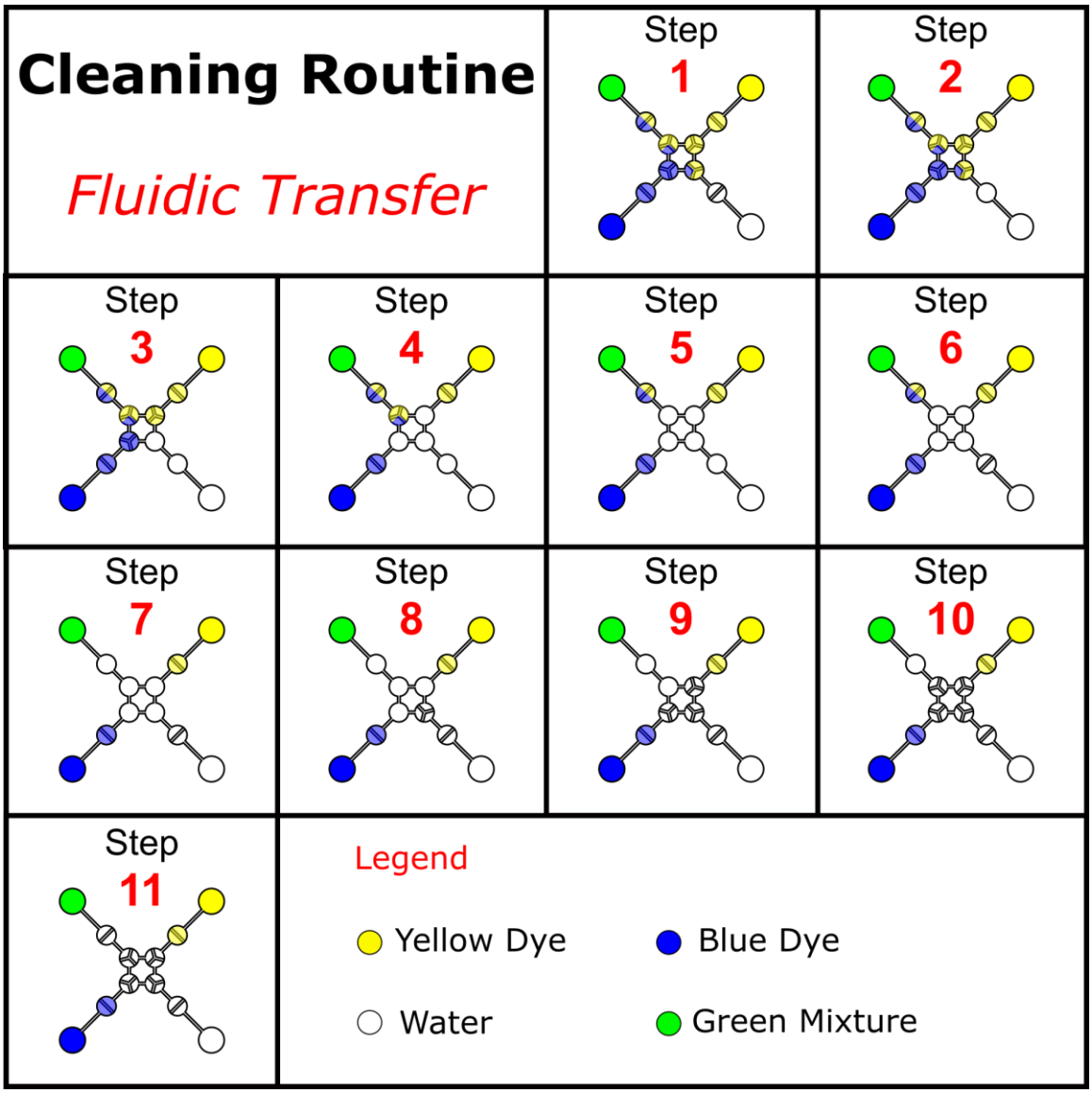

Figure D-11 – Schematics of the cleaning routine used in the fluidic processor.

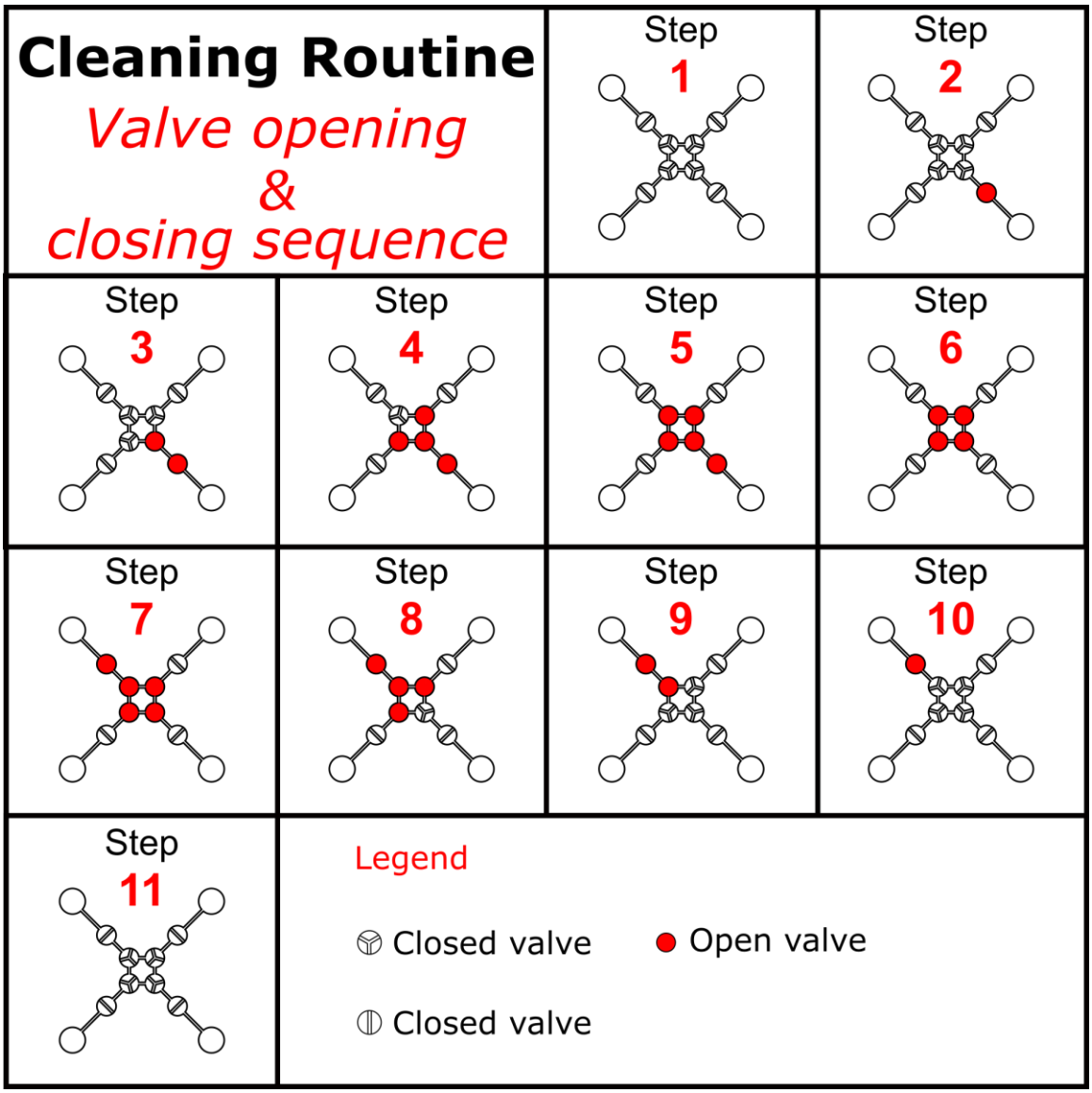

Figure D-12 – Schematics of the opening and closing valve sequence used for the cleaning routine depicted in Figure D-11.

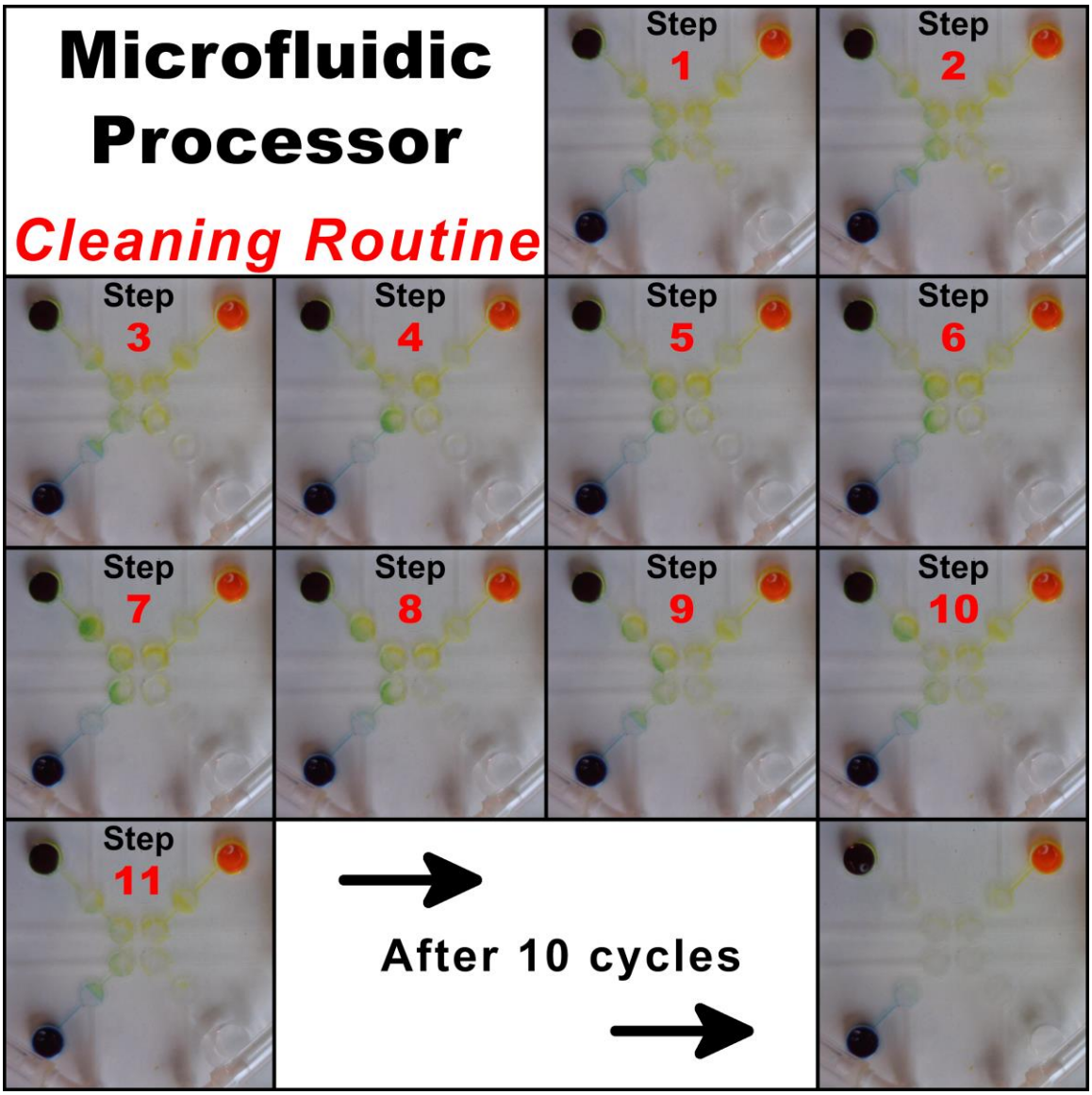

Figure D-13 – 2x2 microfluidic processor used to perform a cleaning routine, after mixing the dyes. Water in a fourth inlet is pumped through all the processor valves, cleaning the residues of dye present from the mixing protocol. After 10 cycles, the processor valves are clean, and can be used for other protocols.

D.5 Glue Film Composition

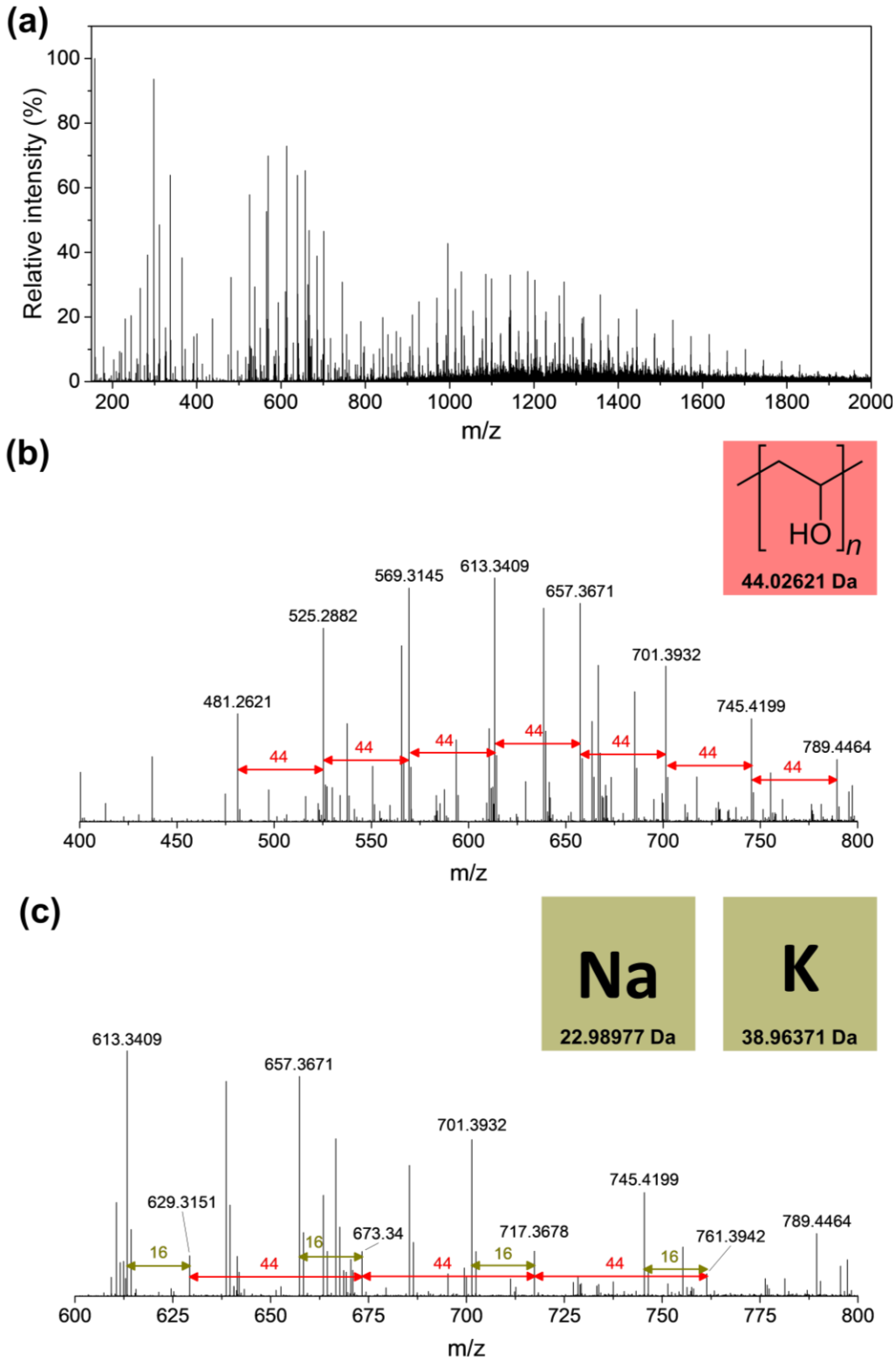

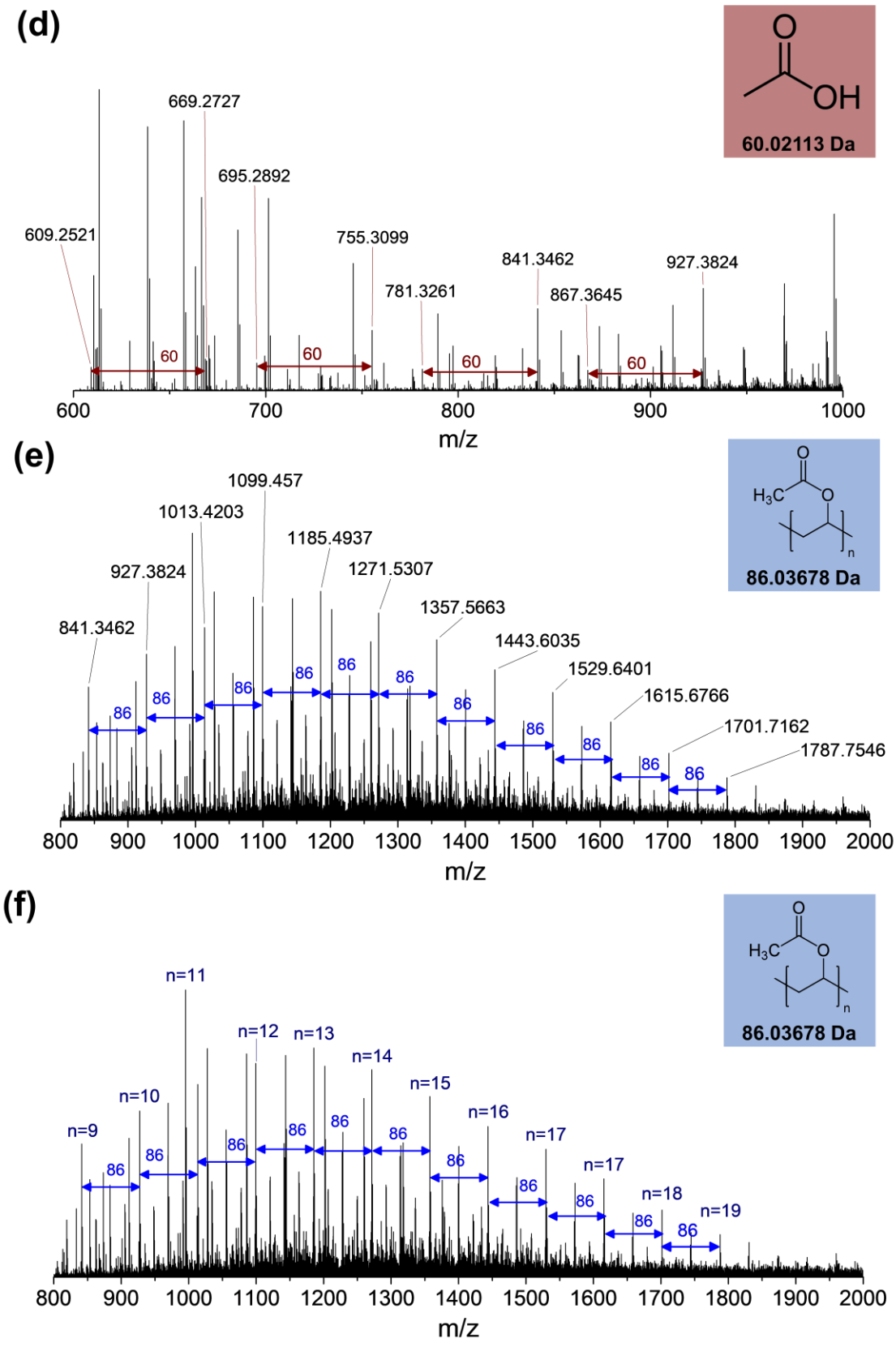
(d)
60.02113 Da
669.2727
695.2892
609.2521
755.3099
841.3462
927.3824
781.3261
867.3645
60
60
60
60
600
700
800
900
1000
m/z
(e)
86.03678 Da
1099.457
1013.4203
1185.4937
927.3824
1271.5307
1357.5663
841.3462
1443.6035
1529.6401
1615.6766
1701.7162
1787.7546
86
800
900
1000
1100
1200
1300
1400
1500
1600
1700
1800
1900
2000
m/z
(f)
86.03678 Da
n=11
n=12
n=13
n=14
n=15
n=16
n=17
n=17
n=18
n=19
n=10
n=9
86
800
900
1000
1100
1200
1300
1400
1500
1600
1700
1800
1900
2000
m/z

Figure D-14 – ESI-orbitrap mass spectrum of white glue. (a) Mass spectrum with m/z ranging from 150 to 2000 Th. (b) Expanded region of the mass spectrum (m/z from 400 to 800 Th). The difference between peaks is annotated with red arrows and corresponds to the mass of a vinyl alcohol monomer (44 Da). (c) Expanded region of the mass spectrum (m/z from 600 to 800 Th). The difference between peaks (16 Da) is annotated with gold arrows and corresponds to the mass difference between sodium (23 Da) and potassium (39 Da) adducts of polymers with the same chain size. (d) The loss of acetic acid (60 Da) from PVAc polymeric chains is annotated with maroon arrows between peaks. (e) Expanded region of the mass spectrum (m/z from 800 to 2000 Th). The difference between peaks is annotated with blue arrows and corresponds to the mass of a vinyl acetate monomer (86 Da). (f) Same region from (e), with peaks annotated with their degree of polymerization (denotated as n). Peaks in all spectra are marked with their m/z values, if not stated otherwise. Sample preparation: a white glue sample (0.5 g) was dissolved in 1 mL of a solution of H_2O : Acetonitrile (50:50 (V/V)) with 0.1% (V/V) of formic acid, and subsequently diluted with methanol (100-fold). Analysis was performed using a Thermo Scientific LTQ Orbitrap XL mass spectrometer, with an electrospray ion source. Analysis conditions: Positive ion mode; Direct infusion with methanol, syringe pump flow rate = 8 µL min^{-1}; ESI source: Spray Voltage = 5 kV, Capillary Voltage = 80.03 V, Capillary Temperature = 235.06 °C.

Table D-1 – Compositional analysis of PVAc oligomers represented in Figure D-14

n	Compositional Assignment	Experimental mass (Da)	Theoretical Data (Da)	ppm error
9	$[(C_2H_5(C_4H_6O_2)_9CH_3)Na]^+$	841.3462	841.3828	43
10	$[(C_2H_5(C_4H_6O_2)_{10}CH_3)Na]^+$	927.3824	927.4196	40
11	$[(C_2H_5(C_4H_6O_2)_{11}CH_3)Na]^+$	1013.4203	1013.4564	36
12	$[(C_2H_5(C_4H_6O_2)_{12}CH_3)Na]^+$	1099.457	1099.4932	33
13	$[(C_2H_5(C_4H_6O_2)_{13}CH_3)Na]^+$	1185.4937	1185.53	31
14	$[(C_2H_5(C_4H_6O_2)_{14}CH_3)Na]^+$	1271.5307	1271.5667	28
15	$[(C_2H_5(C_4H_6O_2)_{15}CH_3)Na]^+$	1357.5663	1357.6035	27
16	$[(C_2H_5(C_4H_6O_2)_{16}CH_3)Na]^+$	1443.6035	1443.6403	25
17	$[(C_2H_5(C_4H_6O_2)_{17}CH_3)Na]^+$	1529.6401	1529.6771	24
18	$[(C_2H_5(C_4H_6O_2)_{18}CH_3)Na]^+$	1615.6766	1615.7139	23
19	$[(C_2H_5(C_4H_6O_2)_{19}CH_3)Na]^+$	1701.7162	1701.7506	20
20	$[(C_2H_5(C_4H_6O_2)_{20}CH_3)Na]^+$	1787.7546	1787.7874	18

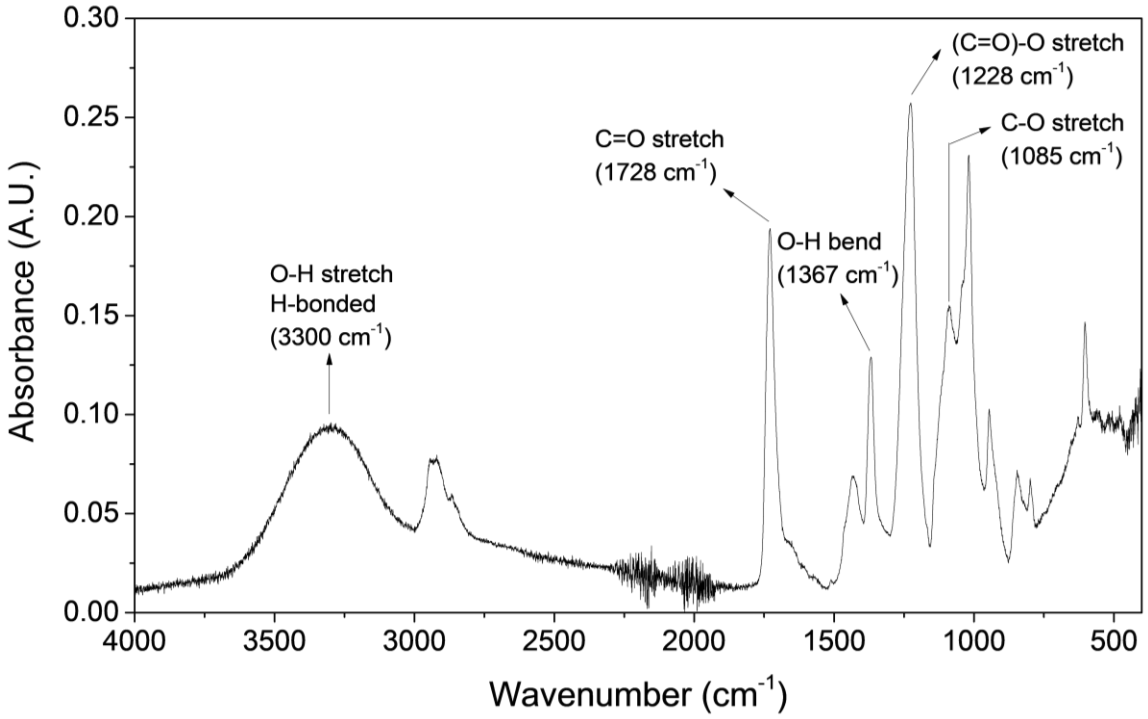

Figure D-15 – ATR-FTIR spectrum of a dried glue film. The polymeric film is composed of poly (vinyl acetate), evidenced by the C=O and (C=O)-O stretches, and poly (vinyl alcohol), evidenced by the H-bonded O-H stretch and O-H bend. Analysis was performed using a Thermo Nicolet Nexus 4700 FT-IR spectrometer with a diamond crystal horizontal ATR cell in the reflectance mode. Scan settings are: resolution 1.0 cm^{-1}, 64 scans, range: 400 to 4000 cm^{-1}.

D.6 Laser Cutter Characterization

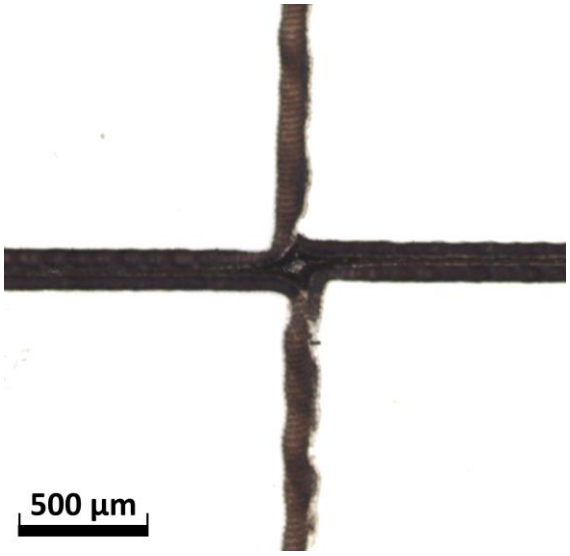

Figure D-16 – Confocal laser micrograph of a glue mold cut into a cross-shape with a laser cutter. Channel width was designed to 100 µm. The glue was totally ablated from the substrate in the vertical orientation (horizontal belt mechanism) because the nominal width was designed with a size smaller than the laser cutter offset.

Table D-2 – Statistical z-test comparing the line width of molds cut in vertical and horizontal orientations with the laser cutter, using the regression parameters from Table D-3. Both cutting orientations did not show a statistically significant difference for nominal lines over 200 µm with a confidence interval of 95% ($p_{(z)}>p_{(0.05)}$)

	Calculated z	p(z)	p(0.05)	p(z)>p(0.05)?	Reject Null Hypothesis?
Intercept	1.149	0.8749	0.05	True	No
Slope	-0.09732	0.4602	0.05	True	No

Table D-3 – Comparison between the linear regressions of the vertical cutting orientation and horizontal cutting orientation, with a confidence interval (C.I.) of 95%*

	Vertical		Horizontal	
r^2	0.999		0.996	
Confidence interval	2.50%	97.50%	2.50%	97.50%
Intercept / µm	-144	-128	-170	-130
Slope / A.U.	1	1.02	1	1.04

* Obtained using Origin 2016 Software.

D.7 Equation Correlating Spin Coating Speed and Film Thickness

$$\delta \propto \frac{1}{\sqrt{\omega}} \tag{8}$$

δ is the film thickness;

ω is the rotational speed.

Table D-4 – White glue viscosity measurements

Measurement	Temp. (ºC)	Viscosity (cP)	Flow rate (µL min $^{-1}$)	Shear rate (s^{-1})	Shear stress (Pa)	Volume (µL)	r^2
1	22.89	2862	59.4	62.8	179.73	17.1	1
2	22.88	2852	59.4	62.8	179.09	19	1
3	22.86	2810	59.4	62.8	176.45	63.5	1
4	22.92	2797	56	59.2	165.63	13.8	1
5	22.92	2862	56	59.2	169.45	13.8	1
6	22.91	2934	56	59.2	173.73	16.2	1
Average	**22.9**	**2853**	**58**	**61**	**174**	**24**	**1**
Std. dev.	**0.02**	**50**	**2**	**2**	**6**	**20**	**0**

Analysis was performed using a RheoSense microVISC Viscometer/Rheometer-on-a-Chip.

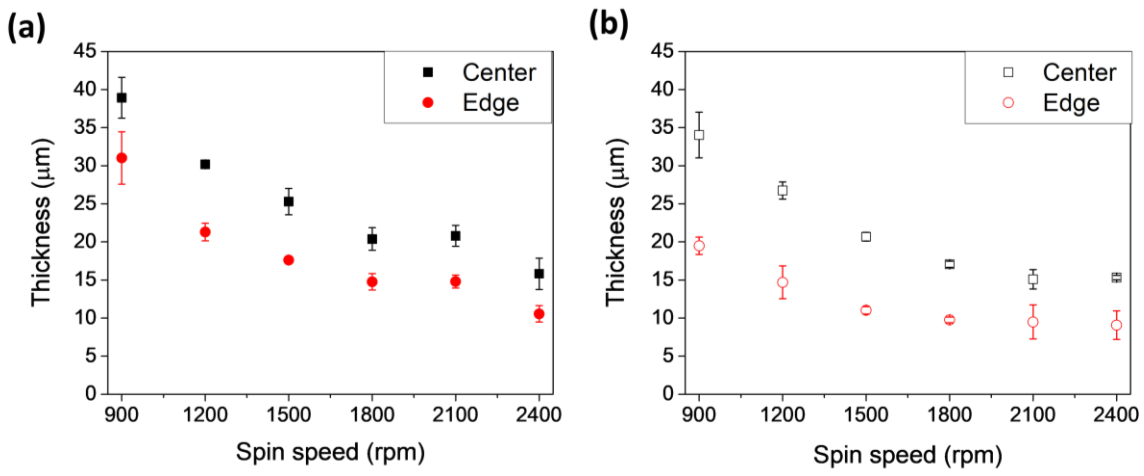

Figure D-17 – Characterization of glue molds. (a) Glue mold film thicknesses spun at different speeds in the spin coater on glass substrates. (b) Glue mold film thicknesses spun at different speeds in the spin coater on PDMS substrates. The values in all plots represent the average of 3 measurements ± 1 standard deviation.

Table D-5 – t-tests comparing the height of glue molds and the height of PDMS channels cast on its respective glue mold (C.I. 95%). There is no significant statistical difference between the height of glue molds and the PDMS channels cast on its respective mold ($t_{calc}<t_{crit}$)

	1 Spin		2 Spins		3 Spins	
	Mold	*PDMS*	*Mold*	*PDMS*	*Mold*	*PDMS*
Average	22.55	21.16	59.86	60.01	103.01	103.84
Variance	2.35	0.55	7.5	5.69	22.27	14.99
Number of observations	3	3	3	3	3	3
Pearson correlation	1.45		6.59		18.63	
Hypothesis test for difference of means	0		0		0	
df	4		4		4	
t calc	1.411		-0.073		-0.235	
P(T<=t) one-tailed	0.115		0.472		0.413	
t crit one-tailed	2.132		2.132		2.132	
P(T<=t) two-tailed	0.231		0.945		0.825	
t crit two-tailed	2.776		2.776		2.776	

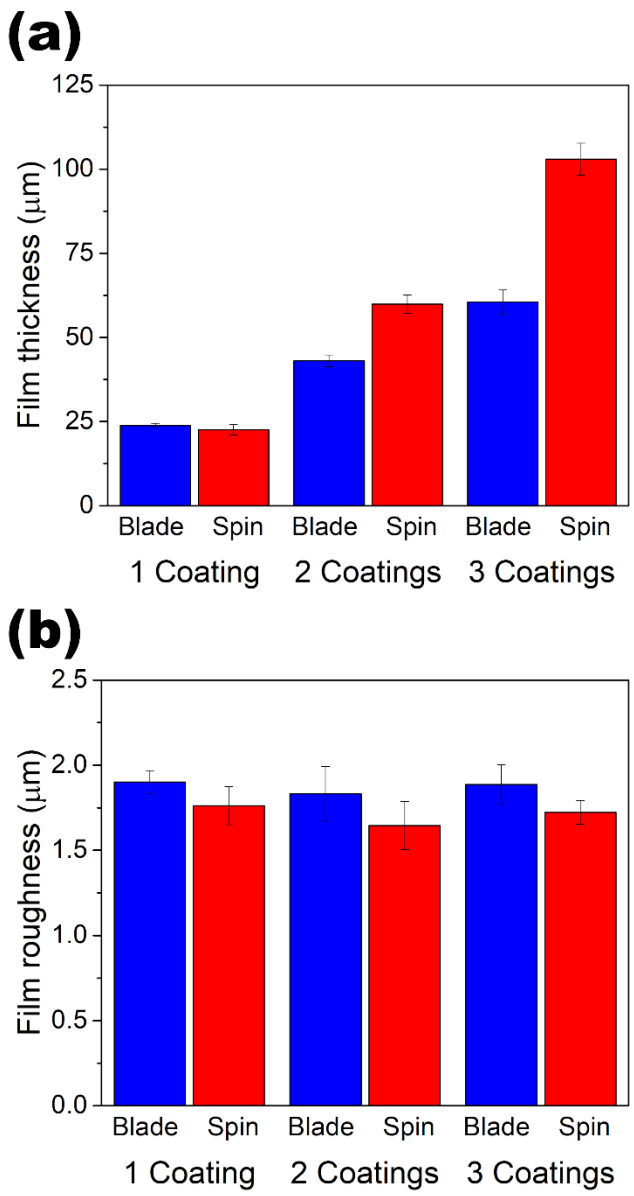

Figure D-18 – Characterization of glue molds fabricated using the two methods. (a) Film thickness of glue molds created using multiple layers of tape via the blade method and via multiple depositions using the spin coating method. (b) Glue thin film surface roughness (root-mean-square of laser confocal profiles) of films made via both methods. The values in all plots represent the average of 3 measurements ± 1 standard deviation.

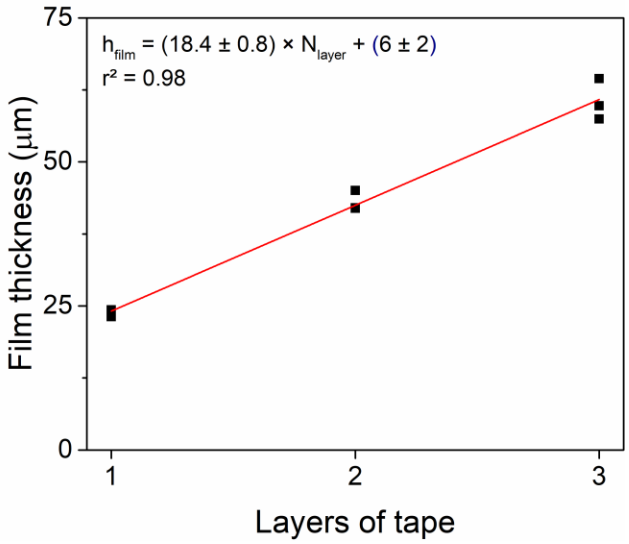

Figure D-19 – Variation of glue mold thickness with the number of layers of tape used in the blade coating method. For each additional layer of tape added, the height of the glue mold increases 18.4 ± 0.8 μm, accordingly to the best fit regression.

Table D-6 – One-way ANOVA test comparing the surface roughness of glue molds fabricated with multiple layers of PVC tape or multiple spins of glue. There is no statistically significant differences between glue molds fabricated using 1, 2 or 3 layers of PVC tape ($F_{calc}<F_{crit}$); between glue molds fabricated with 1,2 or 3 spins ($F_{calc}<F_{crit}$); or between blade coating and spin coating methods ($F_{calc}<F_{crit}$)

Raw data					
Surface roughness (root mean square (RMS)) (μm)					
1 Layer	2 Layers	3 Layers	1 Spin	2 Spins	3 Spins
1.911	1.764	2.019	1.721	1.657	1.779
1.962	1.717	1.802	1.888	1.497	1.644
1.83	2.015	1.837	1.677	1.78	1.744

One-way ANOVA – Surface roughness of blade coating using multiple layers of tape						
Source of Variation	*SS*	*df*	*MoS*	*F*	*P-value*	*F crit*
Between groups	0.0079	2	0.004	0.271	0.771	5.143
Within groups	0.08735	6	0.015			
Total	0.09525	8				

One-way ANOVA – Surface roughness of spin coating with multiple spins of glue						
Source of Variation	*SS*	*df*	*MoS*	*F*	*P-value*	*F crit*
Between groups	0.0214	2	0.011	0.856	0.471	5.143
Within groups	0.0749	6	0.0125			
Total	0.0962	8				

One-way ANOVA – Surface roughness of blade coating and spin coating						
Source of Variation	*SS*	*df*	*MoS*	*F*	*P-value*	*F crit*
Between groups	0.1493	5	0.03	2.209	0.121	3.106
Within groups	0.1622	12	0.014			
Total	0.3115	17				

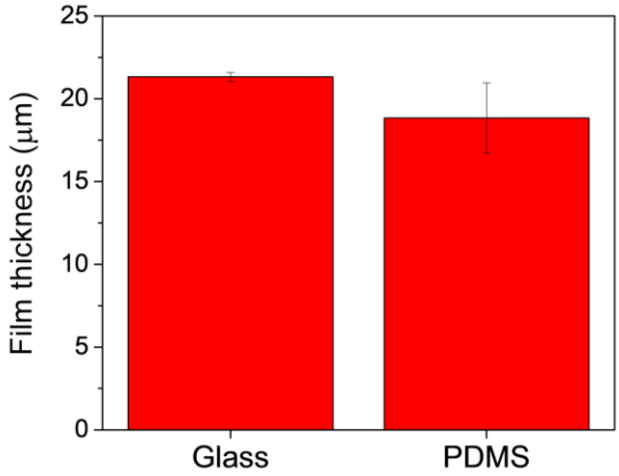

Figure D-20 – Film thickness of glue molds fabricated using the blade coating method on a glass substrate and on a PDMS substrate.

Table D-7 – t-test comparing the height of glue molds fabricated using the blade coating method on a glass substrate and on a PDMS substrate (C.I. 95%). There is no significant statistical difference between the height of glue molds prepared on a glass substrate or on a PDMS substrate ($t_{calc}<t_{crit}$)

	Glass	*PDMS*
Average	21.321	19
Variance	0.07	5
Number of observations	3	3
Pearson correlation	-0.9888	
Hypothesis test for difference of means	0	
df	2	
t calc	1.801	
P(T<=t) one-tailed	0.10675	
t crit one-tailed	2.91999	
P(T<=t) two-tailed	0.2135	
t crit two-tailed	4.30265	

D.8 Inverse Xurography Method

D.8.1 Inverse Xurography Process

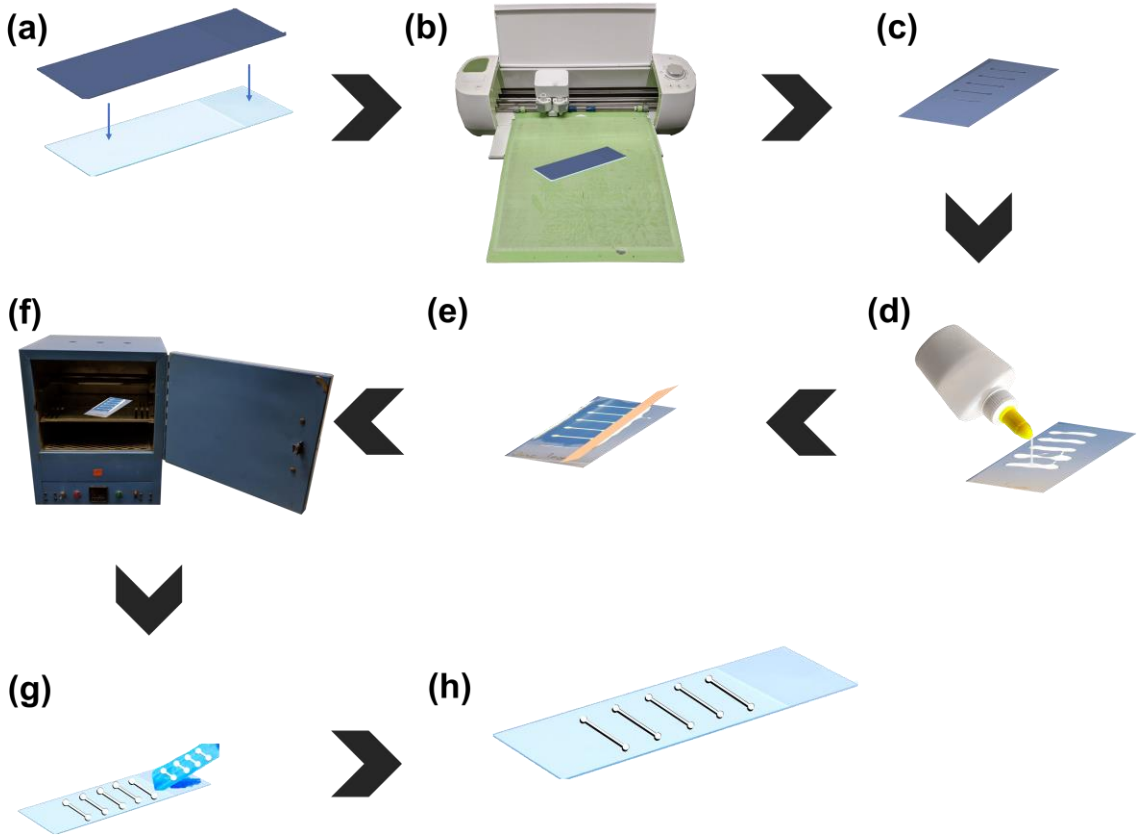

Figure D-21 – Step-by-step fabrication of PDMS-based microfluidic devices using the inverse xurography method. (a) PVC tape adhesion to a glass backing substrate. (b) CAD designs cutting on tape using a cutting plotter. (c) Removal of the 'internal' molds, leaving the excess of tape on the backing substrate. (d) Water-soluble glue deposition on the cut parts of the mold. (e) Glue spreading onto the mold using a flat edge tool. (f) Glue curing in an oven. (g) Tape removal. (h) Glue mold.

D.8.2 Inverse Xurography Mold Characterization

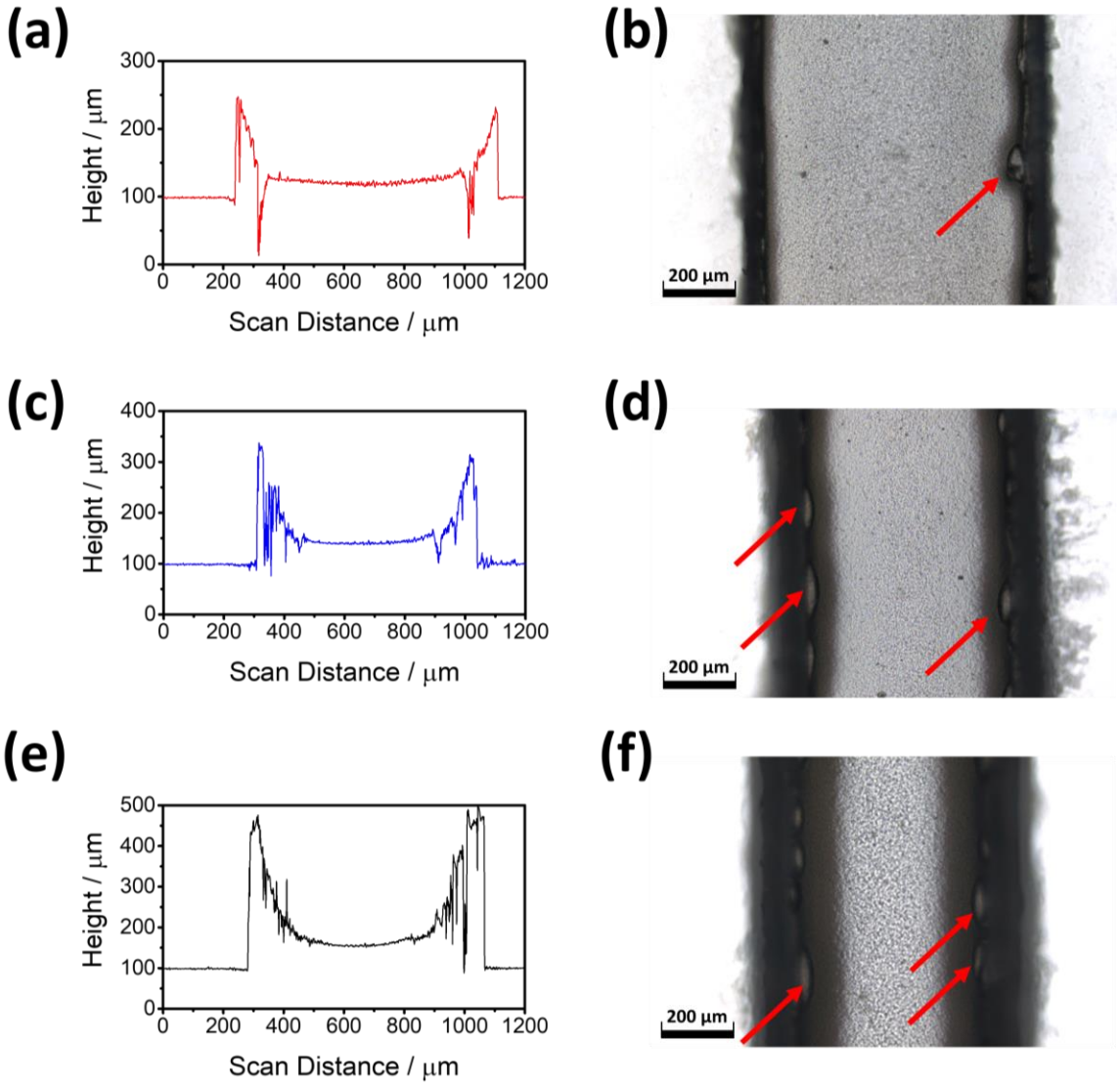

Figure D-22 – Characterization of glue molds fabricated using the inverse xurography method. (a) Profile of a glue mold fabricated using 1 layer of tape. (b) Laser confocal micrograph of the 1 layer of tape glue mold. (c) Profile of a glue mold fabricated using 2 layers of tape. (d) Laser confocal micrograph of the 2 layers of tape glue mold. (e) Profile of a glue mold fabricated using 3 layers of tape. (f) Laser confocal micrograph of the 3 layers of tape glue mold. The arrows in the micrographs indicate air bubbles entrapped in the glue mold at the tape walls.

Table D-8 – One-way ANOVA test comparing the surface roughness of molds raster etched using increasing laser speeds (at a constant laser power (12.5%). Raster etched molds using 45% to 70% laser speed did not show a statistically significant difference in surface roughness ($F_{calc}<F_{crit}$)

Raw data					
Surface roughness (root mean square (RMS)) (µm)					
Speed 45%	Speed 50%	Speed 55%	Speed 60%	Speed 65%	Speed 70%
3.069	4.07	4.364	4.563	5.621	3.71
2.879	4.989	4.152	4.692	4.239	3.667
3.976	5.596	4.55	3.664	4.226	4.566

One-way ANOVA – Surface roughness of the raster molds						
Source of Variation	*SS*	*df*	*MoS*	*F*	*P-value*	*F crit*
Between groups	4.72614	5	0.94523	2.59316	0.08184	3.10588
Within groups	4.37411	12	0.36451			
Total	9.10025	17				

Table D-9 – One-way ANOVA test comparing the surface roughness of molds raster etched using increasing laser speeds (at a constant laser power (12.5%) and the native glue mold. Raster etched molds using 45% to 70% laser speed showed a statistically significant difference in surface roughness in comparison with the native mold ($F_{calc}>F_{crit}$)

Raw data						
Surface roughness (root mean square (RMS)) (µm)						
Native Film	Speed 45%	Speed 50%	Speed 55%	Speed 60%	Speed 65%	Speed 70%
2.03	3.069	4.07	4.364	4.563	5.621	3.71
2	2.879	4.989	4.152	4.692	4.239	3.667
2.059	3.976	5.596	4.55	3.664	4.226	4.566

One-way ANOVA – Surface roughness of the raster molds						
Source of Variation	*SS*	*df*	*MoS*	*F*	*P-value*	*F crit*
Between groups	17.462	6	2.91034	9.31129	0.00032	2.84773
Within groups	4.37585	14	0.31256			
Total	21.8379	20				

Table D-10 – Fabrication costs of glue molds

Material	**Quantity**	**Price ($)**	**Amount**	**Cost per device [c] ($)**
Elmer's School Glue	3.78 L	27.79	1 mL	0.01
Glass slides	720 slides [a]	367.1	1 [b]	0.51
		Cost per mold		**0.52**

[a] 75 mm by 50 mm.

[b] Can be reused indefinitely, because the molds are water-soluble.

[c] $Cost\ per\ device = \frac{Material\ total\ cost\ x\ Material\ required\ to\ fabricate\ 1\ mold}{Total\ material\ content}$

Table D-11 – One-way ANOVA test comparing the height of glue molds after reuse. Mold heights did not show a statistically significant difference after 3 uses ($F_{calc}<F_{crit}$)

Raw data			
Before	First Cast	Second Cast	Third Cast
Height / µm	Height / µm	Height / µm	Height / µm
23.808	22.421	20.722	23.209
20.841	20.45	22.042	20.31
23.002	23.741	21.316	20.816

One-way ANOVA – Mold reuse - height						
Source of Variation	*SS*	*df*	*MoS*	*F*	*P-value*	*F crit*
Between groups	3.042	3	1.014	0.511	0.686	4.066
Within groups	15.863	8	1.983			
Total	18.905	11				

Table D-12 – One-way ANOVA test comparing the channel roughness (as the root-mean-square (rms) of laser confocal profiles) after reuse. The surface roughness of molds did not show a statistically significant difference after 3 uses ($F_{calc}<F_{crit}$)

Raw data			
Before	First Cast	Second Cast	Third Cast
rms / µm	rms / µm	rms / µm	rms / µm
1.721	1.746	1.889	2.253
1.888	2.025	1.832	2.032
1.677	2.06	1.801	1.822

One-way ANOVA – Mold reuse – surface roughness						
Source of Variation	*SS*	*df*	*MoS*	*F*	*P-value*	*F crit*
Between groups	0.128	3	0.043	1.893	0.209	4.066
Within groups	0.181	8	0.023			
Total	18.905	11				

D.9 Hagen-Poiseuille Equation

$$R_H = C_{geo}\,\frac{\eta\, Le}{Ar^2} \tag{9}$$

R_H is the fluidic resistance of the channel (Pa m^{-3} s);

η is the dynamic viscosity of the fluid (Pa s);

Le is the length of the channel (m);

Ar is the cross-sectional area (m^2);

C_{geo} is the geometric constant of the channel.

For an elliptical channel (which fitted our data better):

$$C_{geo} = \frac{\mathrm{w}(1 + \frac{\mathrm{H}^2}{Hw})^2}{H} \quad (10)$$

H is the channel height (m);

w is the channel width (m).

D.10 Backpressure Calculation

$$\Delta P = R_H \, Q \quad (11)$$

ΔP is the backpressure (Pa)

R_H is the fluidic resistance of the channel (Pa m^{-3} s);

Q is the fluid flow (m^3 s^{-1});

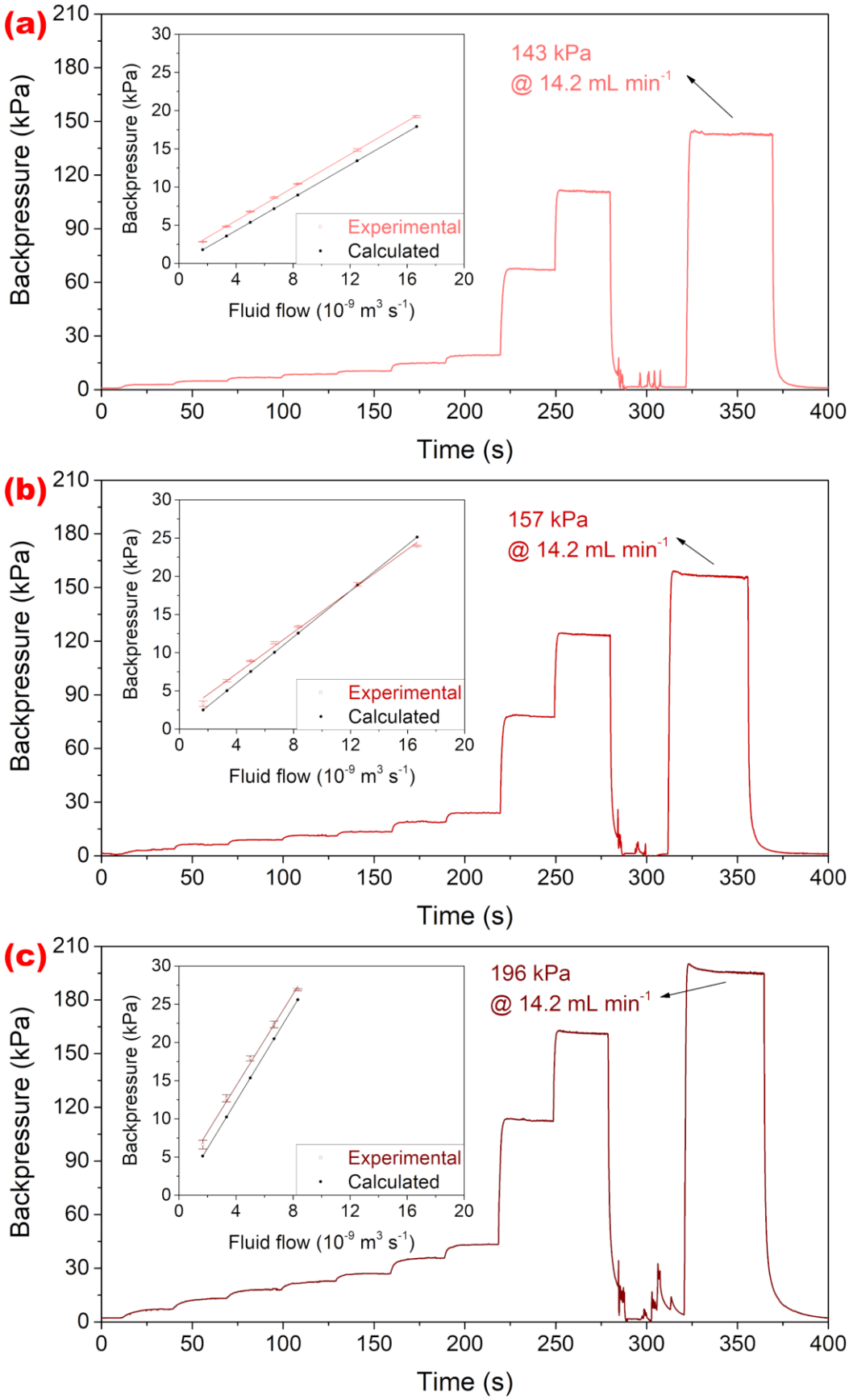
(a)
143 kPa
@ 14.2 mL min-1
Backpressure (kPa)
Time (s)
Experimental
Calculated
Fluid flow (10-9 m3 s-1)
(b)
157 kPa
@ 14.2 mL min-1
Backpressure (kPa)
Time (s)
Experimental
Calculated
Fluid flow (10-9 m3 s-1)
(c)
196 kPa
@ 14.2 mL min-1
Backpressure (kPa)
Time (s)
Experimental
Calculated
Fluid flow (10-9 m3 s-1)

Figure D-23 – Pressure testing of scaffolded PDMS devices. (a) The maximum working pressure registered for this device was 143.0 ± 0.4 kPa (@ 14.2 mL min^{-1}). (b) This device registered a maximum working pressure of 156.7 ± 0.6 kPa (@ 14.2 mL min^{-1}). (c) This device registered a maximum working pressure of 196.1 ± 0.9 kPa (@ 14.2 mL min^{-1}). The region around 300 s in each plot displays noise because the syringe was being refilled with fluid to test the device at the maximum flow of the syringe pump.

The experimental points and the error bars in the inset plots of Figure D-23 represent the time average (20 s) and the standard deviation of the backpressure measurements in the main plot, for different fluid flows. Only fluid flows ranging from 100 µL min^{-1} to 1 mL min^{-1} were used to estimate the fluidic resistance for each device, which is the slope of the curves of the inset plots. For device C, the flow range used to estimate the fluidic resistance of the channel was from 100 µL min^{-1} to 500 µL min^{-1}, because elastomeric channels presenting high fluidic resistance deform at higher flow rates, which in turn causes a deviation from linearity of pressure vs. flow plots. It is relevant to point out that none of the devices delaminated during the pressure testing, for the conditions described. The calculated backpressure points were obtained using Equation 11, and the results are summarized on Table D-13.

Table D-13 – Scaffolded PDMS device dimensions and their respective fluidic resistances

Device	Real Width (µm)	Real Height (µm)	Max. Working Pressure (kPa)	Max. Flow (mL min^{-1})	Resistance (10^{12} Pa s m^{-3})	Calculated resistance (10^{12} Pa s m^{-3})
A	439	59	143.0 ± 0.4	14.2	1.09 ± 0.01	1.07
B	449	52	156.7 ± 0.6	14.2	1.36 ± 0.04	1.51
C	430	41	196.1 ± 0.9	14.2	3.0 ± 0.1	3.07
Average [a]	439 ± 9	51 ± 9	170 ± 30	14.2	2 ± 1	2 ± 1

[a] The average row shows the average ± the standard deviation of the measurements for the individual devices

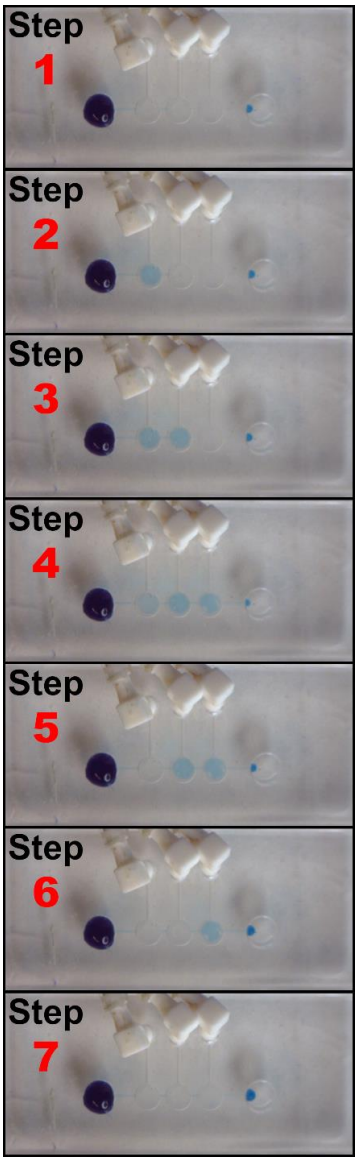

Figure D-24 – Double chamber pumping routine in a 3-valve normally open pneumatic pump. The valve opening and closing routine is depicted in Figure D-8.

APPENDIX E. SUPPLEMENTARY INFORMATION OF CHAPTER 7: AN AUTOMATED LOW-COST MODULAR PLATFORM FOR VERSATILE MICROFLUIDIC DEVICE TESTING AND DEVELOPMENT

E.1 Modular Manifold Blueprints

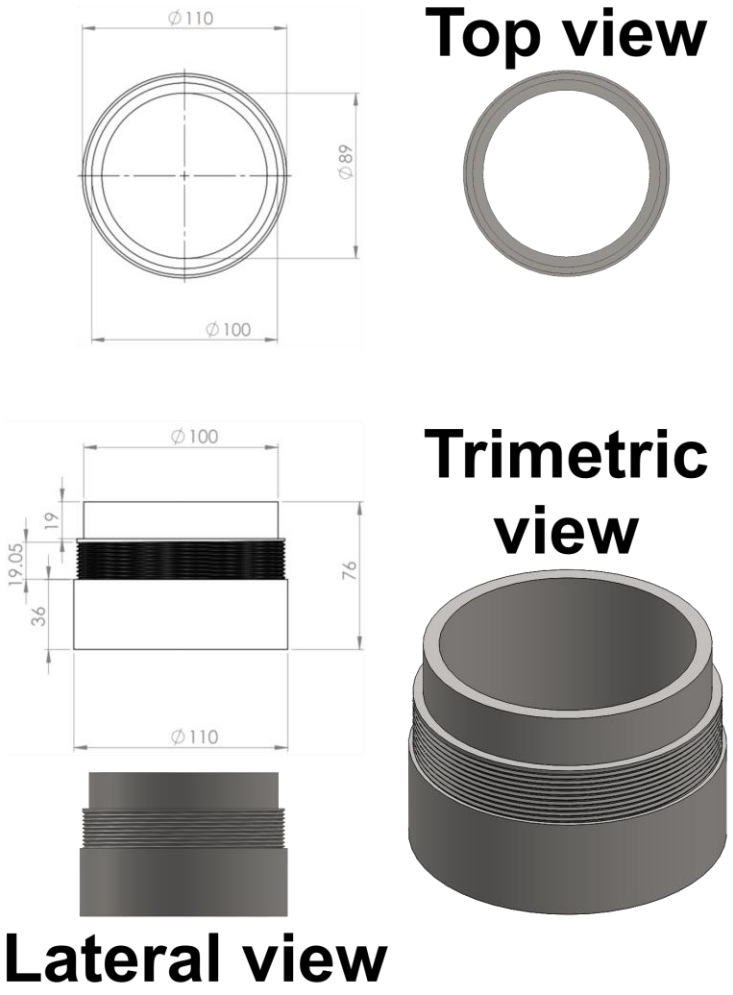

Figure E-1 – Design of the base of the manifold. All dimensions are in mm, if not denoted otherwise.

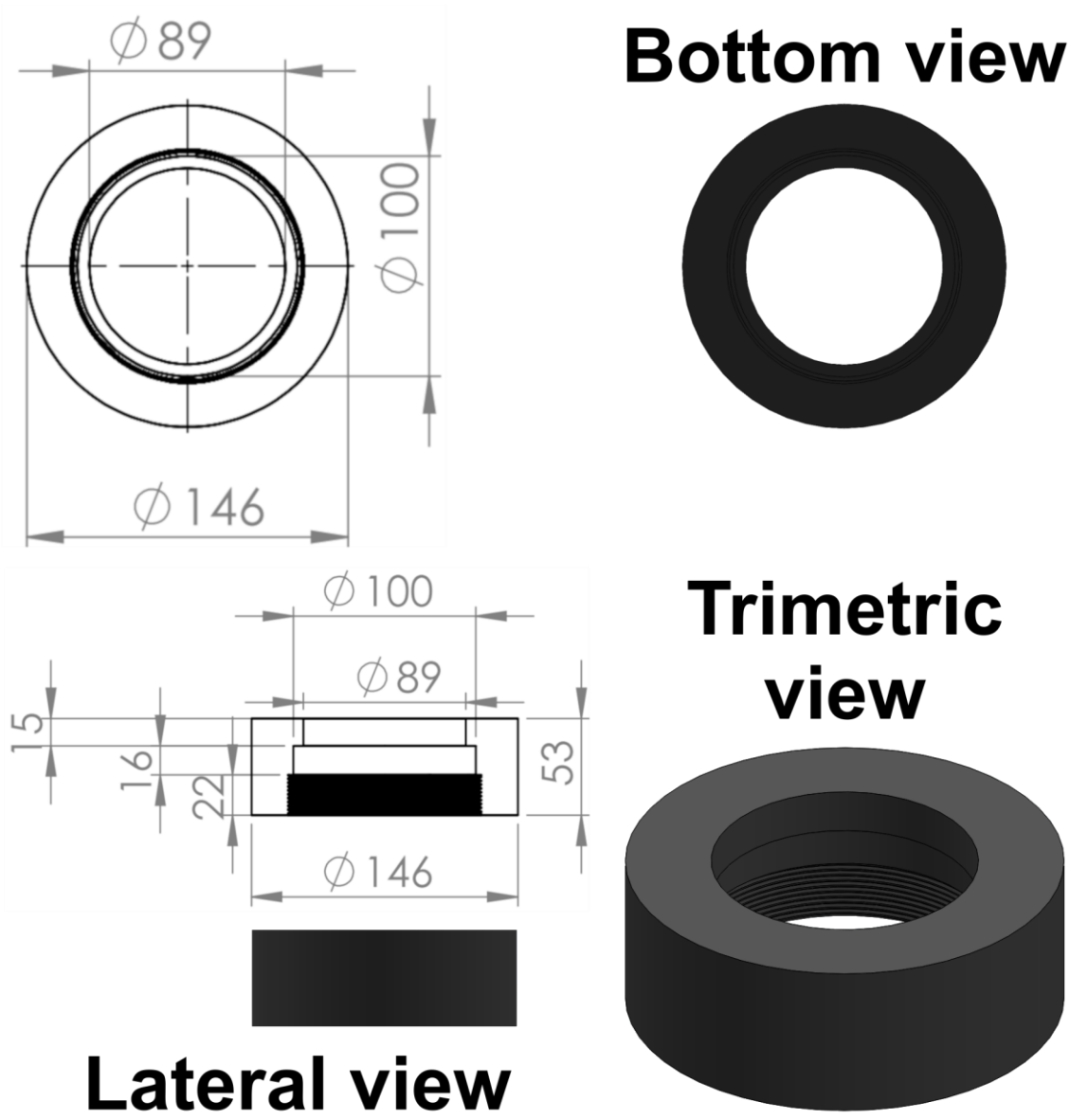

Figure E-2 – Design of the top of the manifold. All dimensions are in mm, if not denoted otherwise.

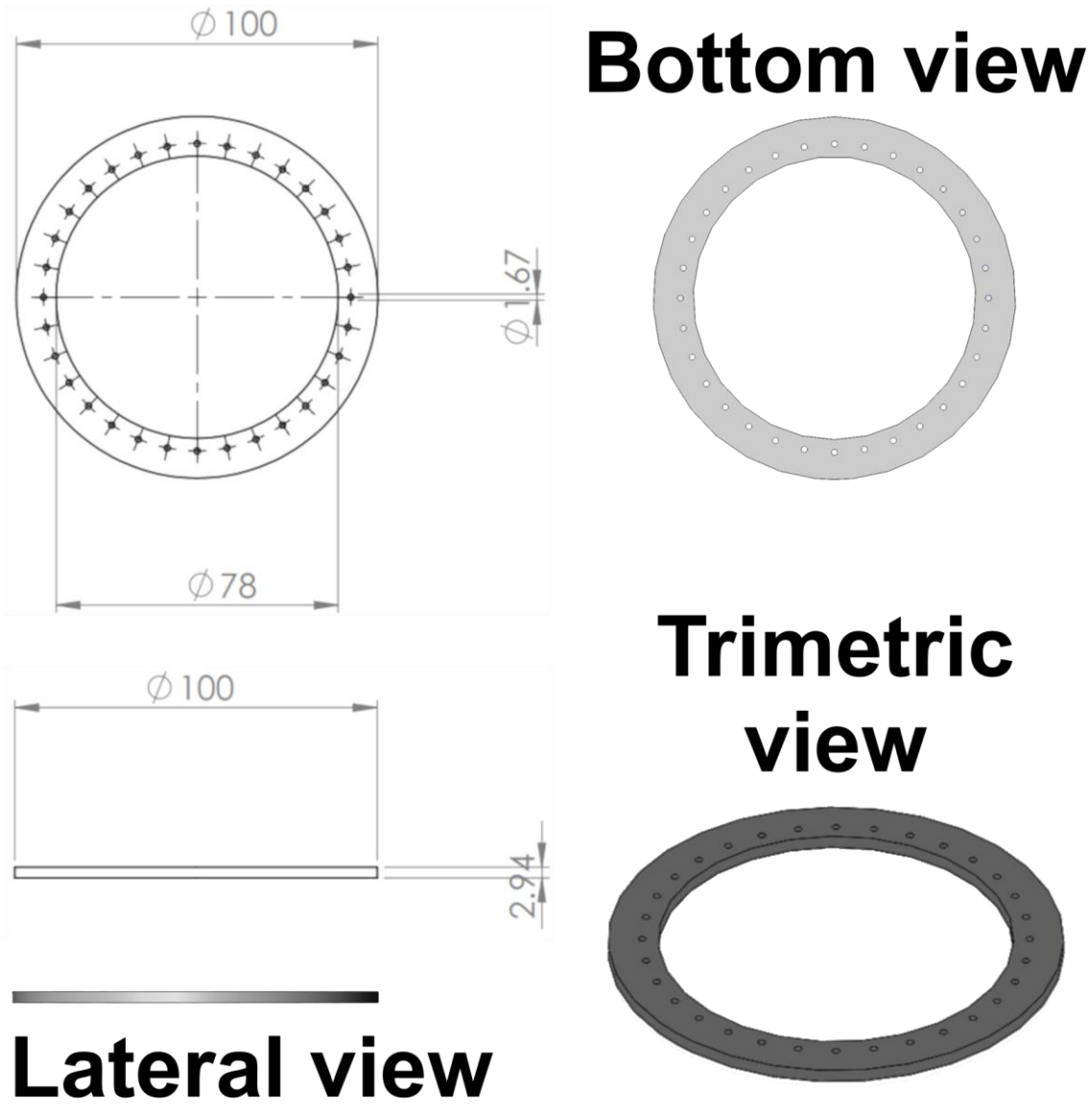

Figure E-3 – Design of the connector. The connector design depends on the pneumatic connections of the microfluidic chip, so the dimensions presented here are used to demonstrate the outer dimensions needed to connect this module to the rest of the manifold. Two connectors might be present in the system, sandwiching the microdevice, if the dimensions of the device are smaller than the lip of the top manifold body. All dimensions are in mm, if not denoted otherwise.

E.2 Microchip Design

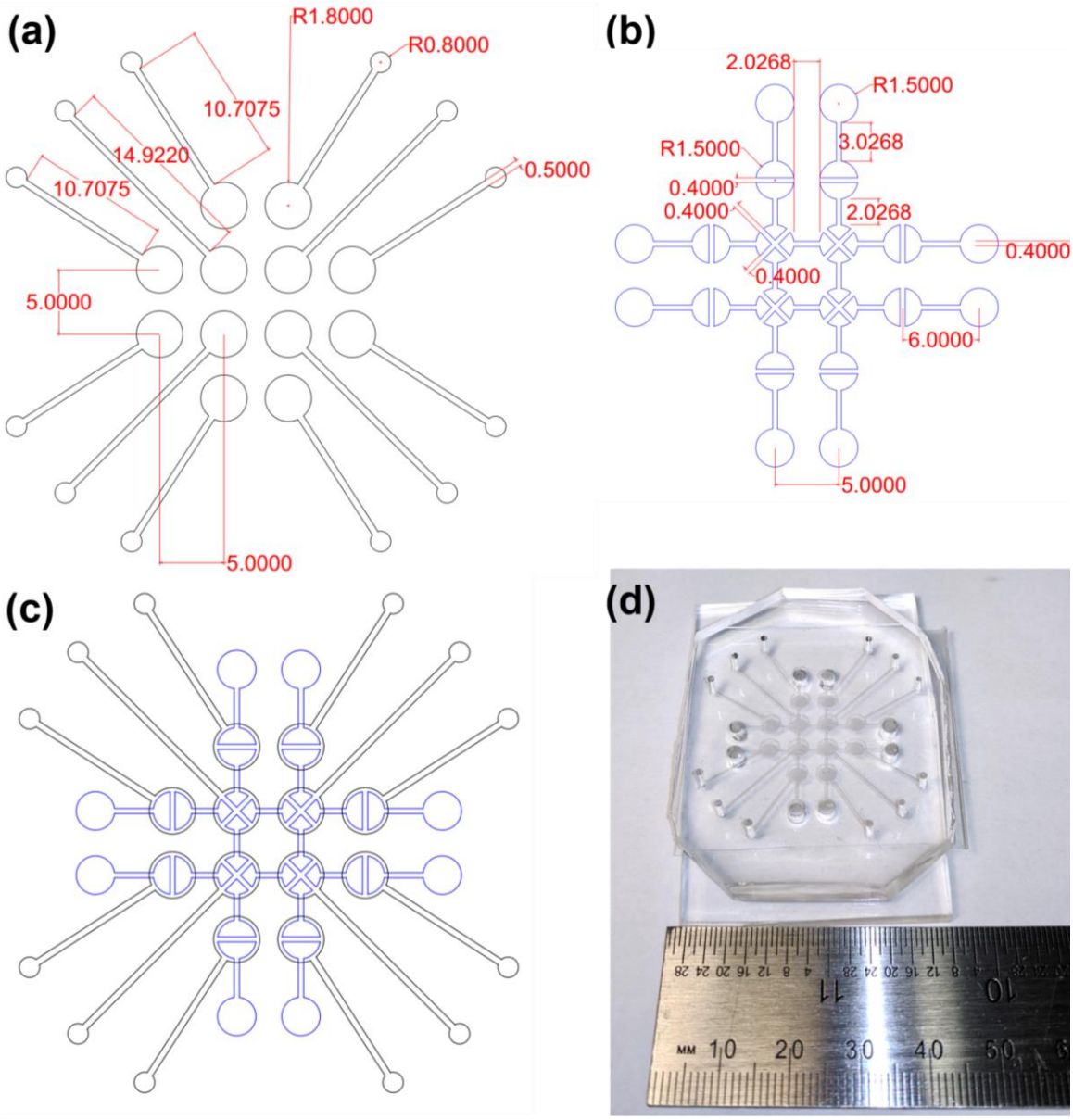

Figure E-4 – Design of a 2x2 pneumatic lifting gate microfluidic processor. (a) Pneumatic layer design with dimensions. (b) Fluidic layer design with dimensions. (c) Layers aligned. (d) Photograph of the final device. All dimensions are in mm, if not denoted otherwise.

E.3 Electronics

E.3.1 Circuit to operate solenoids

The Arduino ATmega2560 board can provide up to 50 mA DC current from each 3.3 V pin to power external components connected to it [244]. The solenoid valves used in the fluidic processor require 750 mW to be operated (3-Way Solenoid LHDA0523112H, The Lee Company [245]), meaning that each individual solenoid require 150 mA DC at 5 V to be actuated, 3 times higher than the provided by the microcontroller board. To provide the necessary current, an external power supply (5 V DC, 10 A max) was connected to the system, and an NPN bipolar transistor was used to switch to a larger DC current. The solenoid is an inductor, and after being actuated it can discharge the current back to the Arduino board, which can damage it. A diode was used to prevent the current returning to the microcontroller, allowing it to flow in just one direction. LEDs were used to indicate the operation of a solenoid, aiding in troubleshooting steps. A circuit diagram of a single solenoid valve is depicted in Figure E-5.

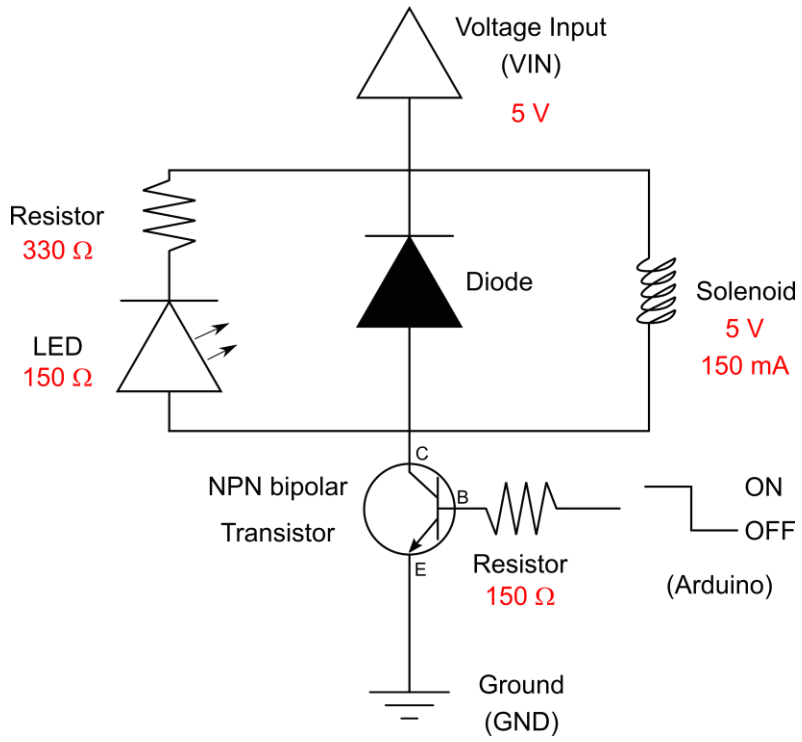

Figure E-5 – Diagram of the electronic circuit used to operate a solenoid valve.

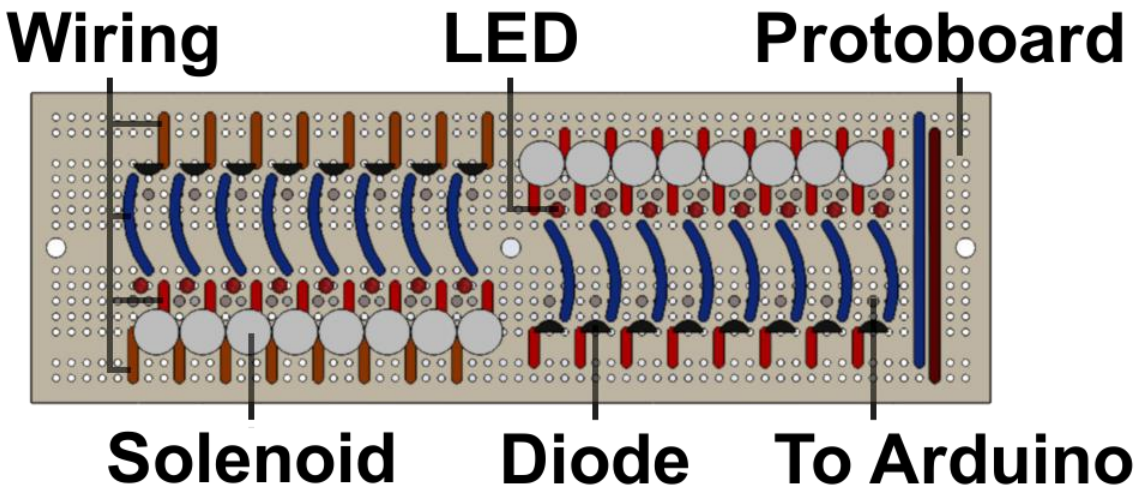

Figure E-6 – Diagram of the protoboard used to connect the solenoid valves to the Arduino board.

E.3.2 Arduino Pin connections

Each solenoid valve was connected to a pin in the Arduino board, which was used to actuate that valve. Table E-1 shows the pin number and the solenoid valve connected to that pin. It is important to stress that this scheme is used for a specific design of microfluidic processor with 32 valves. For different designs, it is necessary to update the dictionary file of the Fluidic Manipulation App, which codes the valve being operated and the Arduino pin that controls that valve.

Table E-1 – Arduino Pin connections to solenoid valves

Front, left (B)				
Board		Dictionary Key	Arduino Pin	Valve Number
8	Orange	'24'	4	24
7	Yellow	'23'	5	23
6	White	'22'	6	22
5	Blue	'21'	7	21
4	Green	'20'	9	20
3	Black	'19'	10	19
2	Brown	'18'	11	18
1	Red	'17'	12	17

Front, right (D)				
Board		Dictionary Key	Arduino Pin	Valve Number
8	Orange	'9'	42	9
7	Yellow	'10'	44	10
6	White	'11'	46	11
5	Blue	'12'	48	12
4	Green	'13'	49	13
3	Black	'14'	47	14
2	Brown	'15'	45	15
1	Red	'16'	43	16

Back, left (A)				
Board		Dictionary Key	Arduino Pin	Valve Number
1	Red	'32'	23	32
2	Brown	'31'	25	31
3	Black	'30'	27	30
4	Green	'29'	29	29
5	Blue	'28'	28	28
6	White	'27'	26	27
7	Yellow	'26'	24	26
8	Orange	'25'	22	25

Back, right (C)				
Board		Dictionary Key	Arduino Pin	Valve Number
1	Red	'1'	33	1
2	Brown	'2'	35	2
3	Black	'3'	37	3
4	Green	'4'	39	4
5	Blue	'5'	38	5
6	White	'6'	36	6
7	Yellow	'7'	34	7
8	Orange	'8'	32	8

E.4 System assembling

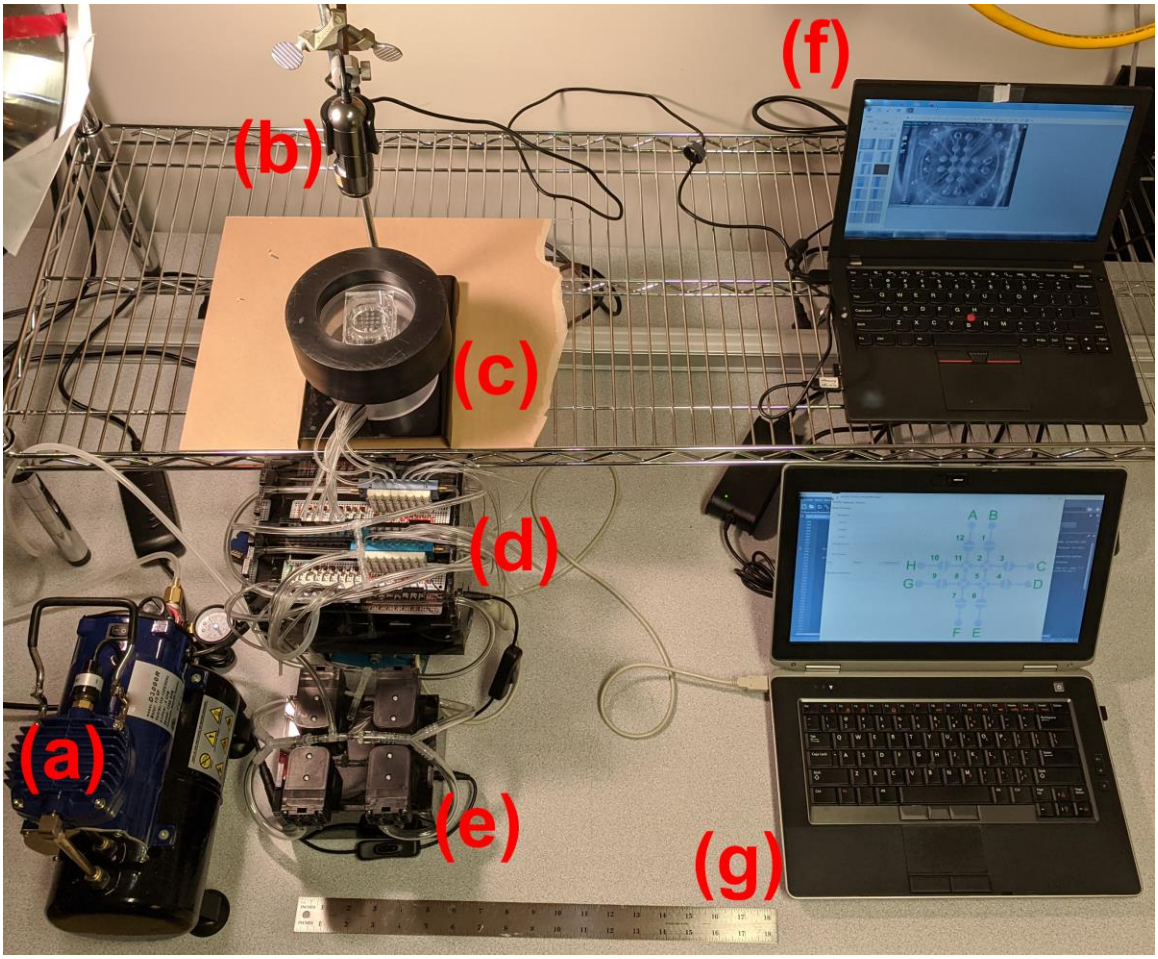

Figure E-7 – Photograph of the experimental setup for the testing apparatus. (a) Pump. (b) Microscope. (c) Modular manifold assembled with the microfluidic device. (d) Electronic circuit to operate the solenoid valves, controlled by the Arduino board. (e) Four 12-V pumps. (f) Computer to operate the microscope. (g) Computer to operate the Arduino board.

E.5 Automatic fluidic manipulation application principle of operation

First, the device is designed [223]. Then, reservoirs, stop valves and valves of the device are identified: letters are used to assign reservoirs, and numbers are used to assign stop valves and valves (Table E-2). After identifying the components of the processor, the

design of the device is drawn on a cartesian system, and coordinates are attributed to the feature's positioning (Figure E-8).

Table E-2 – Description of the function and characteristics of microfluidic processor components

Feature	Assignment	Function	Characteristic
Reservoirs	Letter	Indicate the Inlet / Outlet.	Do not code a valve, and therefore cannot be actuated.
Stop Valves	Number	Block the Inlet / Outlet from the content of the processor.	Do not present all degrees of freedom, in comparison with valves.
Valves	Number	Responsible for routing and mixing fluid within the processor.	Connect with other valves and / or stop valves.
Walls	None	Used to block the assignment of a coordinate.	Do not code any feature, and therefore cannot be actuated.

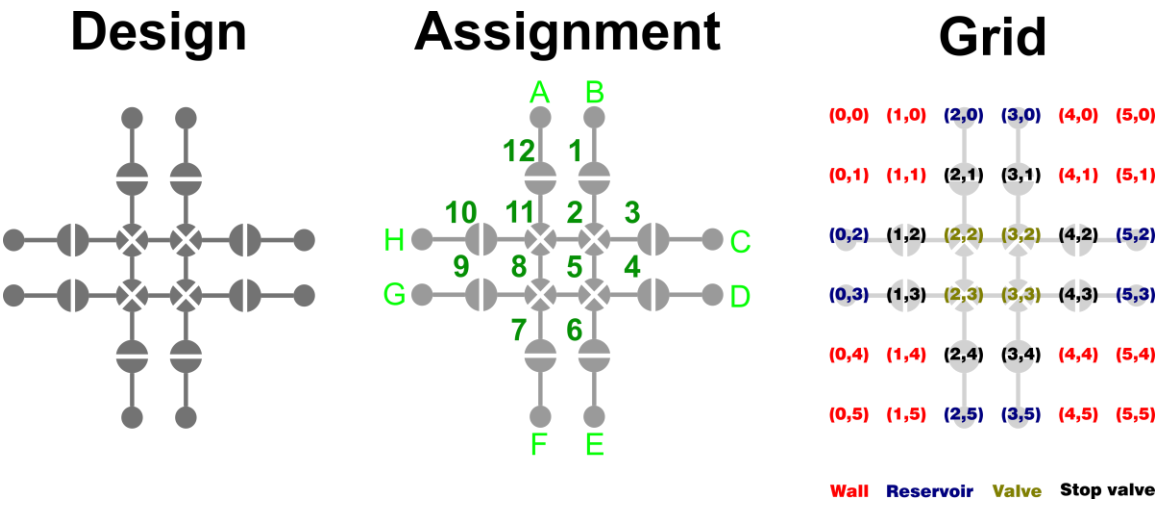

Figure E-8 – Variable assignment used in the code that automates fluidic manipulation on-chip, for a 2x2 fluidic processor.

The automated fluidic manipulation code is based on Dijkstra's algorithm [233], which finds the shortest path from one point to every other point in the graph. Here, we define path length in terms of the graph distance - number of edges traversed in the path.

E.5.1 4x4 fluidic processor example

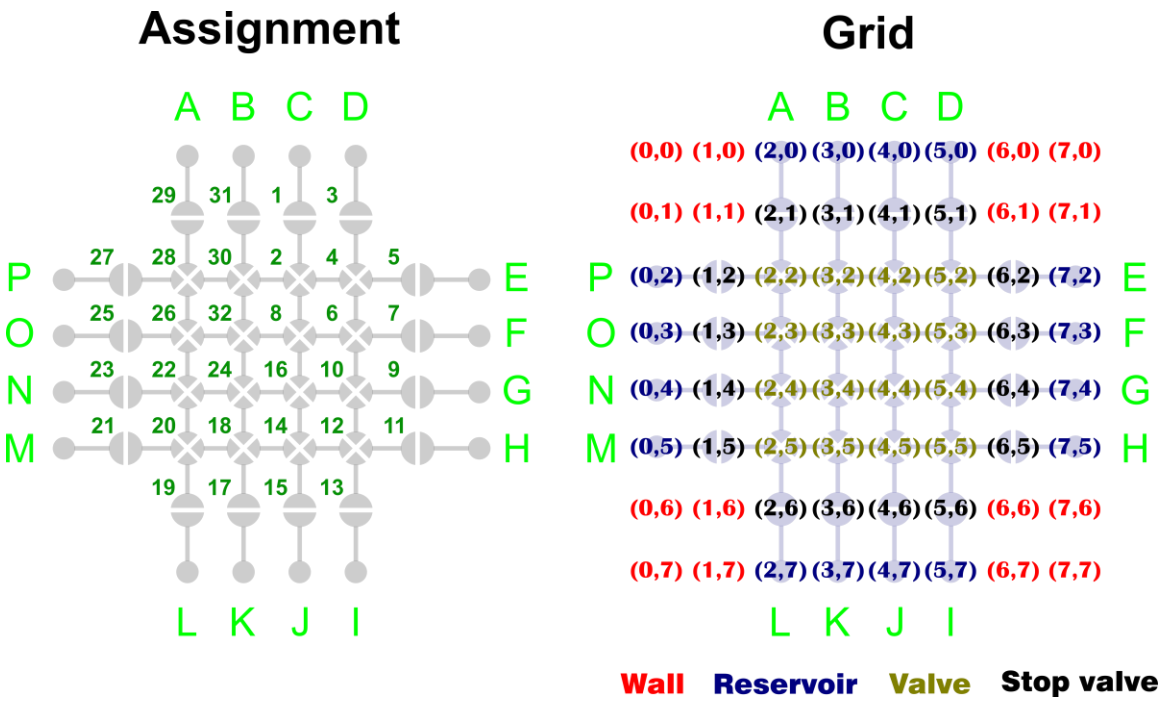

Figure E-9 – Variable assignment and cartesian coordinates for a 4x4 fluidic processor.

It is necessary to determine which points are neighbors of each other and, therefore, which movements are allowed within this system. The code identifies them by taking unit steps along the coordinate directions ((x±1,y) and (x,y±1)), as exemplified in Figure E-10. This only allows horizontal or vertical movements in this system. If one would like to include diagonal movements, then the neighbor coordinates calculation would need to be

adjusted accordingly ((x±1,y) and (x,y±1) and (x±1,y±1)). For stop valves, we allow movement on exactly one axis ((x±1,y) or (x,y±1)).

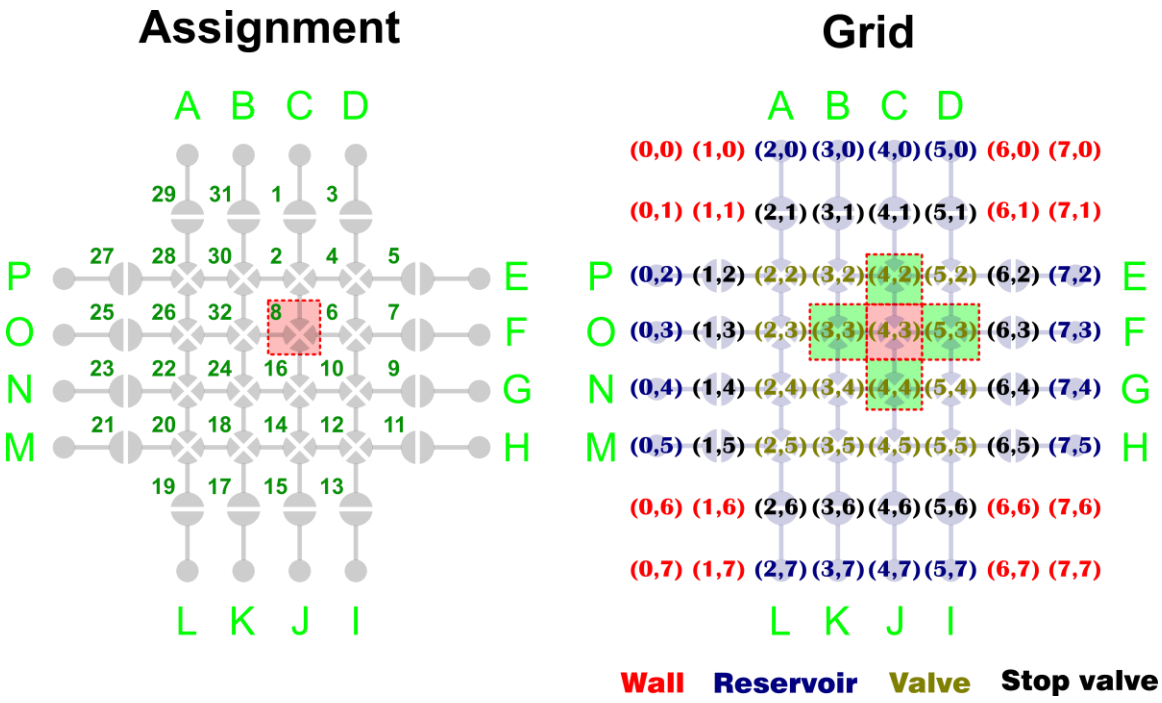

Figure E-10 – Neighbors' coordinates calculations. The neighbors of valve 8 (x=4,y=3) are: valve 2 (x=4, y=3-1), valve 32 (x=4-1, y=3), valve 6 (x=4+1, y=3) and valve 16 (x=4, y=3+1). Valve 8 is marked with a red dotted box, neighbors are highlighted in green.

After obtaining the neighbor coordinates, the algorithm analyzes if that point is available. The vertex can be unavailable if it is being used by another process, or if the point was included in the avoid list, or if the point was assigned as a wall. If the vertex is available, it is included into the search queue.

Two lists are created (visited and unvisited points). The algorithm takes a current point (given by the user) and assigns a very large cost (infinity) to travel to all other points. The algorithm then calculates the cost required to travel from the current point to an

unvisited neighbor point in the graph (neighbors are herein defined as adjacent points that can be reached by the current point). If the cost to travel to the neighbor is smaller than the current cost (which was firstly assigned as infinite), the new cost is reassigned as the distance between current point and neighbor point, and the current point is stored in the visited nodes list, while the neighbor becomes the new current point. We update the current point (by choosing one with the minimum distance) and repeat the process, until all points are visited in the graph and there are no points left in the unvisited points list. By comparing the costs associated with the travelling between the start and end points (both defined by the user) in the grid, the algorithm provides the smallest cost path travelled (Figure E-11).

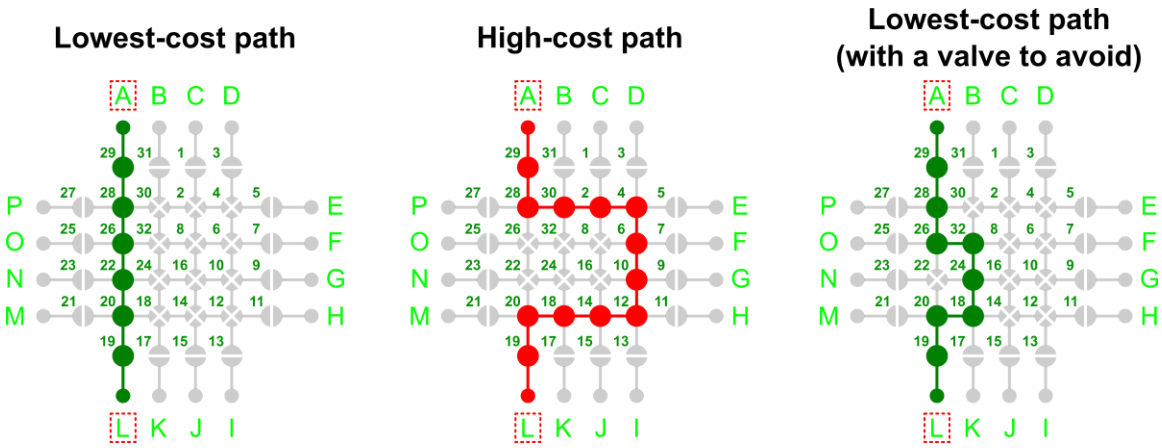

Figure E-11 – Examples of paths calculated by the algorithm, from A inlet to L outlet, both marked with red-dotted boxes. The lowest-cost path (6-points distance) is marked with green dots: A → 29 → 28 → 26 → 22 → 20 → 19 → L. An example of a high-cost path (12-points distance) is marked with red dots: A → 29 → 28 → 30 → 2 → 4 → 6 → 10 → 12 → 14 → 18 → 20 → 19 → L. The lowest-cost path when valve 22 is marked unavailable (8-points distance) is marked with green dots: A → 29 → 28 → 26 → 32 → 24 → 18 → 20 → 19 → L.

After calculating the lowest cost path, the algorithm checks for the number of valves used, based on the user's input: if fewer valves are required by the process, the code

adjusts the number of valves open to be equal to the user's input by excluding valves. If more valves are required, the algorithm looks for neighbor valves from the list of valves in use, and adds them to the path.

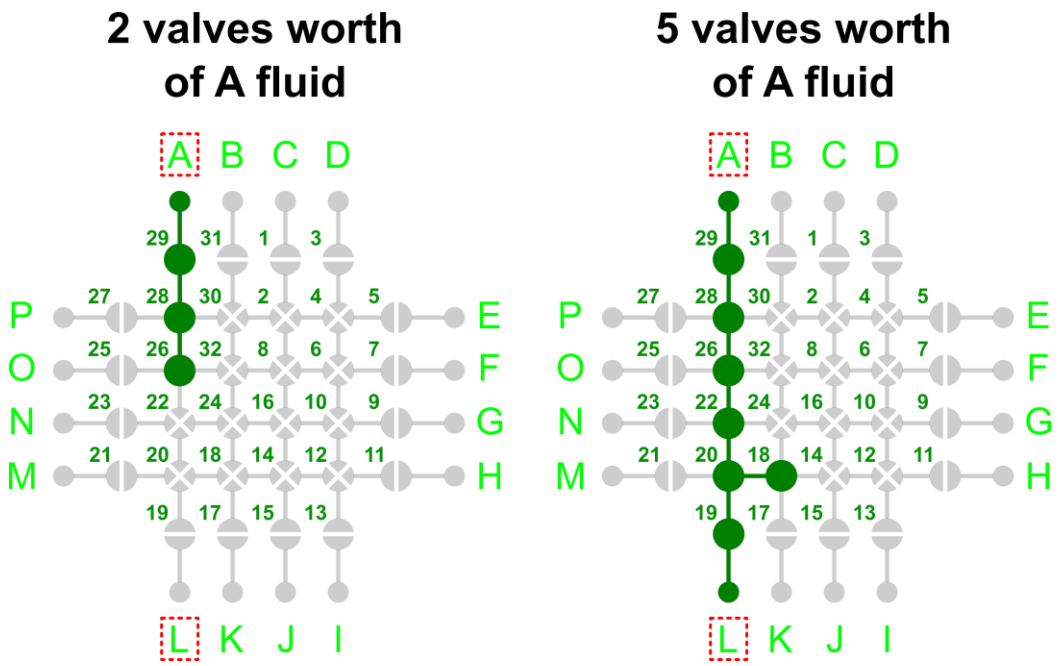

Figure E-12 – Examples of paths calculated by the algorithm, from A inlet to L outlet, both marked with red-dotted boxes. The algorithm calculates the complete route from the inlet to the outlet, and when fewer valves are required (2, in the representation), the program removes valves, starting from the outlet. If more valves are required (5, in the representation), the algorithm adds them to the list of valves used.

The program stores the information regarding the valves being used during a process as a list (used valves), and takes this information into account when more than one inlet is required, using other valves to perform the requested routine (Figure E-13).

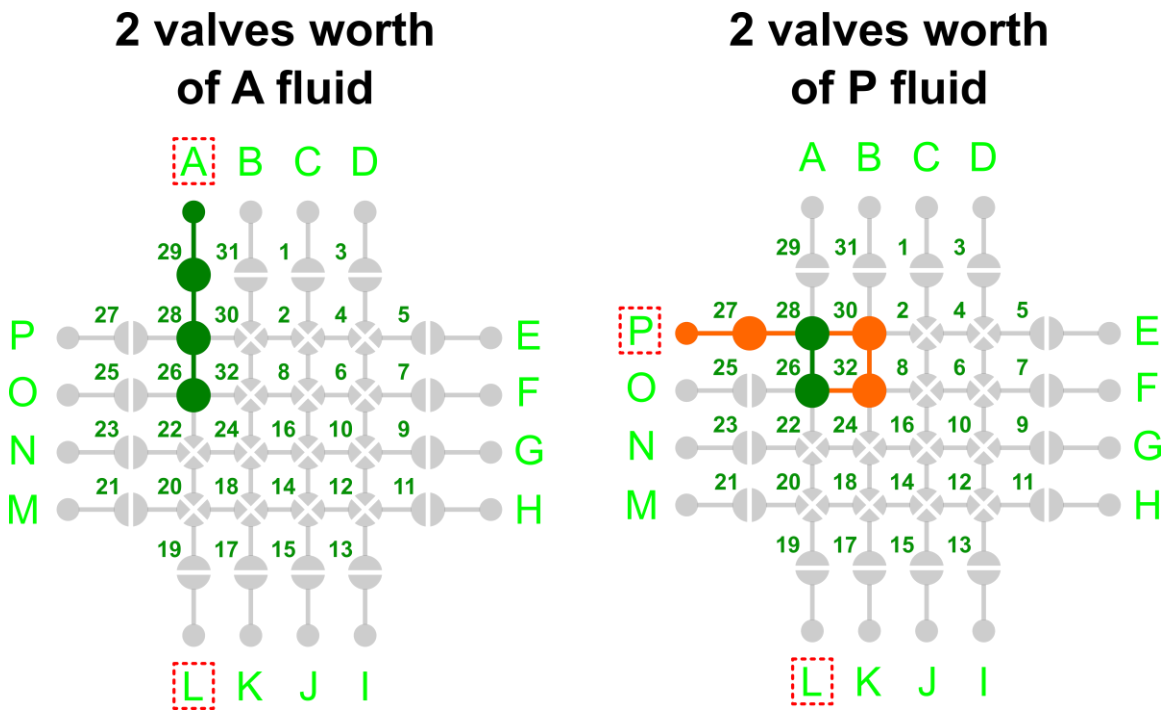

Figure E-13 – Representation of fluidic transfer from A to L and P to L (marked with red dotted boxes). 2 valves worth of fluid from A reservoir are in the processor (marked with green dots), and 2 valves worth of fluid from P reservoir are added in the processor (marked with orange dots).

When transferring the fluid from the processor to the desired outlet, if there is no direct connection between the valves being used by the processor and the stop valve of the outlet, Dijkstra's algorithm is used again: the algorithm searches for the path with the smallest cost, starting from the outlet going to the closest valve being used.

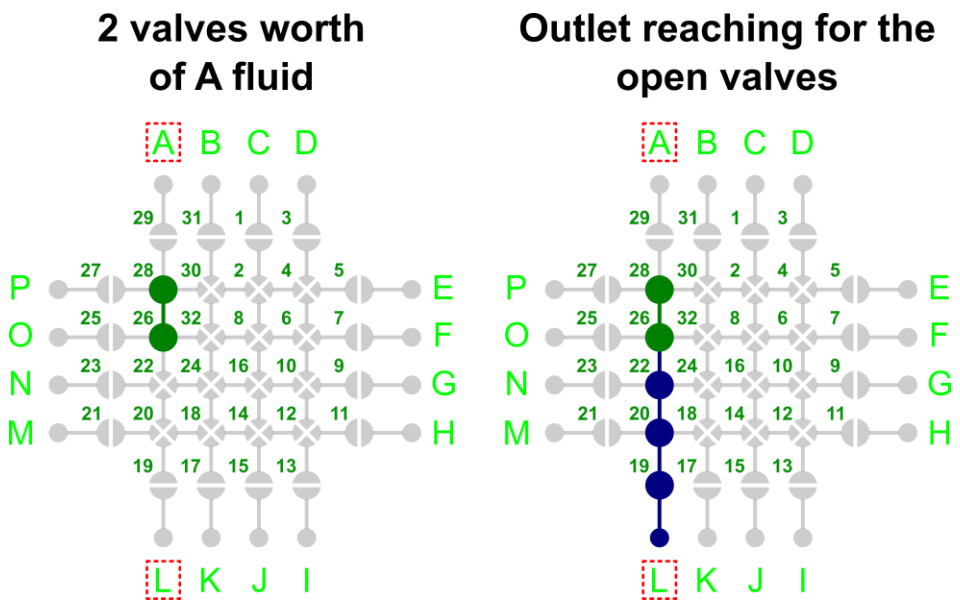

Figure E-14 – Representation of fluidic transfer from A to L (marked with red dotted boxes). Two valves worth of fluid from A reservoir are in the processor (marked with green dots). To transfer them to L, the algorithm uses Dijkstra's algorithm once again, starting from the outlet to the first valve being used in the processor.

After filling the processor and establishing a path towards the outlet, the algorithm closes the valves to pump the fluids inside the processor to the outlet reservoir. The closing routine was designed to avoid trapping fluid inside the processor. It also empties the whole processor before starting a new cycle. If a valve with fluid closes without a path to drain its content (Figure E-15), it can damage the processor by delaminating adjacent layers.

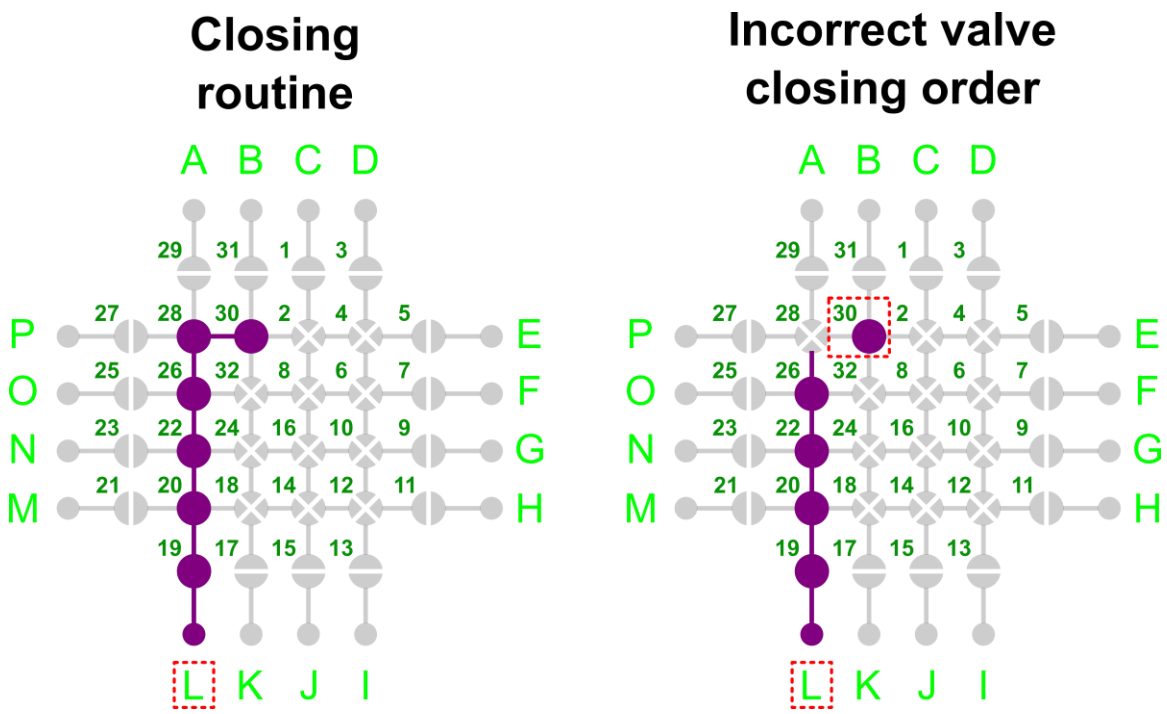

Figure E-15 – Representation of fluidic transfer towards L outlet (marked with a red dotted box). The proper closing order of open valves (represented with purple dots) follows the order: 30 → 28 → 26 → 22 → 20 → 19 → L. If valve 28 closes before valve 30 (marked with a red dotted box), valve 30 would have fluid trapped inside.

E.5.2 Method creation

After creating individual pumping routines, they can be combined to create methods (Figure E-16). Methods are used to perform a series of analytical steps on chip, such as the combination of reagents in a specific order, followed by the washing of the processor, for example. Another example is serial dilutions on chip, useful for on-chip calibration curves.

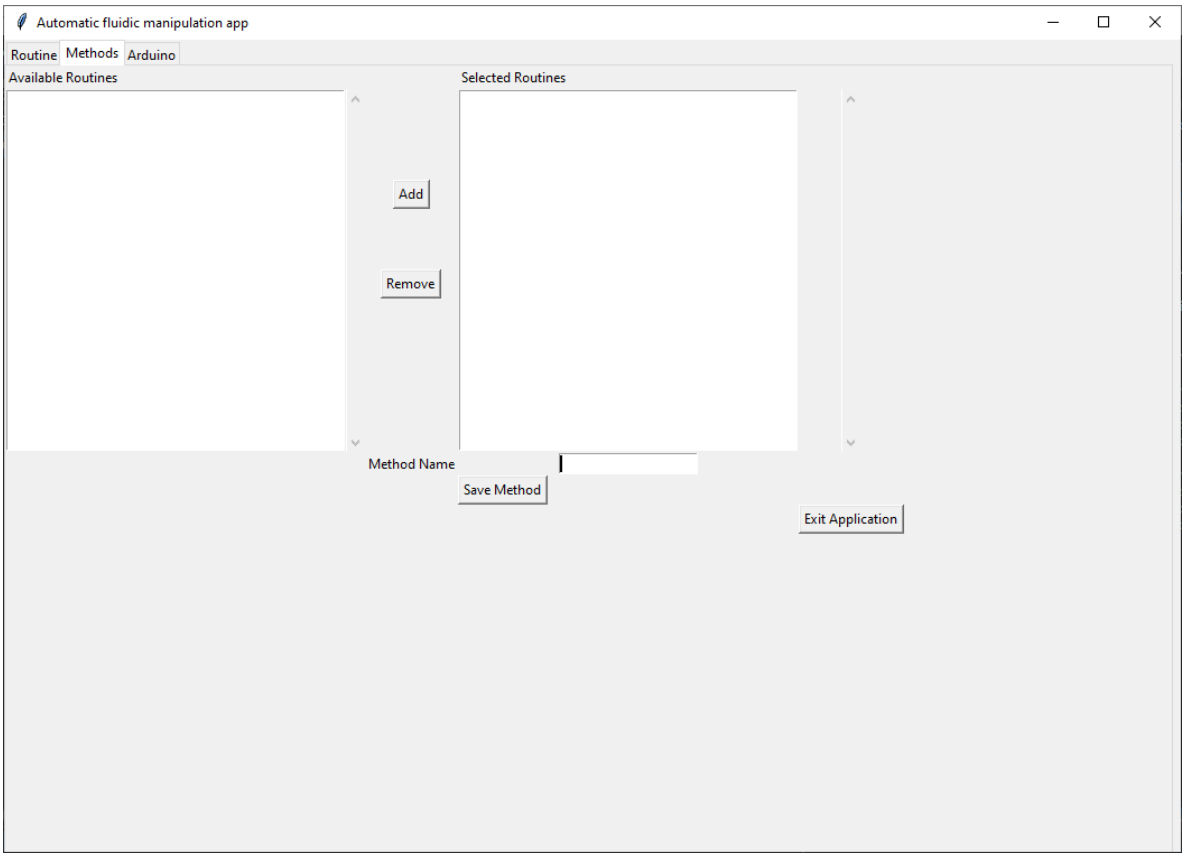

Figure E-16 – Fluidic Manipulation App at the Method development tab.

E.5.3 Solenoid actuation using Arduino

After creating the protocol to operate the valves in the fluidic processor, in terms of opening, waiting and closing valves, the Fluidic Manipulation App generates a string of commands, which can be read either by a commercial LabView system [224], or by an Arduino, used in this work. The Arduino can be operated straight from the Fluidic Manipulation App, in the 'Arduino' tab in the program (Figure E-17). Alternatively, it can be programmed directly by writing C++ code (with the proper pin assignment, as presented in Table E-2).

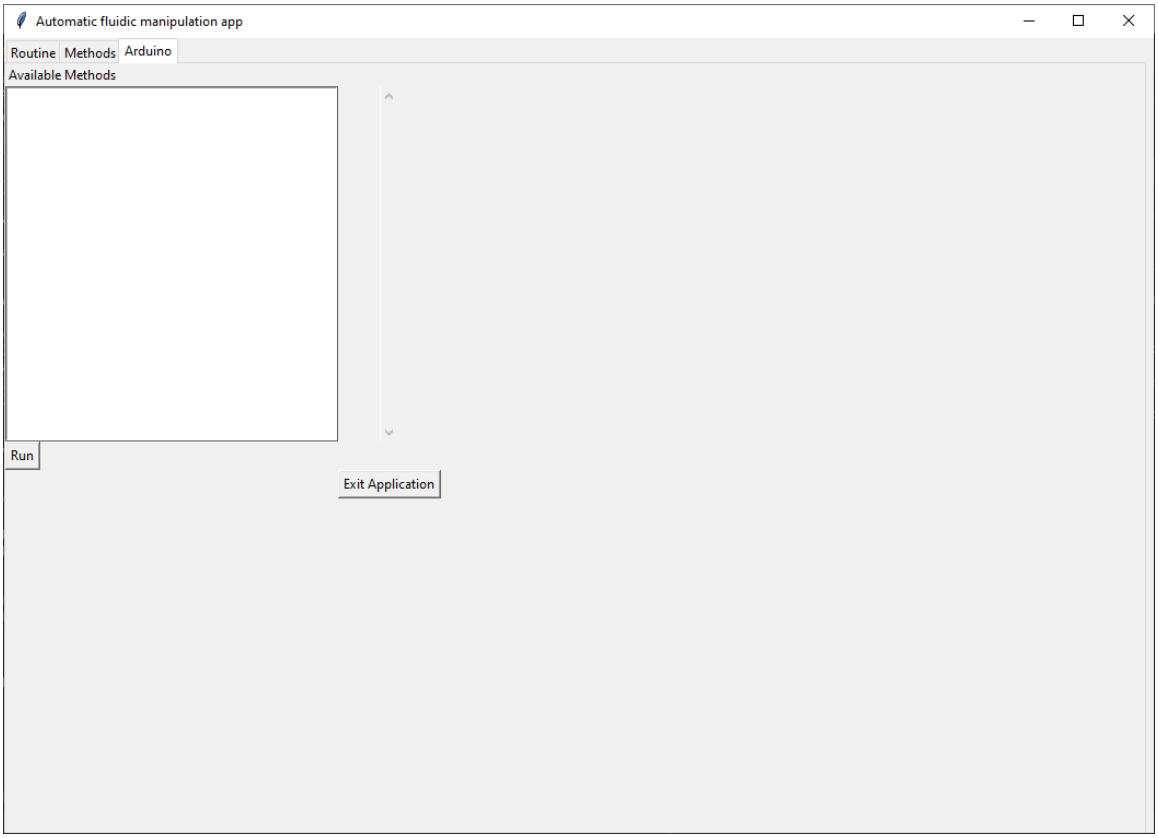

Figure E-17 – Fluidic Manipulation App screen at the Arduino tab.

E.6 Pumps assembling configuration

Four 12 V pumps were used in this work, owing to their low-cost. These pumps provide enough vacuum to operate the elastomeric microfluidic device. All pumps were connected, and the resulting vacuum was distributed to the solenoid mounts, to enable a more homogeneous vacuum in the system. Another advantage of this configuration is the possibility of operation of the entire system (4 solenoid mounts) in case one of the pumps breaks down. If each vacuum pump were to be connected individually to each solenoid

mounts, the failure of one pump would hinder the operation of 8 solenoid valves attached to 1 mount, being a major issue for remote operations.

E.7 Cost

Table E-3 – Costs associated with solenoid valves operation

Equipment	Conventional method [224]	New method (this work)	Price ($)
Sourcing Digital Output [a]	✓	✗	120.00
Compact Data Acquisition Chassis [b]	✓	✗	1433.00
Arduino [c]	✓	✓	40.30
Final price	**$1593.30**	**$40.30**	

[a] Digital Output Sourcing CSeries Module (NI-9472, National Instruments). Available at: https://www.ni.com/en-us/shop/select/c-series-digital-module?modelId=122223 - Access on 05/30/2020.

[b] Compact Data Acquisition chassis (cDAQ-9178, National Instruments). Available at: https://www.ni.com/en-us/shop/select/compactdaq-chassis?modelId=125699 - Access on 05/30/2020.

[c] Arduino board (MEGA 2560, Arduino). Available at: https://store.arduino.cc/usa/mega-2560-r3 - Access on 05/30/2020.

REFERENCES

[1] A. Manz, H.M. Widmers, N. Graber, Miniaturized total chemical analysis systems: A novel concept for chemical sensing, Sensors Actuators B Chem. 1 (1990) 244–248. doi:10.1016/0925-4005(90)80209-I.

[2] R.M. Van Dam, Solvent-Resistant Elastomeric Microfluidic Devices and Applications, Caltech, 2005. doi:10.7907/4EJF-1V78.

[3] H. Ryu, K. Choi, Y. Qu, T. Kwon, J.S. Lee, J. Han, Patient-Derived Airway Secretion Dissociation Technique to Isolate and Concentrate Immune Cells Using Closed-Loop Inertial Microfluidics, Anal. Chem. 89 (2017) 5549–5556. doi:10.1021/acs.analchem.7b00610.

[4] P. Cui, S. Wang, Applications of microfluidic chip technology in pharmaceutical analysis: A review, J. Pharm. Anal. (2018). doi:10.1016/j.jpha.2018.12.001.

[5] J. Kim, E.C. Jensen, A.M. Stockton, R.A. Mathies, Universal microfluidic automaton for autonomous sample processing: Application to the mars organic analyzer, Anal. Chem. 85 (2013) 7682–7688. doi:10.1021/ac303767m.

[6] J. Cleary, D. Maher, C. Slater, D. Diamond, In situ monitoring of environmental water quality using an autonomous microfluidic sensor, 2010 IEEE Sensors Appl. Symp. SAS 2010 - Proc. (2010) 36–40. doi:10.1109/SAS.2010.5439385.

[7] G.M. Whitesides, The origins and the future of microfluidics., Nature. 442 (2006) 368–73. doi:10.1038/nature05058.

[8] G.G. Morbioli, N.C. Speller, M.E. Cato, T.P. Cantrell, A.M. Stockton, Rapid and low-cost development of microfluidic devices using wax printing and microwave treatment, Sensors Actuators B Chem. 284 (2019) 650–656. doi:10.1016/j.snb.2018.12.053.

[9] N.C. Speller, G.G. Morbioli, M.E. Cato, T.P. Cantrell, E.M. Leydon, B.E. Schmidt, A.M. Stockton, Cutting edge microfluidics: Xurography and a microwave, Sensors Actuators B Chem. 291 (2019) 250–256. doi:10.1016/j.snb.2019.04.004.

[10] M.J. Madou, Fundamentals of Microfabrication, 2nd ed., CRC Press, Boca Raton,

2002.

[11] P.J.A. Kenis, R.F. Ismagilov, G.M. Whitesides, Microfabrication inside capillaries using multiphase laminar flow patterning, Science (80-.). 285 (1999) 83–85. doi:10.1126/science.285.5424.83.

[12] V. Hessel, H. Löwe, F. Schönfeld, Micromixers - A review on passive and active mixing principles, Chem. Eng. Sci. 60 (2005) 2479–2501. doi:10.1016/j.ces.2004.11.033.

[13] G.G. Morbioli, T. Mazzu-Nascimento, L.A. Milan, A.M. Stockton, E. Carrilho, Improving Sample Distribution Homogeneity in Three-Dimensional Microfluidic Paper-Based Analytical Devices by Rational Device Design, Anal. Chem. 89 (2017) 4786–4792. doi:10.1021/acs.analchem.6b04953.

[14] D.C. Duffy, J.C. McDonald, O.J.A. Schueller, G.M. Whitesides, Rapid prototyping of microfluidic systems in poly(dimethylsiloxane), Anal. Chem. 70 (1998) 4974–4984. doi:10.1021/ac980656z.

[15] N. Bao, Q. Zhang, J.J. Xu, H.Y. Chen, Fabrication of poly(dimethylsiloxane) microfluidic system based on masters directly printed with an office laser printer, J. Chromatogr. A. 1089 (2005) 270–275. doi:10.1016/j.chroma.2005.07.001.

[16] V.I. Vullev, J. Wan, V. Heinrich, P. Landsman, P.E. Bower, B. Xia, B. Millare, G. Jones, Nonlithographic Fabrication of Microfluidic Devices, J. Am. Chem. Soc. 128 (2006) 16062–16072. doi:10.1021/ja061776o.

[17] G. V Kaigala, S. Ho, R. Penterman, C.J. Backhouse, Rapid prototyping of microfluidic devices with a wax printer., Lab Chip. 7 (2007) 384–7. doi:10.1039/b617764f.

[18] D.A. Bartholomeusz, R.W. Boutté, J.D. Andrade, Xurography: Rapid prototyping of microstructures using a cutting plotter, J. Microelectromechanical Syst. 14 (2005) 1364–1374. doi:10.1109/JMEMS.2005.859087.

[19] N.C. Speller, G.G. Morbioli, M.E. Cato, Z.A. Duca, A.M. Stockton, Green, Low-Cost, User-Friendly, and Elastomeric (GLUE) Microfluidics, ACS Appl. Polym. Mater. 2 (2020) 1345–1355. doi:10.1021/acsapm.9b01201.

[20] R. Gojo, Y. Morimoto, S. Takeuchi, Quick and easy fabrication of microfluidic channels with water- soluble molds, Lab Chip. (2008) 1000–1002.

[21] A.W. Martinez, S.T. Phillips, E. Carrilho, S.W. Thomas, H. Sindi, G.M. Whitesides, Simple telemedicine for developing regions: camera phones and paper-based microfluidic devices for real-time, off-site diagnosis., Anal. Chem. 80 (2008) 3699–707. doi:10.1021/ac800112r.

[22] R.W. Peeling, K.K. Holmes, D. Mabey, a Ronald, Rapid tests for sexually transmitted infections (STIs): the way forward., Sex. Transm. Infect. 82 Suppl 5 (2006) v1-6. doi:10.1136/sti.2006.024265.

[23] L. Ge, S. Wang, X. Song, S. Ge, J. Yu, 3D origami-based multifunction-integrated immunodevice: low-cost and multiplexed sandwich chemiluminescence immunoassay on microfluidic paper-based analytical device., Lab Chip. 12 (2012) 3150–8. doi:10.1039/c2lc40325k.

[24] X. Gong, X. Yi, K. Xiao, S. Li, R. Kodzius, J. Qin, W. Wen, Wax-bonding 3D microfluidic chips., Lab Chip. 10 (2010) 2622–7. doi:10.1039/c004744a.

[25] G.G. Lewis, M.J. DiTucci, M.S. Baker, S.T. Phillips, High throughput method for prototyping three-dimensional, paper-based microfluidic devices., Lab Chip. 12 (2012) 2630–3. doi:10.1039/c2lc40331e.

[26] A.W. Martinez, S.T. Phillips, G.M. Whitesides, Three-dimensional microfluidic devices fabricated in layered paper and tape., Proc. Natl. Acad. Sci. U. S. A. 105 (2008) 19606–11. doi:10.1073/pnas.0810903105.

[27] D. Zang, L. Ge, M. Yan, X. Song, J. Yu, Electrochemical immunoassay on a 3D microfluidic paper-based device., Chem. Commun. (Camb). 48 (2012) 4683–5. doi:10.1039/c2cc16958d.

[28] M. Zhang, L. Ge, S. Ge, M. Yan, J. Yu, J. Huang, S. Liu, Three-dimensional paper-based electrochemiluminescence device for simultaneous detection of Pb2+ and Hg2+ based on potential-control technique., Biosens. Bioelectron. 41 (2013) 544–50. doi:10.1016/j.bios.2012.09.022.

[29] H. Liu, R.M. Crooks, Three-dimensional paper microfluidic devices assembled using the principles of origami, J. Am. Chem. Soc. 133 (2011) 17564–17566. doi:10.1021/ja2071779.

[30] A. Abbas, A. Brimer, J.M. Slocik, L. Tian, R.R. Naik, S. Singamaneni, Multifunctional analytical platform on a paper strip: separation, preconcentration, and subattomolar detection., Anal. Chem. 85 (2013) 3977–83. doi:10.1021/ac303567g.

[31] K. Abe, K. Suzuki, D. Citterio, Inkjet-printed microfluidic multianalyte chemical sensing paper, Anal. Chem. 80 (2008) 6928–6934. doi:10.1021/ac800604v.

[32] M.M. Mentele, J. Cunningham, K. Koehler, J. Volckens, C.S. Henry, Microfluidic paper-based analytical device for particulate metals., Anal. Chem. 84 (2012) 4474–80. doi:10.1021/ac300309c.

[33] T.S. Park, W. Li, K.E. McCracken, J.-Y. Yoon, Smartphone quantifies Salmonella from paper microfluidics., Lab Chip. 13 (2013) 4832–40. doi:10.1039/c3lc50976a.

[34] R.S.J. Alkasir, M. Ornatska, S. Andreescu, Colorimetric paper bioassay for the detection of phenolic compounds., Anal. Chem. 84 (2012) 9729–37. doi:10.1021/ac301110d.

[35] E. Carrilho, A.W. Martinez, G.M. Whitesides, Understanding wax printing: a simple micropatterning process for paper-based microfluidics., Anal. Chem. 81 (2009) 7091–5. doi:10.1021/ac901071p.

[36] D.M. Cate, W. Dungchai, J.C. Cunningham, J. Volckens, C.S. Henry, Simple, distance-based measurement for paper analytical devices., Lab Chip. 13 (2013) 2397–404. doi:10.1039/c3lc50072a.

[37] C.A. Chaplan, H.T. Mitchell, A.W. Martinez, Paper-based standard addition assays, Anal. Methods. 6 (2014) 1296. doi:10.1039/c4ay00205a.

[38] C.-M. Cheng, A.W. Martinez, J. Gong, C.R. Mace, S.T. Phillips, E. Carrilho, K. a Mirica, G.M. Whitesides, Paper-based ELISA., Angew. Chem. Int. Ed. Engl. 49 (2010) 4771–4. doi:10.1002/anie.201001005.

[39] M.S. Khan, G. Thouas, W. Shen, G. Whyte, G. Garnier, Paper diagnostic for instantaneous blood typing., Anal. Chem. 82 (2010) 4158–64. doi:10.1021/ac100341n.

[40] B.R. Lutz, P. Trinh, C. Ball, E. Fu, P. Yager, Two-dimensional paper networks:

programmable fluidic disconnects for multi-step processes in shaped paper., Lab Chip. 11 (2011) 4274–8. doi:10.1039/c1lc20758j.

[41] A.W. Martinez, S.T. Phillips, G.M. Whitesides, E. Carrilho, Diagnostics for the developing world: microfluidic paper-based analytical devices., Anal. Chem. 82 (2010) 3–10. doi:10.1021/ac9013989.

[42] D.M. Cate, J.A. Adkins, J. Mettakoonpitak, C.S. Henry, Recent Developments in Paper-Based Microfluidic Devices, Anal. Chem. 87 (2015) 19–41. doi:10.1021/ac503968p.

[43] K.M. Schilling, A.L. Lepore, J. a Kurian, A.W. Martinez, Fully enclosed microfluidic paper-based analytical devices., Anal. Chem. 84 (2012) 1579–85. doi:10.1021/ac202837s.

[44] G.G. Morbioli, Funcionalização de celulose para ensaios bioanalíticos em dispositivos microfluídicos baseados em papel (μPADs), Universidade de São Paulo, 2015. doi:10.11606/D.75.2015.tde-23062015-105938.

[45] H. Noh, S.T. Phillips, Metering the capillary-driven flow of fluids in paper-based microfluidic devices., Anal. Chem. 82 (2010) 4181–7. doi:10.1021/ac100431y.

[46] K.M. Schilling, D. Jauregui, A.W. Martinez, Paper and toner three-dimensional fluidic devices: programming fluid flow to improve point-of-care diagnostics., Lab Chip. 13 (2013) 628–31. doi:10.1039/c2lc40984d.

[47] Y. Zhang, L. Li, L. Zhang, S. Ge, M. Yan, J. Yu, In-situ synthesized polypyrrole-cellulose conductive networks for potential-tunable foldable power paper, Nano Energy. 31 (2017) 174–182. doi:10.1016/j.nanoen.2016.11.029.

[48] A.W. Martinez, S.T. Phillips, M.J. Butte, G.M. Whitesides, Patterned Paper as a Platform for Inexpensive, Low-Volume, Portable Bioassays, Angew. Chemie Int. Ed. 46 (2007) 1318–1320. doi:10.1002/anie.200603817.

[49] J.T. Connelly, J.P. Rolland, G.M. Whitesides, “Paper Machine” for Molecular Diagnostics, Anal. Chem. 87 (2015) 7595–7601. doi:10.1021/acs.analchem.5b00411.

[50] K.W. Oh, K. Lee, B. Ahn, E.P. Furlani, Design of pressure-driven microfluidic

networks using electric circuit analogy., Lab Chip. 12 (2012) 515–45. doi:10.1039/c2lc20799k.

[51] E. Elizalde, R. Urteaga, C.L.A. Berli, Rational design of capillary-driven flows for paper-based microfluidics, Lab Chip. 15 (2015) 2173–2180. doi:10.1039/C4LC01487A.

[52] N.K. Thom, K. Yeung, M.B. Pillion, S.T. Phillips, "Fluidic batteries" as low-cost sources of power in paper-based microfluidic devices, Lab Chip. 12 (2012) 1768. doi:10.1039/c2lc40126f.

[53] J. Khandurina, A. Guttman, Bioanalysis in microfluidic devices, J. Chromatogr. A. 943 (2002) 159–183. doi:10.1016/S0021-9673(01)01451-0.

[54] K. Landers, J. (Ed.), Begley, M., Scanlan, C., Khurana, T., Monahan, J., Carrilho, E., Guijt, R., Macka, M., Lindner, H., Huber, D., Cullen, C., Wootton, R., Marko-Varga, G., van Midwoud, P., Fuentes, H., Mohamadi, M., Kaji, N., Baba, Y., Stachowiak, T., Dre, Handbook of Capillary and Microchip Electrophoresis and Associated Microtechniques, 3rd Editio, 2007.

[55] B.P. Regmi, M. Agah, Micro Gas Chromatography: An Overview of Critical Components and Their Integration, Anal. Chem. 90 (2018) 13133–13150. doi:10.1021/acs.analchem.8b01461.

[56] Z. Cao, C. Lu, A Microfluidic Device with Integrated Sonication and Immunoprecipitation for Sensitive Epigenetic Assays, Anal. Chem. 88 (2016) 1965–1972. doi:10.1021/acs.analchem.5b04707.

[57] S. Ma, Y.P. Hsieh, J. Ma, C. Lu, Low-input and multiplexed microfluidic assay reveals epigenomic variation across cerebellum and prefrontal cortex, Sci. Adv. 4 (2018). doi:10.1126/sciadv.aar8187.

[58] R.S. Adams, C.J. Atman, Cognitive processes in iterative design behavior, in: FIE'99 Front. Educ. 29th Annu. Front. Educ. Conf. Des. Futur. Sci. Eng. Educ. Conf. Proc. (IEEE Cat. No.99CH37011, Stripes Publishing L.L.C, 2000: pp. 11A6/13-11A6/18. doi:10.1109/FIE.1999.839114.

[59] S. Kruni, Ć.M. Perini, Ć.S. Mari, C.A.D. Cam, C.A.D. Cam, RAPID PROTOTYPING APPLICATION, Eng. Rev. 2 (2010) 91–100.

[60] Y. Chen, L. Zhang, G. Chen, Fabrication, modification, and application of poly(methyl methacrylate) microfluidic chips, Electrophoresis. 29 (2008) 1801–1814. doi:10.1002/elps.200700552.

[61] S. Roy, C.Y. Yue, Y.C. Lam, Z.Y. Wang, H. Hu, Surface analysis, hydrophilic enhancement, ageing behavior and flow in plasma modified cyclic olefin copolymer (COC)-based microfluidic devices, Sensors Actuators, B Chem. 150 (2010) 537–549. doi:10.1016/j.snb.2010.08.043.

[62] G.S. Fiorini, R.M. Lorenz, J. Kuo, D.T. Chiu, Rapid prototyping of thermoset polyester microfluidic devices, Anal. Chem. 76 (2004) 4697–4704. doi:10.1021/ac0498922.

[63] W.I. Wu, K.N. Sask, J.L. Brash, P.R. Selvaganapathy, Polyurethane-based microfluidic devices for blood contacting applications, Lab Chip. 12 (2012) 960–970. doi:10.1039/c2lc21075d.

[64] G. Whitesides, Microfluidics in Late Adolescence, (2018). http://arxiv.org/abs/1802.05595.

[65] C. Iliescu, H. Taylor, M. Avram, J. Miao, S. Franssila, A practical guide for the fabrication of microfluidic devices using glass and silicon, Biomicrofluidics. 6 (2012) 1–16. doi:10.1063/1.3689939.

[66] E. Roy, J.C. Galas, T. Veres, Thermoplastic elastomers for microfluidics: Towards a high-throughput fabrication method of multilayered microfluidic devices, Lab Chip. 11 (2011) 3193–3196. doi:10.1039/c1lc20251k.

[67] K. Domansky, D.C. Leslie, J. McKinney, J.P. Fraser, J.D. Sliz, T. Hamkins-Indik, G.A. Hamilton, A. Bahinski, D.E. Ingber, Clear castable polyurethane elastomer for fabrication of microfluidic devices, Lab Chip. 13 (2013) 3956–3964. doi:10.1039/c3lc50558h.

[68] S. Park, K. Mondal, R.M. Treadway, V. Kumar, S. Ma, J.D. Holbery, M.D. Dickey, Silicones for Stretchable and Durable Soft Devices: Beyond Sylgard-184, ACS Appl. Mater. Interfaces. 10 (2018) 11261–11268. doi:10.1021/acsami.7b18394.

[69] R. Mukhopadhyay, When PDMS isn't the best, Anal. Chem. 79 (2007) 3249–3253. doi:10.1021/ac071903e.

[70] J.N. Lee, C. Park, G.M. Whitesides, Solvent Compatibility of Poly(dimethylsiloxane)-Based Microfluidic Devices, Anal. Chem. 75 (2003) 6544–6554. doi:10.1021/ac0346712.

[71] M.W. Toepke, D.J. Beebe, PDMS absorption of small molecules and consequences in microfluidic applications, Lab Chip. 6 (2006) 1484–1486. doi:10.1039/b612140c.

[72] J.L. Fritz, M.J. Owen, Hydrophobic recovery of plasma-treated polydimethylsiloxane, J. Adhes. 54 (1995) 33–45. doi:10.1080/00218469508014379.

[73] A. Zahid, B. Dai, R. Hong, D. Zhang, Optical properties study of silicone polymer PDMS substrate surfaces modified by plasma treatment, Mater. Res. Express. 4 (2017). doi:10.1088/2053-1591/aa8645.

[74] M.-C. Bélanger, Y. Marois, Hemocompatibility, biocompatibility, inflammatory and in vivo studies of primary reference materials low-density polyethylene and polydimethylsiloxane: A review, J. Biomed. Mater. Res. 58 (2001) 467–477. doi:10.1002/jbm.1043.

[75] Y. Xia, G.M. Whitesides, Soft Lithography, Annu. Rev. Mater. Sci. 28 (1998) 153–184. doi:10.1146/annurev.matsci.28.1.153.

[76] B.E. Slentz, N.A. Penner, E. Lugowska, F. Regnier, Nanoliter capillary electrochromatography columns based on collocated monolithic support structures molded in poly(dimethyl siloxane), Electrophoresis. 22 (2001) 3736–3743. doi:10.1002/1522-2683(200109)22:17<3736::AID-ELPS3736>3.0.CO;2-Y.

[77] J.H.L. Beal, A. Bubendorfer, T. Kemmitt, I. Hoek, W. Mike Arnold, A rapid, inexpensive surface treatment for enhanced functionality of polydimethylsiloxane microfluidic channels, Biomicrofluidics. 6 (2012). doi:10.1063/1.4740232.

[78] J. Zhou, A.V. Ellis, N.H. Voelcker, Recent developments in PDMS surface modification for microfluidic devices., Electrophoresis. 31 (2010) 2–16. doi:10.1002/elps.200900475.

[79] C. Hong, D. Bao, M.S. Thomas, J.M. Clift, V.I. Vullev, Print-and-peel fabrication of microelectrodes, Langmuir. 24 (2008) 8439–8442. doi:10.1021/la801752k.

[80] V. Studer, G. Hang, A. Pandolfi, M. Ortiz, W.F. Anderson, S.R. Quake, Scaling properties of a low-actuation pressure microfluidic valve, J. Appl. Phys. 95 (2004) 393–398. doi:10.1063/1.1629781.

[81] A.E. Özçam, K. Efimenko, J. Genzer, Effect of ultraviolet/ozone treatment on the surface and bulk properties of poly(dimethyl siloxane) and poly(vinylmethyl siloxane) networks, Polym. (United Kingdom). 55 (2014) 3107–3119. doi:10.1016/j.polymer.2014.05.027.

[82] T.K. Meister, K. Riener, P. Gigler, J. Stohrer, W.A. Herrmann, F.E. Kühn, Platinum Catalysis Revisited-Unraveling Principles of Catalytic Olefin Hydrosilylation, ACS Catal. 6 (2016) 1274–1284. doi:10.1021/acscatal.5b02624.

[83] C. Dow, PDMS datasheet Dow corning, n.d.

[84] Z. Wang, A.A. Volinsky, N.D. Gallant, Crosslinking effect on polydimethylsiloxane elastic modulus measured by custom-built compression instrument, J. Appl. Polym. Sci. 131 (2014) 1–4. doi:10.1002/app.41050.

[85] J.H. Seo, K. Sakai, N. Yui, Adsorption state of fibronectin on poly(dimethylsiloxane) surfaces with varied stiffness can dominate adhesion density of fibroblasts, Acta Biomater. 9 (2013) 5493–5501. doi:10.1016/j.actbio.2012.10.015.

[86] J.C. McDonald, M.L. Chabinyc, S.J. Metallo, J.R. Anderson, A.D. Stroock, G.M. Whitesides, Prototyping of microfluidic devices in poly(dimethylsiloxane) using solid-object printing, Anal. Chem. 74 (2002) 1537–1545. doi:10.1021/ac010938q.

[87] H.N. Chan, Y. Chen, Y. Shu, Y. Chen, Q. Tian, H. Wu, Direct, one-step molding of 3D-printed structures for convenient fabrication of truly 3D PDMS microfluidic chips, Microfluid. Nanofluidics. 19 (2015) 9–18. doi:10.1007/s10404-014-1542-4.

[88] C.N. LaFratta, T. Baldacchini, R.A. Farrer, J.T. Fourkas, M.C. Teich, B.E.A. Saleh, M.J. Naughton, Replication of two-photon-polymerized structures with extremely high aspect ratios and large overhangs, J. Phys. Chem. B. 108 (2004) 11256–11258. doi:10.1021/jp048525r.

[89] A.K. Soe, S. Nahavandi, Degassing a PDMS mixture without a vacuum desiccator or a laboratory centrifuge and curing the PDMS chip in an ordinary kitchen oven, Chips Tips. (2011). https://blogs.rsc.org/chipsandtips/2011/05/26/degassing-a-

pdms-mixture-without-a-vacuum-desiccator-or-a-laboratory-centrifuge-and-curing-the-pdms-chip-in-an-ordinary-kitchen-oven/.

[90] M. Lake, M. Lake, C. Narciso, K. Cowdrick, T. Storey, S. Zhang, J. Zartman, D. Hoelzle, Microfluidic device design, fabrication, and testing protocols, Protoc. Exch. (2015) 1–26. doi:10.1038/protex.2015.069.

[91] D. Qin, Y. Xia, G.M. Whitesides, Soft lithography for micro- and nanoscale patterning, Nat. Protoc. 5 (2010) 491–502. doi:10.1038/nprot.2009.234.

[92] C.J. Easley, R.K.P. Benninger, J.H. Shaver, W. Steven Head, D.W. Piston, Rapid and inexpensive fabrication of polymeric microfluidic devices via toner transfer masking, Lab Chip. 9 (2009) 1119. doi:10.1039/b816575k.

[93] E.T. Thostenson, T.-W. Chou, Microwave processing: fundamentals and applications, Compos. Part A Appl. Sci. Manuf. 30 (1999) 1055–1071. doi:10.1016/S1359-835X(99)00020-2.

[94] J.A. Vickers, M.M. Caulum, C.S. Henry, Generation of hydrophilic poly(dimethylsiloxane) for high-performance microchip electrophoresis, Anal. Chem. 78 (2006) 7446–7452. doi:10.1021/ac0609632.

[95] A.L. Briseno, M. Roberts, M.M. Ling, H. Moon, E.J. Nemanick, Z. Bao, Patterning organic semiconductors using “dry” poly(dimethylsiloxane) elastomeric stamps for thin film transistors, J. Am. Chem. Soc. 128 (2006) 3880–3881. doi:10.1021/ja058226v.

[96] L.J. Millet, M.E. Stewart, R.G. Nuzzo, M.U. Gillette, Guiding neuron development with planar surface gradients of substrate cues deposited using microfluidic devices, Lab Chip. 10 (2010) 1525–1535. doi:10.1039/c001552k.

[97] J. Zhou, A.V. Ellis, N.H. Voelcker, Recent developments in PDMS surface modification for microfluidic devices, Electrophoresis. 31 (2010) 2–16. doi:10.1002/elps.200900475.

[98] EPA, (n.d.). https://www.epa.gov/greenchemistry/basics-green-chemistry.

[99] D.T. Eddington, J.P. Puccinelli, D.J. Beebe, Thermal aging and reduced hydrophobic recovery of polydimethylsiloxane, Sensors Actuators, B Chem. 114

(2006) 170–172. doi:10.1016/j.snb.2005.04.037.

[100] M.J. Owen, P.J. Smith, Plasma treatment of polydimethylsiloxane, J. Adhes. Sci. Technol. 8 (1994) 1063–1075. doi:10.1163/156856194X00942.

[101] S. Bhattacharya, A. Datta, J.M. Berg, S. Gangopadhyay, Studies on surface wettability of poly(dimethyl) siloxane (PDMS) and glass under oxygen-plasma treatment and correlation with bond strength, J. Microelectromechanical Syst. 14 (2005) 590–597. doi:10.1109/JMEMS.2005.844746.

[102] H.Y. Chen, J. Lahann, Fabrication of discontinuous surface patterns within microfluidic channels using photodefinable vapor-based polymer coatings, Anal. Chem. 77 (2005) 6909–6914. doi:10.1021/ac050964e.

[103] Z. Niu, F. Gao, X. Jia, W. Zhang, W. Chen, K. Qian, Synthesis studies of sputtering TiO2 films on poly(dimethylsiloxane) for surface modification, Colloids Surfaces A Physicochem. Eng. Asp. 272 (2006) 170–175. doi:10.1016/j.colsurfa.2005.07.024.

[104] G. Sui, J. Wang, C.C. Lee, W. Lu, S.P. Lee, J. V. Leyton, A.M. Wu, H.R. Tseng, Solution-phase surface modification in intact poly(dimethylsiloxane) microfluidic channels, Anal. Chem. 78 (2006) 5543–5551. doi:10.1021/ac060605z.

[105] I. Hoek, F. Tho, W.M. Arnold, Sodium hydroxide treatment of PDMS based microfluidic devices, Lab Chip. 10 (2010) 2283–2285. doi:10.1039/c004769d.

[106] K. Aran, L.A. Sasso, N. Kamdar, J.D. Zahn, Irreversible, direct bonding of nanoporous polymer membranes to PDMS or glass microdevices, Lab Chip. 10 (2010) 548–552. doi:10.1039/b924816a.

[107] R.M. Pasternack, S.R. Amy, Y.J. Chabal, Attachment of 3-(aminopropyl)triethoxysilane on silicon oxide surfaces: Dependence on solution temperature, Langmuir. 24 (2008) 12963–12971. doi:10.1021/la8024827.

[108] W. Stöber, A. Fink, E. Bohn, Controlled growth of monodisperse silica spheres in the micron size range, J. Colloid Interface Sci. 26 (1968) 62–69. doi:10.1016/0021-9797(68)90272-5.

[109] Y. Wang, D. Lee, L. Zhang, H. Jeon, J.E. Mendoza-Elias, T.A. Harvat, S.Z. Hassan,

A. Zhou, D.T. Eddington, J. Oberholzer, Systematic prevention of bubble formation and accumulation for long-term culture of pancreatic islet cells in microfluidic device, Biomed. Microdevices. 14 (2012) 419–426. doi:10.1007/s10544-011-9618-3.

[110] C.D. García, B.M. Dressen, A. Henderson, C.S. Henry, Comparison of surfactants for dynamic surface modification of poly(dimethylsiloxane) microchips, Electrophoresis. 26 (2005) 703–709. doi:10.1002/elps.200410290.

[111] Y. Xu, J. Li, E. Wang, Microchip micellar electrokinetic chromatography based on one functionalized ionic liquid and its excellent performance on proteins separation, J. Chromatogr. A. 1207 (2008) 175–180. doi:10.1016/j.chroma.2008.08.062.

[112] G.G. Morbioli, T. Mazzu-Nascimento, A.M. Stockton, E. Carrilho, 6. How are these devices manufactured?, in: Pap. Diagnostics Curr. Status Futur. Appl., Springer, 2018: p. In preparation.

[113] J.W. Lee, S.R. Daly, A.Y. Huang-Saad, C.M. Seifert, J. Lutz, Using design strategies from microfluidic device patents to support idea generation, Microfluid. Nanofluidics. 22 (2018) 1–22. doi:10.1007/s10404-018-2089-6.

[114] Stanford, Designing Your Own Device, (n.d.). https://stanford.ilabsolutions.com/service_center/show_external/22/microfluidics-foundry#Foundry_Design_ValveTypes (accessed November 2, 2019).

[115] Inkscape, (n.d.). https://inkscape.org/.

[116] D.I. Walsh, D.S. Kong, S.K. Murthy, P.A. Carr, Enabling Microfluidics: from Clean Rooms to Makerspaces, Trends Biotechnol. 35 (2017) 383–392. doi:10.1016/j.tibtech.2017.01.001.

[117] M.A. Unger, H.-P. Chou, T. Thorsen, A. Scherer, S.R. Quake, Monolithic Microfabricated Valves and Pumps by Multilayer Soft Lithography, Science (80-.). 288 (2000) 113–116. doi:10.1126/science.288.5463.113.

[118] N.C. Speller, G.G. Morbioli, M.E. Cato, J.L. McNeice, A.M. Stockton, Characterization and evaluation of ionic liquids for use in rapidly-actuated hydraulic microvalves, Sensors Actuators B Chem. 303 (2020) 127124. doi:10.1016/j.snb.2019.127124.

[119] A.M. Stockton, M.F. Mora, M.L. Cable, P.A. Willis, Design rules and operational optimization for rapid, contamination-free microfluidic transfer using monolithic membrane valves, Sensors Actuators, B Chem. 177 (2013) 668–675. doi:10.1016/j.snb.2012.11.039.

[120] Q. Chen, G. Li, Y. Nie, S. Yao, J. Zhao, Investigation and improvement of reversible microfluidic devices based on glass-PDMS-glass sandwich configuration, Microfluid. Nanofluidics. 16 (2014) 83–90. doi:10.1007/s10404-013-1222-9.

[121] K. Anwar, T. Han, S.M. Kim, Reversible sealing techniques for microdevice applications, Sensors Actuators, B Chem. 153 (2011) 301–311. doi:10.1016/j.snb.2010.11.002.

[122] Y. Temiz, R.D. Lovchik, G. V. Kaigala, E. Delamarche, Lab-on-a-chip devices: How to close and plug the lab?, Microelectron. Eng. 132 (2015) 156–175. doi:10.1016/j.mee.2014.10.013.

[123] S. Satyanarayana, R.N. Karnik, A. Majumdar, Stamp-and-stick room-temperature bonding technique for microdevices, J. Microelectromechanical Syst. 14 (2005) 392–399. doi:10.1109/JMEMS.2004.839334.

[124] L.S. Shiroma, M.H.O. Piazzetta, G.F. Duarte-Junior, W.K.T. Coltro, E. Carrilho, A.L. Gobbi, R.S. Lima, Self-regenerating and hybrid irreversible/reversible PDMS microfluidic devices, Sci. Rep. 6 (2016) 1–12. doi:10.1038/srep26032.

[125] Research Gate, (n.d.). https://www.researchgate.net/.

[126] K. Efimenko, W.E. Wallace, J. Genzer, Surface modification of Sylgard-184 poly(dimethyl siloxane) networks by ultraviolet and ultraviolet/ozone treatment, J. Colloid Interface Sci. 254 (2002) 306–315. doi:10.1006/jcis.2002.8594.

[127] A. Lai, N. Altemose, J.A. White, A.M. Streets, On-ratio PDMS bonding for multilayer microfluidic device fabrication, J. Micromechanics Microengineering. 29 (2019) 107001. doi:10.1088/1361-6439/ab341e.

[128] J. Friend, L. Yeo, Fabrication of microfluidic devices using polydimethylsiloxane, Biomicrofluidics. 4 (2010) 1–5. doi:10.1063/1.3259624.

[129] M. Zhang, J. Wu, L. Wang, K. Xiao, W. Wen, A simple method for fabricating

multi-layer PDMS structures for 3D microfluidic chips, Lab Chip. 10 (2010) 1199–1203. doi:10.1039/b923101c.

[130] J. Liu, M. Enzelberger, S. Quake, A nanoliter rotary device for polymerase chain reaction, Electrophoresis. 23 (2002) 1531–1536. doi:10.1002/1522-2683(200205)23:10<1531::AID-ELPS1531>3.0.CO;2-D.

[131] T. Dahlberg, T. Stangner, H. Zhang, K. Wiklund, P. Lundberg, L. Edman, M. Andersson, 3D printed water-soluble scaffolds for rapid production of PDMS micro-fluidic flow chambers, Sci. Rep. 8 (2018) 1–10. doi:10.1038/s41598-018-21638-w.

[132] V. Saggiomo, A.H. Velders, Simple 3D Printed Scaffold-Removal Method for the Fabrication of Intricate Microfluidic Devices, Adv. Sci. 2 (2015) 1500125. doi:10.1002/advs.201500125.

[133] A.M. Christensen, D.A. Chang-yen, B.K. Gale, Characterization of interconnects used in PDMS microfluidic systems, J. Micromechanics Microengineering. 928 (2005) 928–934. doi:10.1088/0960-1317/15/5/005.

[134] P.J. Hung, P.J. Lee, P. Sabounchi, N. Aghdam, R. Lin, L.P. Lee, A novel high aspect ratio microfluidic design to provide a stable and uniform microenvironment for cell growth in a high throughput mammalian cell culture array, Lab Chip. 5 (2005) 44–48. doi:10.1039/b410743h.

[135] J. Atencia, G.A. Cooksey, A. Jahn, J.M. Zook, W.N. Vreeland, L.E. Locascio, Magnetic connectors for microfluidic applications, Lab Chip. 10 (2010) 246–249. doi:10.1039/b913331c.

[136] H. Chen, D. Acharya, A. Gajraj, J.C. Meiners, Robust interconnects and packaging for microfluidic elastomeric chips, Anal. Chem. 75 (2003) 5287–5291. doi:10.1021/ac034179i.

[137] A. Chen, T. Pan, Fit-to-Flow (F2F) interconnects: Universal reversible adhesive-free microfluidic adaptors for lab-on-a-chip systems, Lab Chip. 11 (2011) 727–732. doi:10.1039/c0lc00384k.

[138] C.W. Li, C.N. Cheung, J. Yang, C.H. Tzang, M. Yang, PDMS-based microfluidic device with multi-height structures fabricated by single-step photolithography using printed circuit board as masters, Analyst. 128 (2003) 1137–1142. doi:10.1039/b304354a.

[139] E.O. Lobo-Júnior, E.F.M. Gabriel, R.A. dos Santos, F.R. de Souza, W.D. Lopes, R.S. Lima, A.L. Gobbi, W.K.T. Coltro, Simple, rapid and, cost-effective fabrication of PDMS electrophoresis microchips using poly(vinyl acetate) as photoresist master, Electrophoresis. 38 (2017) 250–257. doi:10.1002/elps.201600209.

[140] T. Scharnweber, R. Truckenmüller, A.M. Schneider, A. Welle, M. Reinhardt, S. Giselbrecht, Rapid prototyping of microstructures in polydimethylsiloxane (PDMS) by direct UV-lithography, Lab Chip. 11 (2011) 1368–1371. doi:10.1039/c0lc00567c.

[141] A. Grimes, D.N. Breslauer, M. Long, J. Pegan, L.P. Lee, M. Khine, Shrinky-Dink microfluidics: Rapid generation of deep and rounded patterns, Lab Chip. 8 (2007) 170–172. doi:10.1039/b711622e.

[142] S. Cosson, L.G. Aeberli, N. Brandenberg, M.P. Lutolf, Ultra-rapid prototyping of flexible, multi-layered microfluidic devices via razor writing, Lab Chip. 15 (2015) 72–76. doi:10.1039/c4lc00848k.

[143] M.K.S. Verma, A. Majumder, A. Ghatak, Embedded template-assisted fabrication of complex microchannels in PDMS and design of a microfluidic adhesive, Langmuir. 22 (2006) 10291–10295. doi:10.1021/la062516n.

[144] Z. Li, J. Yang, K. Li, L. Zhu, W. Tang, Fabrication of PDMS microfluidic devices with 3D wax jetting, RSC Adv. 7 (2017) 3313–3320. doi:10.1039/C6RA24884E.

[145] S.H. Chao, R. Carlson, D.R. Meldrum, Rapid fabrication of microchannels using microscale plasma activated templating (μPLAT) generated water molds, Lab Chip. 7 (2007) 641–643. doi:10.1039/b618269k.

[146] Y. Xia, E. Kim, X.-M. Zhao, J.A. Rogers, M. Prentiss, G.M. Whitesides, Complex Optical Surfaces Formed by Replica Molding Against Elastomeric Masters, Science (80-.). 273 (1996) 347–349. doi:10.1126/science.273.5273.347.

[147] E. Delamarche, A. Bernard, H. Schmid, B. Michel, H. Biebuyck, Patterned delivery of immunoglobulins to surfaces using microfluidic networks, Science (80-.). 276 (1997) 779–781. doi:10.1126/science.276.5313.779.

[148] D. Qin, Y. Xia, G.M. Whitesides, Rapid prototyping of complex structures with feature sizes larger than 20 ?m, Adv. Mater. 8 (1996) 917–919. doi:10.1002/adma.19960081110.

[149] PhotoPlot, (2020). https://photoplotstore.com/ (accessed August 5, 2020).

[150] Y. Xia, G.M. Whitesides, Soft Lithography, Angew. Chemie Int. Ed. 37 (1998) 550–575. doi:10.1002/(SICI)1521-3773(19980316)37:5<550::AID-ANIE550>3.0.CO;2-G.

[151] M.S. Thomas, B. Millare, J.M. Clift, D. Bao, C. Hong, V.I. Vullev, Print-and-peel fabrication for microfluidics: what's in it for biomedical applications?, Ann. Biomed. Eng. 38 (2010) 21–32. doi:10.1007/s10439-009-9831-x.

[152] A. Tan, K. Rodgers, J.P. Murrihy, C. O'Mathuna, J.D. Glennon, Rapid fabrication of microfluidic devices in poly(dimethylsiloxane) by photocopying, Lab Chip. 1 (2001) 7–9. doi:10.1039/b102905n.

[153] T. Deng, H. Wu, S.T. Brittain, G.M. Whitesides, Prototyping of masks, masters, and stamps/molds for soft lithography using an office printer and photographic reduction, Anal. Chem. 72 (2000) 3176–3180. doi:10.1021/ac991343m.

[154] R. Lu, W. Shi, L. Jiang, J. Qin, B. Lin, Rapid prototyping of paper-based microfluidics with wax for low-cost, portable bioassay, Electrophoresis. 30 (2009) 1497–1500. doi:10.1002/elps.200800563.

[155] Color Solid Ink Printing, (n.d.). http://www.imaging.org/site/IST/Resources/Imaging_Tutorials/Color_Solid_Ink_Printing/IST/Resources/Tutorials/Solid_Ink.aspx?hkey=51a9403c-0474-49d9-a5cd-22cd5abface6.

[156] Xerox, (n.d.). https://www.xerox.com/en-us/office/solid-ink.

[157] G. Comina, A. Suska, D. Filippini, PDMS lab-on-a-chip fabrication using 3D printed templates, Lab Chip. 14 (2014) 424–430. doi:10.1039/c3lc50956g.

[158] PC Magazine, (n.d.). https://www.pcmag.com/picks/the-best-3d-printers.

[159] T. Femmer, A.J.C. Kuehne, M. Wessling, Print your own membrane: Direct rapid prototyping of polydimethylsiloxane, Lab Chip. 14 (2014) 2610–2613. doi:10.1039/c4lc00320a.

[160] Y. Lu, B. Lin, J. Qin, Patterned paper as a low-cost, flexible substrate for rapid prototyping of PDMS microdevices via liquid molding, Anal. Chem. 83 (2011) 1830–1835. doi:10.1021/ac102577n.

[161] X. Liu, Q. Wang, J. Qin, B. Lin, A facile “liquid-molding” method to fabricate PDMS microdevices with 3-dimensional channel topography, Lab Chip. 9 (2009) 1200–1205. doi:10.1039/b818721e.

[162] J.C. Jokerst, J.M. Emory, C.S. Henry, Advances in microfluidics for environmental analysis, Analyst. 137 (2012) 24–34. doi:10.1039/C1AN15368D.

[163] J. Kim, A.M. Stockton, E.C. Jensen, R.A. Mathies, Pneumatically actuated microvalve circuits for programmable automation of chemical and biochemical analysis, Lab Chip. 16 (2016) 812–819. doi:10.1039/c5lc01397f.

[164] P.K. Yuen, SmartBuild–A truly plug-n-play modular microfluidic system, Lab Chip. 8 (2008) 1374. doi:10.1039/b805086d.

[165] D. Bak, Rapid prototyping or rapid production? 3D printing processes move industry towards the latter, Assem. Autom. 23 (2003) 340–345. doi:10.1108/01445150310501190.

[166] L.C. Duarte, C.L.S. Chagas, L.E.B. Ribeiro, W.K.T. Coltro, 3D printing of microfluidic devices with embedded sensing electrodes for generating and measuring the size of microdroplets based on contactless conductivity detection, Sensors Actuators, B Chem. 251 (2017) 427–432. doi:10.1016/j.snb.2017.05.011.

[167] K.B. Anderson, S.Y. Lockwood, R.S. Martin, D.M. Spence, A 3D printed fluidic device that enables integrated features, Anal. Chem. 85 (2013) 5622–5626. doi:10.1021/ac4009594.

[168] Xerox, No Title, (n.d.). http://www.support.xerox.com/support/colorqube-8580/documentation/enus.html.

[169] W. Wang, S. Zhao, T. Pan, Lab-on-a-print: from a single polymer film to three-dimensional integrated microfluidics, Lab Chip. 9 (2009) 1133. doi:10.1039/b816287e.

[170] Xerox, No Title, (n.d.). https://www.xerox.com/download/ehs/msds/S-9511.en-

us.pdf.

[171] S. Arulanandam, D. Li, Liquid transport in rectangular microchannels by electroosmotic pumping, Colloids Surfaces A Physicochem. Eng. Asp. 161 (2000) 89–102. doi:10.1016/S0927-7757(99)00328-3.

[172] L. Perreux, A. Loupy, A tentative rationalization of microwave effects in organic synthesis according to the reaction medium, and mechanistic considerations, Tetrahedron. 57 (2001) 9199–9223. doi:10.1016/S0040-4020(01)00905-X.

[173] C. Sutton, J.E. Mark, Dipole moments of dimethylsiloxane oligomers and poly(dimethylsiloxane), J. Chem. Phys. 54 (1971) 5011–5014. doi:10.1063/1.1674790.

[174] D.A. Lewis, Microwave Processing of Polymers - An Overview, MRS Proc. 269 (1992) 21. doi:10.1557/PROC-269-21.

[175] A. Loupy, A. Petit, J. Hamelin, F. Texier-Boullet, P. Jacquault, D. Mathé, New Solvent-Free Organic Synthesis Using Focused Microwaves, Synthesis (Stuttg). 1998 (1998) 1213–1234. doi:10.1055/s-1998-6083.

[176] J.C. McDonald, D.C. Duffy, J.R. Anderson, D.T. Chiu, H. Wu, O.J. Schueller, G.M. Whitesides, Fabrication of microfluidic systems in poly(dimethylsiloxane)., Electrophoresis. 21 (2000) 27–40. doi:10.1002/(SICI)1522-2683(20000101)21:1<27::AID-ELPS27>3.0.CO;2-C.

[177] M. Geppi, G. Mollica, S. Borsacchi, M. Marini, M. Toselli, F. Pilati, Solid-state nuclear magnetic resonance characterization of PE-PEG/silica hybrid materials prepared by microwave-assisted sol-gel process, J. Mater. Res. 22 (2007) 3516–3525. doi:10.1557/jmr.2007.0434.

[178] C. Leonelli, M. Messori, F. Pilati, P. Veronesi, Non-conventional curing of organic-inorganic hybrids, Macromol. Symp. 228 (2005) 229–235. doi:10.1002/masy.200551020.

[179] J. Kim, R. Surapaneni, B.K. Gale, Rapid prototyping of microfluidic systems using a PDMS/polymer tape composite, Lab Chip. 9 (2009) 1290–1293. doi:10.1039/b818389a.

[180] W. Jung, J. Han, J.W. Choi, C.H. Ahn, Point-of-care testing (POCT) diagnostic systems using microfluidic lab-on-a-chip technologies, Microelectron. Eng. 132 (2015) 46–57. doi:10.1016/j.mee.2014.09.024.

[181] J. Kim, A.M. Stockton, E.C. Jensen, R.A. Mathies, Pneumatically actuated microvalve circuits for programmable automation of chemical and biochemical analysis, Lab Chip. 16 (2016) 812–819. doi:10.1039/c5lc01397f.

[182] P.N. Nge, C.I. Rogers, A.T. Woolley, Advances in microfluidic materials, functions, integration, and applications, Chem. Rev. 113 (2013) 2550–2583. doi:10.1021/cr300337x.

[183] R.O. Rodrigues, R. Lima, H.T. Gomes, A.M.T. Silva, Polymer microfluidic devices: an overview of fabrication methods, U.Porto J. Eng. 1 (2017) 67–79. doi:10.24840/2183-6493_001.001_0007.

[184] J. Wu, M. Gu, Microfluidic sensing: state of the art fabrication and detection techniques, J. Biomed. Opt. 16 (2011) 080901. doi:10.1117/1.3607430.

[185] Z. Isiksacan, M.T. Guler, B. Aydogdu, I. Bilican, C. Elbuken, Rapid fabrication of microfluidic PDMS devices from reusable PDMS molds using laser ablation, J. Micromechanics Microengineering. 26 (2016). doi:10.1088/0960-1317/26/3/035008.

[186] V.N. Goral, Y.C. Hsieh, O.N. Petzold, R.A. Faris, P.K. Yuen, Hot embossing of plastic microfluidic devices using poly(dimethylsiloxane) molds, J. Micromechanics Microengineering. 21 (2011). doi:10.1088/0960-1317/21/1/017002.

[187] H. Yagyu, K. Sugano, S. Hayashi, O. Tabata, Micropowder blasting with nanoparticles dispersed polymer mask for rapid prototyping of glass chip, J. Micromechanics Microengineering. 15 (2005) 1236–1241. doi:10.1088/0960-1317/15/6/014.

[188] D.J. Guckenberger, T.E. De Groot, A.M.D. Wan, D.J. Beebe, E.W.K. Young, Micromilling: A method for ultra-rapid prototyping of plastic microfluidic devices, Lab Chip. 15 (2015) 2364–2378. doi:10.1039/c5lc00234f.

[189] T. Kanai, M. Tsuchiya, Microfluidic devices fabricated using stereolithography for preparation of monodisperse double emulsions, Chem. Eng. J. 290 (2016) 400–404.

doi:10.1016/j.cej.2016.01.064.

[190] D.J. Kinahan, P.L. Early, A. Vembadi, E. Macnamara, N.A. Kilcawley, T. Glennon, D. Diamond, D. Brabazon, J. Ducrée, Xurography actuated valving for centrifugal flow control, Lab Chip. 16 (2016) 3454–3459. doi:10.1039/c6lc00568c.

[191] C.N. Lim, K.S. Koh, Y. Ren, J.K. Chin, Y. Shi, Y. Yan, Analysis of liquid-liquid droplets fission and encapsulation in single/two layer microfluidic devices fabricated by xurographic method, Micromachines. 8 (2017). doi:10.3390/mi8020049.

[192] J. Liu, J.B. Mahony, P.R. Selvaganapathy, Low-cost and versatile integration of microwire electrodes and optical waveguides into silicone elastomeric devices using modified xurographic methods, Microsystems Nanoeng. 3 (2017) 1–7. doi:10.1038/micronano.2017.40.

[193] E. Pinto, V. Faustino, R.O. Rodrigues, D. Pinho, V. Garcia, J.M. Miranda, R. Lima, A rapid and low-cost nonlithographic method to fabricate biomedical microdevices for blood flow analysis, Micromachines. 6 (2015) 121–135. doi:10.3390/mi6010121.

[194] L.E. Stallcop, Y.R. Álvarez-García, A.M. Reyes-Ramos, K.P. Ramos-Cruz, M.M. Morgan, Y. Shi, L. Li, D.J. Beebe, M. Domenech, J.W. Warrick, Razor-printed sticker microdevices for cell-based applications, Lab Chip. 18 (2018) 451–462. doi:10.1039/c7lc00724h.

[195] X. Yuan, L. Renaud, M.C. Audry, P. Kleimann, Electrokinetic Biomolecule Preconcentration Using Xurography-Based Micro-Nano-Micro Fluidic Devices, Anal. Chem. 87 (2015) 8695–8701. doi:10.1021/acs.analchem.5b01352.

[196] M.A. Eddings, B.K. Gale, A PDMS-based gas permeation pump for on-chip fluid handling in microfluidic devices, J. Micromechanics Microengineering. 16 (2006) 2396–2402. doi:10.1088/0960-1317/16/11/021.

[197] J.I. Martínez-López, H.A. Betancourt, E. García-López, C.A. Rodriguez, H.R. Siller, Rapid fabrication of disposable micromixing arrays using xurography and laser ablation, Micromachines. 8 (2017). doi:10.3390/mi8050144.

[198] J.I. Martínez-López, M. Mojica, C.A. Rodríguez, H.R. Siller, Xurography as a rapid fabrication alternative for point-of-care devices: Assessment of passive

micromixers, Sensors (Switzerland). 16 (2016) 1–21. doi:10.3390/s16050705.

[199] J. Kim, R. Surapaneni, B.K. Gale, Rapid prototyping of microfluidic systems using a PDMS/polymer tape composite, Lab Chip. 9 (2009) 1290–1293. doi:10.1039/b818389a.

[200] P.K. Yuen, V.N. Goral, Low-cost rapid prototyping of flexible microfluidic devices using a desktop digital craft cutter, Lab Chip. 10 (2010) 384–387. doi:10.1039/b918089c.

[201] M. Islam, R. Natu, R. Martinez-Duarte, A study on the limits and advantages of using a desktop cutter plotter to fabricate microfluidic networks, Microfluid. Nanofluidics. 19 (2015) 973–985. doi:10.1007/s10404-015-1626-9.

[202] J. Greer, S.O. Sundberg, C.T. Wittwer, B.K. Gale, Comparison of glass etching to xurography prototyping of microfluidic channels for DNA melting analysis, J. Micromechanics Microengineering. 17 (2007) 2407–2413. doi:10.1088/0960-1317/17/12/003.

[203] I.D. Johnston, D.K. McCluskey, C.K.L. Tan, M.C. Tracey, Mechanical characterization of bulk Sylgard 184 for microfluidics and microengineering, J. Micromechanics Microengineering. 24 (2014). doi:10.1088/0960-1317/24/3/035017.

[204] J. Dubose, J. Zhu, S. Patel, X. Lu, N. Tupper, J.M. Stonaker, X. Xuan, Electrokinetic particle separation in a single-spiral microchannel, J. Micromechanics Microengineering. 24 (2014). doi:10.1088/0960-1317/24/11/115018.

[205] J. DuBose, X. Lu, S. Patel, S. Qian, S.W. Joo, X. Xuan, Microfluidic electrical sorting of particles based on shape in a spiral microchannel, Biomicrofluidics. 8 (2014). doi:10.1063/1.4862355.

[206] J. Zhu, X. Xuan, Curvature-induced dielectrophoresis for continuous separation of particles by charge in spiral microchannels, Biomicrofluidics. 5 (2011). doi:10.1063/1.3599883.

[207] C. Church, J. Zhu, J. Nieto, G. Keten, E. Ibarra, X. Xuan, Continuous particle separation in a serpentine microchannel via negative and positive dielectrophoretic focusing, J. Micromechanics Microengineering. 20 (2010). doi:10.1088/0960-1317/20/6/065011.

[208] N.G. Vanifatova, B.Y. Spivakov, J. Mattusch, R. Wennrich, Separation of unmodified polystyrene nanosphere standards by capillary zone electrophoresis, J. Chromatogr. A. 898 (2000) 257–263. doi:10.1016/S0021-9673(00)00850-5.

[209] C.J. Easley, J.M. Karlinsey, J.M. Bienvenue, L.A. Legendre, M.G. Roper, S.H. Feldman, M.A. Hughes, E.L. Hewlett, T.J. Merkel, J.P. Ferrance, J.P. Landers, A fully integrated microfluidic genetic analysis system with sample-in-answer-out capability, Proc. Natl. Acad. Sci. 103 (2006) 19272–19277. doi:10.1073/pnas.0604663103.

[210] C.M. McGraw, S.E. Stitzel, J. Cleary, C. Slater, D. Diamond, Autonomous microfluidic system for phosphate detection, Talanta. 71 (2007) 1180–1185. doi:10.1016/j.talanta.2006.06.011.

[211] H. Becker, C. Gärtner, Polymer microfabrication methods for microfluidic analytical applications, Electrophoresis. 21 (2000) 12–26. doi:10.1002/(SICI)1522-2683(20000101)21:1<12::AID-ELPS12>3.0.CO;2-7.

[212] S. Wang, N. Yu, T. Wang, P. Ge, S. Ye, P. Xue, W. Liu, H. Shen, J. Zhang, B. Yang, Morphology-Patterned Anisotropic Wetting Surface for Fluid Control and Gas-Liquid Separation in Microfluidics, ACS Appl. Mater. Interfaces. 8 (2016) 13094–13103. doi:10.1021/acsami.6b01785.

[213] T.M.G. Cardoso, F.R. de Souza, P.T. Garcia, D. Rabelo, C.S. Henry, W.K.T. Coltro, Versatile fabrication of paper-based microfluidic devices with high chemical resistance using scholar glue and magnetic masks, Anal. Chim. Acta. 974 (2017) 63–68. doi:10.1016/j.aca.2017.03.043.

[214] M. Heymann, S. Fraden, D. Kim, Multi-height precision alignment with selectively developed alignment marks, J. Microelectromechanical Syst. 23 (2014) 424–427. doi:10.1109/JMEMS.2013.2279231.

[215] Elmer’s Glue, (n.d.). http://elmers.com/about/faqs/general.

[216] B.M. Budhlall, O.L. Shaffer, E.D. Sudol, V.L. Dimonie, M.S. El-Aasser, Atomic Force Microscopy Studies of the Film Surface Characteristics of Poly(vinyl acetate) Latexes Prepared with Poly(vinyl alcohol), Langmuir. 19 (2003) 9968–9972. doi:10.1021/la0270340.

[217] E. Tisdale, C. Wilkins, Method development for compositional analysis of low

molecular weight poly(vinyl acetate) by matrix-assisted/laser desorption-mass spectrometry and its application to analysis of chewing gum, Anal. Chim. Acta. 820 (2014) 92–103. doi:10.1016/j.aca.2014.02.042.

[218] L.E. Scriven, Dip Coating and Spin Coating, MRS Proc. 121 (1988) 717–729.

[219] S. Roy, K.J. Ansari, S.S.K. Jampa, P. Vutukuri, R. Mukherjee, Influence of substrate wettability on the morphology of thin polymer films spin-coated on topographically patterned substrates, ACS Appl. Mater. Interfaces. 4 (2012) 1887–1896. doi:10.1021/am300201a.

[220] S. Bhattacharya, A. Datta, J.M. Berg, S. Gangopadhyay, Studies on surface wettability of poly(dimethyl) siloxane (PDMS) and glass under oxygen-plasma treatment and correlation with bond strength, J. Microelectromechanical Syst. 14 (2005) 590–597. doi:10.1109/JMEMS.2005.844746.

[221] T. Isemura, A. Imanishi, The dissolution of water-insoluble polymers in the surfactant solution. The polyelectrolyte-like behavior of the dissolved polymers, J. Polym. Sci. 33 (1958) 337–352. doi:10.1002/pol.1958.1203312632.

[222] W. Shi, J. Qin, N. Ye, B. Lin, Droplet-based microfluidic system for individual Caenorhabditis elegans assay, Lab Chip. 8 (2008) 1432–1435. doi:10.1039/b808753a.

[223] G.G. Morbioli, N.C. Speller, A.M. Stockton, A practical guide to rapid-prototyping of PDMS-based microfluidic devices: A Tutorial, Anal. Chim. Acta. (Submitted (2020).

[224] Z.A. Duca, G.K. Tan, T. Cantrell, M. Van Enige, M. Dorn, M. Cato, N.C. Speller, A. Pital, R.A. Mathies, A.M. Stockton, Operation of pneumatically-actuated membrane-based microdevices for in situ analysis of extraterrestrial organic molecules after prolonged storage and in multiple orientations with respect to Earth's gravitational field, Sensors Actuators, B Chem. 272 (2018) 229–235. doi:10.1016/j.snb.2018.05.040.

[225] P.A. Willis, A.M. Stockton, Microchip Capillary Electrophoresis For In Situ Planetary Exploration, in: C.D. Garcia, K.Y. Chumbimuni-Torres, E. Carrilho (Eds.), Capill. Electrophor. Microchip Capill. Electrophor. Princ. Appl. Limitations, Wiley, 2013: pp. 277–291.

[226] W.H. Grover, R.A. Mathies, An integrated microfluidic processor for single nucleotide polymorphism-based DNA computing, Lab Chip. 5 (2005) 1033–1040. doi:10.1039/b505840f.

[227] A.T. Ciftlik, H.A. Lehr, M.A.M. Gijs, Microfluidic processor allows rapid HER2 immunohistochemistry of breast carcinomas and significantly reduces ambiguous (2+) read-outs, Proc. Natl. Acad. Sci. U. S. A. 110 (2013) 5363–5368. doi:10.1073/pnas.1211273110.

[228] William H. Grover, GitHub Dr. Grover, (2020). https://github.com/groverlab (accessed April 5, 2020).

[229] W. Zhang, S. Lin, C. Wang, J. Hu, C. Li, Z. Zhuang, Y. Zhou, R.A. Mathies, C.J. Yang, PMMA/PDMS valves and pumps for disposable microfluidics, Lab Chip. 9 (2009) 3088–3094. doi:10.1039/b907254c.

[230] P. Scherz, S. Monk, Practical Electronics for Inventors, 4th ed, McGraw-Hill Education, New York, 2016.

[231] Python, (2020). https://www.python.org/ (accessed April 5, 2020).

[232] SciPy, (2020). https://www.scipy.org/about.html (accessed April 5, 2020).

[233] E.W. Dijkstra, A Note on Two Problems in Connexion with Graphs, Numer. Math. 1 (1959) 269–271. doi:https://doi.org/10.1007/BF01386390.

[234] A.M. Stockton, T.N. Chiesl, T.K. Lowenstein, X. Amashukeli, F. Grunthaner, R. a Mathies, Capillary electrophoresis analysis of organic amines and amino acids in saline and acidic samples using the Mars organic analyzer., Astrobiology. 9 (2009) 823–831. doi:10.1089/ast.2009.0357.

[235] J.M. Ottino, S. Wiggins, Introduction: Mixing in microfluidics, Philos. Trans. R. Soc. A Math. Phys. Eng. Sci. 362 (2004) 923–935. doi:10.1098/rsta.2003.1355.

[236] G.G. Morbioli, T. Mazzu-Nascimento, A. Aquino, C. Cervantes, E. Carrilho, Recombinant drugs-on-a-chip: The usage of capillary electrophoresis and trends in miniaturized systems – A review, Anal. Chim. Acta. 935 (2016) 44–57. doi:10.1016/j.aca.2016.06.019.

[237] G.G. Morbioli, T. Mazzu-Nascimento, A.M. Stockton, E. Carrilho, Technical aspects and challenges of colorimetric detection with microfluidic paper-based analytical devices (μPADs) - A review, Anal. Chim. Acta. 970 (2017) 1–22. doi:10.1016/j.aca.2017.03.037.

[238] F.A. Kappi, G.Z. Tsogas, D.C. Christodouleas, D.L. Giokas, Calibrant-loaded paper-based analytical devices for standard addition quantitative assays, Sensors Actuators, B Chem. 253 (2017) 860–867. doi:10.1016/j.snb.2017.07.007.

[239] L. Gervais, E. Delamarche, Toward one-step point-of-care immunodiagnostics using capillary-driven microfluidics and PDMS substrates †, Lab Chip. 9 (2009) 3330–3337. doi:10.1039/B906523G.

[240] International Telecommunication Union, (n.d.). https://www.itu.int/en/ITU-D/Statistics/Pages/stat/default.aspx.

[241] I.M. Hutchings, G.D. Martin, eds., Inkjet Technology for Digital Fabrication, John Wiley & Sons, Ltd, Chichester, UK, 2012. doi:10.1002/9781118452943.

[242] W. Su, B.S. Cook, Y. Fang, M.M. Tentzeris, Fully inkjet-printed microfluidics: A solution to low-cost rapid three-dimensional microfluidics fabrication with numerous electrical and sensing applications, Sci. Rep. 6 (2016) 1–12. doi:10.1038/srep35111.

[243] D.T. Chiu, A.J. deMello, D. Di Carlo, P.S. Doyle, C. Hansen, R.M. Maceiczyk, R.C.R. Wootton, Small but Perfectly Formed? Successes, Challenges, and Opportunities for Microfluidics in the Chemical and Biological Sciences, Chem. 2 (2017) 201–223. doi:10.1016/j.chempr.2017.01.009.

[244] Arduino Store, (2020). https://store.arduino.cc/usa/mega-2560-r3 (accessed April 5, 2020).

[245] The Lee Company, (2020). https://www.theleeco.com/products/electro-fluidic-systems/solenoid-valves/control-valves/lhd-series/3-port/face-mount/ (accessed April 5, 2020).